STUDIES ON ETCHING AND POLYMER DEPOSITION IN HALOCARBON PLASMAS.

October 1st. 1987.

P.J.Astell-Burt.

Chemical Crystallography Laboratory.

South Parks Road,

OXFORD.

Dedicated to Paddy and John.

"The time has come," the Walrus said,

"To talk of many things:

Of shoes-and ships-and sealing wax-

Of cabbages-and kings-

And why the sea is boiling hot-

And whether pigs have wings."

Alice through the Looking-Glass

C.L.Dodgson, Christ Church.

D.Phil Thesis 1987

Table of Contents

Table of Figures

Table of Tables

ABSTRACT.

A Thesis concerning

Surface Chemical Effects In Ionised Environments.

submitted for the degree of Doctor of Philosophy, University of Oxford by P.J.Astell-Burt, Christ Church, 1987.

Plasma etching, the selective removal of materials by reaction with chemically active species formed in a glow-discharge, is widely used by the electronics industry because of the advantages over 'wet' processes. The full potential has yet to be realised because chemical processes occuring in the plasma and at the plasma/substrate interface are incompletely understood. In this work attention was focussed on the accumulation of polymers on surfaces during plasma etching in fluorocarbon gases.

An apparatus was designed and constructed to explore the conditions which give rise to these deposits by:

i) The detection of the excited species such as CF and CF_2 (by optical emission spectroscopy); and

ii) The rate of accumulation or removal of deposits (by means of a quartz crystal microbalance).

The gases CF_4, C_2F_6, C_3F_8 and CHF_3 were used at pressures between 200-600mT, together with mixtures with H_2 and a few runs with other gases to vary the partial pressures of etching and polymerizing species. Both substrate effect of, viz silicon and thermally oxidised silicon (SiO_2), and electrode materials effects have been examined.

Polymer production from C_3F_8 has been found to be more sensitive to electrode composition than that from CHF_3, but the material formed is overall less thermally stable. On the other hand, polymers produced from C_3F_8 accumulate at similar rates on Si and SiO_2, whereas those from CHF_3 show a much greater liklihood of building up on Si than SiO_2. XPS and infra-red spectroscopy have been used to demonstrate that polymers arising from these two gases exhibit marked structural differences, which can be minimised by mixing H_2 with C_3F_8. These effects can be correlated with the decomposition products expected in the plasma.

ACKNOWLEDGEMENTS.

I would like to thank my supervisor Dr.A.K.Cheetham for his constant help and interest. Also I am indebted to Dr.J.A.Cairns for allowing me the equipment to carry out this work and providing many useful scientific insights, and to Dr.C.B.Amphlett for allowing me access to the facilities and staff of Chemistry Division at A.E.R.E. Harwell. I am particularily grateful to the Special Processing Group; especially Ken Hyde, Dr.E.S.Lane, Chris Markiw; and also to D.Stone, P.S.Drew, K.Cole, and R.M.Hazel.

From other divisions at Harwell I would like to thank:
Environmental and Medical Sciences: Dr.C.Pickford, N.J.D.Prosser, J.M.Butcher.
Instrumentation and Applied Physics: G.F.Snelling, E.M.Wittam, M.J.Fisher, G.Phillips.
Metallurgy/Materials Development: J.E.Bainbridge, C.Kenway-Jackson.
Nuclear Physics: Dr.C.J.Sofield, P.M.Read, Dr.N.J.Eyre, R.A.Saint.
Engineering Projects: R.A.Preston, R.Perrins.
Site services: The ladies of the tracing office, J.H.Slade and his team from the Recovery section, J.H.Marns and the staff of the library, the Harwell Photographic group and D.T.C.Wadler of CSSD.

I would like to acknowledge the helpful guidance I have had from Dr.R.F.Barrow and Dr.G.Hancock of the Physical Chemistry Laboratory, Oxford University.

I am indebted to the project assessors, Dr.V.S.Deshmukh and Dr.T.Cox from R.S.R.E. Malvern. From other organisations I would particularily like to thank Dr.E.Kay, IBM San Jose; C.Dobson, Electrotech Ltd.; D.Carr, Plasma Technology Ltd; and C.Starbuck, Southampton University. I acknowledge financial support from the Ministry of Defence via A.E.R.E. Harwell under the terms of a research contract RP 27/5.

Lastly to the many people who made my time in Oxford, Harwell and Weston so much more enjoyable, particularily Dave and Sue Coles, James Pettifar, John Wylie, Kim, Brendan, Ian and Penny, and Wendy and Jason.

1)INTRODUCTION.

The introduction begins with a brief review of some of the processes that are utilised in semiconductor device fabrication, concentrating on Silicon based structures. The formation and nature of plasmas is then discussed, and the uses of plasmas in dry etching processes is described in some detail. Some of the previous literature in this area is reviewed and the aims of the present work are presented.

1.1)Fabrication of Integrated Circuits.

A typical Very Large Scale Integration (VLSI) device consists of a $20mm^2$ slice of single crystal silicon on which a circuit consisting of up to 250,000 circuit elements may be present[1]. A sample circuit with 5 micron feature sizes is shown in a photomicrograph in the Appendix[2].

The process for forming Metal Oxide Semiconductor (MOS), Metal Semiconductor Field Effect Transistor (MESFET), and Bipolar Junction Transistor (BJT) Integrated circuits will include at least some of the following main stages[3-8]:

1. Substrate preparation -Silicon.

Polycrystalline silicon, synthesised from SiO_2 + C

in an electric furnace, is the starting material. This is converted to trichlorosilane and chemically purified before decomposition in a H_2 atmosphere to give semiconductor grade silicon. Another method of purification used is zone refining. Growth of the large single crystals of Si material required for device fabrication is then accomplished from the melt by one of three main methods[9-10]:

The Czochralski Technique.

The Float Zone method.

The Bridgman or Gradient Freeze technique.

Most often used is the Czochralski Technique in which the material is contained in a quartz vessel and melted by inductive or resistive heating. A seed crystal of the required orientation is then dipped into the liquid and when its end is molten it is slowly withdrawn at about 10 micron s^{-1}, resulting in a single crystal which grows by progressive freezing at the liquid-solid interface. The crystal diameter is controlled by adjusting the heat input and pull rate.

In the Float Zone method a molten volume is passed upwards through a polycrystalline bar of silicon positioned vertically inside a furnace chamber. A seed crystal is mounted in contact with the lower end of the bar and a molten zone is established by R.F. heating which fuses the seed crystal to the end. As the molten zone is moved up,

the material freezing along the lower interface has the single crystal structure and crystallographic orientation of the seed crystal.

The Bridgman technique involves melting the polycrystalline material in a long boat which is then cooled from one end. A seed crystal placed at the narrow end of the boat allows a single grain to propagate at the liquid-solid interface, eventually resulting in the whole melt freezing in a particular crystalline structure. Since the boat grown material crystal structure is highly defected from the expansion of the silicon on freezing this method is usually only found for polycrystalline solar cells.

After growth, a flat face is ground on the side of the large single crystal that parallels the growth axis. This is used as a reference for alignment for later processing and measurement stages. Finally the ingot is sliced into wafers by means of a diamond saw. The sliced wafers are then lapped to remove the damage and irregularities caused by the slicing operation and finally are polished to an optically flat surface. The backside of the wafer is then often damaged mechanically to provide defect gettering sites.

2. Epitaxy.

This is a deposition technique to grow a thin single crystal layer upon the surface of a single crystal substrate. These layers have advantages where high speeds or current carrying capability are required, but add increased complexity to the fabrication process. Molecular Beam[11], Vapour Phase[12], or Liquid Phase[13] Epitaxy can be used, but are more common for III/V and II/VI semiconductors than for silicon.

3. Thermal processes.

Heating semiconductor grade silicon wafers at typically 1000-1200^{o}C in an oxidising atmosphere results in the formation of a SiO_2 layer. The experimental methods used in this study are outlined in "2.7 Preparation of samples". The SiO_2 films formed are used for diffusion or implant masks, surface passivation, electrical isolation of individual devices, the gate oxides and capacitor dielectrics in MOS devices, and use as a tunnelling oxide in Electrically Alterable ROMS. Another thermal process is diffusion which is discussed in the next section. Wafers are also heated in inert atmospheres for the annealing out of charge traps and damage caused by ion implantation, and for alloying of contact zones (silicides).

4. Doping.

The introduction of p-type or n-type impurities may be carried out by diffusion or ion implantation[14], thus changing the electrical characteristics of the material. Diffusion involves the thermally induced distribution of impurity atoms through the crystal lattice. This is generally achieved by a pre-treatment stage in which vaporised dopant is passed across the wafer surface into which it will penetrate a short distance. This surface saturated material is then heated to allow diffusion into the substrate to the required junction depth. Increasingly for VLSI, ion implantation[14] is used to place the impurity or doping ions at precisely controlled depths in the semiconductor layers at accurately controlled concentrations in areas designated by means of beam steering and masking. The depth is determined by means of the ion energy because as the energetic ions penetrate the target they lose energy due to collisions with atomic nuclei and electrons in the substrate and eventually come to rest. The range-energy relationship to predict the depth is usually obtained from LSS theory[15]. The dosage is determined by means of the total charge. This can even be extended so as to form buried SiO_2 layers by means of oxygen ion implantation. A subsequent annealing process is required since the damage caused by the ion beam

causes the silicon surface to become amorphous, and the ions need to become substitutional to become electrically active.

5. Lithography.

This involves the use of photomasks and photosensitive organic, and to a very much lesser extent inorganic, films for masking for subsequent pattern definition[16-17]. These films are applied by spraying or spin coating onto the surface of a layer which is to be etched, followed by evaporation of the solvent and baking at ca. 100°C. The photoresist is then selectively exposed to sensitising radiation, generally in the far UV. For very high resolution work exposures to very short wavelengths, such as X-Ray radiation, is required. The exposure is through a mask or by a modulated scanned beam as in Electron Beam Lithography, or Ion Beam Lithography. Subsequent development of the exposed portions of the photoresist causes either the exposed or the unexposed portions to be removed depending on whether the material is a positive or negative photoresist. Positive photoresist developers are dilute alkaline solutions, and those for negative photoresists are organic solvents:

The photoresists themselves are often removed by 'plasma-ashing', exposure to an O_2 plasma, or by means of a wet chemical stripper.

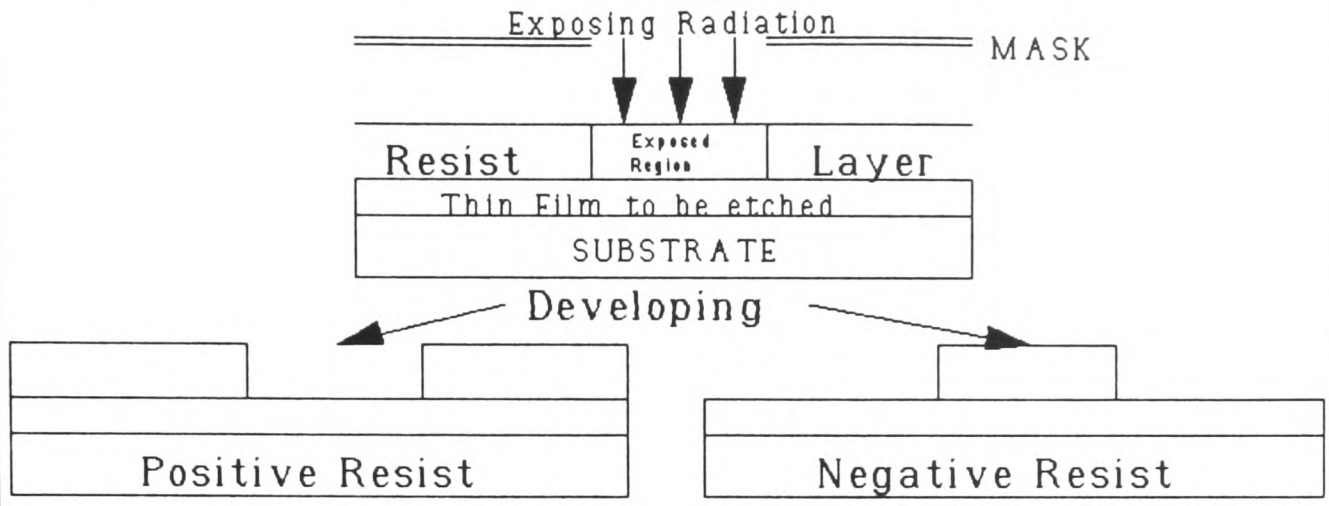

Figure 1.

Characteristics of the two Resist Types.

6. Wet Processes.

These include wafer cleaning to remove unwanted particles, films and chemical impurities from the surface, photoresist development and later removal, and solution etching techniques. 'Lift-off' patterning techniques can also be included here.

7. Etching.

This is the use of 'wet' chemical or 'dry' plasma etching agents[18-19] to remove material from the substrate or from thin films on its surface. When there is a masking layer present the goal is to selectively remove material from the uncovered areas. Typical processes include:

a) Opening of windows in SiO_2, SiON, or SiN_x prior to doping, implantation or formation of contacts to the individual devices.

b) Definition of metal interconnect patterns.

c) Removal of substrate material in certain isolation processes, e.g. by formation of a surrounding trench; or for the formation of through wafer contacts -vias.

d) Photoresist removal after use, and occasionally for pattern definition.

'Dry' processes are dealt with in detail in "1.2 Plasma Etching." as are some of the advantages and disadvantages compared with 'wet' etching.

8. Deposition.

Various techniques are used[19-20] to deposit metals, semiconductors and insulators. The commonest films are thermally grown or deposited from the vapour phase, such as Plasma Enhanced Chemical Vapour Deposition (PECVD) or Low Pressure CVD (LPCVD). These are for materials such as amorphous Si, polycrystalline Si, SiO_2, and Si_3N_4. Induced decomposition of SiH_4 gives amorphous Si. SiH_4 with CO, CO_2 or O_2 is used for SiO_X, and SiH_4 with NH_3 and/or N_2 for SiN_X. These are used for protective layers -encapsulants, dielectric layers, or masks for etching or diffusion. Their production is discussed further in "1.7.1 Deposition of Inorganic Materials". As encapsulants these can be used for either electrical isolation or for a barrier to contaminants such as Na^+ or H_2O. High density SiN_X can be used below the first interconnect level, and

phosphorous doped silicon dioxide layers are deposited on the level above for both isolation and mechanical strength. There is interest in the use of organic polymers for these purposes due to their relative ease of formation at low temperatures in plasma based systems. Evaporation and sputtering techniques are also employed, more usefully for metals rather than non-metals.

9. Metallisation.

This involves deposition over the diffused regions, usually by Aluminium or its alloys with Si or Cu. This layer is then etched to form the interconnects between devices formed on the silicon, and also connections to the edge of the complete die. The metallisation is applied by sputtering or by evaporation from filament or e-beam sources. Pattern definition is again by either dry or wet etching processes.

1.2)Plasma Etching.

New methods for making semiconductor devices have had to evolve in response to the demands for VLSI[21-29]. Though improvements in lithographic techniques have enabled replication of high density patterns, the transfer of these patterns into the underlying substrate can no longer be accomplished by the 'traditional' method of wet etching. This involves, in for example an oxide etch, the use of a buffered HF solution through a resin-based photolithographic masking layer. Current devices are now tending towards sub-micron dimensions, causing severe problems for an isotropic etch process (Figure 2).

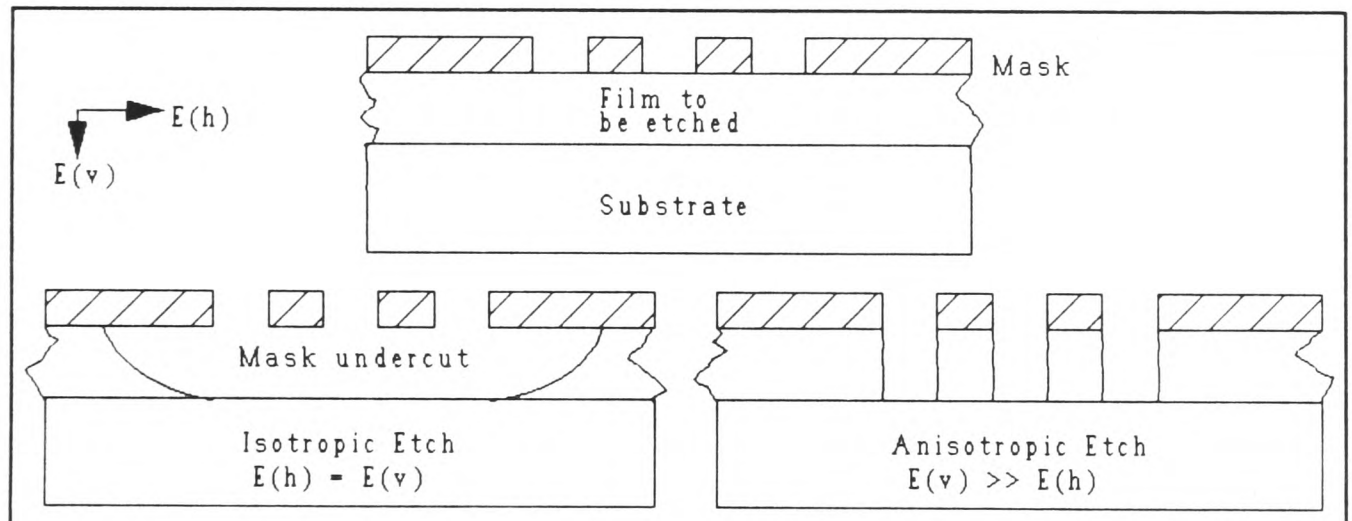

Figure 2.

Isotropic vs. Anisotropic etching processes.

For the very small geometries now required, wet etching suffers from several further drawbacks. Surface tension effects can prevent the liquid from

penetrating through the photoresist to the surface, or the capillary action of the liquid etchant can undercut the photoresist. Small gas bubbles may hinder access of the reagents as can contamination by sub-micron dust particles. There are also the problems associated with the handling, use and disposal of relatively large quantities of toxic acids and solvents as used in the wet etching and resist strip processes and their associated health hazards.

The alternative is a process based on gas phase, plasma assisted etching which, under certain circumstances, can produce the very high resolution pattern transfer required. This retention of pattern fidelity requires a high degree of anisotropy during the etch, with the vertical etch rate substantially exceeding the lateral etch rate. Further explanation of anisotropic etching is in the section "1.5 Effects of Ion Bombardment".

A typical plasma etching process involves the loading of the wafer(s) into the reactor chamber which is then evacuated. The reagent gas mixture is then flowed through the system at a pressure maintained in the region 5mT - 1 Torr by means of control of reagent gas flows and pump throttling. The gas is then ionised by an applied R.F. field and the resultant species diffuse to, react, and then the products desorb from the wafer surface. Upon

completion of the etching cycle the R.F. and gas flows are switched off. The chamber is then pumped out, vented with an inert gas such as N_2 and the wafer(s) removed. Some sample gases and materials are shown in Table 1. It should be noted that there are wide differences in the mechanisms of 'overall' plasma etching with different types of gases, reactor configurations and plasma conditions, but these techniques have in common the use of plasma activated species to achieve etching.

Etching gas.	Some etchable materials.
CF_4, CF_4/O_2	Si, SiO_2, SiN_x, Ti, Mo, W
C_2F_6, CHF_3	SiO_2, SiN_x
CF_4/H_2	SiO_2
$CClF_3$	Si, Au, Ti
$CBrF_3$	Si, Ti, Pt, Nb, Mo
CCl_2F_2	GaAs, InP, Au
SF_6, $+O_2$	SiN_x
ClF_3	Si
NF_3,PF_5	Si, Mo, $MoSi_2$, SiO_2
HF	Si, SiO_2
F_2, Cl_2, Br_2	Si, GaAs, InP
H_2	InP, GaAs
CCl_4, $+O_2$, $+Cl_2$	GaAs, Al, Si, Cr, $TiSi_2$
Cl_2, Cl_2/O_2	InP, GaAs, Si, Cr
BCl_3, BCl_3/Cl_2	Al
SiF_4	SiN_x
$SiCl_4$, $+Cl_2$	Al-alloys, GaAs
O_2	Organics, Resists

Table 1.
Some typical gases and etchable materials.

Plasma assisted etching methods include ion etching (ion milling and sputter etching)[30-32], reactive ion etching (RIE) and reactive sputter etching[33-35], reactive ion beam etching (RIBE) and chemically assisted ion beam etching (CAIBE)[36-38],

and planar etching[39-41]. Ion milling relies on physical sputtering by energetic inert gas ions with energy ranges from several hundreds to thousands of electron volts. The strongly directional incident ions allow removal of substrate material to be highly anisotropic. However since this process relies on physical momentum transfer, rates are low; and selectivity to the mask and underlying layers is poor due to the small sputter yield differences between materials. Characteristic surface and sidewall redeposition, as well as trenching of the material is often found as the ejected species are not inherently volatile. The high ion energies can also cause radiation damage. At the other extreme is Planar Etching which can be described as the formation of a volatile product by reaction between a solid and the active species created in a comparatively high pressure molecular gas discharge. With such a chemical process, very high selectivities and rates, along with low radiation damage to devices can be achieved; but isotropic etching is usually as well as polymer deposition. Reactive Ion Etching and RIBE lie intermediate in effect, in that there is a contribution from both physical and chemical processes, potentially offering adequate selectivity along with controlled anisotropy, without problems such as faceting of the substrate and ion damage to MOS devices.

In the basic dry etch process there are six main steps. A relatively inert molecular gas which breaks down to form species (atoms, molecules and ions) that are chemically reactive with the material to be etched is decomposed in a glow discharge by inelastic collisions with energetic electrons. These species then diffuse, or are accelerated by the electric field to the surface of the wafer. Three steps then take place at the actual gas/solid interface. Firstly there is absorption onto the surface, spontaneous or stimulated chemical reaction, and then desorption of the product from the surface. Finally the desorbed species diffuse away into the gas phase and are pumped away. For Si semiconductor processing, the halocarbon gases used produce, among other things, fluorine or chlorine atoms which will attack silicon and SiO_2 leading to volatilisation of the surface as SiF_4 or $SiCl_4$, gaseous products which simplify disposal problems.

In contrast to D.C. and R.F. sputtering, species arriving at the sample are chemically active, so there is concern with both the chemistry at the gas/surface interface as well as the physics and chemistry of the discharge itself. However the complexity of the system can easily be seen in that neutrals, radicals such as CF_x species and $F^{\bullet}$, as well as ions and higher order unsaturated fluorocarbons and free electrons will be present. The concentrations of these species depend on

parameters such as power, pressure, feed gas composition and flow rate, and the materials present in the reactor. These will influence the competition between 'useful' reactions and undesirable ones such as low etch rates, loss of selectivity and anisotropy, and contaminants such as polymer deposition or sputtering of extraneous material as well as damage to the substrate. All of these factors must be carefully controlled in a practical etching system. Important parameters to be considered in dry etching processes are:

1. The rates of reaction.

The throughput of wafers can greatly affect the economics of the process[42]. The rate should also be reproducible from run to run.

2. Anisotropy.

The ratio of vertical to horizontal etch rates must be controllable as this will affect the feature sizes[43-48]. Not all processes are required to be completely anisotropic (vertical), as sometimes a process needs a slight wall slope such as for a subsequent metallisation step.

3. Substrate temperature.

This can influence etch rates, mask erosion and thermal damage to the devices[49-50].

4. Selectivities.

The etch should be highly selective with respect to both the material under the film being etched and

also the mask layer. This is because the etch rate over the wafer and the film thickness itself may not be uniform, and hence an additional overetch is required beyond the point at which the average film thickness would have etched to completion. The materials of the system itself should also be unaffected[51-53].

5. Loading effect.

One example is the depletion of active species by increased substrate area[54-55], thus giving variable etch rates for wafers with different exposed areas, or for a different number of wafers present in the chamber.

6. Uniformity.

The etch should be uniform over the wafer surface and over each wafer if in a batch system[56]. The etch rate should also be uniform from run to run.

7. Side reactions.

Typical ones to avoid are; mask attack, polymer or particulate formation[57-59], and ion bombardment induced damage[60-64].

1.3)Physics and Chemistry of Discharges.

1.3.1)Formation and Nature of Plasmas.

In the presence of an applied electric field of sufficient magnitude charged species found as a small fraction of a neutral gas (from natural radiation, photoionisation or field emission) can be accelerated and undergo elastic and inelastic collisions. In the case of an elastic collision between an electron and a gas molecule, very little energy will be lost by the electron because of the large difference in masses. Eventually the electron kinetic energy will become large enough to undergo an inelastic collision leading to ionisation or excitation of a gas molecule e.g.:

$$Ar + e^- \longrightarrow Ar^+ + 2e^-$$
$$O_2 + e^- \longrightarrow O_2^+ + 2e^-$$

Ionisation frees a second electron and an avalanche effect will occur if the applied voltage exceeds the breakdown potential. This results in an abundance of positive ions and electrons[65-69]. Inelastic collisions with energy less than the ionisation potential also happen causing promotion of gas molecule orbital electrons to a higher energy state. Subsequent radiative relaxation causes a glow whose colour depends on the spectral features of the species present. A second type of non-ionising collision is electron impact dissociation of

chemical bonds which can give rise to highly reactive fragments[70-72], as discussed further in the next section.

In the vicinity of surfaces regions of reduced luminosity a few millimetres wide, called sheaths or dark spaces are formed. In a D.C. discharge at the cathode, positive ions are present at a higher density. This causes a localised space charge and due to the difference in their comparative masses they are attracted more slowly to the cathode than the electrons are repelled. Thus they have a higher instantaneous concentration, increasing the electric field in front of the cathode and screening the rest of the discharge from the cathode voltage. As the glow region is a good conductor most of the voltage between the anode and cathode is dropped across these sheaths and the charged species experience their greatest acceleration here. As a result electrons rapidly acquire large amounts of kinetic energy and are more likely to cause ionisation on collision than excitation in this region. The cathode, and to a lesser extent the chamber walls, also act as a source of electrons by secondary emission when struck by ions, thus replenishing electrons lost (to the anode for example). Ions can cause sputtering of heavy particles which may deposit on surfaces where they can also be catalytically active[73]. The secondary electron emission leads in turn to further ionisation of the

gas at an overall concentration of about one ion in 10^4-10^6 molecules. The charged particle concentration is of the order of 10^9-10^{12} cm^{-3}, with a Debye length (screening distance) of 10^{-2} cm. This results in the generation of a non-equilibrium situation in which the gas has a very high electronic temperature. The large difference between the electronic temperature, about 10^5K and the mean rotational/vibrational temperature is due to the inefficient transfer of kinetic energy during elastic collisions between electrons and gas molecules.

With an alternating current supply each electrode in turn acts as a cathode. The glow discharge is still established but with a superimposed periodic polarity reversal. Above a minimum frequency, of about 2MHz, the ions created by the breakdown will no longer have sufficient time to be extracted from the sheath before the polarity change. At a higher frequency still, in the R.F. range, a large fraction of the electrons will oscillate in the gap between the electrodes without being able to drift to the positive electrode. Above this point the electrons sustain the discharge independently of secondary electron emission as they can pick up sufficient energy during oscillations cause ionisation. The ionisation collision probability is also increased by the oscillation so the discharge can be sustained at lower pressures, and this effect can also be

caused by magnetic confinement of the electrons. Typically these systems are run at an allocated frequency of 13.56MHz. A further advantage of the higher frequencies is that insulating electrodes, or electrodes that become covered with an insulating film, can be used. In a D.C. discharge the surface would charge up to the plasma potential and the glow would extinguish as soon as the insulator surface potential dropped below the value required to sustain the discharge. With an R.F. discharge the positive charge accumulated during one half-cycle can be neutralised by electron bombardment during the next half.

With systems with insulating electrodes or run with a blocking capacitor in the power feed, a D.C. bias of up to half the applied R.F. peak to peak voltage is established, the driven electrode being offset negatively. This is due to the difference in acceleration of the electrons and the ions, by the same potential in the plasma, because of their differing masses. This gives alternatively low energy electron bombardment followed by a lesser flux of high energy ions at the cathode, resulting in secondary electron emission and some sputtering.

The energy of ions incident upon the substrate depends on the applied a.c. field, as illustrated in Figure 3. $V_{(t)}$ is the potential of the smaller electrode, $V_{(p)}$ the potential of the glow itself.

There is also a dependence on the area ratio of driven to grounded surfaces and on which electrode the substrate is placed.

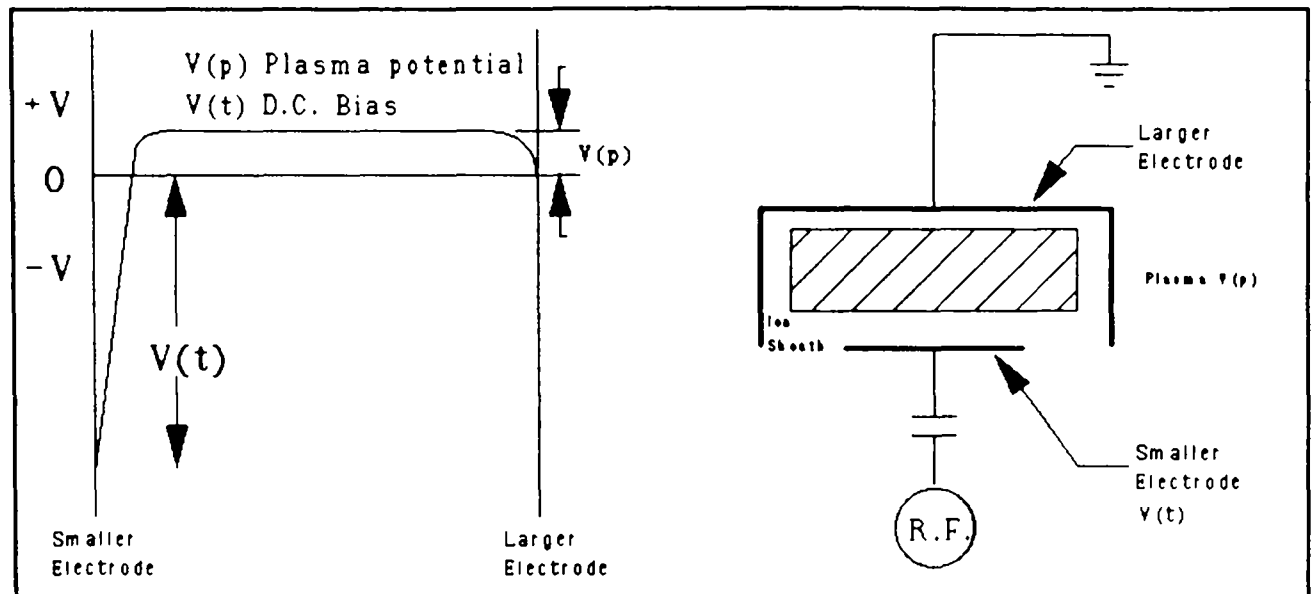

Figure 3.

Potential Distribution Across the Plasma.

1.3.2)Species Production in Discharges.

Apart from electronic excitation as a result of a comparatively low energy inelastic collision between an electron and a molecule, fragmentation of the molecule can also occur. This leads to the production of atoms, radicals and negative ions, e.g.:

$$(F + e^- \rightarrow F^* + e^- \rightarrow F + h\nu_F)$$
$$O_2 + e^- \rightarrow 2O + e^- \rightarrow O + O^-$$
$$CF_4 + e^- \rightarrow CF_3 + F + e^-$$
$$C_2F_6 + e^- \rightarrow 2CF_3 + e^-$$

and these species are the ones responsible for the etching of the substrates, since the parent molecules react only slowly or not at all without a discharge present.

Electron impact ionisation in the discharge is the primary ion generation mechanism, but this can also cause simultaneous fragmentation, e.g.:

$$(O_2 + e^- \longrightarrow O_2^+ + 2e^-)$$
$$CF_4 + e^- \longrightarrow CF_3^+ + F + 2e^-$$
$$CF_4 + e^- \longrightarrow CF_3^+ + F^- + e^-$$

The loss of electrons and ions from the discharge occur by a combination of recombination, diffusion, attachment and drift. Electron recombination or attachment with a molecular ion can also be dissociative. Atoms and radicals are lost by either homogeneous or heterogeneous reactions:

$$A + A + M \longrightarrow A_2 + M$$
$$A^* + M \longrightarrow A + M$$

Typically the plasma reactor contains 70-98% reagent gas molecules, 2-20% etch product molecules, 0.1-2% radicals and finally 0.001-0.01% charged species[3].

1.4)Previous Studies.

1.4.1)Halocarbon Plasma Etching.

R.F. discharges in flowing mixtures of halocarbons and hydrogen or oxygen are known to be efficient and selective in etching surfaces of semiconductors and overlying films. Recently there have been several good reviews of these processes[74-94]. It is clear that most of the

improvements in plasma etching processes have been largely empirical with, for example, the effects of changes in discharge power or amount of substrate on the etching behaviour being studied. An idea of some of the processes that can occur, for a CF_4 plasma are shown in Figure 4, noting that in the absence of a discharge CF_4 does not etch Si since it does not chemisorb. Fluorine on the other hand is known to spontaneously etch Si.

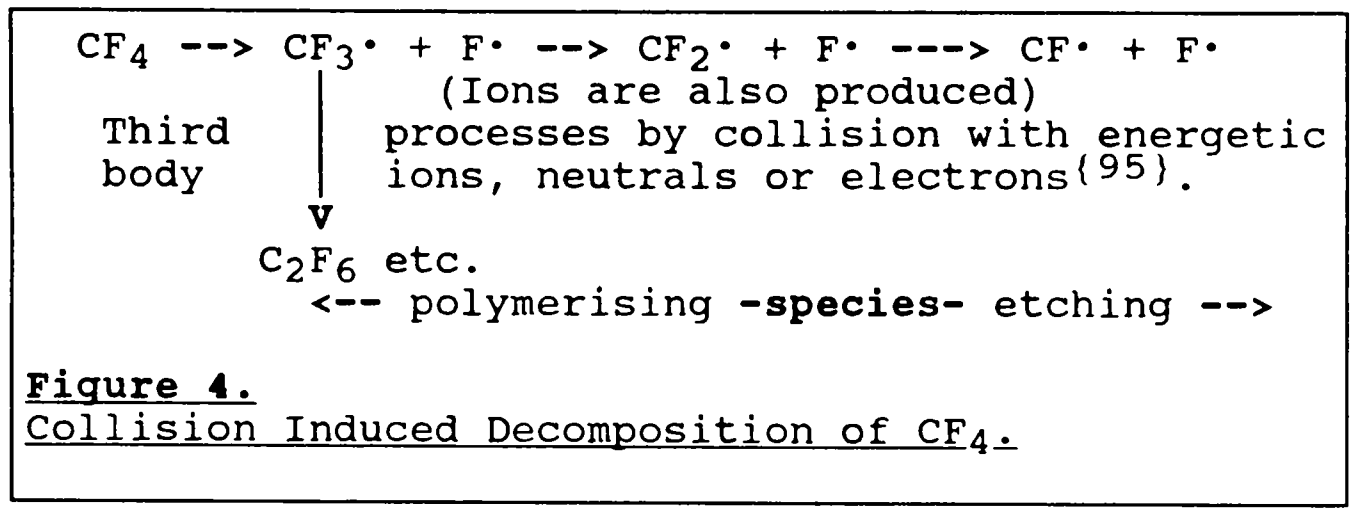

Figure 4.
Collision Induced Decomposition of CF_4.

The reason why halocarbon gases are used instead of, for example, F_2, HF or XeF_2 is ease of handling, and more importantly, if there is preferential polymer formation on the substrate the polymer film may act as an etch stop. This will prevent or slow further attack giving an etching selectivity. Anisotropy can also be enhanced by polymer deposition masking the sidewall, which is not subjected to ion bombardment, and thus passivating it against chemical attack. However excess deposition of material, either inorganic[96-97] or organic[98-99] can lead to problems of inconsistent etch rate and poor pattern transfer. On the other

hand as the films are pin-hole free, in some cases controlled film build up can be used to advantage for sealing of devices, planarization, or insulating purposes as for example as capacitor dielectrics. Organic deposition processes are more fully discussed in Section 1.7.

1.5)Effects of Ion Bombardment.

In capacitively coupled systems, both the driven electrode, grounded and floating surfaces are subject to ion bombardment[100-105]. This effect, together with the relative concentrations of species such as F and $(CF_2)_n$ present in halocarbon plasmas, account for major phenomena such as:

1.Ion enhanced polymerization:

$(CF_2)_n + X^{+/-} \longrightarrow (CF_{2-x})_{n\ (s)}$.

2.Ion enhanced fluoridation:

$F_{(g)} + X^{+/-} \longrightarrow MF_{x\ (g)}$ Volatile fluoride.

$F_{(g)} + X^{+/-} \longrightarrow MF_{x\ (s)}$ Involatile fluoride.

3.Chemical sputtering of deposited material:

$(CF_{2-x})_n + F_{(g)} + X^{+/-} \longrightarrow C_nF_{2n+2}$

4.Physical sputtering:

$M,\ MF_{x\ (s)} \text{ -- } X^{+/-} \text{ --> }$ sputtered neutrals, secondary ions

where M is electrode material and $X^{+/-}$ is any active ion. Often it is observed that samples on the grounded electrode, subject to low energy

bombardment, may form polymeric material; while samples on the driven electrode, subject to energetic ion bombardment, may etch predominantly. This is illustrated later in Figure 5. as the two points at the same gas composition, but differing biases. The driven samples may also show a profile with an enhanced vertical etch rate over the horizontal -anisotropic etching.

There are several possible steps in the etching mechanism that could be proposed to explain anisotropy, due to the ion bombardment caused by the acceleration of charged particles across the dark space. This can cause an effect due to a combination of all or some of the following factors[106-107]. There is firstly chemical attack by incident ions by impact dissociation of reactant molecules and ions. There is the formation of surface and several monolayers deep damage and defects that can catalyse or enhance chemisorption or etching compared to an undamaged surface. There also may be the provision of some of the reaction energy required, by momentum transfer, for activation of processes at the surface, and also stimulated product desorption or removal of involatile residues and any polymer films formed. Thus material exposed to the bombardment will be removed and hence allow access to the substrate, (the polymer breakdown species may themselves take place in the attack), but material deposited on the sidewalls will protect the

substrate against attack. This mechanism of polymer sidewall passivation has a major application in allowing dry etching of deep vias in GaAs substrates[110]. Thus the etch rate normal to the surface is enhanced but not the lateral etching rate. This mechanism also gives an explanation for two observed effects, viz why samples mounted on the driven or smaller electrode show greater anisotropy (the voltage offset is greater here than for the grounded electrode); and why there is an increase as the pressure is lowered (the ion mean free path and subsequent energy increases). This was examined by **Coburn and Winters**[108-109], who studied the reactions of Si, SiO_2, SiC, and SiN_x with XeF_2, F_2, and Cl_2 and the enhancements in rate caused by energetic radiation, ions and electrons. It was found that the etch rate of a surface subjected to energetic ion bombardment in a simulated plasma etching system was greater than the sum of etch rates of chemical attack and physical sputtering.

1.6)The Role of O_2 or H_2 Additions.

The behaviour of the halocarbon gases used in plasma etching can often be related to the relative amounts of fluorine and carbon present in the molecules, the F : C ratio model[81,111-121]:

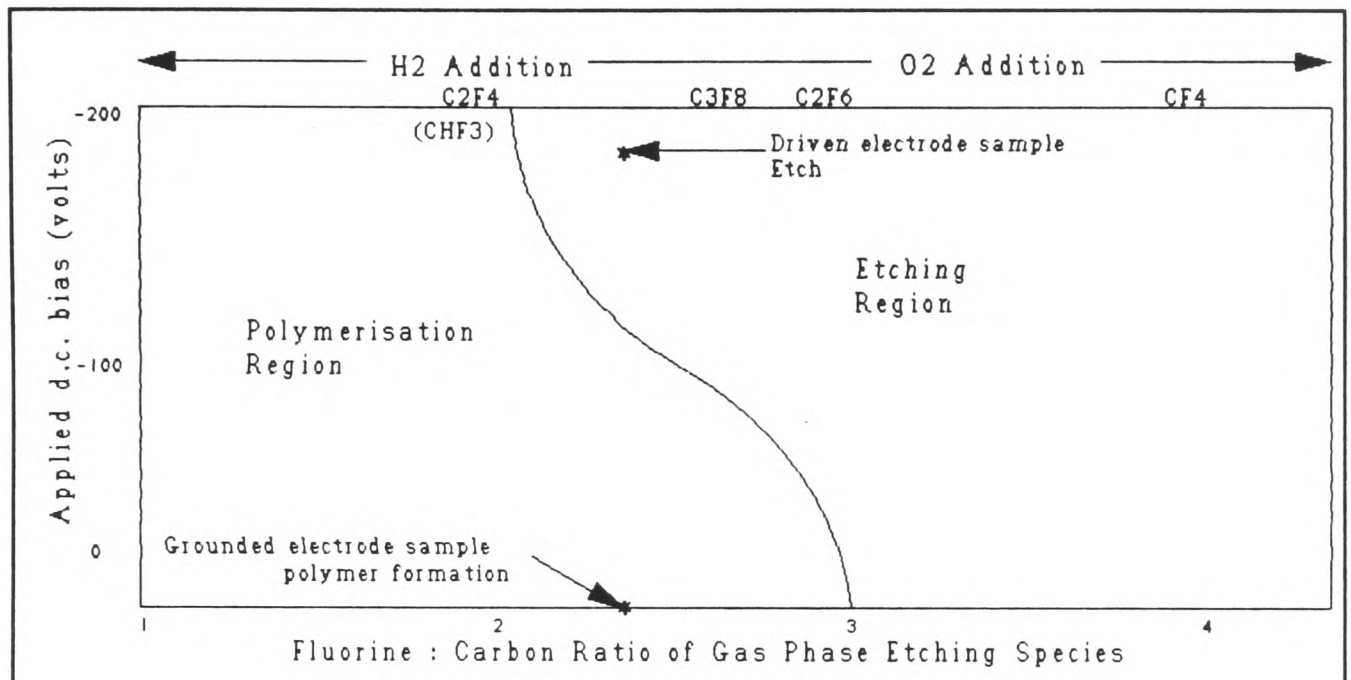

Figure 5.

Etch/Polymerisation Boundary Conditions.

This model does not account for specific mechanisms, but is used to predict the behaviour of fluorocarbon plasmas as conditions are changed. For example it has been found that the etch rate of silicon, and its selectivity to oxide can be markedly affected by the additions of O_2[122], or H_2[123], to fluorocarbon gas mixtures. The etch rate of SiO_2 under the same conditions is changed a great deal less.

1.6.1)Oxygen Additions.

Studies on Systems by Optical Spectroscopy.

Some of the earliest semiconductor orientated examinations of the emissions from a discharge was a study of photoresist stripping in an Oxygen discharge by **Degenkolb**, **Griffiths et al**[124-125], by monitoring electronically excited CO and OH in both the UV and visible regions of the spectrum.

The first comprehensive study was done by **Harshbarger et al**[126-128]. They studied the optical emission from CF_4/O_2 in a simple parallel plate system. The species monitored were atomic O and F, and molecular CO. They observed a large increase in the emission of F, when a small amount of O_2 was added to the fluorocarbon plasma, and an increase in the rate of etching of Si and SiN_x. The emission intensities of both F and O were found to be significantly lower when the plasma was actively etching these materials as well. This was used as an end-point monitor and as a diagnostic tool. **Flamm et al**[129], showed that though the F atom emission increases with the amount of added O_2, to about 20% O_2, the corresponding curve for the increase in etch rate of the Si substrate peaks earlier. This was shown by titration with Cl_2 not to be due simply to the concentration of fluorine, as measured by the

atomic emission of excited state F. This was proposed to be due to a competition between O and F for chemisorption onto the Si surface.

As the percentage of O_2 added to a fluorocarbon gas plasma is increased the Si etch rate increases, passes through a maximum at about 8% O_2, and then decreases. The corresponding SiO_2 etch rate increases less dramatically to a maximum at about 20% O_2. The F atom density in the plasma also increases as can be seen by the 703.7 emission intensity. This indicates that the function of oxygen is to remove carbon from both C_xF_y[122,130-133], and C_xCl_y[134-136] molecules in the gas phase; and also from species adsorbed on the Si surface. This increases the active fluorine concentration allowing for highly selective etching of Si over SiO_2 by:

* Reaction with the carbon on the surfaces liberating fluorine and also lessening the number of fluorine atoms that would be consumed by reaction with this adsorbed layer to form species such as C_2F_6. More of the silicon surface is also exposed.

* Reacting with CF_3, both on the surface and in the gas phase, to liberate more fluorine for etching:

$CF_{3(abs)} + O \rightarrow 3F_{(abs)} + CO$ Surface Reaction.

or

$CF_3 + O \rightarrow COF_2 + F \rightarrow CO + F_2$ Gas Phase.

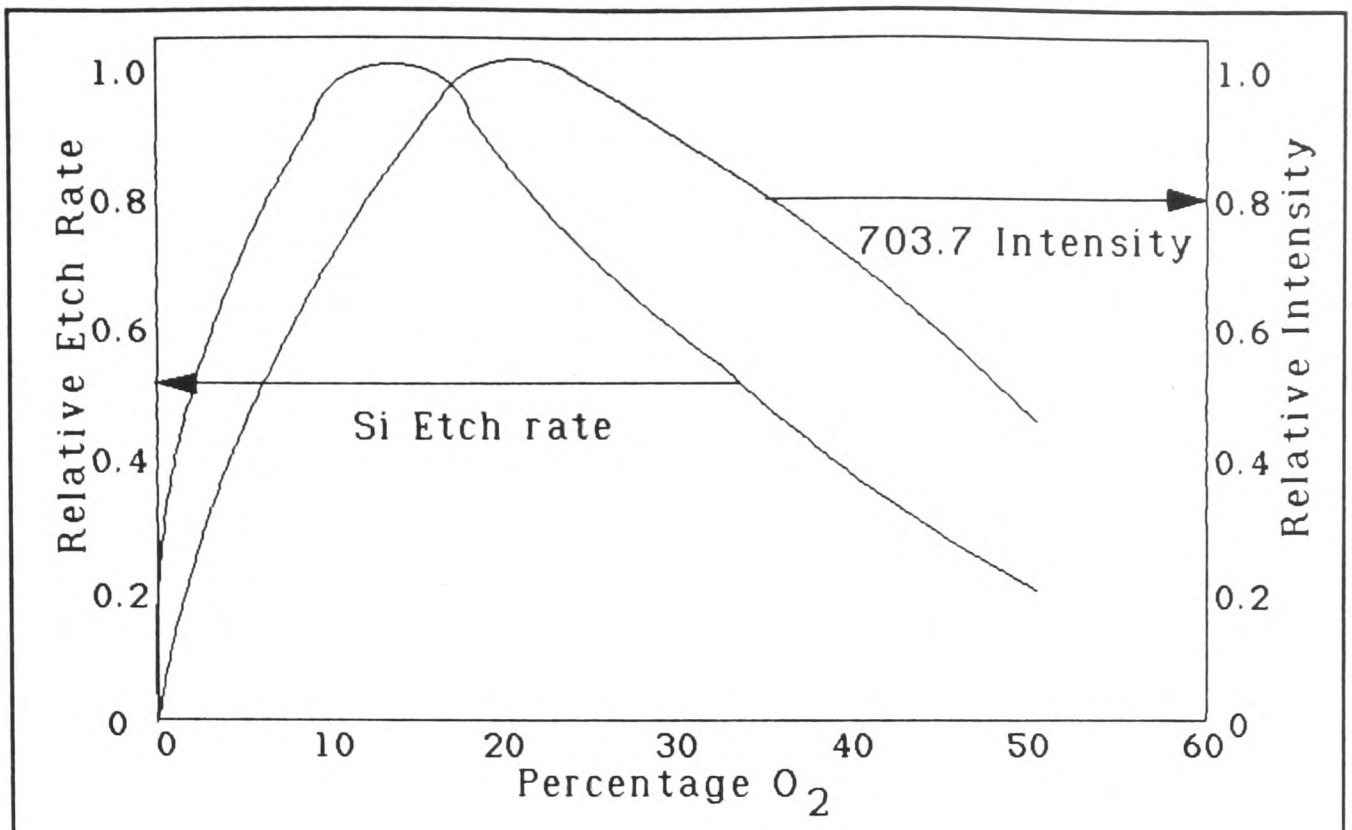

Figure 6.

Etch Rate vs. F (704nm) Emission.

When oxygen is added:

i) For small amounts, (to approx. 10% by volume).

CO, CO_2, COF_2 formed as effluent and more active etching agent, fluorine, is liberated as evidenced by the observed enhancement of 703.7nm F atom emission. There is probably no direct reaction between oxygen and CF_2[137], but rather by one of two routes:

$$2CF_2 \text{ ---M---> } C_2F_4, \text{ then}$$

$$C_2F_4 + O \text{ ---> } C_2F_4O \text{ ---}O_2 \text{ ---> } 2CF_2O + O$$

or $C_2F_4^* + O \text{ ---> } 2CF_2O.$

ii) Excess O_2 leads to chemisorption on surface -blocks fluorine attack ('SiO2' etching by F is slower). The etching gas is also ultimately diluted.

In terms of the F : C model the ratio is increased by addition of O_2, (or even CO_2 or N_2O) because more carbon than fluorine is consumed. Also the effect of the oxygen in the SiO_2 lattice is to locally increase the ratio thus allowing etching to proceed as though the incident plasma had a greater F : C value. Addition of fluorine to the discharge can also be predicted in terms of increasing the ratio, hence the etch rate of silicon is increased.

1.6.2)Hydrogen Additions.

Studies on Systems by Optical Spectroscopy.

D'Agostino et al[138-139] examined C_xF_y/H_2 systems to obtain information as to the likely decomposition channels for these gases in an R.F. discharge. From this they concluded that the most likely polymer forming species were CF and/or CF_2. For Si, at least, they proposed that the etching species present were fluorine atoms. This was extended further by **Millard and Kay**[140] who showed that there was a relationship between difluorocarbene emission and the rates of polymer deposition. They found that the spectra obtained

from inductive plasma discharges of fluorocarbon gases, including CF_4 and C_3F_8, had the emission from CF_2 for primarily polymer forming gases, and the emission from CF for the etching gases as one of the main features. Addition of H_2 to CF_4 reduced the fluorine atom emission and also increased the CF_2 emission. They saw the HF spectrum as well provided there was greater than 8% H_2 in the discharge. In a parallel plate reactor they found that there was a linear relationship between the emission from CF_2 and the rate of polymer formation as a function of changing power or flow rates.

As the percentage of H_2 in a fluorocarbon plasma is increased, the etch rate of Si and photoresists is monotonically decreased, reaching almost zero at about 40% H_2. There is however little effect on the SiO_2 rate except at very high H_2 concentrations when there is a dilution effect. The addition of hydrogen or hydrogen containing molecules to the feed gas of the plasma suppresses the F atom concentration by scavenging to form HF and there is an increase in the deposition rates of polymeric material. However even H_2 plasmas themselves can be used to etch Si, SiO_2 and III/V semiconductors such as GaAs, but probably the mechanism has a high sputtering component as well as hydride formation.

The combination of the Si and SiO_2 rate changes gives a reversal in selectivity allowing SiO_2 to be

selectively etched over Si. This effect is also seen when fluorohydrocarbon plasmas such as CHF_3 are used, or the F atom concentration is reduced by the presence of large areas of F consuming materials including the substrate, (the loading effect). Overall the difference between Si and SiO_2 etching is the presence of the oxygen in the SiO_2 lattice, which is liberated as the reaction proceeds. This can react with the carbonaceous layer that is forming on the surfaces during the reaction from dissociation of CF_3 or other fluorocarbon radicals upon being chemisorbed to form volatiles such as CO CO_2. Thus in the case of SiO_2 etching, added O_2, or H_2 has little effect, however with an excessive rate of film formation all etching will eventually cease.

In order to achieve a high selectivity for the etching of Si rather than SiO_2 the Si etch rate must be made to exceed the SiO_2 by a reasonable factor. One way this can be achieved is by increasing the active fluorine concentration. Methods to achieve this include adding O_2 to fluorocarbon plasmas or the use of inorganic fluorides such as SF_6, NF_3 or XeF_2. To reverse the selectivity when etching through an oxide layer to underlying silicon for a contact hole for example, free fluorine must be suppressed and the larger fluorocarbon fragments such as CF_3 and CF_2 increased. Either H_2 can be added or the gases with lower C:F ratios employed such as C_3F_8 or CHF_3. The exact process conditions

are found to be highly reactor dependent as the system must be operated very close to the polymerisation/etching borderline for maximum selectivity.

Again the F : C ratio model predicts that increase in substrate area or addition of H_2 will consume F atoms without affecting any carbon thus reducing the etch rate of silicon. Similarly the use of gases such as CHF_3 or C_3F_8 will have similar effects.

1.6.3)<u>The Role of Other Gas Additions.</u>

When gases other than O_2 or H_2 are added to fluorocarbon plasmas[357,498-502] their effects can be divided into either their influence on the physics of the discharge, affecting the electron energy/distribution; or may themselves take place in the chemistry. In the first case they may be electron donating species, electron acceptors or possibly simply as dilutants; in the second they could have an influence on the kinetics and mechanisms of any polymer formation.

1.7)Fundamentals of Plasma Deposition.

1.7.1)Deposition of Inorganic Materials.

Interest in low temperature deposition processes for the semiconductor industry[20,150-152] is focussed on three main areas:

1. Semiconductors for use as solar cells, photoreceptors, or thin film transistors. Some examples are PECVD of aSi:H at 220^{o}C, and MOCVD of GaAs.

2. Deposition of insulating films for interlayer dielectrics or passivation purposes: encapsulants for planarization or hermetic sealing using SiO_2, SiC, SiO_xN_y, or even organo-silicon polymers. Plasma deposited SiN_x is frequently found as a dielectric, and phosphorosilicate glass (PSG) grown by simultaneous oxidation of silane and phosphine at low temperatures (350-500^{o}C) and with about 8%P by weight is a popular choice for a planarising or sealing layer. Organic polyimide films have been tried for this purpose[153], but so far plasma deposited organic polymers[57] have not found widespread use.

3. Metallisations using metals, alloys or silicides.

The advantage of glow discharge process is that sufficient energy is supplied for the reaction at a relatively low substrate temperature, thus minimising thermal effects such as the diffusion of shallow junctions and the interdiffusion of metals. The problems of pin hole formation from dust generated by sputtering and LPCVD systems can also be minimised.

1.7.2)Polymer Films.

There is a growing interest in plasma polymerised materials due to their unique characteristics[154-156]. The basic types of layers that can be produced are General Organic Polymers, usually $C_xH_y(O,N)_z$ and related materials[157-165]; Fluoropolymers which are of particular interest to this study; and Metal containing Polymer films which consist of finely divided material in an inert dielectric matrix.

The wide differences between the formation and stability of hydrocarbons and fluorocarbons in a glow discharge can often be explained by consideration of the relevant bond energies such as C-F/C-H and H-H $(436)^X$, F-F $(157)^X$, H-F $(569)^X$; and the difference in stability as seen by the heat of formation of the two radicals CH_2 $(+423)^X$ and CF_2 $(-194)^X$. For more values see the section "5.3 Thermodynamic

^{X}kJ/mol

calculations". These values were used, particularly in conjunction with the data obtained from the gas breakdown studies in the mass spectrometer, to understand the polymer forming behaviour of the systems.

1.7.3)Fluoropolymers.

The use of plasma polymerised fluorocarbon monomers has developed to a large extent from firstly the work done with hydrocarbon materials (with the aims of producing more chemically and thermally stable polymers); and secondly from their formation as a by-product of high selectivity gas mixtures used for etching. The latter has led to attention being concentrated on their cause and ways to control their formation while using low F:C ratio etching gases or mixtures[166-169] used to enhance or reverse the selectivity of Si to SiO_2 during etching. As already stated, polymer formation which can ultimately stop the etching is favoured by factors such as low F : C fluorocarbon plasmas, low ion energies and D.C. bias voltages, and low pressures. Excess polymer formation on the walls of the reactor, as well as on the substrate, can cause problems with the absorption of contaminants which are subsequently released. They can also degrade at later stages in a multistep sequence in the same

chamber, which could release fluorine as an undesirable etching agent during, for example, an O_2 based dry resist strip.

1.7.4)Metal Containing Polymer Films.

Interest in metal containing fluoropolymer films has arisen for two main reasons[170-192]. Firstly to extend the scope and usefulness of the fluoropolymers because of their novel electrical, magnetic and optical characteristics; and secondly as a means of studying the behaviour of the metal clusters either as isolated or interacting species in a dielectric matrix. Conversely the modification of the physical properties of the matrix as a function of the incorporation of the clusters can be studied. There are five main routes to these materials:

1. The evaporation in vacuum of separate metal and polymer sources[170].

2. Cosputtering from a composite or separate targets[171].

3. Plasma polymerisation of organometallics[172].

4. Evaporation of metal in a system where plasma polymerisation is taking place[173-174].

5. Sputtering of metal from an electrode in a system where simultaneous plasma etching and polymerisation is taking place[175-192].

The last method is of most relevance to the present work and has also been the most widely studied as a method of examining electrode processes during plasma etching[180]. The bulk of the studies have been done by **Kay and coworkers at IBM**. with Co, Ge, Mo, and W driven electrode materials[181-188], with mainly C_3F_8 or C_3F_8/Ar as the fluorocarbon monomer. Other electrode materials used include Au[188-189], Al[190-191], and Co/Al[192]. Of the different processes proposed for the transport of the electrode material the most likely are physical sputtering of the parent metal[188-189], sputtering of involatile fluorides such as CuF, CuF_2, and CoF_2, or by chemical reaction followed by loss of volatile fluoride e.g. MoF_6, which then incorporates into the growing polymer film.

1.8)Purpose of the Present Work.

The production of Si devices is a complex and expensive process. The yield of usable die from a wafer can be very low, and thus it is essential to understand the processes that take place during plasma etching to achieve improvements in at least one area of device fabrication. In this study an apparatus was designed and constructed to investigate the conditions under which polymer deposition occurs during etching of systems consisting of a layer of metal, oxide or photoresist on a silicon substrate, in a range of fluorocarbon gas plasmas.

Optical emission spectroscopy was used to measure excited species in situ, this technique having previously been shown to be very useful in identifying important gas phase species. The rate of polymer film formation or etching was monitored by the use of a quartz crystal microbalance. Mass spectrometry was also attempted. In addition, the deposits themselves were subjected to a range of characterisation techniques. The most useful were X-ray Photoelectron Spectroscopy and Auger Electron Spectroscopy, Rutherford Backscattering Spectroscopy, Elastic Recoil Detection Analysis, Thermogravimetric Analysis, and Infrared Spectroscopy.

From this work, some of the polymer deposition characteristics of these fluorocarbon discharges have been further rationalised. The usefulness of reliable ways of end-point monitoring[193-195] methods were also borne in mind. Current methods include; optical techniques such as fluorescence[196-197], observing changes in atomic or molecular emission[198-203] as a function of time, e.g. F atom[199], mass spectrometry[200-206], laser interferometry[207-212] and other techniques[213-216].

Chapter 2 details the design and construction of the apparatus used for this work, followed by preparative work on the samples and electrodes. In the following chapter analytical techniques used to investigate firstly the surfaces of the samples and the electrodes, and then the bulk properties of the materials are discussed. The data obtained by the various techniques is then assessed, followed by a discussion of the results obtained from (i) pure fluorocarbon and (ii) fluorocarbon/hydrogen mixtures.

The appendices also describe some subsidiary work done with a controlled atmosphere scanning electron microscope, some studies of cracking patterns of fluorocarbon gases in a mass spectrometer, and finally some thermodynamic values.

2)EXPERIMENTAL.

This section deals with all the basic experimental work in constructing the apparatus and sample preparation.

2.1)Design and Construction of Plasma Rig.

At the commencement of this work there was no suitable facility available at Harwell for conducting experiments on fundamental aspects of plasma etching/deposition. Considerable time was therefore devoted to the design and construction of a suitable rig. This section deals with the evolution of the current hardware and the present state of the apparatus, a photograph of which is included in photographs in the Appendix.

2.1.1)Support Frame.

Square-section tubing was supplied for the initial framework. This was soon replaced by a base frame 75cm square by 180cm in height constructed from 1" Kee Klamps units and 1" galvanised pipe. This enabled changes and additions in equipment to be readily accommodated. Some sections of pipe were subsequently replaced by synthetic laminate insulating rod so as to break any continuous loops

of metal that could act as resonant aerial lengths. With large amounts of Radio Frequency Interference found to be present, a lot of effort was put into reducing its effects. This led finally to the adoption of a star earthing system, where all electrical units are only earthed by one common point. This is explained in more detail in "2.4.1 R.F. interference problems". The main copper earth block of the star earthing system was mounted on the top aluminium plate on a high voltage insulator. A cable was taken this block to the main building earth and thence to a local substation. This gave less than 3 ohms resistance to earth.

The bottom aluminium plate provided a base for the vertical reactor assemblies plate and the horizontal reactor system. The latter was itself built into a smaller frame, also made out of insulated rod. This second framework also carried the R.F. power matching unit. The 13.56MHz R.F. power from the cathode end of the matching unit coil was fed directly to the electrode via a cable which was as straight and short as possible to minimise inductive losses. On the underside of the lower aluminium plate was bolted the main diffusion pump, as was the R.F. head electronics for the quadrupole mass spectrometer. This was mounted on a small insulated plate below the main bottom plate.

Attached to the lower part of the frame but electrically isolated from it; were the mass flow meters, valves and mixing chamber for the gas flow system (see Figure 12).

A side rail supported the weight of the magnetic isolation valve and main valve D, which was connected by a short flexible pipe to the baffle chamber, which smoothed the pump flow and trap any particulate matter which might otherwise damage the main pump. A flexible length of pipe connected the pumping system to the reaction chamber and along with anti-vibration mounts on the base of the rotary pump prevented movement being transmitted to the main framework and thence to the reaction chamber and sample. Any vibration here was found to affect the quartz crystal microbalance.

The frame can be enclosed on all four sides, if necessary by wire mesh to make a Faraday cage as a further measure to reduce Radio Frequency interference. These screens and the frame itself were earthed by means of copper straps as was the pump system.

A lathe bed was modified to support the optical spectrometer and the associated quartz focussing lens and focal point translation mirror. The horizontal travel of the lathe bed and the x,y,z mirror mount allowed the spectrometer to view different regions of the discharge- radial for

barrel systems, or linear for parallel plate (see Figure 18). All the associated electronics for the spectrometer system were mounted on and earthed to the lathe bed which was in turn earthed directly to the copper earth block.

2.1.2)Vacuum System.

Current requirements of the semiconductor industry are for vacuum systems with pumps and fluids that are proof against many corrosive materials[219-222]. Both reactant gases such as O_2,H_2, AsH_3, and PH_3; and by-product gases such as SiF_4, HF, and HCl have to be safely pumped without allowing them to reach explosive or toxic concentrations. With this in mind, considerable care was taken in the design of the pumping system for this apparatus[223-225].

For nearly all of the experimental work the main pump for the rig was a single stage Edwards mechanical rotary pump, model ISC 450B, with a swept volume of 33.3 lhr^{-1} and an ultimate vacuum (hydrocarbon oil) of 5mT. This pump was modified by thorough degreasing and the adjustment of tolerances on rebuilding, to run on Montedison Y-25G Fomblin oil. Fomblin fluids are fluorinated polyethers, often described as a 'liquid PTFE', with general formulae $CF_3O\ (C_3F_6O)_m\ (CF_2O)_n\ CF_3$, and the use of

this Fomblin oil was recommended as a means of avoiding pump and oil degradation[226]. The oils are chemically inert below 300°C, to the species found in plasma effluents, e.g. halogens, halogenated compounds, oxygen and acids. The pump was at all times gas-ballasted with, for example N_2[227], since the Fomblin oil has a greater tendency to absorb gas than hydrocarbon oils.

With the roughing pump running, typically at about 50°C, an ultimate vacuum of 25mT was obtained. Though by no means 'high vacuum' this limit was sufficient for the processes for which the system was designed. Common operating pressures for commercial Planar Etch and Deposition reactors are about 200-1000mT; and Reactive Ion Etch systems are operated at pressures between 2mT-100mT. It was noticeable that the rather high vapour pressure of the oil leads to significant losses when the system was running at high gas throughputs and gas ballast, so an outlet mist filter was fitted later to recover the fluid that was exhausted, particularly during pumpdown. It could be seen that an emulsion was also formed with water vapour. Though degradation of the oil itself was not found, occasional filtering and drying was required since acid residues were visible floating on the liquid surface. The pump must be run continuously or exposed internal metal surfaces would readily corrode as the oil is non-wetting. Particulate matter accumulated also, despite the

trap, which ultimately caused scoring of the pump chamber leading to an irreversible loss of pump efficiency. Subsequent analysis by Infrared showed that the particulate matter strained out of the oil was composed mainly of a mixture of metal fluorides from attack of the pump surfaces and $(O\text{-}Si\text{-}O)_n$ polymeric material. Adequate exhausting of fumes was required because there is production of free fluorine when the reactor was run, and also if the Fomblin oil temperature exceeds 300^{o}C. Other species generated in the effluent can include COF_2, HF and SiF_4 -all highly toxic[228].

An alternative was the use of a standard hydrocarbon oil[229]. It has the disadvantage that it degrades slowly under the corrosive running conditions but is comparatively cheap to renew and produces a better vacuum overall. Since the oil is wetting it protects the pump if it stops for any reason, the Fomblin oil is better at preventing damage to the pump when actually running -probably due to the fact that the aqueous based effluents and Lewis acids do not dissolve in the oil.

Major problems with reproducibility in commercial systems are known to be qualitatively caused by the chamber being exposed to atmospheric water and contaminants when the reactor is loaded and unloaded, so in the present system unwanted contaminants were minimised. The system was brought

up to atmospheric pressure with high purity Argon. Argon was used instead of N_2 so that a leak could be readily detected by the initial colour of the plasma. After roughing, the chamber was hard pumped with the help of an additional air cooled 150 $lmin^{-1}$ nitrogen cold trapped oil diffusion pump type EO2, filled with $75cm^3$ of Dow Corning 740 oil after each sample change. A 50 watt oxygen plasma was then run for 15 minutes, before running as a plasma etch/deposition system. This however was seen to cause sputtering of electrode material in a few cases.

The system could be set up in three different ways, the roughing pump being run continuously (see Figure 7).

i) Standby
Overnight.
Valves **B,C,D** open; **A** closed
Diffusion pump heater off.
Longer periods.
Valves **A,D** open; **B,C** closed
Diffusion pump heater off.
Ultimate chamber pressure 25mT.

ii) Pre-run
Valves **B,C,D** open; **A** closed
Diffusion pump heater on.
Ultimate chamber pressure < 10^{-5} Torr.

iii) Run (or roughing pump down.)
Valves **A,D** open; **B,C** closed
Diffusion pump heater off.

The operating chamber pressure could be from 1mT to near atmospheric, but was typically in the region of 200-500mT. At present the combined use of input gas flow control and valve **A** as a throttling valve

sets the pressure in the reactor chamber, but a combined mass flow control system and throttling valve would have been the next logical step to have taken[230].

Other points to note are that the diffusion pump cannot, except at very low flow rates, cope with the required gas volumes due to the long pumping line. On the other hand contamination of the system by backstreaming of the Fomblin oil was found to be a problem, but CF_3^+ was observed in the mass spectrum of the empty chamber. At some stage either a foreline trap or a rootes blower should be fitted.

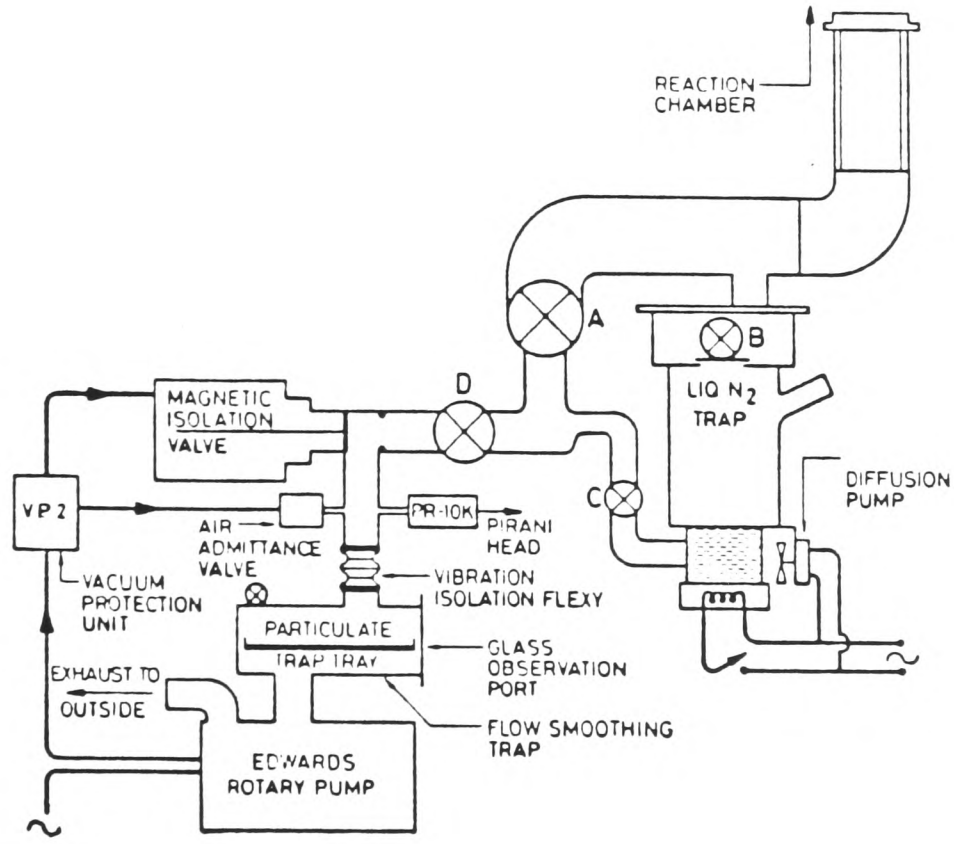

Figure 7.

Pump System Layout.

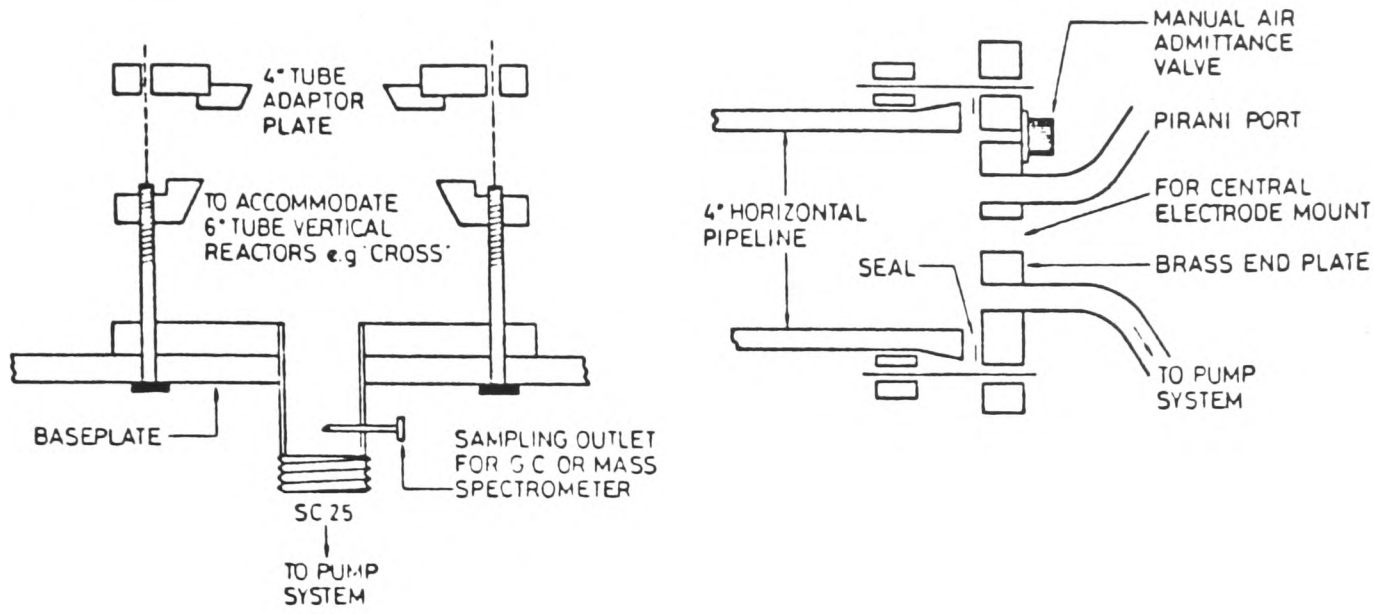

Figure 8.

System Mounting Layout.

2.1.3)Reactors.

There were two types of reaction chambers considered, the present cylindrical system and a more complex glass 'cross' with commercial electrodes.

2.1.3.1)Pipeline Systems.

Based around standard lengths of 4" pipeline, similar to commercial barrel reactors in principle, a gas inlet and an offset spectral observation port was made in a brass end plate. Because of the risk of contamination this was later changed for a

stainless steel plate which was directly clamped to the end of the tube. This plate was fitted with a central gas inlet, spectral observation port, an insulated contact for the driven electrode and two welded Swagelock fittings for the cooling water feed and return for the ground electrode. At the other end a second plate had connections for a vacuum outlet, manual air-admittance valve, Pirani port and a fitting for a central electrode, as shown in Figure 8. The Pirani head has been replaced by a capacitance manometer gauge, as detailed in "2.2 Pressure measurement".

Side ports of smaller bore pipeline were fitted onto the main glass tube to accommodate ancillaries such as the mass spectrometer for which a 300mm length of 40mm bore pipe was inserted at right angles to the tube axis.

R.F. power was initially supplied to the system via inductive coupling so that the optical spectra of the halocarbon plasmas could be examined with minimal electrode effects. To confine the plasma more and to obtain conditions similar to commercial systems the present capacitively coupled electrode system was designed and installed.

2.1.3.2)Glass 'Cross' System.

This system, though built, was not used because the glass pipeline systems were found to be ideal for all the experimental work as a parallel plate etching system. It is currently set up as a Reactive Ion Etcher, with 4" diameter electrodes, using the baseplate illustrated in Figure 8(a).

Figure 9. Layout of Etching Chamber.

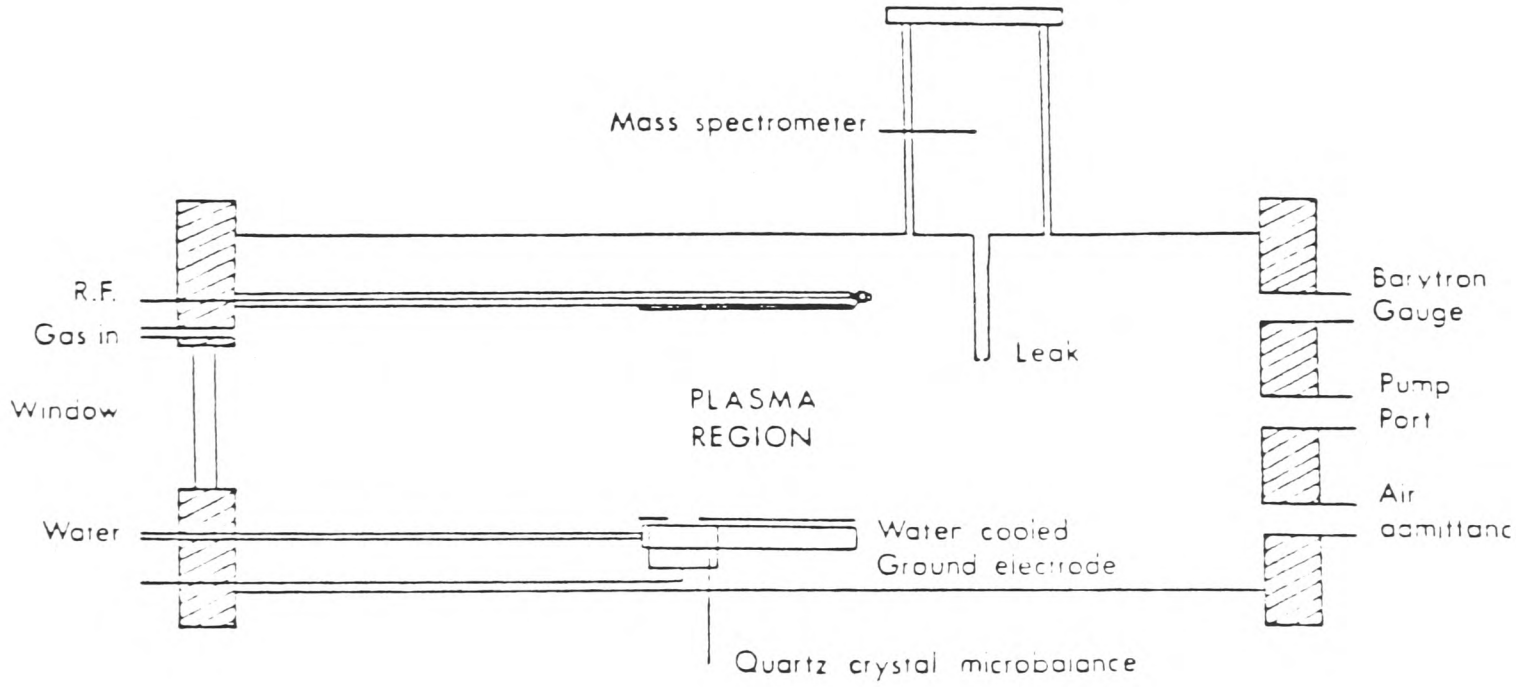

2.1.4)Electrode Assemblies.

Both inductively and capacitively coupled systems were used in this study, the initial spectroscopic measurements being made with the inductive system and most of the etching and deposition work being done with a capacitively coupled electrode assembly.

2.1.4.1)Inductive Electrodes.

The driving electrode was a water cooled copper coil. This was used either coiled around the outside of the pyrex pipeline, or remotely mounted close to the apparatus with power tapped off from the coil to a separate stainless steel mesh wrapped around the reactor[231-232].

Two types of central electrode assemblies were utilised. The first had a fixed central electrode made of copper tube, Figure 10(a), thermally isolated by a short length of poorly conducting cryogenic stainless steel tube. Knowing the mass (241.3g), the plasma power at the electrode could be measured by the rate of heating with time as measured by a thermocouple inserted in to the copper. This setup was also used as a support for tubular samples. It was attached to the end-plate, but electrically isolated from it by a glass sleeve, and thus could be earthed, floated to near the

plasma potential or held at a fixed potential. The second, Figure 10(b), allowed the electrode to be detached from the end plate and was designed for the purpose of monitoring potential electrode material behaviour. Two major designs were used, firstly various metallic electrodes for corrosion and deposition studies, and secondly substrate holders for etching work on the Si/SiO_2 system made from e.g. PTFE, SiO_2. These also contained single wire Langmuir probes for measurements of the electrical characteristics of the plasmas as well as thermocouples. Again the electrodes were electrically isolated from the grounded end plate by a glass sleeve. Both plates had installed in them pressure measuring and pumping ports. The apparatus was used in this configuration to study both the spectroscopy of the fluorocarbon plasmas without the influence of samples and electrodes, and as a 'barrel' etching system to study isotropic processes such as photoresist degradation. Some erosion of the glass tube was noticed so the discharges were never completely free of substrate effects.

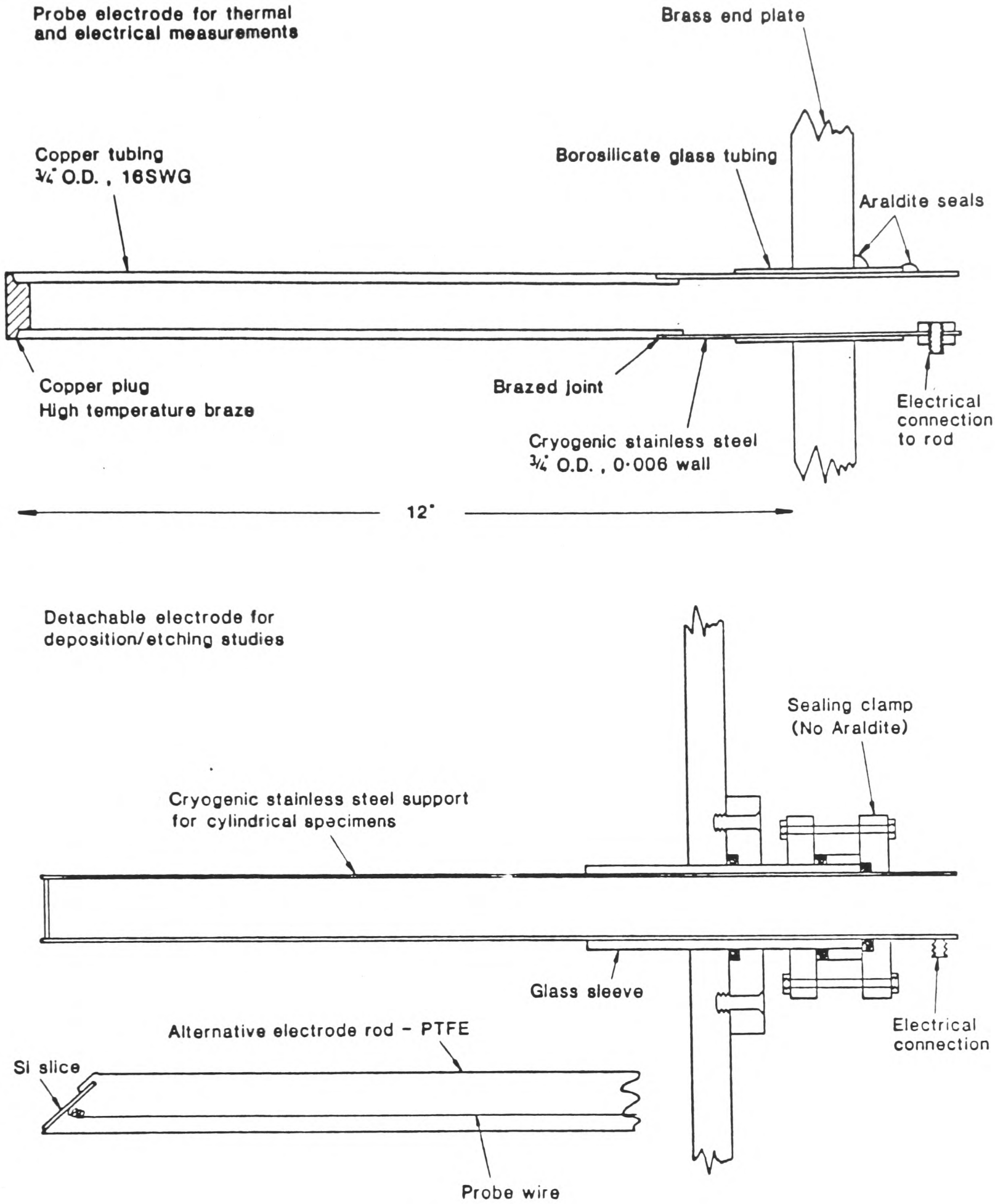

Figure 10.

Inductive Electrode Assemblies.

2.1.4.2)Capactively Coupled Electrodes.

A characteristic of this type of system is that the voltage offset[233], caused by the differences in mobilities of the ions and electrons, gives positive ion bombardment of the driven electrode. This can lead to sputtering of potentially catalytically active material which can cause polymer formation either in the gas phase or on the substrate surface. Typical values of elemental sputtering rates are given in Table 2.

Target	Argon ion energy.			
	100eV	200eV	300eV	600eV
Al	0.11	0.35	0.65	1.2
Si	0.07	0.18	0.31	0.5
Ti	0.081	0.22	0.33	0.6
V	0.11	0.31	0.41	
Cr	0.30	0.67	0.87	
Fe	0.20	0.53	0.76	
Co	0.15	0.57	0.81	
Ni	0.28	0.66	0.95	1.5
Cu	0.48	1.10	1.57	
Ge	0.22	0.50	0.74	
Mo	0.13	0.40	0.58	0.9
Ta	0.10	0.28	0.41	0.6
W	0.068	0.29	0.40	0.6
Yield in atoms per incident ion[234]				

Table 2.
Sputter rates for bombardment by Ar^+.

The reason for the choice of titanium for some current etchers, despite the volatility of the fluoride, can be seen in terms of the low sputtering rate for this material. Sputtering of impurity elements present in the parent material, especially true for Group 1 metals[236], can have long term

effects on device characteristics as the slow diffusion of the ions can lead to a time-delayed device failure. They form deep level traps and affect minority carrier lifetimes and junction leakage currents. It was found in the present system that with most electrode materials a fine residue was left on the surface of the etched sample due to micromasking effects of sputtered electrode material except in the case of Ti and Carbon and could normally be seen in the SEM. It should be borne in mind that all surfaces in the reactor can also serve as recombination sites for reactive species produced in the discharge.

For most of the etching and deposition experiments, the top driven electrode was constructed from a metal sheet with a tab to couple to the power feed. After considerable evolution the design shown in Figure 11. was used as it proved to be very reliable. This is a coaxial arrangement with a 3mm stainless steel conductor inside an earthed length of 6mm stainless-steel tube packed with ceramic beads which act as spacers and high voltage insulators. This arrangement also helped reduce the unshielded length of R.F. conductor. Ideally this electrode should be watercooled, as incorporation of a thermotropic strip indicated that the temperature during the fluorocarbon plasmas was in excess of 260^{o}C. The consequences of this high temperature with respect to the type of polymer formed are

discussed in section "4.1.3.1 electrode effect". The electrode plate was backed by a recrystallised alumina insulating plate and another stainless steel plate of the same dimensions which was earthed. The bottom electrode plate was mounted by means of colloidial graphite on a grounded stainless steel block which had a channel machined in it for cooling water. This block had a large hole drilled through it at one end to house the Quartz Crystal Microbalance.

The two electrode plates, 5cm x 5cm, gave an overall power density at 40W of 1.6W cm^{-2} and they were also separated by a 5cm gap.

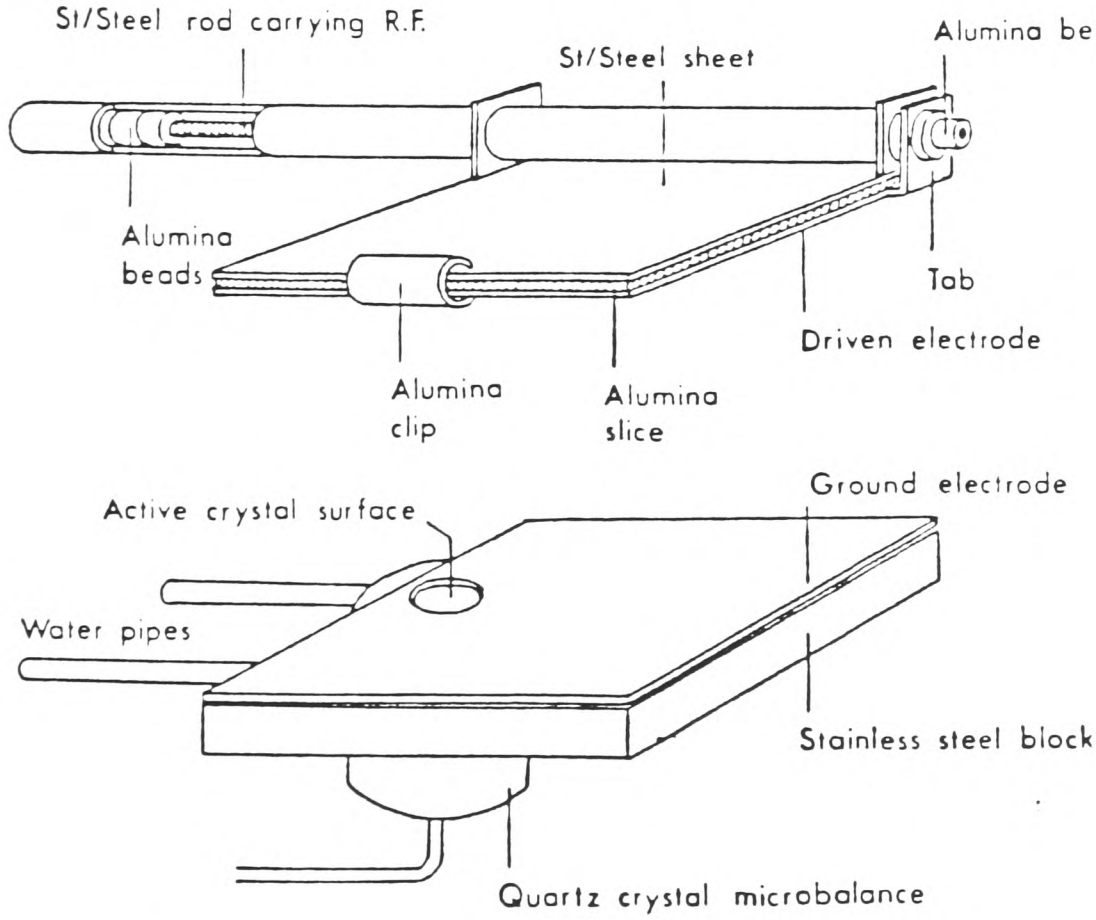

Figure 11.

Capacitively Coupled Electrode Assembly.

2.2)Pressure Measurement.

The vacuum pressure of the system was measured by three PR-10K Pirani heads connected to an Edwards model 101 controller. The first was just above the roughing pump particulate trap, the second was above the diffusion pump baffle valve and the third connected directly to an end plate of the chamber coupled to the pump. Despite filters in the power supplies the readings when the system was running were not accurate due to the R.F. fields. The pressure readings were subject to correction, even when the power was not applied, because they were calibrated for systems where the thermal properties of the gas were the same as air. Slow degradation of the heads was found due to the hollow cathode effect formed inside the gauge -despite an earthed mesh across the orifice; which enhanced the reaction of fluorine with the tungsten filaments, leading to their eventual breakage. Therefore a capacitance manometer pressure measuring system was obtained to replace the Pirani head connected to the chamber. This consisted of two metal diaphragms forming a capacitor whose spacing changes as a result of pressure changes on the vacuum system side of the diaphragm. This change in capacitance is measured and related to the system pressure[237]. The unit was coupled to a three gas mass flow controller on the input to allow control of pressure in the system

by changing the total flow but maintaining a constant ratio, to improve reproducibility. A further refinement would be a throttle valve fitted below the etching chamber and interfaced with the present pressure/mass flow controller.

It should be noted that these systems have a potential for end point monitoring, as there can be a change in total system pressure indicative of a change in 'chemistry' as a film is etched through to a substrate. In this system this was done by observing if there were any changes in total gas flow as the controller readjusted to maintain the set point pressure, the pumping speed being kept nominally constant.

2.3)Gases and Flow Controls.

The tubular reactor system was initially commissioned on high purity Argon gas, since there was on site experience with Argon plasmas at Harwell. A 5psi feed from a standard regulator was fed to the rig through a leak valve to obtain the characteristic blue argon colour due to the visible atomic lines. This helped to check for leaks and contamination problems, and to set up the original spectrometer.

After trying various systems, most work on the pure gases was done with a Brookes model 5841 dual channel mass flow controller, allowing reproducible mixtures of two gases to be established. The first check was to calibrate the unit using a bubble flowmeter. The set up was used to mix a halocarbon gas- CF_4, C_2F_6, C_3F_8, or CHF_3 with either O_2 or H_2, inert gases, when used, being mixed in from an Edwards leak valve. All of this was finally replaced by a MKS 254 three gas controller that can be programmed to flow at set rates, or ratio the gases at a set chamber pressure. It has in fact proved very difficult to set up the flow-controller so as to control the pressure by varying the flow rates in proportion to each other. This is due to the distance between the pressure measuring point in the chamber, and the flow valves, which is constrained by R.F.I. and other design considerations. Two lines are connected to halocarbon gases, and the third to either the oxygen or hydrogen cylinders via appropriate regulators. An interlock was used so both H_2 and O_2 could not be run simultaneously for safety reasons. Maximum flows for the halocarbon gases were 20cc min^{-1} except for C_3F_8 (15cc min^{-1}). This was due to the large differences in specific heat capacity of the gases compared to the standard; N_2 = 1.0, for which the mass flow controllers were calibrated. Though there was a facility for dialling in a gas

correction factor on the control unit for all the gases used, there was still found to be a systematic error of 12% for CF_4, C_2F_6, CHF_3 and 17% for C_3F_8. Thus all the results presented are for actual (corrected) gas flows. A schematic of the gas flow system is shown in Figure 12.

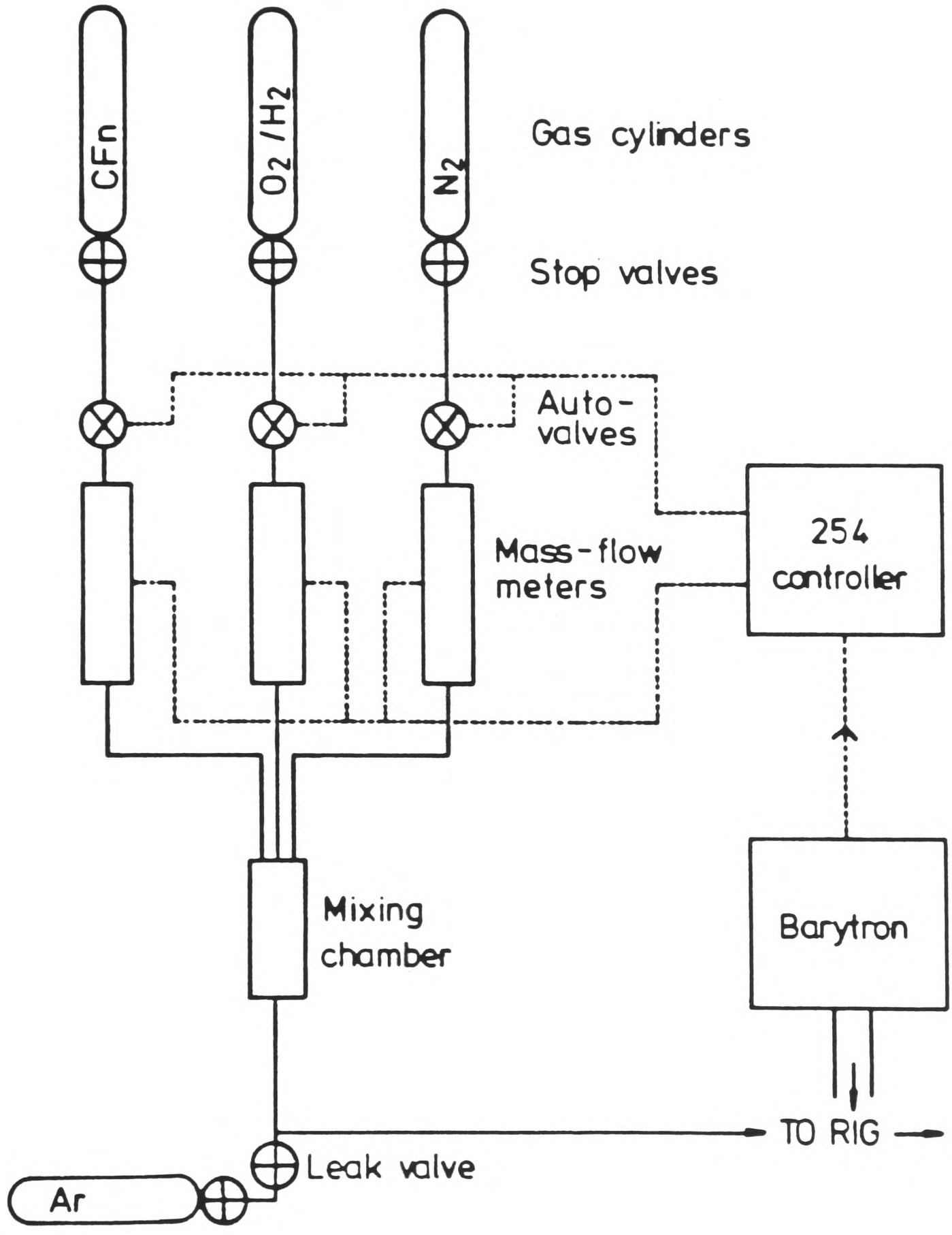

Figure 12.

Gas Flow System.

Among the factors to be considered were the changes in reagent concentrations[238], possible by combinations of pressures and residence times from control of gas input rates and pump exhaust speeds[239-243]. Work was also started on the roles of different carrier gases, since this can have a major effect on the plasma characteristics and hence etching and polymerization behaviour. Additions such as He, Ne, Ar, Xe and SF_6 and other electron sinks have been used, but not chlorine containing gases as the mass flow controllers have not been adapted to pass these corrosive gases.

2.4)R.F. Generators.

The most used source of radio frequency was a HFS-500E 13.56MHz generator with a maximum output of 500W, manufactured by Plasma-Therm Inc. This source is widely used for commercial sputtering, plasma etching, welding and spraying[244].

An alternative source was a nominally 2MHz Radyne generator for investigating frequency dependent effects[259-266].

The HFS-500E is a crystal controlled oscillator in a Colpitts circuit driving a buffer which in turn drives the R.F. power amplifier. A block diagram of the generator is given in Figure 13., and of the matching unit, after modification of the component

values, in Figure 14. The output of the generator was into a 50 ohm quarter wavelength coaxial cable which was fed into a MRC matching unit, as a source/load tuner. The function of the matching unit is to match the output impedance of the generator (50 ohms) into the load impedance (plasma), and to ensure the applied voltage and current are in phase at the load. The matching unit output in turn was then taken directly to the driven electrode by as short a cable as possible to minimise power losses. This arrangement allowed the load to be matched to the generator- i.e. tuned for minimum reflected power (max VSWR). With the planar electrode assembly the bias voltage meter fitted to the cathode plate in the matching unit indicated due to the self rectifying nature of the plasma (the r.f. diode effect)[245-253]. The current system has the lower electrode earthed and the other coupled to the R.F. generator through the matching unit which has an incorporated blocking capacitor. With the system being run unbalanced, with the lower plate earthy, it was found that the plasma became more stable and easier to tune than with the barrel system. The peak to peak a.c. voltage at the driven electrode, as measured by means of an oscilloscope and high voltage probe, was in the region of 1000V, offset by about -20/50V d.c. dependent on the conditions used.

No measurements were made with the incorporated Langmuir probes due to experimental difficulties[254-258].

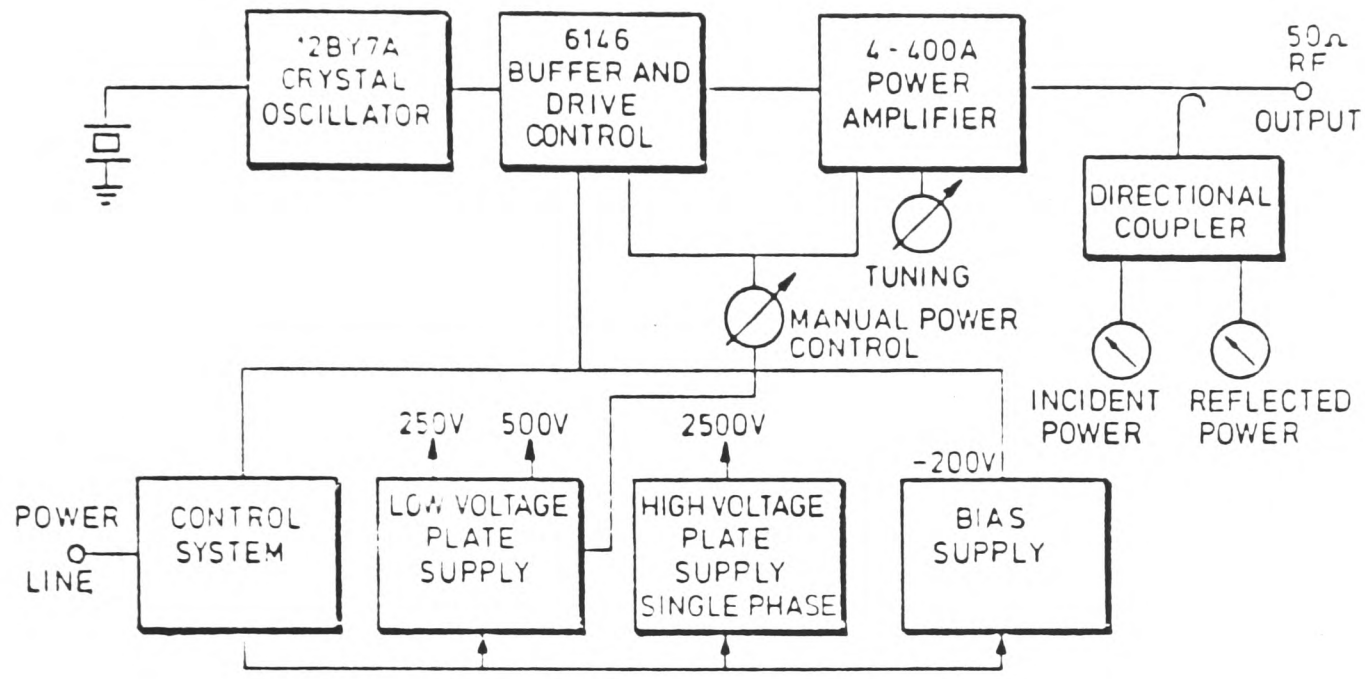

Figure 13.

Diagram of R.F. Supply Unit.

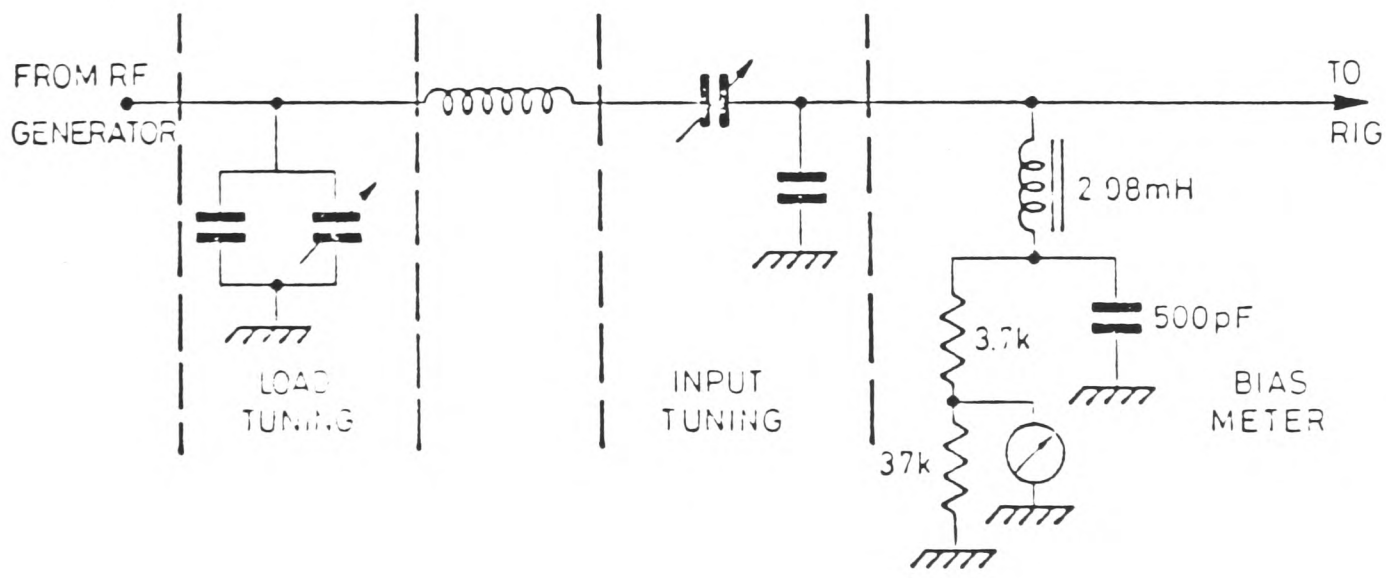

Figure 14.

Circuit of Current Matching Unit.

2.4.1)R.F. Interference Problems.

The R.F. generator was the source of considerable interference in the low level electronics of the ancillary equipment, particularly the quadrupole mass spectrometer, quartz crystal microbalance, and gas flow controllers.

In the case of the quartz crystal microbalance for example, no readings could be taken while R.F. power was applied to the system. Leaving the head amplifier connected to the crystal, even though disconnected from the control electronics eventually led to the breakdown of all the enclosed amplifier circuitry due to stray fields.

Problems with R.F. interference are well known in plasma and glow discharge systems in general. As examples, logic circuits are easily affected by capacitance effects and spurious pulses; this affects stepper motors, computing equipment and A/D converters. The offset voltages affect sensitive analogue circuits such as pico-ammeters used with photomultiplier tubes, and obvious in this particular system was charge build-up especially on the quartz crystal microbalance sensor crystal. There are also body capacity/aerial effects which affect the reproducibility of measurements.

The National Radiological Protection Board was asked to assess the possible hazards associated with the 13.56 MHz Gas Plasma equipment built, and after measurements of the R.F. fields present they produced several more recommendations from an operator safety point of view. It was found that the equipment generated fields which exceeded the limits for continuous exposure that have been adopted or proposed by other countries (but these standards and codes of practice all assume whole body exposure at an appreciable distance from the R.F. source). The high field strengths they found with this equipment were only observed very close to the equipment localised at particular points such as the R.F. power feed-through into the vacuum chamber.

As a result of this a few simple measures were implemented. The R.F. generator was turned through 90^{o} so that its back face was presented to the adjacent wall to allow the R.F. 50 ohm output lead to be routed well above head height. The various monitoring instruments were mounted on the back wall between the generator and the plasma system to restrict access. The intense field close to the generator cabinet was reduced by bridging the ventilation gaps using perforated metal screens and the same effective ventilation area was maintained by adjusting the spacing between the generator modules.

To reduce the problem further, several additional measures were implemented. As already stated in "2.1.1 Support frame", the inner frame, its supporting rods and main frame were partially replaced by non-metallic rods to break aerial loops and the grounding connections have been, as far as possible, separated to eliminate earth loops. Separate mains supplies, via voltage stabilisers, were used to power the thickness monitor and optical spectrometer as one system; the generator as another, and the main rack of electronics containing the pressure measuring and gas flow systems together with the mass spectrometer as the third. The stabilisers here provide two main functions, firstly they smooth the mains feed and minimise returned ripple, and they also cope with fluctuations in mains power caused by nearby furnaces.

Though these measures have helped to virtually eliminate R.F.I., further ideas were in the process of being implemented. These included an all metal screened main assembly with good earth bonding, and an exclusive return path for the main R.F. generator output current with a balanced R.F. feeder. Separate screening of the reactor inner frame was utilised to confine the primary R.F. field., as was screening and lead-through decoupling of all input and output connections to the low level electronics.

2.5)Quartz Crystal Microbalance.

It was necessary in this programme to have a method of measuring the accumulation or removal of deposits{267}. This was accomplished by incorporating a quartz crystal microbalance{268-270} into the ground electrode block, as illustrated in Figure 11. Initially a Nanotech unit was fitted using 5MHz silver coated quartz crystals to measure dynamic weight changes. This proved very unreliable and was replaced by an Intellemetrics IL002 film thickness monitor. This has a 6MHz crystal and is based on digital not analogue electronics around a 8748 microprocessor, with similarities to a Z-80 based thickness monitor reported in the literature{271}.

The basic sensing unit for the balance was a quartz crystal oscillator. The crystal itself was a plano-convex plate approximately 14mm in diameter and 0.25mm thick. It is excited into thickness shear vibrations by the external local oscillator unit at a frequency of about 6MHz. The exact frequency of oscillation is determined by the mass of material which may have been deposited on the exposed part of the crystal surface. As the deposit builds up so the rate of oscillation slows down and hence the difference in frequency between the crystal and a standard frequency source can be used to calculate the mass of material deposited on the crystal

surface. A plano-convex crystal was used since this shape induces most of the oscillation to occur in the central exposed region. This increases the sensitivity of the crystal to deposited material and allows the crystal to be firmly clamped at the rim, so increasing the effectiveness of the water cooling from the steel block surrounding the head. If the crystal temperature is allowed to vary, a temperature effect term must also be included{272}, especially for AT cut crystals.

In practice measurements of changes in frequency of the crystal while the discharge was running suffered from two main of problems. Firstly there was the unequal charge build up on the faces of the crystal, causing it to twist and thus imposing a severe mechanical restraint on its oscillation (it can even cause the crystal to break); and secondly there was Radio frequency Interference from the plasma causing spurious frequencies in the local oscillator.

The possibility of fitting a crystal head that can operate when the R.F. power was present in the system was being investigated. The best alternatives seem to be either the use of an opto-isolator between the head electronics and the control unit or the use of an efficient R.F. filter system to allow the approximately 6MHz signal but not the 13.56MHz signal to pass.

Previous studies.

Sauerbrey was the first to propose the use of a quartz crystal resonator to monitor the deposition of thin films[273-274]. He made the assumption that the deposited film would have the same effect as an equivalent deposited mass of quartz represented thus:

$$T_f = \frac{(N_q P_q)}{(P_f f^2)} \cdot (f_q - f)$$

T_f - Film thickness (cm).

N_q - Frequency constant for crystal.

P_q - Density of quartz (g cm^3).

f - Frequency of loaded crystal (Hz).

P_f - Density of film (g cm^3).

f_q - Frequency of unloaded crystal (Hz).

Often it is adequate to assume that $(1/f^2) = (1/f_q^2)$ then T_f is proportional to (f_q-f), but for thicker deposits it should be noted that the film thickness is not exactly proportional to the change in frequency because the crystal frequency enters into the proportionality constant and because of penetration of the acoustic wave into the surface film[275]. Provided that very heavy depositions were not made however, the linear approximation is adequate. In practice the proportionality constant is made for each material and sensor crystal location empirically, but if an approximate calculation is adequate then:

$$N_q = 1.67 \times 10^{-5} \text{ Hz cm.}$$

$$P_q = 2.20 \text{ g cm}^3.$$

$$f^2 = 3.6 \times 10^{13} \text{ Hz.}$$

Quartz crystal microbalances are in frequent use for measuring deposition rates of materials such as optical coatings, and in sputtering systems. They were used by **Coburn and Winters** in Si/SiO_2 etching studies as very sensitive probes to the build-up of even monolayers on surfaces[277]. They have proved also very useful in measuring the effect of ion beams of, for example, CF_3^+ impinging on Si and SiO_2 surfaces. It was found, when using 500eV CF_3^+ ions, with a clean Si surface deposited on the balance, that there was a decrease in etch rate with increasing dosage. 1900eV ions, on the other hand showed etch rates that were proportional to dosage. The decrease in etch rate at the lower ion energy was due to the build-up of a carbon layer on the surface which they observed simultaneously by AES. At the higher ion energy this coverage was only partial, and there was little impedance to the Si etch rate. Subsequent measurements with Ar^+ ion bombardment indicated that most of this etch rate observed could be accounted for by physical sputtering by the incident CF_3+ ions, with little chemical assistance. For SiO_2 surfaces total coverage by the carbon containing film could not be achieved with the same dosages as those used for Si. This led to the postulate that the oxygen in the

lattice of the oxidised silicon effectively limits the carbon film build-up, and can be used as an explanation for Si/SiO_2 selectivity in etching that is often observed in potentially polymer forming gas mixtures. Hence this supports the F : C model and indicates that the removal of carbonaceous material as well as silicon etch products needs to be considered in fluorocarbon plasmas. A later study was also carried out using microbalance techniques to examine the effect of changes in bias energy and frequency.

Experimental.

The holder for the quartz crystal was machined to fit flush into the water cooled ground electrode by machining, and was sputtered with 200Å of gold to minimise contamination of the plasma and to improve the electrical contact with the crystals fitted. A hole was then made in the ground electrode plates the same size as the exposed crystal area so that, as far as possible, only the crystal surface was exposed to the plasma.

In order to measure the rate of build up of material on the inert gold surface, the power was turned off every fifteen minutes and a reading taken. Despite not knowing densities accurately, attempts were made to relate frequency change displayed in Hertz to the actual thicknesses of

deposited material. Preliminary results indicated a polymer density of approximately 2, and 0.5 Hz change in frequency representing about 1Å thickness of deposit. This however may be an underestimation as the tooling factors can vary for each crystal head. The results are thus presented only in relation to each other and not as absolute thicknesses. Realizing the limitations of the gold surface, it was hoped that a variety of surfaces exposed to the plasma could have been tried, to investigate the rate of polymer deposition on, or removal of material from various potential electrode materials, see "2.7 Preparation of samples". A starting point would be materials such as Si, SiO_2, Al, and Ti, which could have been sputtered over a partially masked crystal surface. An attempt was made to expose part of the crystal silica to see if it was possible to use the crystal material itself, but the crystal would not then oscillate. It was however possible to recover the crystal by recoating the whole surface with sputtered gold.

2.6)Spectrometers.

2.6.1)Spectrometer -Optical.

It was decided to measure the optical emissions from the discharge during both etching and polymer

forming plasmas so as to obtain an insight into the excited species present in the gas phase. A glass window was therefore fitted onto the end plate of the system to allow the plasma to be viewed by an optical spectrometer. This was later replaced with a quartz disc obtained from the end of an old hollow cathode lamp, because of the greater range of quartz (200-420nm) compared with pyrex glass (330-420nm).

Optical emission spectroscopy is widely used for process monitoring and end point detection as it is relatively simple to implement. Spectra are recorded for plasmas that contain and do not contain the material that is desired to be etched and the spectral lines that show the greatest differences are monitored. At the end point there will be a change in emission intensity which can be used as a signal to terminate the process. Both reactant and product species can be used. This technique suffers from disadvantages in that it is an averaging technique over a whole batch and also if the areas that are being etched are small, the change in signal may also be difficult to detect. Relevant species so far monitored in plasma etching/deposition studies are shown in table 3.

To overcome problems such as the build up of polymer on the quartz window, slight variations in applied power and system pressure, all spectra were normalized to a mercury impurity line.

Emitter.	Wavelengths(nm).
CF CF_2 CF_3 CF_4	200-220,220-290 260-350 180-300,450-750 630,1283
CN #CO* CO*	387.1 297.7,483.5,519.8,230-271,283.3 114-280,412-612,266-383
H HF $F F F_2	656.3,486.1,434.0,410.2 486.8,435.1 748.2,731.1,730.9,703.7,690.2 685.6,656.9,651.7,529.1 651.7
N N_2	674,493.5,444.7,410.9,409.9 280-500
O O OH* O_2	845, 777.2, 615.8, 533.1 436.8, 394.7 308.9 777.7
Si Si SiF SiF_3* SiF_4	390.6, 288.2, 252.9, 252.4 251.6, 250.7 424-485, 777 max-630 FWHM=260nm 1031
General references{278-288}; End-point monitoring; # -Resist stripping, $ -Si etch processes.	

Table 3.
Species of prime interest -Optical.

Excited species are most commonly formed by the route:

(i) Collisions with usually secondary electrons

Parent molecule/atom ----e^-----> mostly ions.

(ii) Then collisions mainly with heavy ions, e.g.

CF_2(singlet) ---ions---> CF_2*---> CF_2 + hv, or by non-ionising inelastic collisions with electrons.

2.6.1.1)CF_n Emissions.

A comprehensive study of the literature had to be made to be able to identify some of the many lines that appeared on the measured spectra. There is an extensive literature on the emissions of $\cdot CF$, $\cdot CF_2$ and $\cdot CF_3$, some of which is outlined below[289]:

CF emissions. The two main systems for CF are both in the UV[290-296]. An examination has also been made of matrix isolated material[297].

CF_2 emissions. The spectrum of CF_2 consists of a large number of narrow red degraded bands[298-316]. The half life for CF_2 has been estimated to be of the order of 1 sec, with the loss mechanism being by slow dimerisation to form $C_2F_4^*$ and subsequent collisional stabilisation; or else by wall collision processes. This has been examined further by measurements of rates for dimerisation[317]. This study also found the rates of reaction of CF_2 with olefins and O_2 to be very slow. This is important when compared to the very fast rates for the less stable CH_2. Values measured for the quenching of CF_2^* emission from the $^1B1$ state are:

Quencher	Rate	
H_2	5.6×10^{9}	#
O_2	4.1×10^{11}	#
N_2	4.8×10^{12}	ß
Ne	3.3×10^{12}	ß
CF_2Br_2	2.4×10^{14}	ß

Values in units of $dm^3\ mol^{-1}\ s^{-1}$
ß Values in units of $cm^3\ mol^{-1}\ s^{-1}$

Table 4.
Quenching rates for CF_2[318-323].

The infrared and microwave spectra are also known[324-325].

CF_3 emissions. A study was undertaken into the spectrum and reactions of CF_3 by **Suto and Washida**[326]. An IR study has also been done[327].

2.6.1.2)SiF_n Emissions.

SiF emissions. There are seven major SiF systems in the region 660-250nm[328-335]. There is also one at 220-200nm found by **Dovell and Barrow**[336], and a system in the infrared. Systems below 200nm are also known.

System 660-250 nm.	Transition
alpha	$A^2sigma^+ - X^2pi$
beta	$B^2sigma^+ - X^2pi$
gamma	$C^2D - X^2pi$
epsilon(C')	$^2pi - A^2sigma^+$
epsilon(D')	$^2pi - A^2sigma^+$
zeta	Not known
eta	$a^4sigma- - X^2pi$

There was a delta band originally assigned but this is now said to be SiF_3.

Table 5.
SiF emissions.

SiF_2 emissions. For SiF_2 there is a series of regularly spaced bands 418-365nm{337-338}. Microwave studies of the rotation spectra have been done{339-340}. IR studies of SiF_2 generated at high temperatures and condensed on CsI windows at 20K, have shown that it exists probably as $(SiF_2)_2$. A polymeric material was given on warming{341}.

SiF_3 emissions. As already mentioned, these bands were originally assigned to SiF but by comparison with the spectra of matrix isolated species, they have been reassigned to SiF_3 {342-345}. This species can be used as an end-point monitor e.g.{346-347}.

SiF_4 bands have been observed also{348}.

SiClx emissions- Bands ascribed to SiCl have been measured in the region 283-276nm

Optical Emission Studies of Etching Plasmas.

This has already been discussed in Chapter 1. Some work has also been done on avoiding the problem of assuming the ground state concentration can be measured by use of the emission intensity of an excited state which is only valid if the radiative lifetime of the species being measured is very much less than the mean-free time between collisions. In this case the emission intensity may be taken as a direct measure of the number density of the emitting state. Care must be taken with transitions to any state that is relatively long-lived, in that as the

concentration of this species increases so the amount of radiation trapped will increase leading to a false impression of intensity. A way of avoiding this problem is to measure the ground state concentration using Laser Induced Fluorescence (LIF)[356-357]. Relevant species that have been measured include CHF, CF_2, and CFCl[358-367]. In actual plasma systems CF_2 has been measured[368].

Hardware.

The optical spectrometer first used was a Hilger-Watts medium prism spectrometer presenting 10" X 4" glass plates with a theoretical range of 200 - 900 nanometres. The radiation from the plasma passed through a quartz optical flat attached to the chamber end-plate and was focussed by a quartz lens onto the entrance slit of the spectrometer. However the emulsions used on the plates are only sensitive to certain regions of the spectrum, as can be seen in Figure 15. This spectrometer produced a plate as illustrated in Figure 61. The plates were then scanned on a microdensitometer, to provide relative values for the intensities. Sample traces can be seen in Figure 16 for a N_2 plasma; and Figure 17 for a CF_4 plasma. From this the actual intensities had to be deconvoluted by weighting with the plate sensitivity.

Initial trial experiments were carried out to test the vacuum system, R.F. power supply and the Hilger-Watts optical spectrometer. A series of experiments was done, initially with an inductively coupled system and later with parallel-plates made from hard anodised aluminium, to establish appropriate power levels, exposure times and apertures. The early results obtained with the SA1 photographic plates used in the optical spectrometer indicated that the required information was outside their sensitivity range. Better results were obtained with the 1-N plates but their supply was limited.

Figure 15.

Spectral Sensitivities of 10" x 4" Plates.

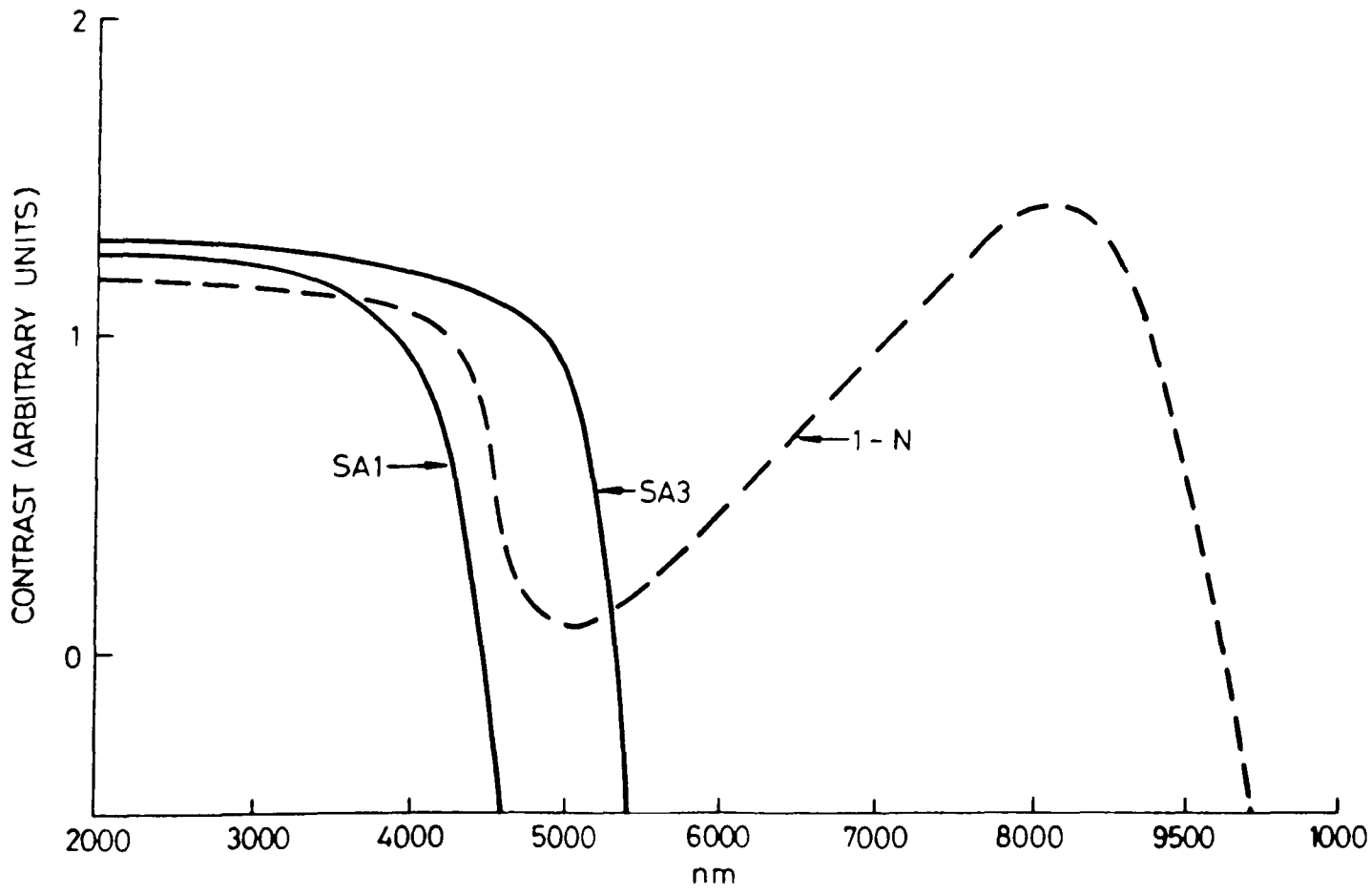

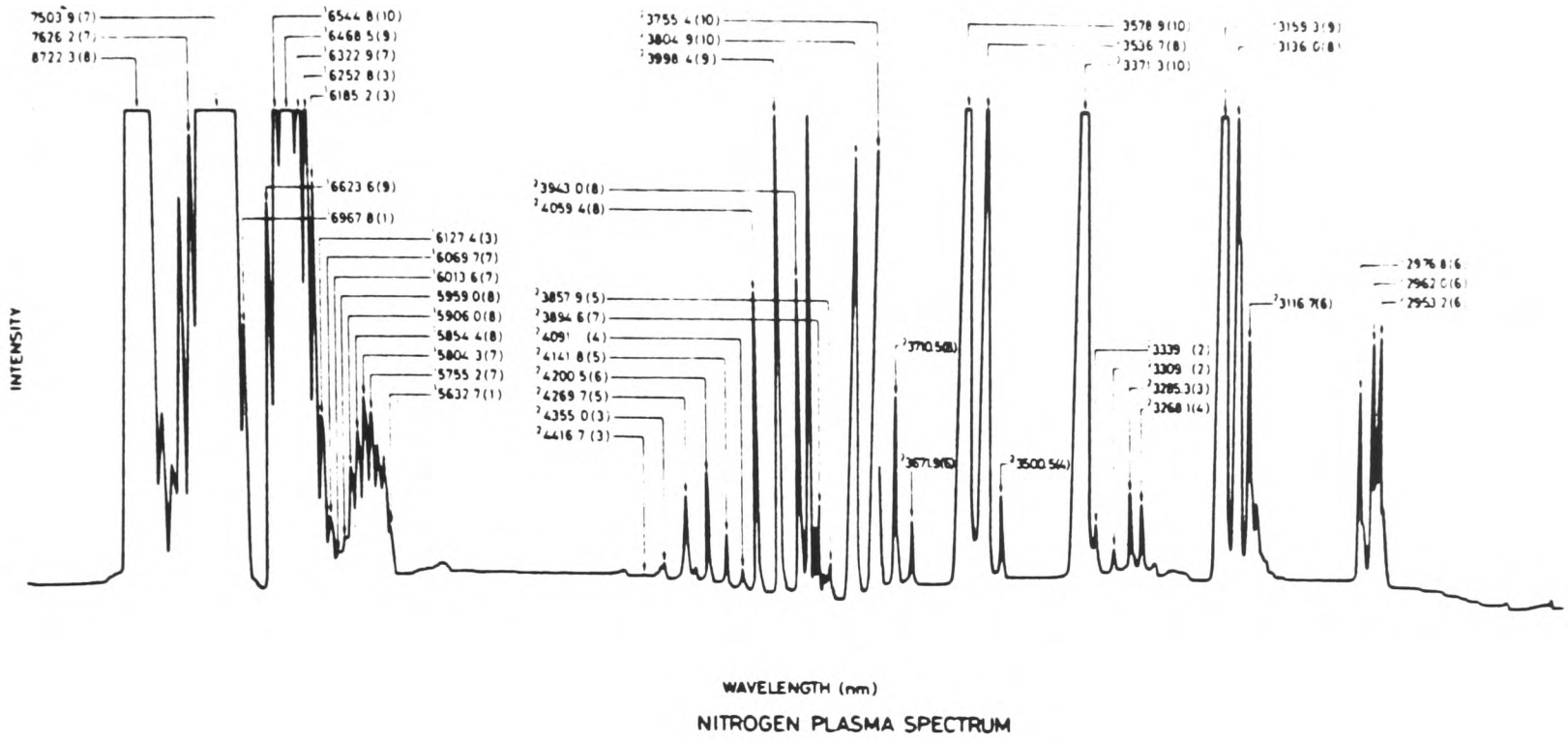

Figure 16.

Microdensitometer Derived Trace -N_2.

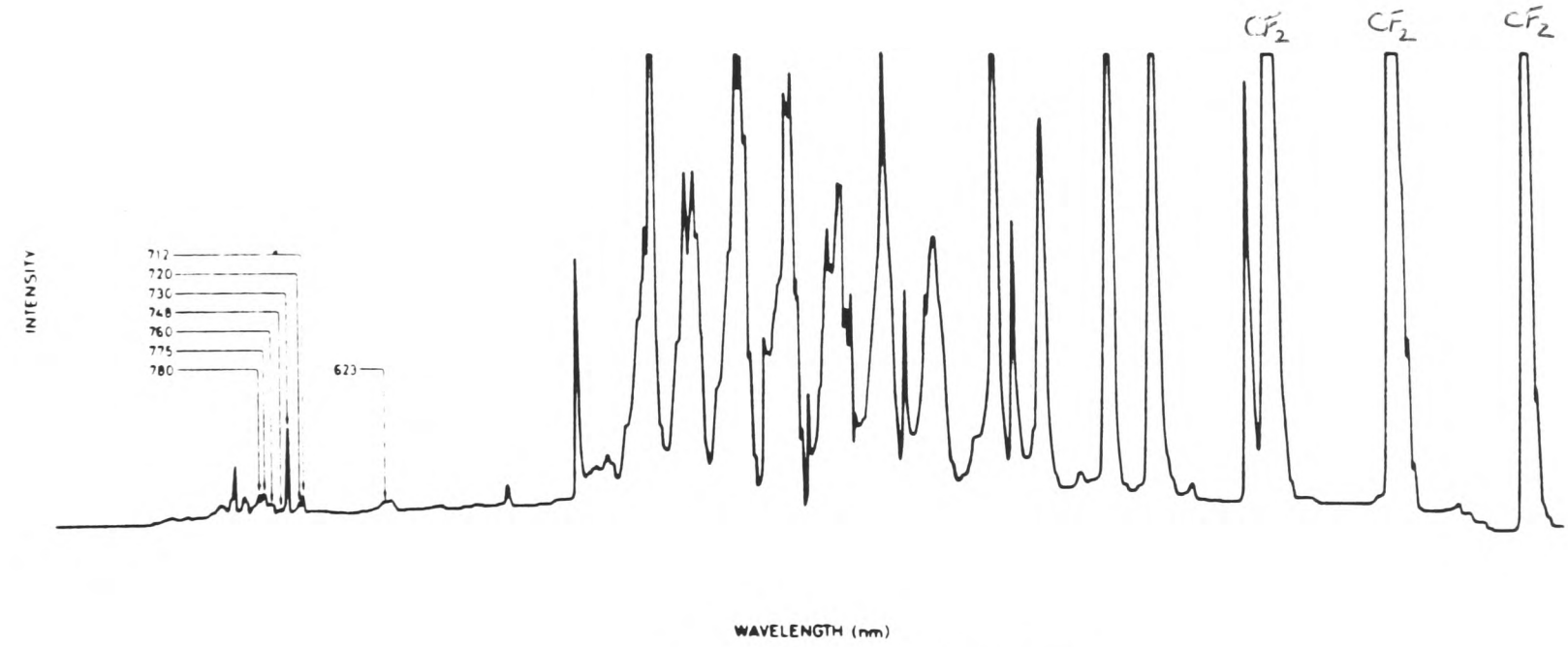

Figure 17.

Microdensitometer Derived Trace -CF_4.

CF emissions.

Emitter. CF	Wavelengths(nm). 220-290			A²D-X²H	
v' \ v"	0	1	2	3	4
0	232.79	239.99	247.84	255.33	263.56
1	223.83	230.47			

Double double-headed bands, violet degraded. P(1) heads.

Figure 30. CF 'A' emission.

CF2 emissions.

Emitter. CF2	Wavelength (nm). 260-350			1 (A)	
nm	I	nm	I	nm	I
321.41	6	286.61	6	267.55	6
319.75	4	285.25	6	265.24	6
305.37	5	279.98	8	262.85	9
303.81	5	277.42	5	259.50	9
302.28	5	276.12	5	255.06	8
292.13	6	274.91	8	251.86	9
289.35	7	271.13	9	248.78	9
		268.81	5	245.76	7
211.87	3	207.95	5	204.28	6
210.17	3	206.35	6	202.84	7
209.99	4	206.25	5	201.13	8
208.33	3	204.53	7	200.80	7

Narrow red degraded bands.

Figure 32. CF2 'A' emission.

The limited sensitivity, slow response time, and practical problems including availability, led to the plate spectrograph being replaced with a 0.5m Czerny-Turner scanning monochromator made by Spex Industries. This has a grating ruled with 1200 lines/mm giving a dispersion of 16 Å/mm and a blaze angle of 17°27" making the instrument most sensitive to the 400-500 nanometres region. This was chosen since initially it was expected to be used in the visible and near ultra-violet region of the spectrum. This work though has concentrated on the 200-300nm region. The detection system consists of a Hamamatsu photomultiplier tube with a spectral range of 185-900nm and a Spex radiometer. The output is recorded directly on a Farnell chart-recorder giving traces as in Figure 19, or by a microcomputer system with an Analogue to digital converter. The slit width used was 150 microns on both entrance and P.M. tube slits. This combined with a dispersion of 16Å mm^{-1} gives a resolution at half band pass of:

$$\text{Resolution} = \frac{150 + 150}{2} \times 16 = 2.4\text{Å}, (.24\text{nm})$$

Experimental.

During the runs the spectrometer was adjusted such that a point between the plates was focussed, by means of the mirror and lens system, onto the

spectrometer entrance slit. The region between 200-275nm was scanned, usually at a rate of 0.1 nm sec^{-1}.

For a few runs measurements were made of the intensity of 2238Å CF, and 2490Å CF_2 as a function of the distance from the electrode surface. Variations in intensity of the various species were shown that would have warranted further investigation. Other systems have used both moving electrode assemblies in front of a fixed spectrometer, and a movable quartz probe as a light guide.

Stepper motor driven mirror.

For the purpose of measuring the spatial distribution between the electrode plates, since both the plasma and spectrometer were effectively fixed, was by means of a tilting mirror driven by a stepper motor. The front aluminised mirror, originally supplied in a fixed holder, was attached to an adjustable mount. This allowed it to be rotated about two axes with a high degree of precision, by means of two micrometer screws acting on shallow wedges. The first permitted the mirror to be rotated about its horizontal axis by means of a stepper motor attached to the micrometer screw. This allowed the concentration of emitting species to be observed as a function of the distance from one electrode plate to the other. The other screw

adjusted the horizontal position of the focal point so as to allow regions both on and to the side of the sample to be viewed.

The micrometer screw, which has a pitch of 40 threads per inch, was coupled to the ten step stepping-motor via a 50:1 reduction gear. Each complete turn of the micrometer screw then corresponded to a horizontal movement of 25 thousandths of an inch. Calculation of the range of movement required to observe from one electrode to the other let to the smallest sensible increment of movement required to be one tenth of a turn, corresponding to 2.5 thou. horizontal movement. The overall range required was ten turns (0.25" horizontal movement. The stepping-motor was moved fifty steps at a time, corresponding to 2.5 thou. horizontal shaft movement. Safety microswitches were provided to detect forward and reverse overrun. The motor could be operated either manually or automatically in conjunction with an automatic data collection system linked to the radiometer. There was a search facility to enable setting any pre-determined mirror orientation to quickly move from one electrode to the other for example, or to go to either overrun limit.

The radiometer had a Binary Coded Decimal option installed to simplify computer controlled data collection. The BCD output was read by a port from

an Intel 8155 I/O chip connected to an 8085 microprocessor which also controlled the stepper-motor drive electronics. This worked by sending a TTL level pulse to the stepper-motor electronics which caused the motor to be driven to its next position. On arrival a pulse was sent back to the 8085 which caused a jump to an interrupt routine which read, converted then printed the radiometer current and relative mirror position. After a set interval a further movement pulse was sent.

Due to the involved nature of the design and hardware implementation, the system was shown to work successfully but no quantitative measurements were obtained.

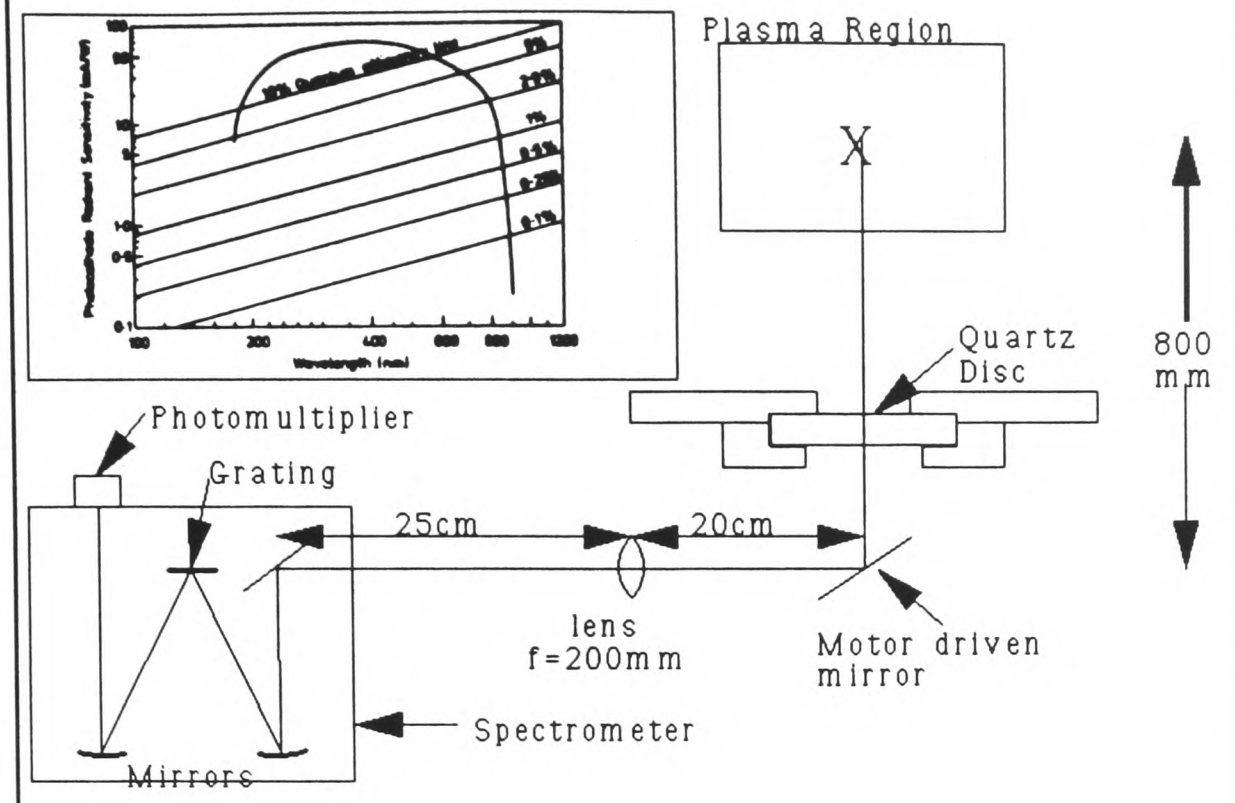

Figure 18.

Present Layout of Optical System.

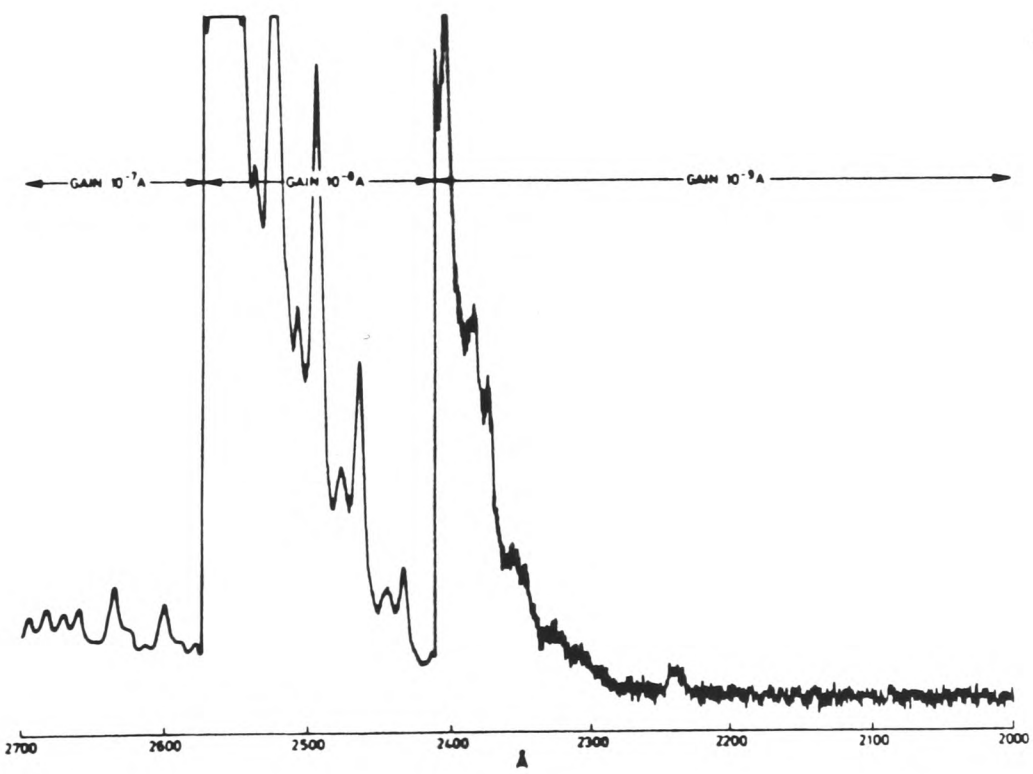

Figure 19.

Sample Spectrum 200 - 250 nm.

2.6.2)Spectrometer- Mass.

Previous studies.

Mass spectrometry is used, almost routinely, in plasma systems for process and end-point monitoring as well as real and virtual leak detection. For etching, particularly SiO_2 or SiN_x over Si, the most commonly monitored species is SiF_3^+[206-207,381-382]; with the equivalent in chlorine containing plasmas being $SiCl_x$ (x=1-3)[383-384]. Special care has to be taken with hydrogen containing species as H^o is formed on the tungsten filaments used in the mass-spectrometer head. This then causes impurity desorption from the wall materials leading to a high background[385].

Early studies concentrated on the elucidation of mechanisms occurring in DC discharges used for sputtering by investigating the types and energy ranges of particles present[386]. This was extended to uses in surface analysis and depth profiling[377-385]. For other related processes, plasma diagnostics have been used in tracing the reaction routes for CF_3Br etching plasmas[386], SF_6 etching of Si[387], and also for plasma polymerisation of hexamethyldisiloxane[388] and silane[389].

The most extensive study of polymerising and etching fluorocarbon glow discharges was undertaken by **Kay, Coburn and Kruppa**[390]. They investigated discharges in CF_4, C_2F_6, C_3F_8 and C_2F_4; and showed that there was a good correlation between the total concentration of the unsaturated species taken as ($C_2F_2^+$, $C_3F_4^+$, $C_3F_6^+$, $C_3F_3^+$, $C_4F_4^+$, $C_4F_5^+$, $C_4F_6^+$, $C_5F_3^+$, $C_5F_6^+$, $C_5F_5^+$) and deposition rate as measured with a quartz crystal microbalance. The overall C to F ratio of the total unsaturates was also close to that found for the polymer film. The effect of hydrogen additions was to cause greater production of unsaturates, but for CF_4 and C_2F_6 there was found to be a maximum in the deposition rate.

Hardware.

The mass spectrometer initially attached to the system was a Supervac quadropole mass spectrometer supplied by V.G. Gas Analysis Ltd. This was capable of detecting m/e from 1 to 100, but the presence of the R.F. field caused malfunctions in the head. While the instrument was being repaired it was decided to upgrade to a 1 to 200 m/e quadrupole with a remote R.F. head. This allows the observation of the higher polymer forming species. The mass spectrometer head is attached to a separate pumping system from the main rig, since differential pumping is required. This consisted of a LN_2 trap over an

Edwards E02 diffusion pump and a model 8 backing pump, to give a vacuum at the head of about 10^{-5} Torr., with the chamber at a pressure of 1 Torr. There are two ion pumps fitted along with a titanium sublimation pump but these cannot be used while gas is passing through the controlled leak in the mass-spectrometer head.

To operate the system the pressure is checked before switching on the quadrupole (so as to minimise the risk of damage to the mass-spectrometer filament), by an Edwards 1002 Penning gauge and an ion gauge. The filament material chosen was thoriated iridium which is less likely to burn out at the higher pressures required to be used. The ion energy ultimately used was set at 5eV, as a signal to noise compromise, but it is hoped to reduce this, at the higher pressures used and also due to the complications introduced by the breakdown of species inside the head itself; see "5.2 Gas breakdown studies by Mass Spectrometry" for some results. The main species noted in the literature as being likely to be identified are given in Table 6.

0 -------	30	60	90
H	CF	Cu	
H_2	O_2;CHF	C_2F_2	
	COF_2^{++}	C_2F_2H	C_3F_3
He	(CF_3^{++})	Cu	C_3F_3H
	Cl		
	HOF	SiF2++;COF_2	
	Cl		$AlCl_2$,CF_3CO
	F_2		
		CF_3	
10	40 Ar;H_2F_2	70	100 C_2F_4
	ArH	$^{13}CF_3$,CHF_3	C_2F_4H
C	(SiF_3^{++})		
	1.4xhcarb		
N	CO_2;SiO		SiF_4
			# TiF_3
CH_4;O		C_3F_2H	
HO;NH_3	SiF;COF		$C_4F_3H_2$
H_2O	CFOH	(D oil)	
F			
20	50 CF_2		110
HF;Ne;Ar	(D);CHF_2	80 Ar_2	
		C_2F_3	C_3F_4
$CO2^{++}$		C_2F_3H	
(SiF_4^{++})	ArN		
	(R)		
CF_2^{++}	Fe	SiF$_3$;COF$_3$	
C_2H_2	(R)	C_4F_2	C_5F_3
Al	$(CH_3)_2CO$	C_4F_2H	
Si;N_2;CO	Ni		C_2F_5

Higher masses: 124-C_4F_4; 131-C_3F_5; 143-C_4F_5; 150-C_3F_6; 155-C_5F_5; 162-C_4F_6; 169-C_3F_7; 181-C_4F_7;
Notes:
1.4x hcarb-Peak height gives oil contamination
Characteristic peak of
Rotary pump **(R)**, Diffusion **(D)**, oil.

Endpoint:
CO_2^+ -Photoresist stripping in O_2.
SiF_3^+ -Si,SiO_2,SiN_x etching in fluorocarbons.
TiF_3^+ -Ti etch in CF_4/O_2.
$AlCl_2^+$ -Al etch in BCl_3, CCl_4 etc.
Table 6. Species of interest (Mass spec).

None of the spectra or measurements made are reported due to the inconsistent results obtained once the equipment was finally made to produce some data. The main use was for residual gas analysis in

terms of the amount of mass 17/18 -water present in the system. This was found to have a major effect on the reproducibility as found by other workers.

2.7)Preparation of Samples.

2.7.1)Substrates.

There were basically two types of substrates to be prepared:

1. The quartz crystals for the microbalance
2. The various types of silicon/silica wafers.

1. The quartz crystals originally supplied were 5MHz AT cut quartz crystals with a thin coating of silver on each surface. The electrical properties of the Ag quickly degraded so a 200Å layer of gold was sputtered over both surfaces. The same procedure was adopted for the 6MHz crystals which, though supplied gold coated, tended to degrade after a while. After this treatment the edges were scraped clean to prevent tracking from one contact face to the other. Some experiments were attempted with Si and SiO_2 sputtered films which necessitated the electrical contact regions at the edge being masked.

2. SiO_2 layers were thermally grown on 3" and 4" semiconductor grade silicon wafers by two separate methods depending on whether the thicknesses required were up to 1000Å, or to 1 micron.

a) For oxide thicknesses to 1000Å, the wafers were first cleaned using a hot peroxide/ammonia mixture followed by a hot peroxide/hydrochloric mixture and finally a deionised water wash. Immediately prior to insertion in the furnace the wafers were dipped in a 10% HF/water mixture to remove any native oxide.

Wafers were inserted into the furnace at 1050^{o}C in an atmosphere of dry nitrogen and left for 15 minutes. The wafers were then oxidised by switching to an oxygen atmosphere, (1 litre/min oxygen flowing through furnace), for 1hr 9mins to give an oxide thickness of 1000Å. This was subsequently confirmed on an optical interferometer or by ellipsometry. The furnace atmosphere was then switched back to nitrogen for fifteen minutes before the wafers were withdrawn.

b) For thicknesses to 1 micron the wafers were cleaned as above, and again inserted into the furnace in a nitrogen atmosphere. After fifteen minutes at 1150^{o}C the furnace atmosphere was changed to wet oxygen. This was produced by bubbling oxygen through deionised water held at 96^{o}C, at the rate of 1 litre/min for 2hrs 30mins. After this time the

atmosphere was once more changed back to dry nitrogen and held for fifteen minutes before the wafers were withdrawn from the furnace. This oxide was measured at 1.03 microns on the interferometer.

To clean off regions of oxide where required the silica was masked off either with positive photoresist -usually Shipley 1350H or AZ-1360 baked at 75^{o}C for half an hour in the dark, exposed to light through a contact mask and then development in 7g/litre NaOH; or the region required was masked off with black wax dissolved in xylene. The substrate was then etched chemically in either HF or buffered HF- (40%-HF / 40%-NH_4F in a ratio of 1 to 7). The masking material was subsequently removed with an acetone rinse in an ultrasonic bath.

To remove Si surfaces the 'CP4' wet etch was used (see Table 7). For example when experiments were done with some ion-implanted wafers, it was used to remove the dosed layer. Measurements were being made at the time of the effect of impurities and damage in the silicon on the etching characteristics.

Etch rate (Si) microns min^{-1} (at 25^{o}C	Ratio of acids. HNO_3 SpGr.1.42	CH_3CO_2H Glacial	HF (40%)
6	5	2	2
4	4	1	1

Table 7.
CP4 recipe.

2.7.2)Electrodes.

The electrodes used in the parallel-plate capacitively coupled system consisted of 5cm x 5cm plates 1mm thick, with a 1.5cm tab in one corner for coupling the power in the case of the top electrode. A 7mm diameter hole was drilled in the bottom plate to expose the face of the Quartz crystal of the balance.

A major aspect of this study was to investigate the role of the electrode in promoting either etching or deposition. The ideal electrode for a plasma etching system should have a combination of the following properties; low sputtering rates, (see Table 2), and minimal contamination effects on the substrate, as well as a high resistance to chemical attack by the plasma, so the plasma reactive species are not depleted, nor is the chamber eventually destroyed.

The majority of experiments were carried out using the following materials:

* Stainless steel electrodes from 18/8/1 stainless steel 1mm thick.

* Nickel electrodes made from 0.4mm metal foil.

* Titanium electrodes made from 130 Ti, 1.0mm thick supplied by IMI.

* Fecralloy electrodes, 1.0mm thick.

* Aluminium electrodes from a 1.0mm sheet of 99.9% purity.

Preliminary experiments were also carried out using '80 Volt' hard anodised aluminium electrodes made in the following way:

* 1.0mm aluminium sheet was cut into 5 cm^2 pieces and abraded with Scotchbrite.

* This was mounted in a Ti holder, between Pb electrodes.

* These were then anodized at 7-10^oC in a stirred solution of;

100 ml/l H_2SO_4 (Sp. Gr. 1.84).

50 g/l Oxalic acid.

* Voltage rising from 20-80 V, in a process time of three hours{391}.

* The electrodes were then rinsed in demineralised water and dried.

Plasma sprayed electrodes were also under consideration with alumina, titania, zirconia and similar coatings, onto Stainless-steel or Fecralloy substrates{392-393}. This was to obtain chemical inertness and low sputtering rates. One problem was the tendency for the porous coatings to outgas for some considerable time, and there was also a problem found with thermal stress crazing the coating on the driven electrode. No problem was found with the electrical characteristics of the coatings with

respect to the R.F., except for a tendency to form a 'hot-spot' -a region of enhanced glow where the film had burnt through.

The electrodes were handled with gloves to minimise contamination and were cleaned before use with a recommended degreasing solution for vacuum components [394] of; HNO_3 (1.37 Sp. Gr.) 250 ml/litre, HF (60%) 35 ml/litre, care had to be taken with the acids and aluminium and alumina components. An attempt was made to evaluate the effect of various cleaning agents on the polymer deposition rate. The types of treatments tried were:

1. Chemical etch cleaning -as above.
2. Bead/sand blasting.
3. Scouring pads such as 'Scotchbrite'.
4. Heating both in air and vacuum.
5. Sputter cleaning, precoating.

along with various rinses such as

7. Alcohol.
8. Acetone.
9. Deionised water.

but overall there was found to be little discernible effect.

3)ANALYTICAL TECHNIQUES.

Several techniques were used to examine the structure and chemical composition of the surfaces remaining after etching or deposition. Since the specimens were exposed to air before analysis, there may be some tendency for hydrolysis at trapped radical sites in the near surface[396-398]. This can be clearly seen in the IR spectra of CF_4 and C_2F_6 plasmas with stainless-steel electrodes, where there is a strong peak due to water associated with the metal fluoride formed which can only have happened as a result of atmospheric contamination. With titanium electrodes the effect was exaggerated due to the copious quantities of TiF_4 formed.

Firstly methods of analysis that are sensitive to the surface or very near surface are discussed, followed by techniques that examine the bulk of the material. All analytical methods for which results were obtained are presented in this section for completeness, but some were found to be more informative than others. In particular in examining the nature of the polymers formed and the changes to the electrode surfaces, XPS and Rutherford Backscattering Spectrometry were found to be the most informative. However SIMS, NMR and Laser Induced Raman Spectroscopy on the other hand were not found to be particularly relevant, once some idea of the results that could be obtained was

known. These latter techniques, not useful enough for a major investigation, are noted separately in Section 3.3.

3.1)Surface Sensitive Techniques.

3.1.1)Surface Profiling, Interferometry.

a) Surface Profiling.

The relative etch rates of Si and SiO_2 were measured by means of a Rank Taylor Hobbs Talystep instrument[399]. This consisted of a diamond tipped stylus which is traversed while in contact with the surface being examined. Thus the device resembled a record player in its mode of operation, except that the output was a trace showing height variations during the scan. The stylus used was chisel shaped with a width of 2 microns and a depth of 0.1 micron. It was maintained in contact with the surface by a load of a fraction of a milligram and could be so traversed for a maximum distance of 2.5mm. Electrical and electronic attachments enabled the trace to be represented at horizontal magnifications of 50X, 200X, or 5,000X, and at a vertical magnification in the range 5,000X - 1,000,000X.

Like all devices, the Talystep suffers from certain limitations. Thus it must be operated in a low-vibration environment, and particular care has

to be taken when one of the higher vertical magnifications is being used. The width of the chart on which the trace is recorded limits the heights of any steps or features which can be measured to less than 10 microns, and the width of the chisel-shaped stylus means that pits which have a diameter of less than 2 microns will not be recorded on the trace.

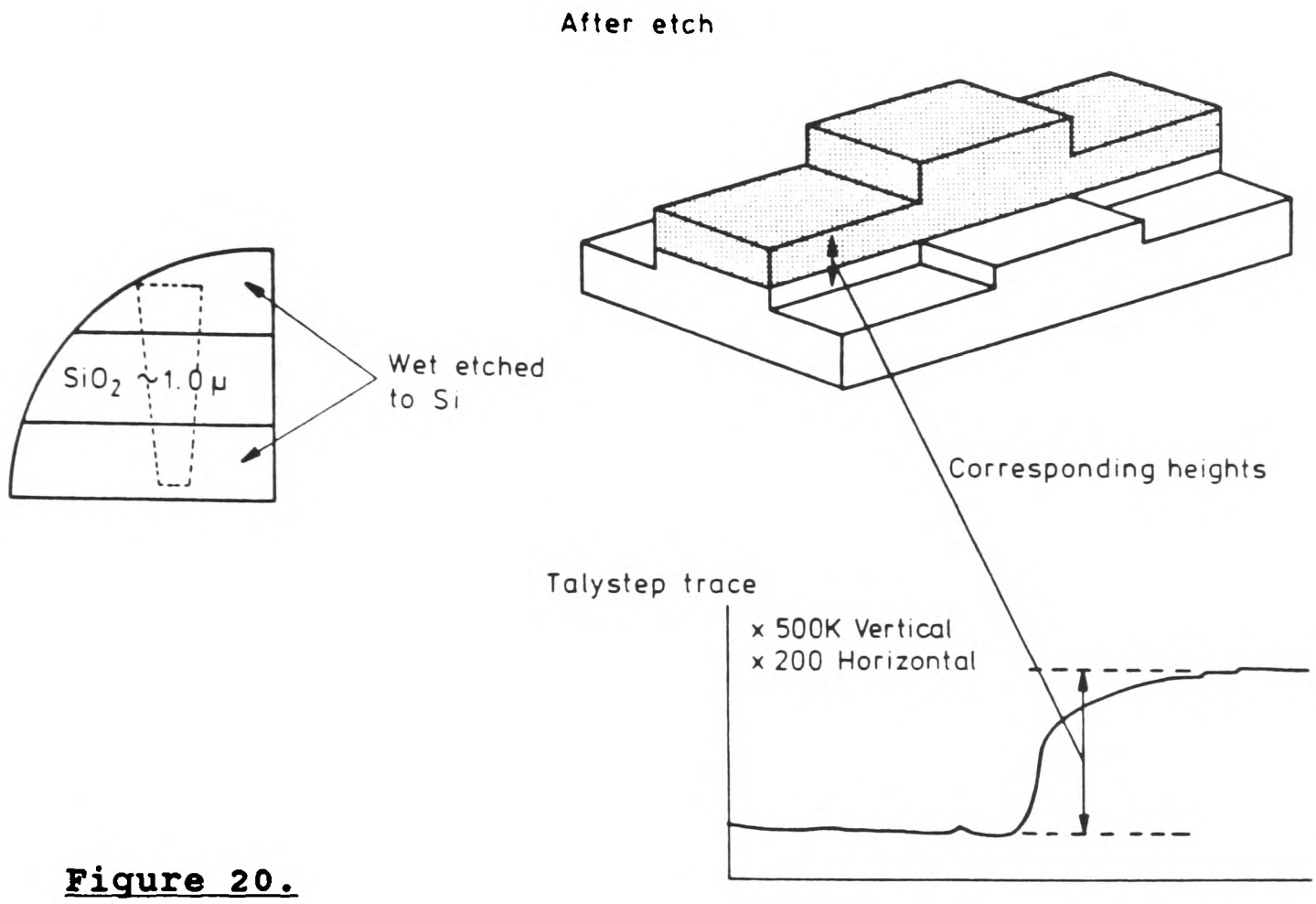

Figure 20.

Talystep Measurement of Etched Sample.

b) Interferometry.

Interferometry studies were carried out by Nomarskii interference contrast microscopy[400]. This involves splitting the illuminating beam into two components which are shone onto the sample surface with a small separation. Upon reflection and recombination, surface features appear as different colours or shades, due to the different optical pathlengths

caused by steps or changes in refractive index in the surface being measured. A Vickers photoplan microscope with a mercury lamp or filtered tungsten lamp as a light source was used. Problems with transparent films were overcome where necessary, by sputtering a thin gold layer{401}.

There was limited access to a Gaertner ellipsometer which was used to confirm the Talystep measurements, by giving a value for the thickness of transparent oxide film remaining on the polished silicon after etching. Where the film appeared to fluoresce, there was found to be polymer present on top of the oxide, so no reading was taken. Since most of the oxide used was thermally grown the refractive index was accurately known to be 1.45. A quick check by comparing the apparent colour of the slice with a published chart when using tungsten filament illumination in the optical microscope was found only to be useful in the lower orders, where the colours were strongest.

3.1.2)XPS/ESCA, Auger Spectroscopy.

The technique of X-Ray photoelectron spectroscopy (XPS), alternatively known as 'Electron Spectroscopy for Chemical Analysis' (ESCA), is relatively new for the purpose of surface analysis. The basic experiment involves the ionisation of inner core

electrons from the sample by irradiation with X-rays. With a known X-ray energy and a measured ejected electron kinetic energy, the electron binding energy is the difference of the two. Since core, unlike valence electrons, retain characteristic energies; their elemental source can be inferred thus leading to a chemical analysis. Structural information is also obtained since electrostatic interactions between the two types will cause a 'chemical shift'. Though the technique of measuring electron kinetic energies resulting from X-Ray irradiation has been reported since the early part of the century[403-407] only recently have sufficiently monochromatic sources and high resolution detectors been available[408-413].

In the related technique of Auger Electron Spectroscopy (AES), electrons in a nearly monoenergetic beam at a current between 10^{-7} and 10^{-4} Amps and typically in the 2-5KeV energy range are focussed onto the surface to be analysed in a 50-500 micron spot. The energies of the secondary electrons backscattered or ejected from the surface are then analysed. Attention is focussed on the small current peaks of electrons at fixed kinetic energies ejected by the Auger process. These can be used to identify the species present in the surface. Ultra-high vacuum must be used here due to the

tendency to build up carbonaceous material on the surface. The electron beam is also comparatively destructive especially for insulating samples.

XPS uses an X-Ray beam corresponding to characteristic atomic emission lines, usually Al-alpha, Mg-alpha or K-alpha, to excite the photo-electron spectrum. The beam is of relatively low energy, and hence less destructive than techniques which use ion or electron bombardment of the surface. The electrons emitted are both photoelectrons and Auger electrons and hence the energy distribution spectrum is more complex than that arising from Auger processes alone. The signal observed from the sample volume in XPS is a function of the photoelectron inelastic mean free path in the sample material which is of the order of 20-50Å. This is also the effect governing the depth profile of Auger spectroscopy, and hence the effective sample observed in both cases is essentially the same. Thus the information obtained from XPS originates in the very near surface, whereas most other techniques rely on fragments knocked out of the surface. As a result XPS does not have an intrinsic depth profiling capacity as it is measuring a fraction of a monolayer, although if required, profiling can be carried out by sputter erosion of the surface, generally by means of an Argon ion gun. It should be noted when undertaking quantitative work, that the mean free

path for electrons is a function of depth, kinetic energy of the escaping electrons and sample composition, and hence the effective sample thickness may not be the same for photoelectron peaks observed at different energies.

One caution is that though the electron mean free path in a polymeric material, such as we are concerned with here, is of the order of 40-100Å there is often a change in sample surface potential. Non conductive materials normally become positive and hence retard the ejected electrons, thus leading to higher apparent binding energies. This combined with the inability to measure hydrogen limits the amount of structural information obtained.

Method.	**XPS.**	**AES.**
Incident particle	Photon (X-Ray)	Electron
Energy.	Al Ka 1487eV.	1-10 KeV.
	Mg Ka 1254eV.	
Flux.	50 - 100W.	10^{-3}-10 microA.
Emergent particle	Photoelectron, Auger electron.	Auger electron.
Energy.	Al 0-1500eV.	0-2000eV.
	Mg 0-1260eV.	
Analysed depth	1-10 monolyr.	1-5 monolayers.
area.	1-50 mm^2.	10^{-9} - $10^{-4}mm^2$.
Elemental sensit.	ca. 10^{-3} atom%	ca. 10^{-3} atom %.
Spread.	< 10.	< 10.

Table 8. Comparison of XPS / AES[414]

Previous studies.

XPS has been demonstrated to be an extremely useful and powerful tool for the investigation of structure, bonding and reactivity in polymeric systems[415-421]. This is aided by the small

sample volume required, the non-destructive nature, and the minimum of preparation required. Fluorine containing systems are well suited to examination by XPS since fluorine is the most electronegative element and induces the largest chemical shifts in the C_{1s} levels. There is also comprehensive data on fluorine containing materials. Often it is the case that XPS provides the only detailed information available about plasma polymerized compounds, especially for the fluorocarbons{422-429}.

Carbon environment.	Carbon 1s peak (eV).
-C-C-, -C-H	284.5 - 285.5
$H_2C-CH_2-CH_2$	285.4
-C-F	286.0 - 287.0
F-C-F	290.7 - 291.3
CF-C-CF	286.0 - 287.0
$CF-CF_n$	288.8 - 289.4
CF_2-CF_3	294.8
$-(CF_3)$	293.0 - 293.4
pi-pi* CF	295.3 - 296.2

Table 9. XPS Carbon 1s peaks.

Figure 21 illustrates the distinctive nature of the C_{1s} levels for typical structural features found in fluoropolymers as well as showing a typical C_{1s} XPS spectrum from a plasma deposited fluorocarbon films. This shows contributions from CF_3, CF_2, CF, and C not directly bonded to fluorine.

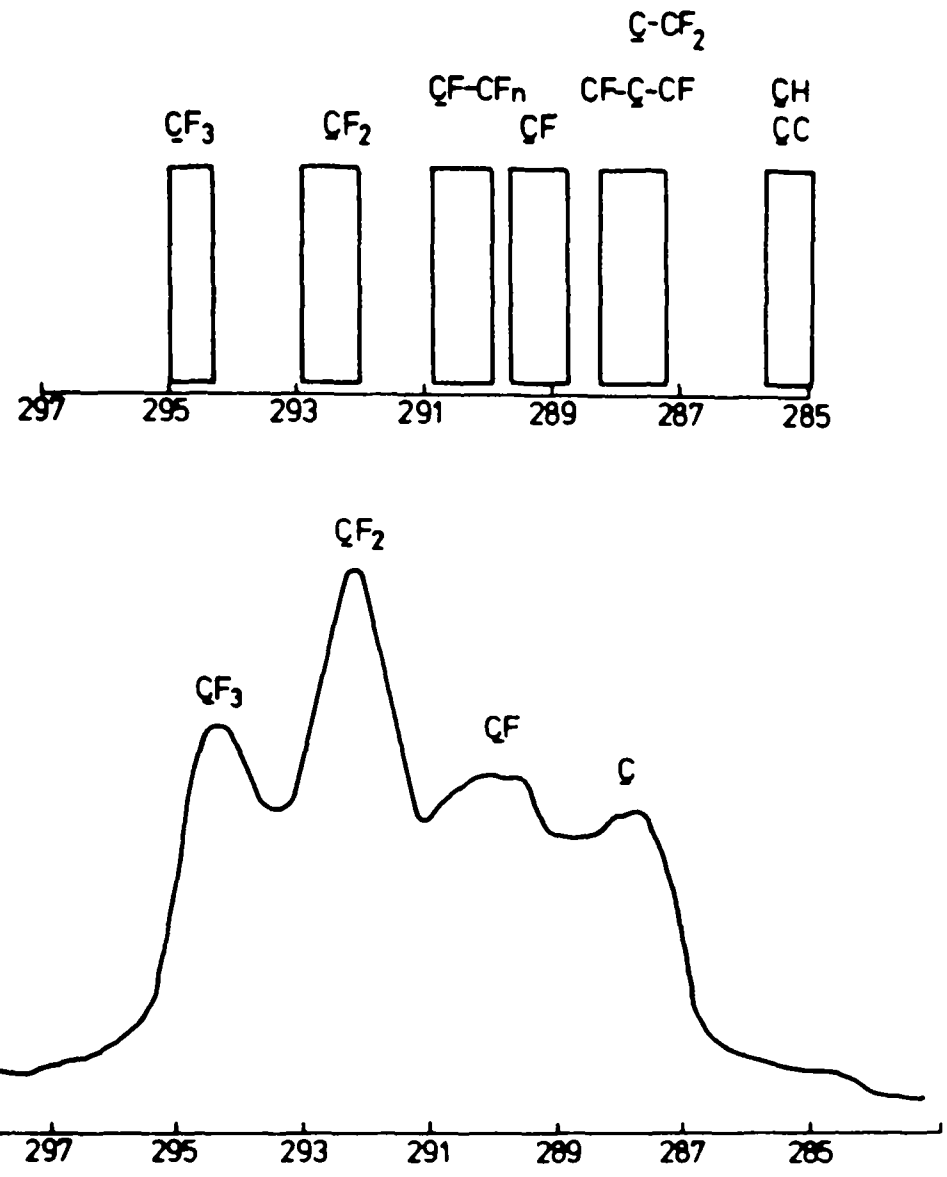

Figure 21.

Typical C_{1s} Binding Energies for fluoropolymers.

Prior studies of material deposited on silicon or silica substrates have been done including inorganic films on silicon substrates[430], cleaning procedures[431], and more importantly the preferential polymer formation on Si rather than SiO_2 surfaces which leads to the selectivity of SiO_2 over Si in certain etching processes. **Davies et. al.**[432], investigated the two types of polymer film that could be formed during plasma etching of SiO_2. These are known as 'persistent' -resistant to removal by O_2 based discharges, and 'non-persistent' -removed quite easily. The motivation for this study was that the formation of the persistent film inhibited completion of the etch process during their silicon device fabrication process.

The non-persistent film was found to be mainly a long chain fluorohydrocarbon polymer, whereas the persistent film was found to be of a shorter chain length (greater $-CF_3$ contribution) with incorporation of electrode materials such as Al and Stainless-Steel throughout. Si-F bonding was also more in evidence at the interface in the latter case.

Experimental.

The solid state instruments service at Harwell uses a MA500 ultra high vacuum scanning electron microscope made by V.G. Ltd. The SEM resolution is better than 500Å and Auger spectra can be obtained on sample areas as small as 1000Å in diameter. A scanning argon ion gun is fitted to allow controlled stripping of the sample surface to give profiles of composition with depth. This was needed since all the samples were exposed to air before measurement.

3.1.3)Microscopy.

The main microscopes used at various times were:

1. Phillips SEM- A.E.R.E. Harwell.

The scanning electron microscope used initially was a Phillips PSEM 500X with an eucentric goniometer stage. The typical working vacuum was 10^{-7} Torr. Theoretical resolution is 70Å, but is usually 100Å. The range of spot sizes was 100Å to 1 micron and

beam powers 1-25KeV, with typically 640Å and 25KeV being used for these studies. The standard signals were obtained; secondary electron, back-scattered, and specimen current (in the range 10^{-11}A). Analysis was by either a wavelength or energy dispersive spectrometer with resolution for the former of 0.01%, and the latter of 0.1%. Magnifications in the range 10-80,000X were possible and photos were taken on 4" X 5" plates. The specimen was held mechanically, not glued, and could be up to 2.5cm in diameter and 1cm high. Both uncoated and gold coated samples were examined to see the surface morphology.

2. JEOL 100CX- Chemical crystallography, Oxford.

For small specimens the JEOL 100CX TEMSCAN at the Department of Chemical Crystallography, Oxford was used. Several attempts were made to examine the heavy metal content of the polymer films and residues left, by transmission electron microscopy, and also by use of the elemental analyser fitted to the instrument.

3. Optical Microscopy.

A few optical micrographs were taken using a Wild M400 microscope with a polaroid attachment. This was capable of magnifications of 6.3-32X. This was also used to examine the gross morphology of the substrates and also to estimate the remaining oxide film thickness by colour.

3.2)Bulk Measurement Techniques.

This section on 'bulk measurement techniques' includes all the methods that produce information on the bulk composition or properties of the substrates, electrodes and polymer films. Samples were submitted to the Harwell Nuclear Physics Division for analysis by Elastic Recoil Detection Analysis and by Rutherford Backscattering. Samples for Infrared analysis were submitted to the Physico-chemical measurement unit (PCMU) and some substrates were also measured on an instrument belonging to the Special Processing group.

3.2.1)Elastic Recoil Detection Analysis.

The light elements present in the polymer films were qualitatively determined by ERDA, also known as Forward Scattering; in the Harwell Tandem Accelerator{450-452}. This is one of the few methods for profiling hydrogen{453}. The target is bombarded with a heavy ion beam and the energy of the recoiling impurity atoms is analysed. This is unlike the Rutherford Backscattering technique which analyses the energy loss of the primary beam. The energy of the recoil, which is dependent on its mass and depth (t) in the target is given by:

$$E_{R_1}(t) = K\left[E_B(0) - \int_0^{x_1} S_B(E)dx \right] = K E_B(t)$$

and the energy it is ejected with is:

$$E_{R_2}(t) = E_{R_1}(t) - \int_0^{x_2} S_R(E)dx$$

where E denotes energy, S denotes stopping power and the subscripts B and R refer to the bombarding projectile and the recoil respectively. x_1 and x_2 are the path lengths for the projectile and recoil and are dependent on the geometry- hence changes in geometry can be used to enhance particular depth profiles with respect to each other. The kinematic factor is:

$$K = \frac{4M_B M_R}{[M_B + M_R]^2}\cos^2\theta$$

where M is the mass and Theta the scattering angle. The cross-section for the recoil is:

$$\left(\frac{\delta\sigma}{\delta\Omega}\right)_R = \left[\frac{Z_B Z_R e^2(M_B + M_R)}{8\pi\epsilon_0 M_R E_B(t)}\right]^2 \cdot \frac{1}{\cos^3\theta}$$

The advantages of a heavy projectile are that they have large Rutherford scattering cross-sections and high stopping powers. The high stopping power gives a high depth resolution and also allows the use of a stopper foil in front of the detector to prevent the scattered primary beam from reaching the detector whilst allowing light recoils through. This absorber also stops recoiling substrate atoms but has the disadvantage that it degrades depth resolution because of the energy straggling of the light recoils as they pass through the foil.

Previous studies.

The two major uses of ERDA in semiconductor technology have been to profile impurities such as hydrogen and boron in hydrogenated amorphous silicon materials and for measurements of doping levels. The technique has also been successfully used to measure oxide thicknesses on Si[454].

Experimental.

In the present studies, a 30MeV beam of ^{35}Cl ions with a current of 10-20 particle nA was obtained from the Harwell Tandem Accelerator and recoiled off the film of interest, with an angle of 70^{o} between the beam and the target normal axis. The experimental arrangement is shown in Figure 22. A surface barrier detector was located at 30^{o} to the beam axis and subtended a solid angle of 0.4msr with an acceptance angle of 12mrad. A 12 micron Mylar absorber, the thickness of which was determined by the energy loss of 5.8 MeV alpha-particles, was employed to remove the heavy ion background. Analysis was carried out at 10^{-6} Torr with additional liquid nitrogen trapping in front of the target to minimise carbon build-up. Owing to the kinematic relation between recoil energy and mass[455] the detector gives a pulse height spectrum which separates the different particle masses and a multichannel analyser was used to record the spectra.

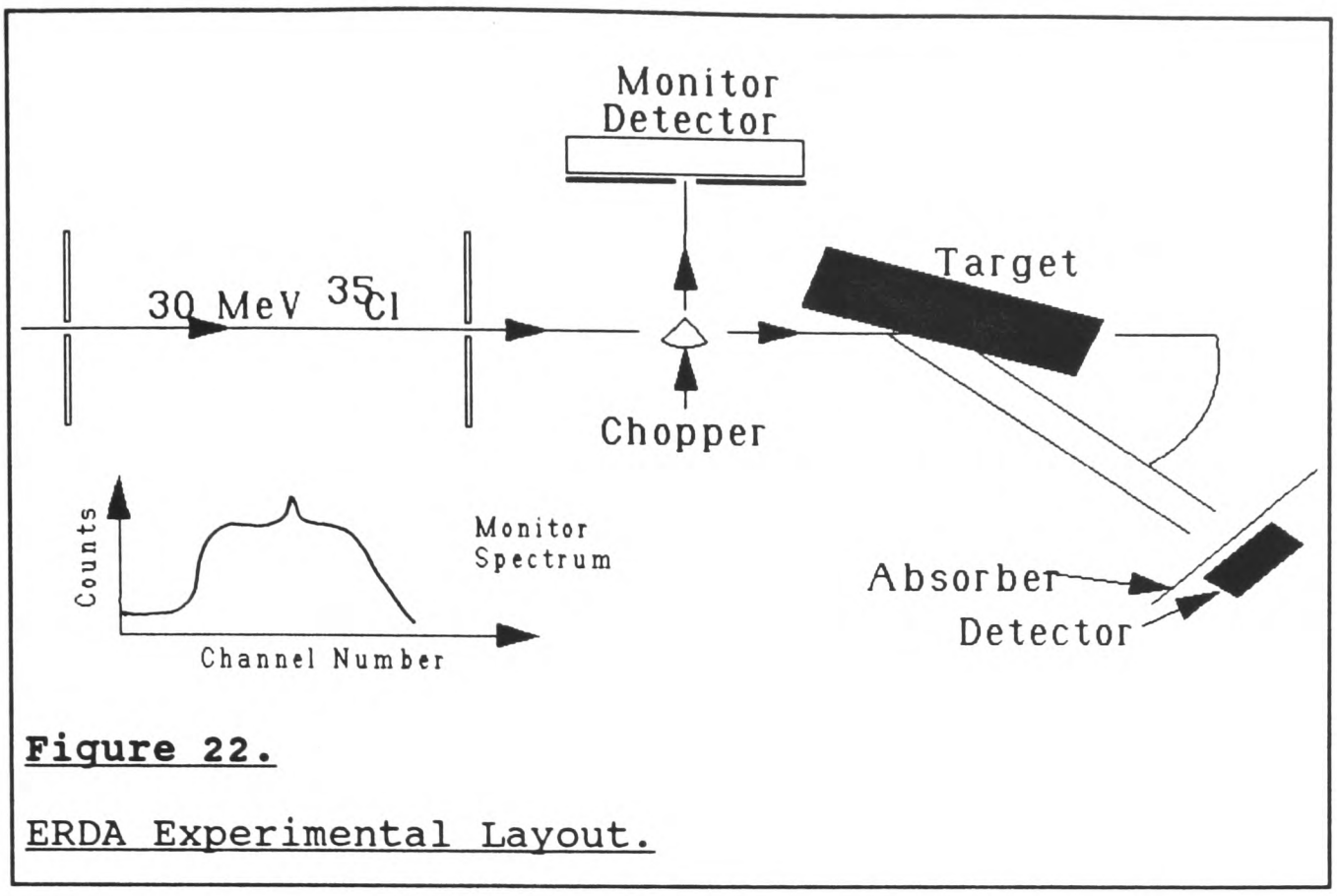

Figure 22.

ERDA Experimental Layout.

To obtain absolute beam fluxes a rotating chopper was used. This consisted of a carbon blade onto which was evaporated a gold film. Approximately 10% of the beam was intercepted, scattered off the gold and detected by a monitor at 90°. An electronic gate was placed round the gold peak and the number of counts fed into a scaler. This monitor was calibrated by passing the beam via the chopper directly into an electrostatically suppressed Faraday cup. In this way a beam of single charge state, as selected by the accelerator analyser magnet, is collected and the integrated charge can be simply related to the beam fluence.

The elastic recoil technique has high sensitivity in this case, firstly due to the small heavy element concentration of these films producing a low

background from primary beam scattering, and secondly because the scattering cross-sections are large (rms radii[456]).

Sample spectra are shown in Figure 35 on page 150. A different geometry was tried to resolve fluorine without much sucess.

3.2.2)Rutherford Backscattering (RBS).

This technique, also known as Nuclear Backscattering Spectrometry, depends on the interactions which occur when energetic charged particles undergo elastic Coulomb scattering by the nuclei of target atoms[457-460]. The incident charged particles, which typically are He^+ in the few MeV energy range, enter a target chamber as a collimated beam, typically $1mm^2$. The principle of RBS is that some of the He^+ ions will undergo close nuclear collisions with target nuclei and consequently be scattered from the target with reduced energy. The energy retained by the He^+ ion after such collisions is dependent on the masses of the target atoms involved. The energy spectrum of backscattered ions was measured by a surface barrier detector, mounted inside the target chamber, close to the bombarded specimen. The ion energy is then directly related to the mass and depth of the struck nucleus; for instance, recoil without energy loss

would take place from an infinitely heavy nucleus, while more energy transfer occurs the lighter the target mass.

The main features of the technique are illustrated schematically in Figure 23.

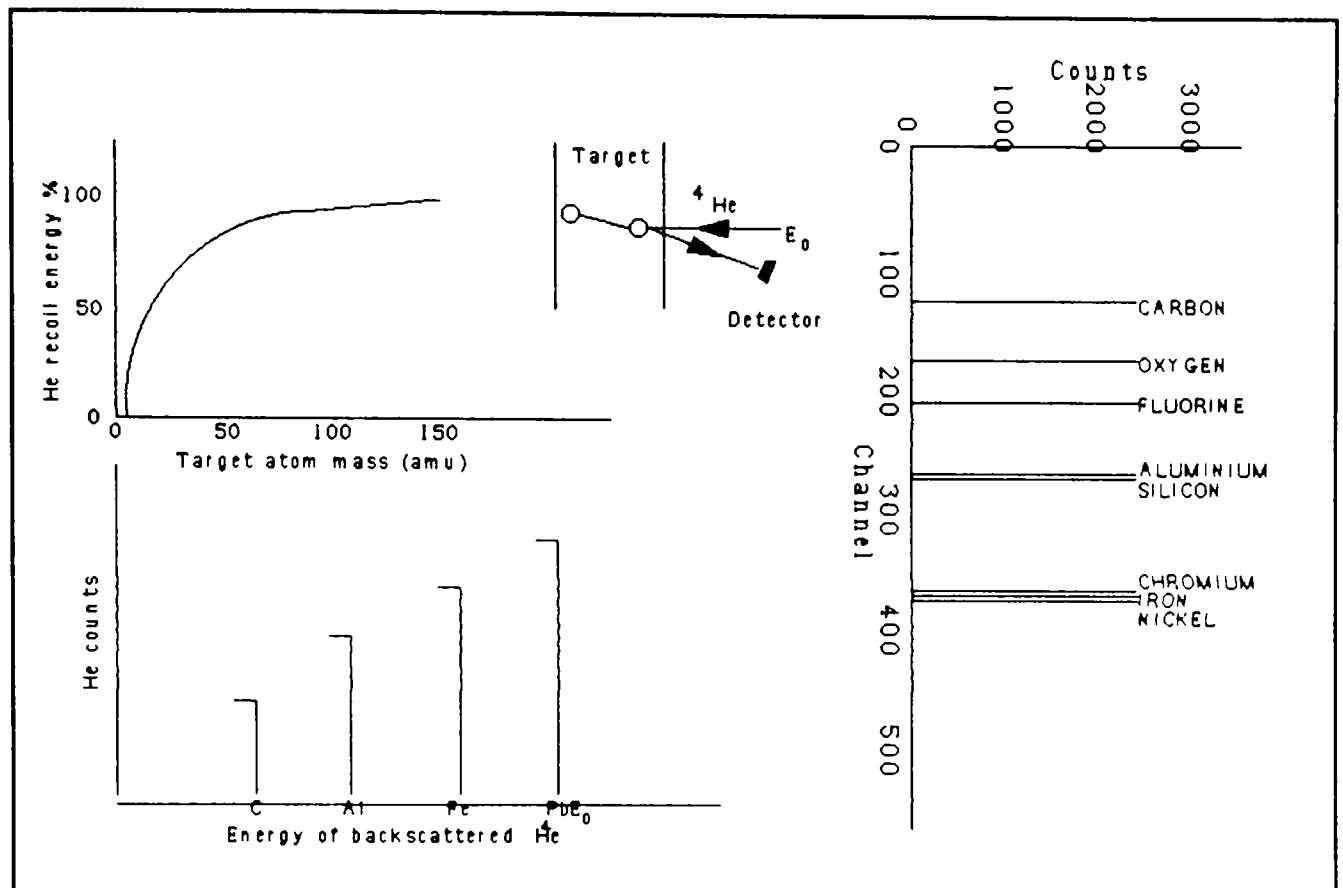

Figure 23.

Some Features of RBS.

Of particular relevance to this work are:

1) The technique is mass sensitive.

When an ion of mass m_1, charge z_1 and energy E_o is scattered at an angle Theta from a nucleus of mass m_2, charge z_2, its energy E as registered at the detector will be given by:

$$E = E_o \left[\frac{\left(m_1 \cos\theta + \left(m_2^2 - m_1^2 \sin^2\theta \right)^{\frac{1}{2}} \right)}{m_1 + m_2} \right]^2$$

Thus the best mass resolution is obtained for lighter elements. Also the relationship of (E/E_o) with m_2 for He^+ is also shown inset in Figure 23.

2) It is quantitative.

The number of He^+ scattered at energy E into a solid angle Theta subtended by the detector is directly proportional to the concentration of scattering nuclei of the corresponding species. For an elemental thin film, the area (total counts) C of a peak in the backscattering spectrum gives a direct measure of the quantity of material present N (atoms cm^{-2}). If the film thickness is only a few thousand Å or less, one may use the relationship:

$$C = N\frac{(\delta s)}{(\delta \theta)}\delta\theta q$$

where q is the number of incident He^+ ions for the run, and ds/dTheta is the differential cross-section for coulomb scattering.

3)It is rapid and non-destructive.

Doses of typically 10 microC in a $1mm^2$ spot for a few minutes were used, not sufficient to heat the test area significantly or cause radiation damage.

It emerges as a technique suited to the quantitative, non-destructive examination of materials consisting of one or a relatively few elements on substrates composed of low atomic number elements. RBS is especially valuable in Silicon device technology because of the low atomic numbers

of the silicon/silica substrates and the polymer films, which makes it easy to observe heavier species such as incorporated electrode material, at or close to the surface.

Previous studies.

This technique has been used to study many species in silicon matrices. These include measurements of diffusion profiles and the diffusivities of, for example arsenic in polysilicon, depth profiles of implants and metallisations, the formation and properties of silicides[459-460] and the growth of SiO_2 films. It has also been used to measure contamination on a silicon surface from tungsten. This was from the ion source of a reactive ion beam etcher[461]. In a channelling orientation, where the beam is aligned with a crystal plane and hence can penetrate further, the signal intensity can be used to indicate disturbances to crystalline perfection[462] or the effects of annealing treatments. One drawback of RBS is the large size of the beam and thus poor spatial resolution, for small device studies.

Experimental.

2MeV He^+ ions were used from the Harwell 3MeV Van de Graaf accelerator, IBIS (Intense Bunched Ion Source), collimated to a beam diameter of 1mm[463].

Backscattered He^+ ions were detected by a silicon diode used as an energy sensitive detector, mounted to receive particles recoiling at an angle of about 160^o to the incident beam. A backwards scattering angle was chosen in order to optimise discrimination between different target masses.

The scattering yield (vertical scale) plotted as a function of ion energy (horizontal scale) is reduced by the dilution of each element by admixture of another, hence the basic differences between the two substrates Si and Si diluted by oxygen -SiO_2.

The thickness of the individual layers is related to the (horizontal) energy scale by the known rate of energy loss for He^+. The information concerning composition as a function of depth is therefore obtained without any removal of material, and quantitative accuracy to a few percent is achievable both for stoichiometry and depth data.

3.2.3)Infrared Studies of Polymers.

Previous studies.

The Infrared spectra of large fluorocarbon molecules are highly complex with most bands in the region of 1400-1000cm^{-1} being associated with C-F stretching vibrations. With mixed

hydrocarbon/fluorocarbon molecules there is also the problem of the very intense C-F bands masking the weaker C-H bands.

Metal fluoride absorptions were also seen, predominantly in the region 650-300cm^{-1} but individual bands are not well documented[464-467]. Bands due to the substrate were also observed and their assignments are listed below:

Assignment.	Substrate material[468].		
	SiO2	SiNx	a-Si:H
OH	3620		
OH	3380		
NH		3340	
BH			2530
SiH	2270	2170	2000
NH		1170	
SiO	1070		
SiOH	940		
SiH,SiOH	885		
SiN		850	
SiO	805		
SiH			630
SiN		465	
SiO	450		

Table 10.
Substrate peak assignments by IR (cm^{-1}).

Experimental.

To detect the presence of fluorocarbon deposits on the electrode surfaces IR double transmission spectra were recorded. Ordinary transmission infrared absorptions were attempted for the silicon/SiO_2 substrates but were difficult to obtain, despite the fact that the Si was infrared

transparent. The very thin polymer films present were easily lost in the combination of noise and the interference pattern generated from the front and back surfaces of the slice. Therefore a multiple reflection technique was tried, using a Perkin-Elmer Model 580 instrument, to enhance the absorptions by increasing the effective path length through the sample. Also once it had been shown, by XPS, that changes in gas composition had a major effect on the rate and a minor effect on the composition of the polymer films produced, Si and SiO_2 substrates which had been exposed to the plasma for longer periods of time, but varying gas ratios, were then used to build up thicker films which were more readily examined by this technique. Si and SiO_2 comparison spectra were also obtained on a spectrometer capable of computing the difference between the two substrates to find if the nature of the surface had an effect on the deposited polymer.

3.2.4)Thermogravimetric Analysis (TGA).

TGA involves measuring the change in weight of a sample{473} as it is subjected to increasing temperature. This was used to measure the thermal stability of polymer scraped off various surfaces in the reactor including the electrodes.

A DuPont 951 Thermogravimetric analyser module in conjunction with a DuPont 1090 thermal analyser was used for measurement of weight loss as a function of temperature. Up to 500mg of sample was mounted in a platinum pan suspended from a quartz rod which is attached to a taut-band meter movement. The balance beam is maintained in position between two photodiodes by an optically controlled servo-loop. A shutter on the beam causes the light from a constant intensity light source to shine equally on the two photodiodes when the balance beam is in its null position. As sample weight is lost or gained the beam will move from the null position and cause a difference in the amount of light striking each photodiode. This unbalances an amplifier and produces a current flow in the meter movement to which the beam is attached. This causes a restoring force to be applied and drives the beam back to the null position. The magnitude of the current flow is directly proportional to the sample weight lost or gained. This signal, after conditioning, is then displayed as weight% lost/gained (Y axis), against a thermocouple output from the sample chamber (X axis).

Previous studies.

Fluorocarbon polymers have been widely used commercially due to their thermal stability and high degree of chemical inertness. The 'parent' compound

is usually PTFE from which thermal stability comparisons have been extended to other fluorine containing organic polymers.

Weight loss techniques have been used to study the thermal stabilities of an extensive series of fluorocarbon polymers in vacuum[474]. Relative stabilities were obtained in the form of a plot of loss in weight at temperature after two hours against temperature. The most stable polymers were found to be PTFE and C_2F_4/C_3F_6 copolymer. Substitution of fluorine atoms by Cl or H was shown to lead to a marked decrease in thermal stability.

In oxygen the same series of polymers was used[475] and the same overall pattern of thermal stability was found, but shifted by about 200°C to lower temperatures.

Experimental.

The balance pan containing 10-20 mg. of sample was heated over the range 25-900°C at 20°C min^{-1}, with an air flow through the system of about 10cm^3 min^{-1}. Care had to be taken that the fine powdered material was not exposed to high air flow rates that would lead to false weight losses caused by physical removal of sample. On the other hand too low a flow rate leads to inaccuracies and damage due to corrosion of the quartz balance beam by fluorine containing vapours.

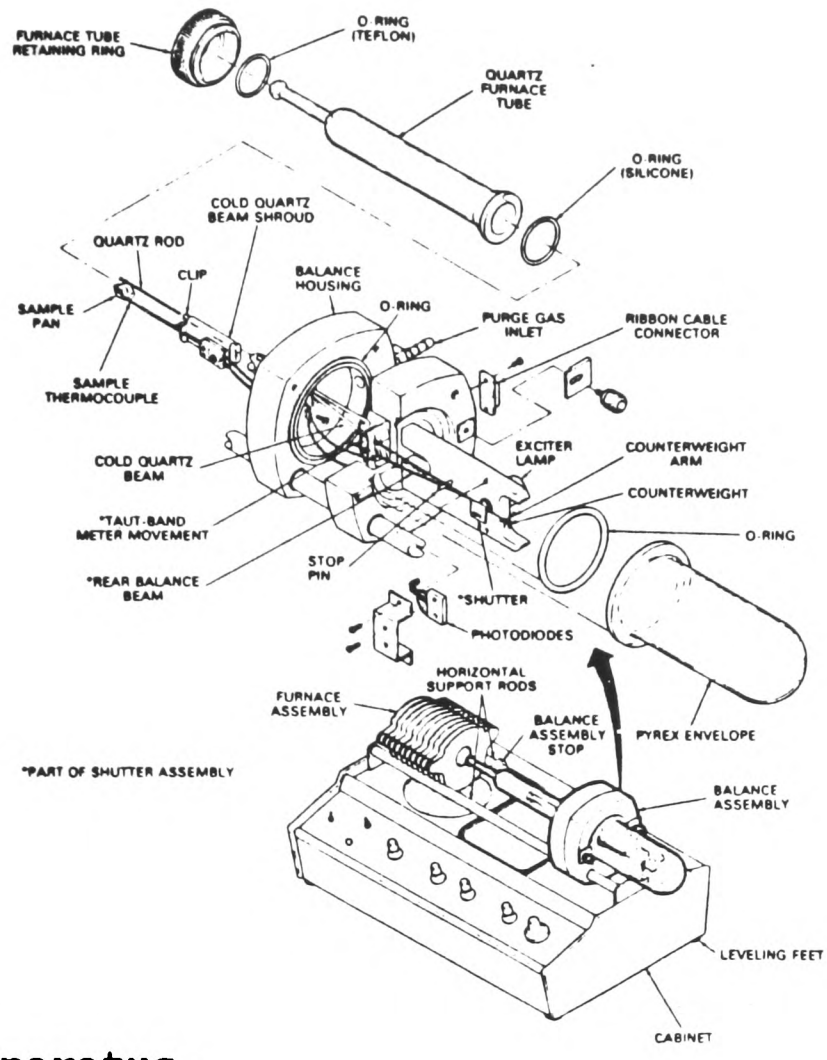

Figure 24.

T951 TGA Apparatus.

3.3)Other Techniques Employed.

Some time was spent using other techniques available at Harwell. These were found to be of limited usefulness, so are only briefly mentioned here.

3.3.1)Secondary Ion Mass Spectrometry.

In this technique an ion beam is used to sputter material from the surface of a sample. This process slowly erodes the surface and the sputtered secondary ions can be extracted and analysed by mass spectrometry. The particular instrument used can

also form images of the elemental distribution on the surface of the sample, as well as providing data on the elemental composition[433-438]. Both positive and negative incident ions can be used at typical beam energies of 5-15KeV. O_2^+ ion beams are used to generate high positive ion yields of species such as $^{11}B^+$, $^{31}P^+$; and beams of e.g. Cs^+ are used for electronegative species such as $^{16}O^-$ from SiO_2 and for $^{75}As^-$. The lateral resolution is of the order of 1-2 microns and the progressive removal of the specimen surface during the analysis allows the distribution in depth of a particular element to be studied with a typical resolution of 1/10 of the eroded depth.

Previous studies.

Most work with this technique on semiconductors has concentrated on the depth profiling of impurities in these materials[439-440], the effect of ion implantation or doping[441-442], and the formation of silicides[443].

Experimental.

Examination of plasma exposed Si and SiO_2 surfaces was carried out using a CAMECA IMS 300 ion analyser. The wafer was scribed and broken to give a $1cm^2$ or smaller sample which was mounted in a holder and bombarded by a beam of oxygen ions. Also tried were argon and nitrogen ion beams, but these

generally gave lower yields. Automatic sequential mass analysis (ASMA), combined with a digital data logging system and an Apple computer utilised as a multi-channel scaler, was used to analyse a 100 micron diameter area.

Problems were usually experienced with samples that consisted of Si/SiO_2/polymer due to the severe charging effects on a highly insulating substrate. Some of this was be minimised by using a sample with a thin layer of sputtered gold. The minimum possible ion current was also employed, consistent with the detection equipment limitations. The masses that were analysed were $^{18}OH_2^-$, $^{19}F^-$, $^{24}C_2^-$, and $^{28}Si^-$ with a rate of erosion of about 45Å per channel. The ASMA ensured that the resultant elemental depth profiles were interrelated. This data was then plotted using the Statistical Analysis System package to produce elemental profiles. Because of the experimental difficulties only a few results were obtained, similar in nature to the XPS data.

3.3.2)Laser Induced Raman Spectroscopy.

Raman spectroscopy involves measuring the wavelength and intensity of radiation emitted when a sample interacts with incident monochromatic radiation. The effect was observed and identified by **Raman**{444}, and involves quantised energy exchange

between molecules and incident photons. The frequency of the photons are either decreased (Stokes), or increased (anti-Stokes). Since most molecules are found in the ground state the Stokes emission due to energy lost from the photon to the molecule is stronger. These shifts in frequency, of which the relevant ones are given in Table 11., correspond to differences in energy levels of the molecules. They are however caused by changes in polarizability rather than dipole moment. Thus the information obtained was complementary to that obtained from Infrared.

Species	**Freq.shift (cm^{-1})**{50/51}.
CF (stretch)	900 - 1300
CF_4 "	v1 904,v2 437,v3 1265,v4 630
CCl "	450 - 850
CH "	2850 - 3050
SiF (stretch)	550 - 1040
SiCl "	400 - 750
SiH "	2100 - 2250
C - O (stretch)	1080 - 2370
O - C - O (bend)	650 - 1070
Si - O (stretch)	800 - 1050
O - Si - O (bend)	500 - 515

Table 11. Important Raman lines.

Previous Studies.

Raman techniques have been used in semiconductor technology for only a few years mainly for analytical purposes. These have included the characterisation of substrates such as wet oxidised

SiO_2[446], Si-O films, or the depth of ordering of laser annealed Si[447]. Contamination studies have been carried out, using laser Raman microprobes, on solder balls[448], hard disks and solder pads[449].

Experimental.

Ordinary Raman spectra were measured in the hope that a surface Raman technique could be used to partially characterise the polymer films in situ. These were obtained by mounting the sample in the path of a focussed beam from a nominally one watt Ar^+ laser. The cavity was tuned such as to cause lasing at 488nm, and a series of prisms were used to remove any contribution from other Ar^+ spectral features. The light scattered from the sample was then directed onto the entrance slits of a monochromator. This was then scanned away from the exciting line so as to observe any Stokes Raman lines. Care had to be taken near the exciting frequency due to stray light components from Rayleigh and Tyndall scattering caused by photons recoiling from collisions with molecules in homogeneous media and by collisions with suspended particles. These contributions can have intensities from 10^5 to 10^{12} that of the Raman light and can easily damage the photon counting system.

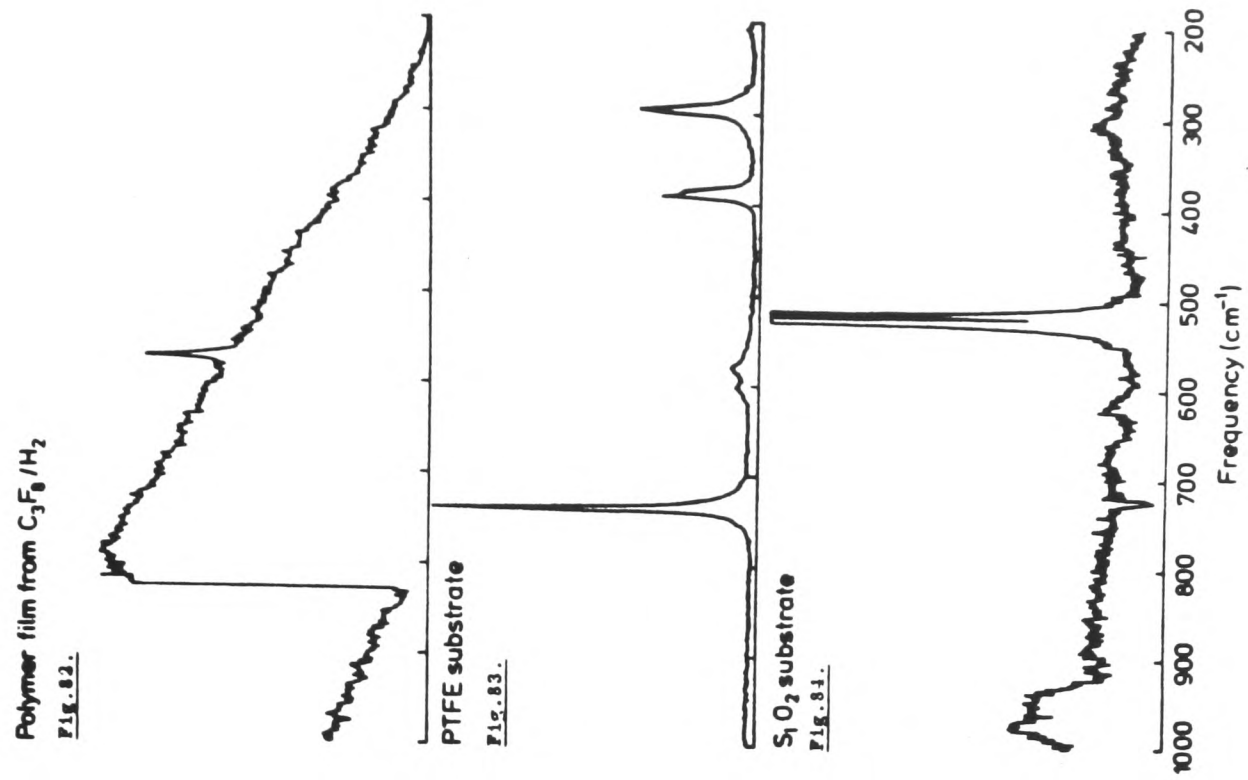

Figure 25. Typical Raman Spectra Obtained.

A series of standard samples were first run in a static system to calibrate the spectrometer and for familiarisation with the equipment. These included standard fluoropolymer materials such as PTFE PVDF -(Polyvinyldifluoride) $-(CH_2CF_2)_n-$), PFA (Perfluoroalkoxy-teflon), and FEP 140 (Hexafluoropropylene); substrate and electrode materials like Al_2O_3 -'Chip carrier', Si, and SiO_2. Both Merck Selectilux P and Shipley AZ1370, since both were used on the SiO_2/Si samples, were measured to see if there were any significant differences between them. In the case of the SiO_2 on Si samples, a range of thicknesses, including the 1 micron standard thickness used, was carefully measured to see if there were any frequency shifts that could be used for thickness monitoring as the etching

proceeded. The Electrotech #2 sample which had deposits of polymer from CF_4/H_2 etching was included.

A high degree of fluorescence, due to absorption of the incident radiation followed by re-emission at longer wavelengths, was noted in the case of the bulk polymer samples, or ones with with organic polymer on the surface. This in nearly all cases caused the very much weaker Raman signal to be swamped, even with a change of exciting frequency. This however led to a quick and easy way of monitoring the polymer build up on the surface, by measuring the fluorescence induced by a laser beam hitting the coated wafer. The polymer films also produce a high intensity of scattered light compared to the normal reflection off the highly polished surface. This can be used in combination with the normal interferometric technique to measure both rates and quality of etching.

Measurements were attempted on polymers on both electrodes and on the silicon substrates. With CHF_3 derived materials, as well as the problems of fluorescence, the samples decomposed in the beam. By adjusting the cavity length to lase at the 514.5nm Ar^+ laser line, no Raman signals were observed from any of these samples. The reduction in intensity of the laser was less than the loss in signal strength of the Raman light. Thus, despite some success with

monitoring the 'quality' of etching by measuring the fluorescence as well as observing a possible end point by the loss of the Si-O peak no further work was done. It was noticed that there was a tendency for the beam to enhance the etch rate leading to anomalous intensity measurements.

Considering the effort involved in moving the entire plasma system to the Raman facility the results were somewhat disappointing. Sample spectra were shown in Figure 25 for the polymer that was produced from C_3F_8/H_2 with a characteristic high polymer induced background fluorescence signal, for PTFE and 1 micron SiO_2 on Si.

3.3.3)NMR Investigations of Polymers.

1. Liquid phase.

Several attempts were made both at Harwell and at Royal Holloway College, University of London{469} to investigate these polymeric materials using both ^{13}C and ^{19}F NMR, but it was not found possible to find a solvent system in which any of these materials was sufficiently soluble for subsequent analysis. All trials resulted in no discernible signal being obtained.

2. Solid State.

There have been a few solid state NMR studies on plasma-polymerised materials to obtain information

complementary to that obtained from techniques such as ESCA[470-472]. Using C_2 hydrocarbons, a study was made of the material formed in a discharge using a 22.36MHz ^{13}C NMR spectrometer. Both cross-polarisation with magic angle spinning and high power decoupling, and delayed decoupling techniques were used. Five main bands were found in the spectrum (with their shifts from TMS), they are: Unsaturated, non protonated =C @ (130-150ppm); Unsaturated =CH, $=CH_2$ @ (100-145ppm); Quaternary C @ (30-55ppm); Methine, methylene -CH, $-CH_2$ @ (12-60ppm); and finally Methyl $-CH_3$ @ (10-30ppm) The overall percentages of unsaturates increased across the series: C_2F_6-(19%), C_2F_4-(24%), to C_2F_2-(38%).

An initial study was also made of the polymerisation of C_2F_2 which gave rise to six bands: Unsaturated, $=CF_2$; Unsaturated non-fluorinated; Trifluoromethyl $-CF_3$; Difluoromethylene $-CF_2$; Fluoromethine -CF; Quaternary C. The contribution from unsaturated CF is buried between ii) and iii). No major differences were seen between the bulk material by NMR and the surface (by ESCA) but the NMR has the advantage of being able to distinguish readily between C=C and C-C.

4)RESULTS AND DISCUSSION.

This section has been divided into two parts, firstly the results using pure halocarbon plasmas, and secondly the results of adding H_2 to the mixtures.

4.1)Runs With Pure Fluorocarbon Gases.

As already indicated in Chapter 2, the various aspects of the system were tested and the initial problems found. Various gases were used, both to set up the Brookes mass flow controllers and to calibrate the emission spectrometer scale. An O_2 plasma was found to clean the system of waste products and residual gases and was subsequently run for 15 minutes between each different gas and whenever the chamber was opened. Lines obtained on the 1-N plates were measured on a microdensitometer as were shown in Figure 16 and Figure 17, and their positions and intensities compared with known flame and arc spectral lines from the literature. A series of trials showed that successful etching was possible in both the inductively and capacitively coupled systems using CF_4 and CF_4/O_2. Attempts were made to use the mass spectrometer with a low measure of success, resulting finally in the necessity for a complete overhaul of the quadrupole system.

The entire rig was then moved to another building since the lasers and spectrometers used for the Raman studies could not themselves be moved. When the equipment was brought back from the Raman trials, the vacuum system was refurbished, the new parallel-plate electrode assembly was installed and the new Spex monochromator and 1-200 amu quadrupole fitted. A series of trials was then repeated to calibrate the scanning monochromator.

4.1.1)Results From Rig.

The relative tendencies for polymer deposition or etching ability for the series CF_4, C_2F_6, C_3F_8, CHF_3 was studied using a range of electrode materials. These included nickel, 18/8/1 stainless steel#, pure aluminium, duralβ and Fecralloy*. A complete series of runs was then done with combinations of:

Electrode materials	Gases	Pressures mT.	Flows $cm^3\ min^{-1}$
St/Steel Aluminium Nickel Titanium Fecralloy	CF_4 C_2F_6 C_3F_8 CHF_3	600 300 200	20(15)+ 10(7.5)+ 5
+ Flow rates of $20cm^3\ min^{-1}$ not possible for C_3F_8, see "2.3 Gases and flow controls". All at 40W power.			

\# -18% Cr, -8% Ni, -1% Si type St/Steel.

β Aluminium alloyed with Cu, Mn and Mg.

* Yttrium, Aluminium containing steel.

4.1.1.1)Quartz Crystal Microbalance.

Since the crystal surfaces when new were either silver (the 5MHz microbalance), or later gold, only deposition of material could be measured on exposure to the plasma. This means that a false impression may be given for etching plasmas since even if the sample is being eroded, the balance will only indicate a weight gain due to any sputtered material.

Rates of deposition for the four fluorocarbon gases were measured with flow rates of 20 cm^3 min^{-1} (15 cm^3 min^{-1} for C_3F_8), at a pressure of 600mT and 40 Watts applied power at 13.56MHz.

As a rough guide, the shift in frequency in Hz s^{-1} corresponds to a change in polymer film thickness of Å s^{-1}. It should be noted that this is a function of film density and this will in turn depend on factors such as the polymer density, metal contamination and sublimate content. The changes in frequency as shown in Figure 26 from CF_4 plasmas, and Figure 27 for C_2F_6, indicate the low characteristic deposition rate due to sputtered material. Neither of these gases would be expected to show any particular tendency towards polymer formation as, referring back to Figure 5 -the F : C ratio etch/polymerisation diagram, both exist as primarily etching gases at all bias voltages.

Figure 26.

Pure Gas Deposition Rates -CF_4.

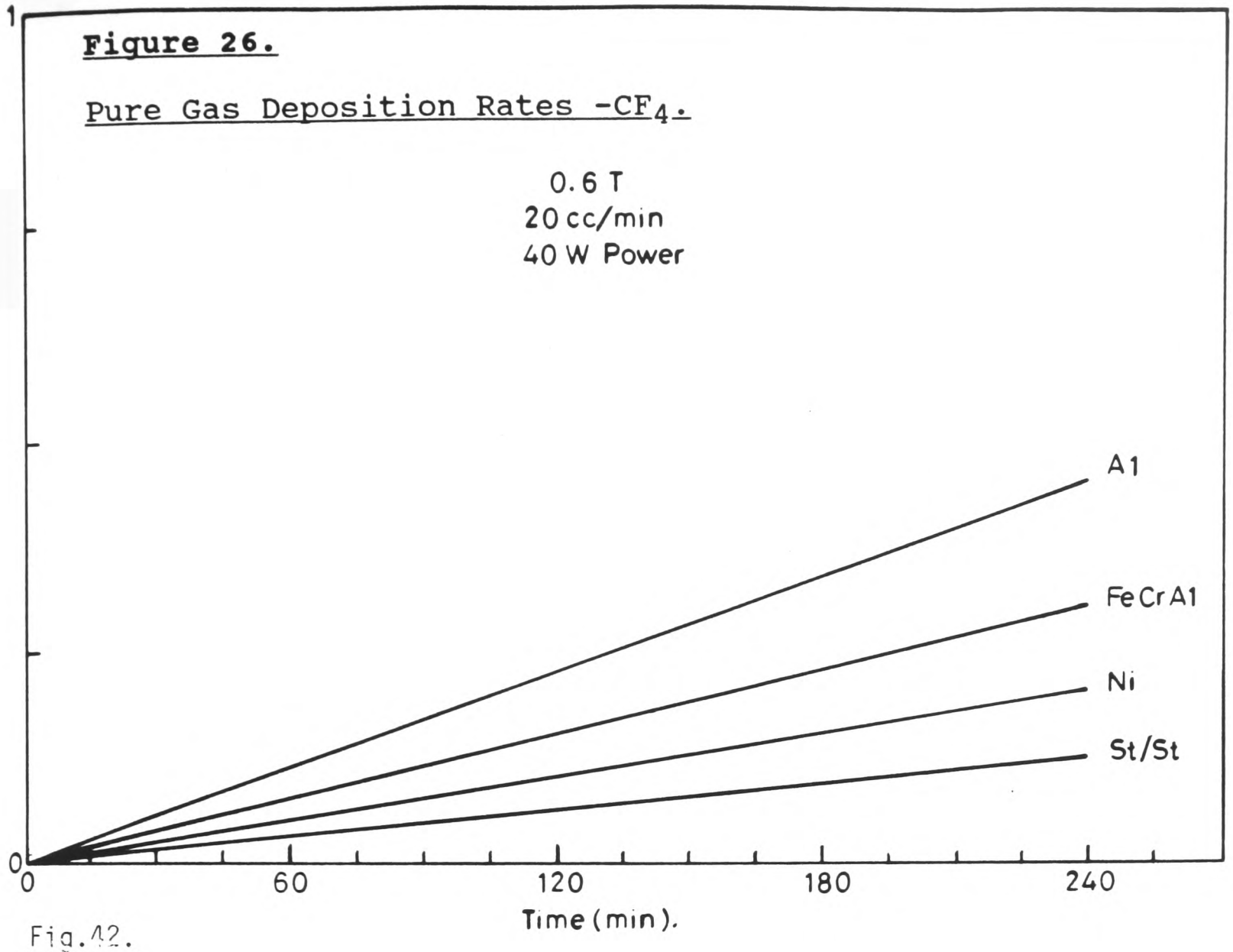

Fig.42.

Figure 27.

Pure Gas Deposition Rates -C_2F_6.

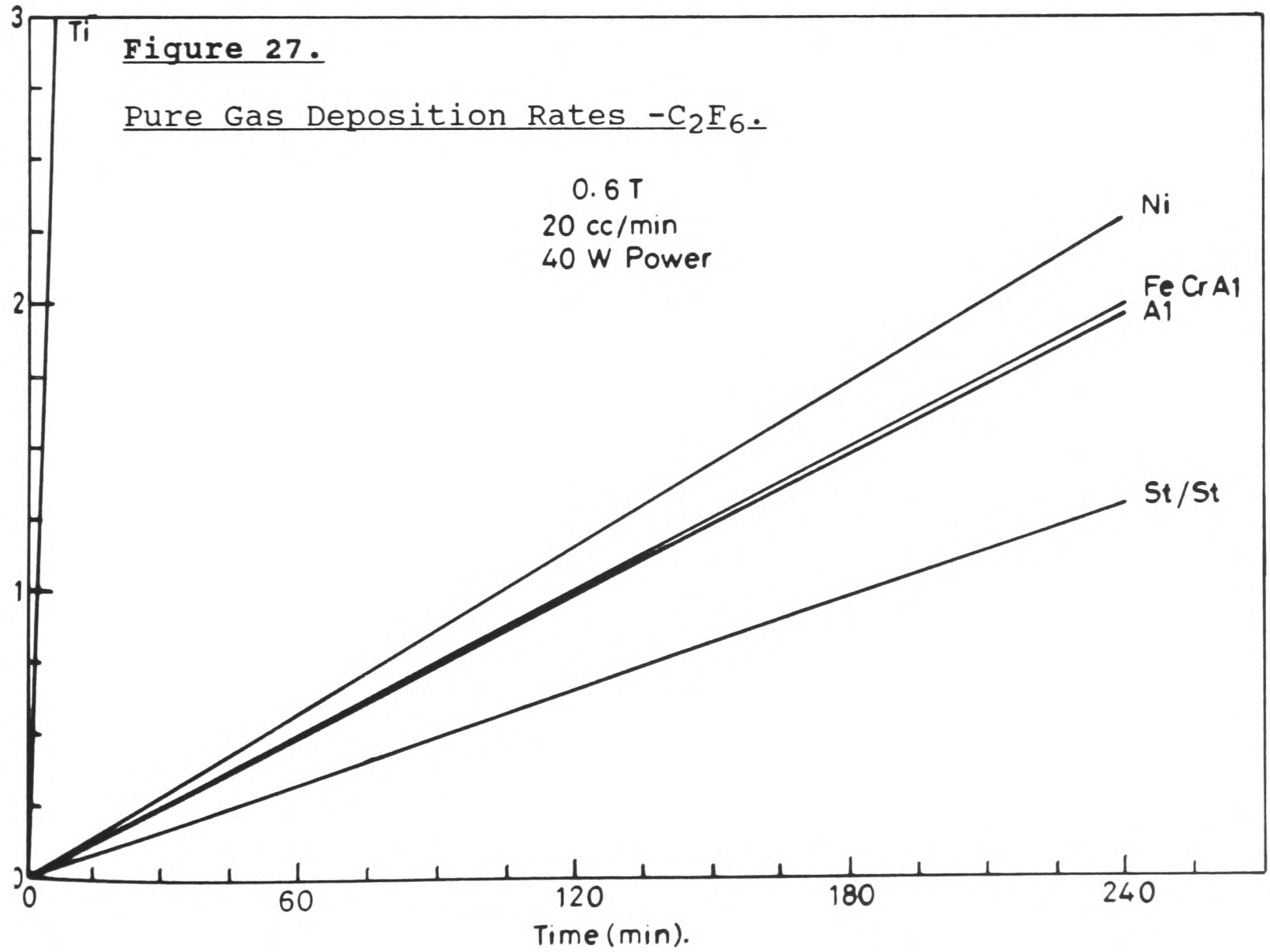

There is an anomalous result obtained from exposing the Titanium electrodes to the discharge. This was due to the formation of what appeared to be a liquid which condensed on the water cooled electrode and deposited on the quartz crystal microbalance surface. A white waxy material simultaneously appeared on the walls of the vacuum chamber downstream of the parallel plate electrode system. On opening the chamber to air, this material gradually turned to red flakes over a period of ten minutes. Some of these were collected and examined using the energy dispersive X-ray analysis system attached to the SEM. These flakes were, not surprisingly, titanium rich. This combined with the corrosion of the tube as the material absorbed atmospheric moisture indicated that it was probably hygroscopic TiF_4. This would sublime, particularly from the hot top electrode, as the sublimation temperature at atmospheric pressure is 284^{o}C. The fluoride would then readily hydrolyse to a mixture of oxyfluoride and hydrous oxide on exposure to moisture in the atmosphere.

The deposition rates from C_3F_8 plasmas, are shown in Figure 28, indicate a variation that is strongly dependent on the electrode material. This effect is not shown to anything like the same extent with any of the other pure gases. Finally the pure CHF_3 plasma deposition rates are seen to be comparable to those from C_3F_8, but without the

electrode material sensitivity. The electrodes also demonstrated the characteristic yellow colour of plasma deposited fluoropolymer, and this combined with the fact that the rates of deposition are independent of electrode material, suggests that the formation of volatile fluorides does not make a significant contribution under these particular conditions. Both the C_3F_8 and CHF_3 deposition rates are more than an order of magnitude greater than that from CF_4.

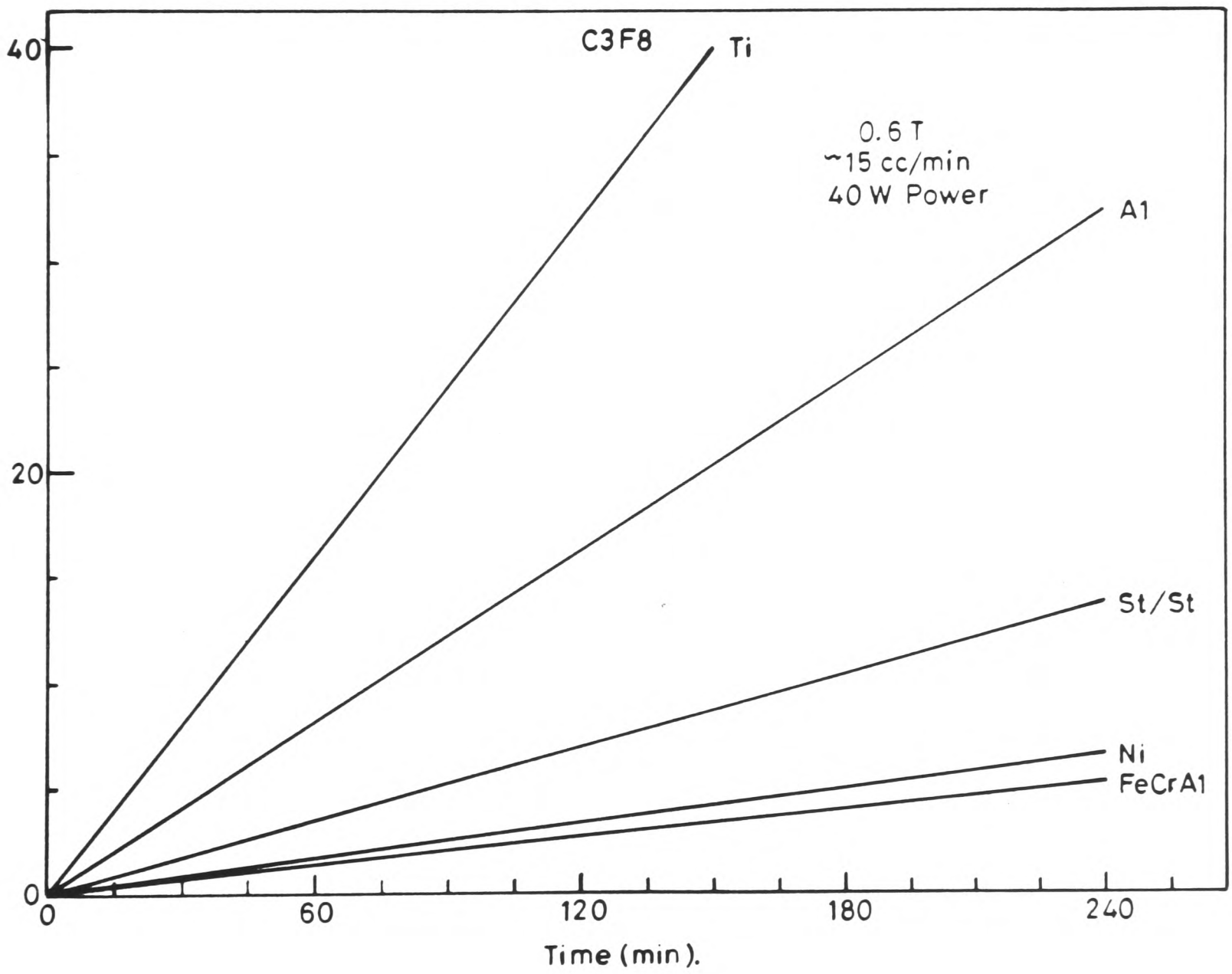

Figure 28.

Pure Gas Deposition Rates -C_3F_8.

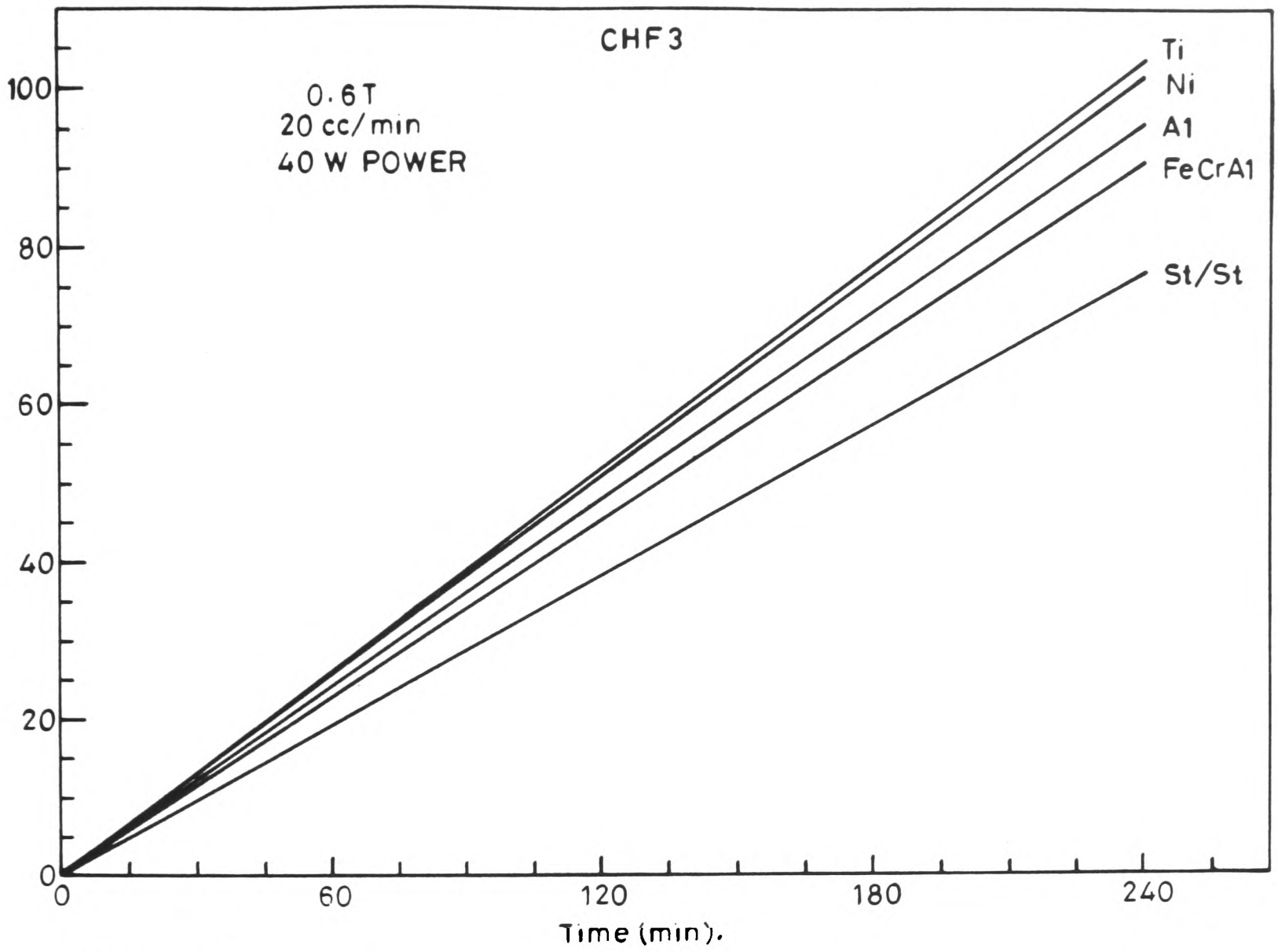

Figure 29.

Pure Gas Deposition Rates -CHF_3.

Next, rates of deposition for C_3F_8 and CHF_3 were measured with flow rates of $5cm^3\ min^{-1}$, 40 Watts and a system pressure of 200mT. These should be compared with the $20cm^3\ min^{-1}$, 600mT results for C_3F_8, and also for CHF_3.

In comparing the 200mT and 600mT results it is interesting that, in the case of C_3F_8, as the pressure is lowered, the deposition rate increases; but in the case of CHF_3, the deposition rate decreases as the pressure is lowered:

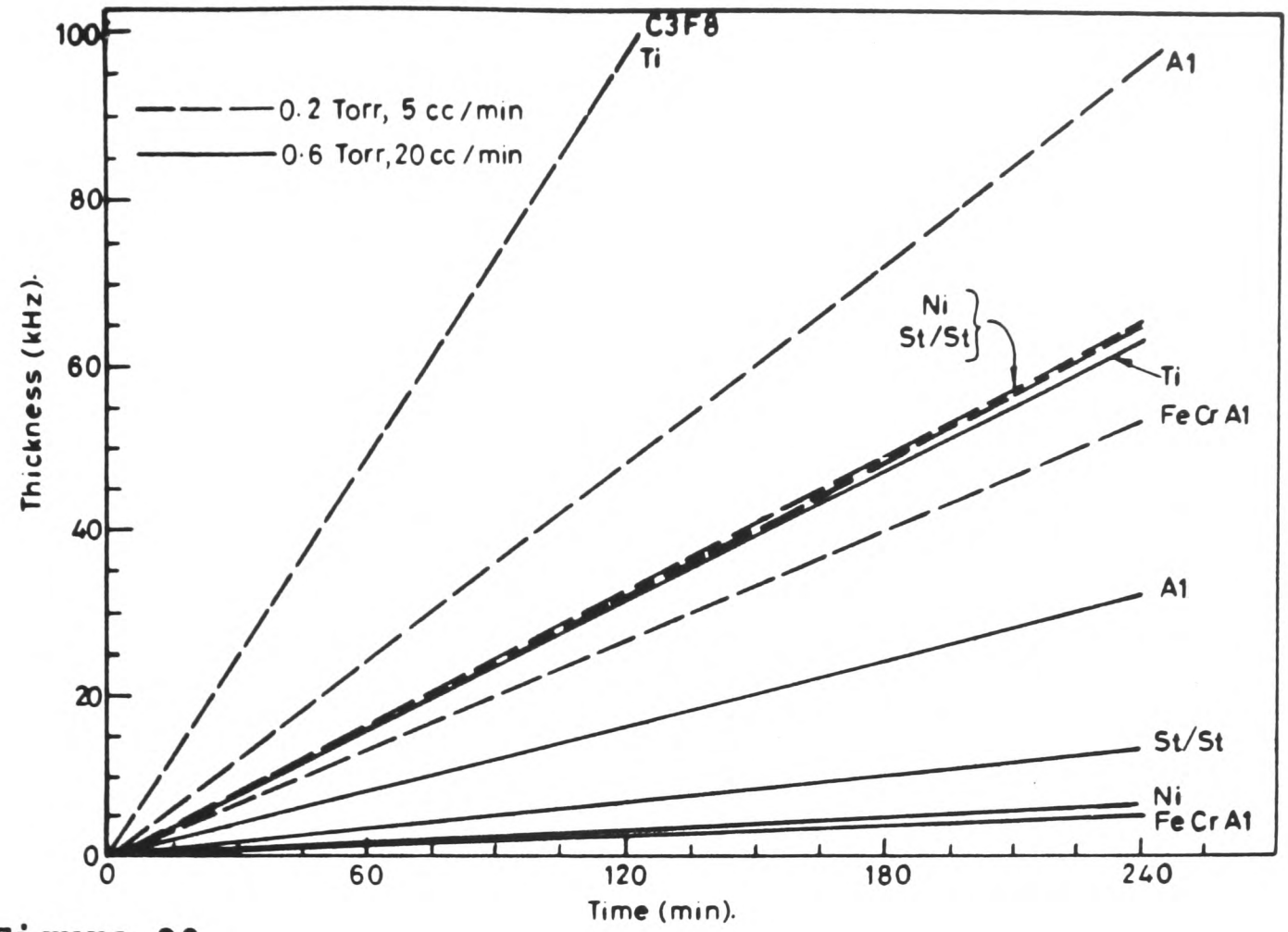

Figure 30.

0.2 and 0.6 Torr results, C_3F_8.

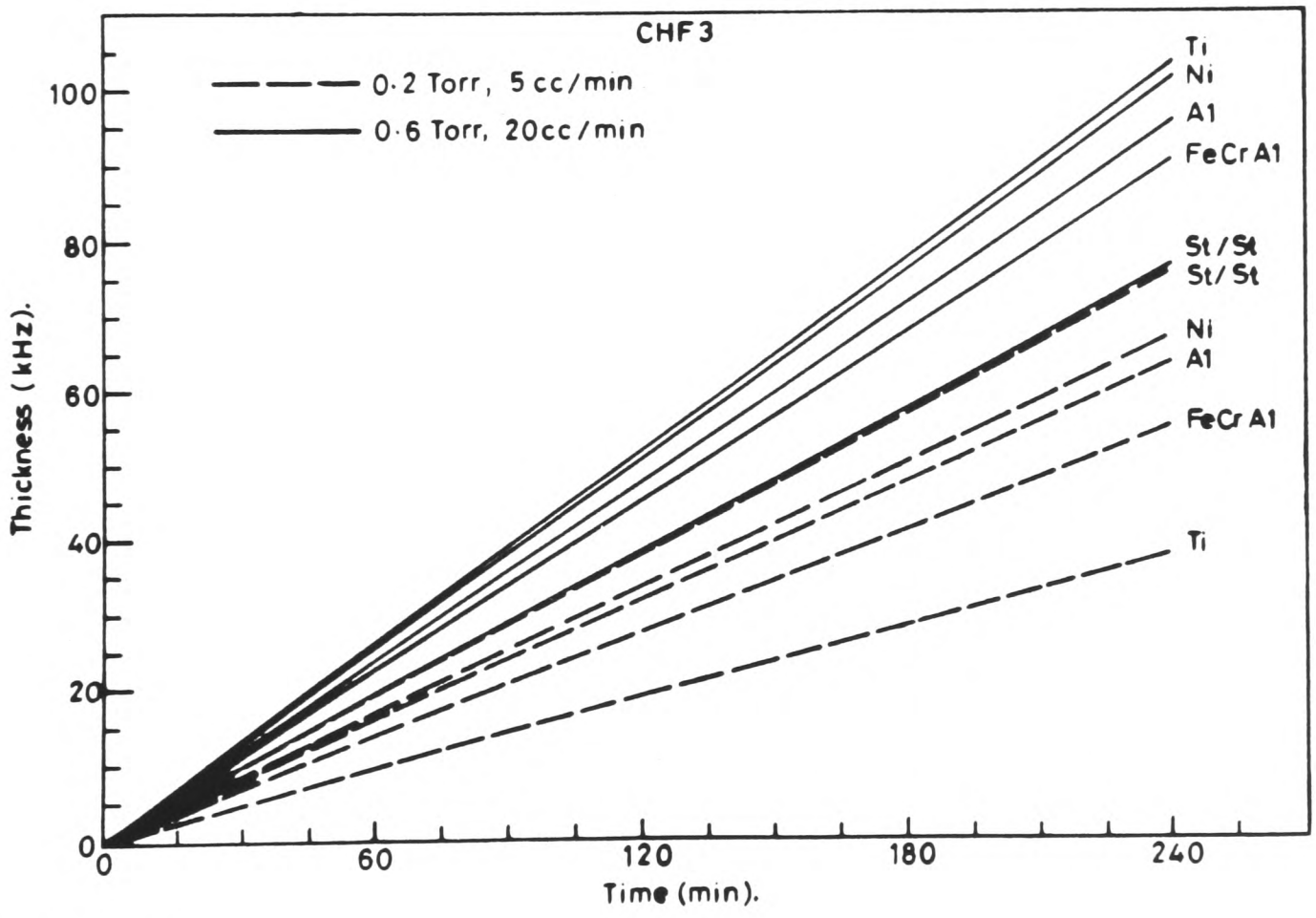

Figure 31.

0.2 and 0.6 Torr results, CHF_3.

Two factors will cause this effect. Firstly the sputtering rates increase as the pressure is lowered. The residence times are shorter of the gas phase species and their collision frequencies decrease. The ion mean free paths get longer and their maximum energy increases. Secondly the rate of sublimation of any fluorides formed will increase as the pressure is lowered. Typical sublimation pressures are 284^{o}C for TiF_4, greater than 1000^{o}C for FeF_3, 1000^{o}C for NiF_2 and 1291^{o}C for AlF_3.

For CHF_3 a certain amount of the decrease is caused by elimination of HF being enhanced by the higher ion and electron energies. This will tend to slow down the rate of film growth but there will probably be a change in density to contend with in working out the absolute differences in deposition rates at the two pressures.

Also as the pressure is decreased the average electron energy will increase. This is due to the fact that, at the same power density, the electric field present has more chance of accelerating the electrons between collisions. Hence these collisions will occur with increased energy, leading to a higher probability of reactive species being formed. There will however be less multiple collision reactions due to the greater energy per impact and the lower species density. This results in an overall shift in the vibrational progression towards

higher energy levels as shown by the optical spectra. These changes are small compared to the overall intensity of the 2238Å line used to monitor CF_2^* so the change in intensity of this emitter is still usable to monitor the overall concentration.

4.1.1.2)Dynamic Optical Spectroscopy.

This was used, as already indicated in "2.5 Quartz crystal microbalance", for a comparison of intensities of CF_2^* (2238Å) vs. polymer build-up rate. One observation is that even the CF_4 and C_2F_6 plasmas show significant concentrations of CF_2 present in the discharge. However there is also a considerable quantity of F which would tend to react with any growing polymer film to reform the gas phase species.

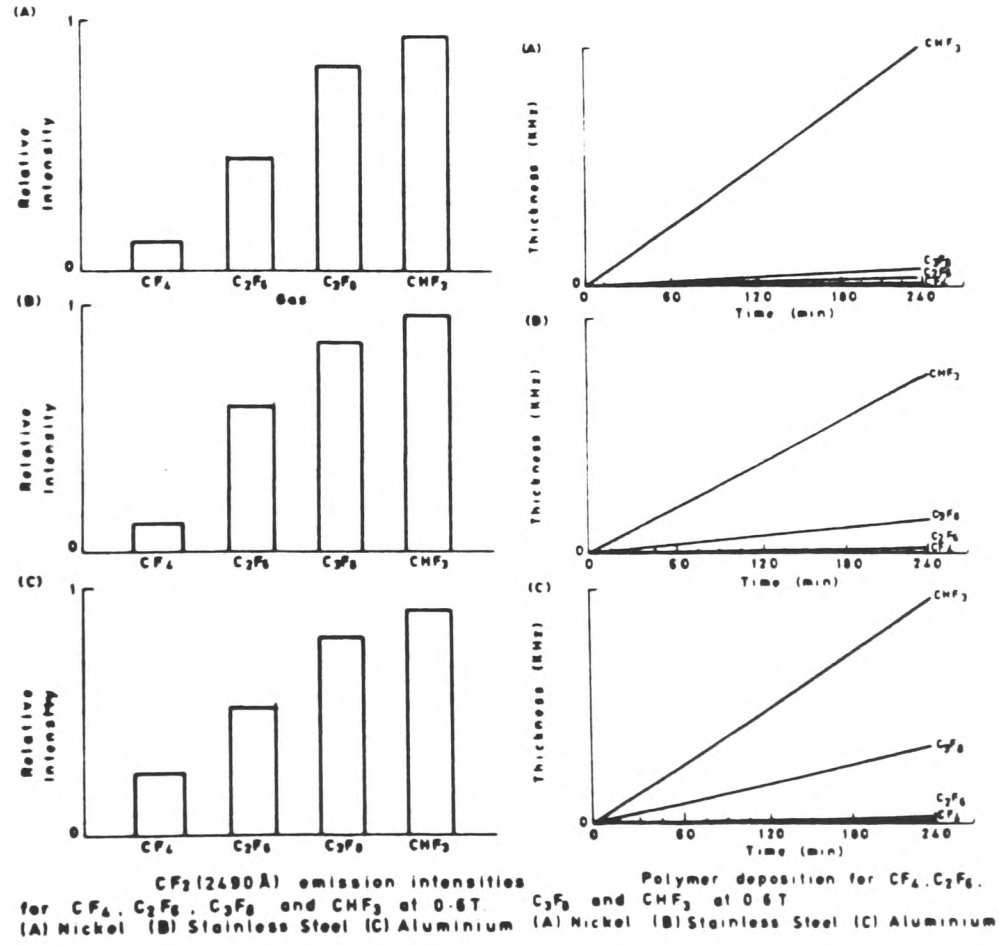

Figure 32.

CF_2 Emission

CF_2 (2490 Å) emission intensities for CF_4, C_2F_6, C_3F_8 and CHF_3 at 0·6 T (A) Nickel (B) Stainless Steel (C) Aluminium

Polymer deposition for CF_4, C_2F_6, C_3F_8 and CHF_3 at 0·6 T (A) Nickel (B) Stainless Steel (C) Aluminium

Measurements of the intensities of particular 'reactant' and 'product' species were also made as a function of time to see the suitability of particular lines as endpoint monitors. It was found that for most lines used to endpoint SiO_2 over Si etching, no more than about 20% Si could be exposed at the beginning of the etch, or the endpoint perturbation was not seen.

Figure 33.

Typical Endpoint Detection Trace.

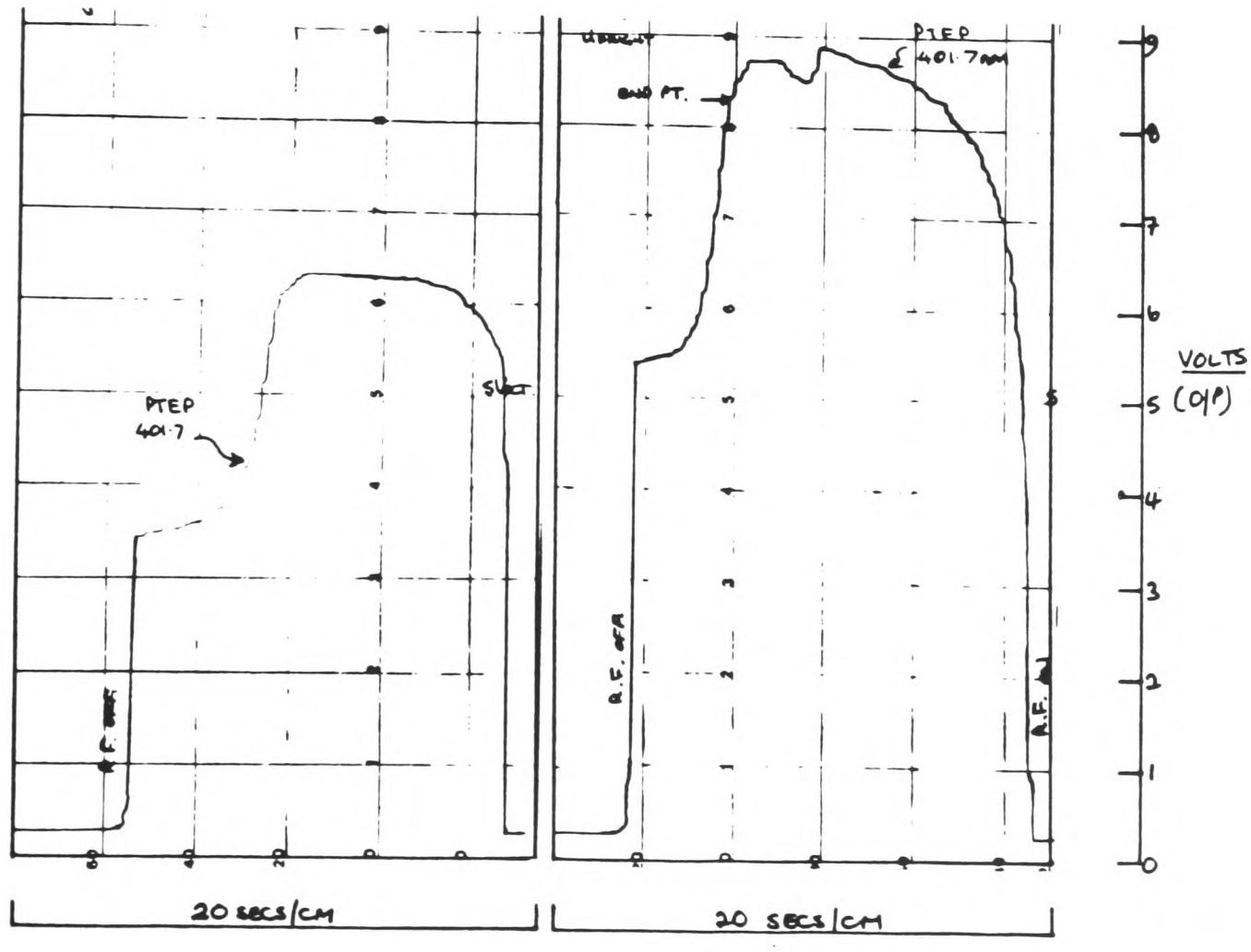

4.1.2)Examination of Surfaces.

With the effect of exposing the polymer to the atmosphere having already been noted, the samples were removed from the vacuum system and then subjected to the analysis as outlined in "3 Analytical techniques employed". From this a better understanding of the results obtained in the previous section was obtained.

4.1.2.1)Step Measurements.

A series of measurements for a set of related runs using the four gases is given below:

SAMPLE	ETCH RATE Åmin^{-1} Si	SiO_2	ETCH RATIO Si/SiO_2	ETCH GAS
up **a001** down	193 -E-	100	0.52	CF_4
	80 -E-	43	0.54	
up **a002** down	18.3	70	0.26	C_2F_6
	25	70	0.36	
up **a003** down	123 -P-	110	"1.2"	C_3F_8
	120 -P-	110	"1.1"	
up **a004** down	-P-	19.3	---	CHF_3
	-P-	17	---	

Notes; upstream of the mask.
downstream of the mask. (see Figure 20.)
E= negative step- etching.
P= positive step- polymer film formed.

From these results the principle findings was the difference in behaviour on the Si and SiO_2

substrates. The polymer forms to an approximately equal thickness on both Si and SiO_2 in the case of C_3F_8; but in the case of CHF_3, the polymer is formed preferentially on Si. No reproducible reading could be obtained on the step caused by the polymer due to its extreme softness. A thin gold layer was sputtered on top to try and give the layer some support, but this was unsuccessful.

4.1.2.2)<u>XPS/ESCA, Auger Spectroscopy.</u>

The first samples submitted for analysis to the Harwell service were two commercial thermal oxide etching samples obtained from Electrotech Ltd[476]. Comparisons were made between specimen #1, etched in CHF_3/Ar; and specimen #2, etched in 70% CF_4/ 30% H_2. The former had etched satisfactorily but the latter has visible evidence of polymer formation, as can be seen in the SEM photographs shown in Figure 41 (P.158). Next the samples were examined by XPS and a comparison made with a PTFE standard. The thickness of the surface layer on the sample was explored by argon ion bombardment to see the extent of atmospheric contamination. The area of sample examined in each case was approximately 3mm in diameter.

In the as received state only carbon, fluorine and oxygen were observed on the surface of both samples. A high resolution scan through the carbon

1s peak showed a substantial proportion of the peak shifted from its normal position, consistent with the presence of C-F bonds. In both cases the F content was high although not as high as the PTFE standard (the fact that hydrogen is not detected is to be noted). On ion bombardment the F peaks on specimen #1 dropped rapidly and Si peaks appeared. The surface polymer layer is only a few monolayers thick. In #2 the F signal dropped less rapidly and no Si peaks were detected even after removing 70Å from the surface. The polymer film here is clearly thicker on #2 than #1, but ion bombardment is not reliable for measuring the thickness of the film since F will be preferentially lost from the polymer.

The drawback with XPS in this case was the presence of a fine circuit pattern on the surface of the specimens with resulting different areas of substrate materials being exposed. AES was attempted, as the beam can be focussed down to a small enough spot size to measure on only one type of substrate feature at one time, Unfortunately the polymer film was readily degraded with loss of fluorine and severe charging effects from the insulating substrates were also observed.

Specimen #1	C	F	O	Si
As received	55	38	7	-
10Å removed	80	11	5	3
30Å removed	88	3	5	4
Specimen #2	**C**	**F**	**O**	**Si**
As received	59	33	8	-
30Å removed	80	18	1.8	-
70Å removed	82	15	2.6	-
PTFE standard	41	58	0.5	-

Table 14. XPS Approx surface (Atom %).

The next set submitted were samples run in each of the gases CF_4, C_2F_6, C_3F_8, CHF_3; in the reactor while using hard anodised aluminium electrodes. XPS measurements were again made on a 3mm diameter area. Depth was profiled by sputtering with an argon ion gun, with each μA min^{-1} approximately corresponding to 1-2Å min^{-1} sputtered from the surface.

Each sample consisted of an area of Si and an area of SiO_2 exposed to the plasma. In the 'as received' state, the surfaces of specimens from CF_4 and C_3F_8 plasmas had traces of aluminium as well as the usual fluorine, oxygen, carbon and silicon. Adventitious carbon, from atmospheric contamination was found on all specimens as a peak at 1200-1203eV kinetic energy. Carbon bonded to fluorine was also found on the surface, as can be seen in the shift of the carbon peak by about 7eV. Carbon was also present 'in' the film, from its presence on depth profiling, in the cases of C_3F_8 and CHF_3 on both Si and SiO_2.

To examine the thermal stability and resistance to ion bombardment of the material, both the silicon area on the substrate and the driven electrode of the parallel plate system were examined in the case of C_3F_8 and CHF_3 plasmas, since these were the most rapid polymer producers. The spectra obtained are shown in Figure 34(a) -C_3F_8, and Figure 34(b) for CHF_3.

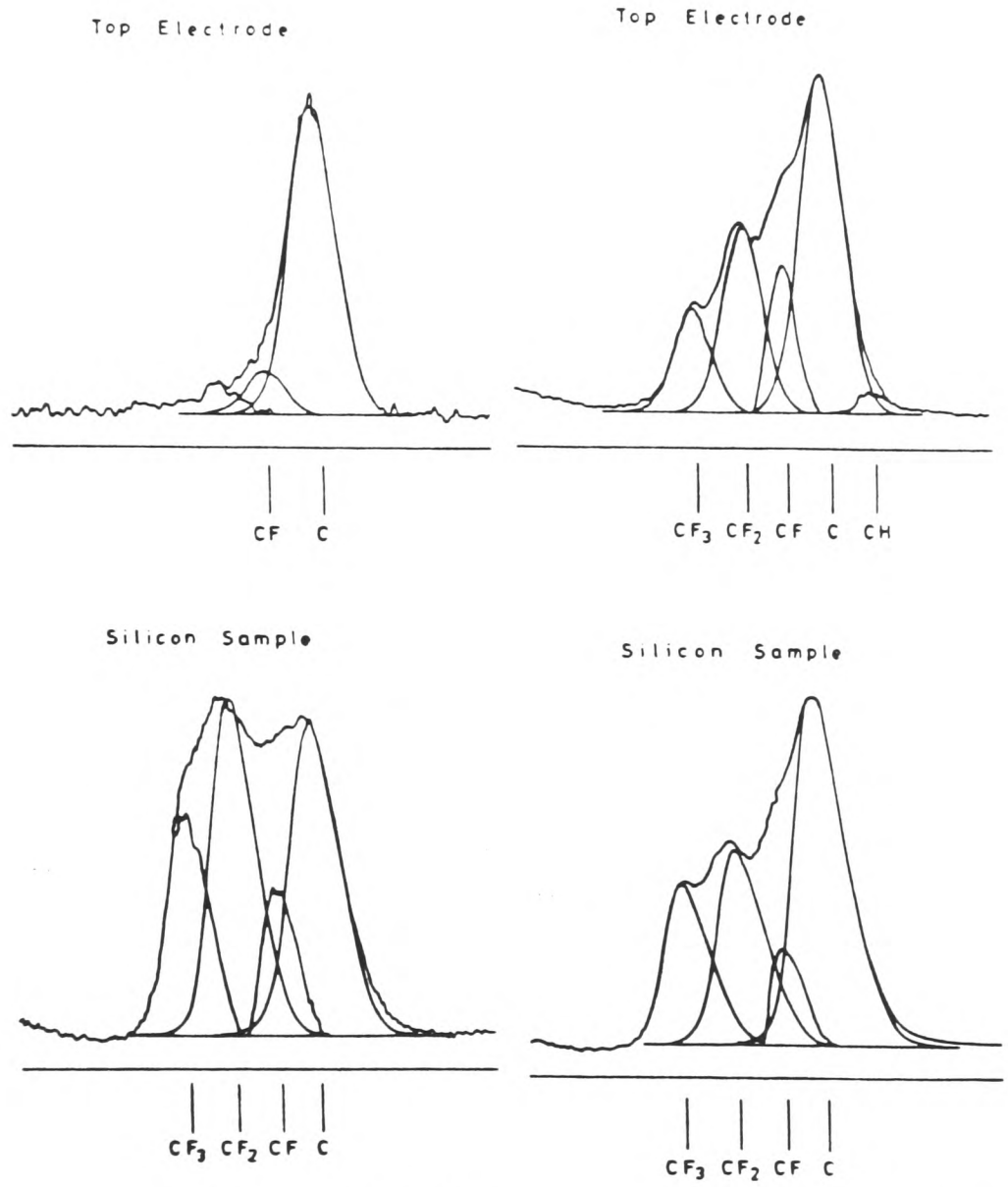

Figure 34.

XPS Results, C_3F_8, CHF_3.

The Carbon 1s spectra of both polymers show contributions from CF_3, CF_2, CF and C not directly bonded to fluorine. However the spectra of the polymer formed from C_3F_8 on the driven electrode is very different in nature from the material deposited on the water-cooled ground surface. On the driven electrode is found a dull black carbonaceous coating along with Al-F 21%-60%. The material on the grounded electrode is a light yellow material. This, when examined on the silicon specimen, is shown to have contributions from all four types of C_{1s} signal.

Gas used.	Top electrode.	Si sample.
C_3F_8		
F	60.7%	53.7%
C	12.4%	44.4%
O	5.9%	1.3%
Al	21.0%	0.5%
CF_3	----	1189
CF_2	1195.3	----
$C\text{-}CF_n$	1200.5	1193.1
CHF_3		
F	47.1%	51.3%
C	51.4%	47.8%
O	1.5%	0.8%
CF_3	1188	1187
CF_2	1190.3	1188.9
CF	1192.7	----
$C\text{-}CF_n$	1194.7	1193.3

Table 15.
% Element in film and C_{1s} peak position.

From CHF_3 plasmas on the other hand the spectra of the polymeric material formed on both surfaces is very similar. There is also a very much greater

contribution from the CF and CF_2 species indicating greater cross-linking and possibly longer chains than for C_3F_8 polymers. This is most likely due to ion bombardment induced cross linking in the polymer by elimination of HF. This is supported by the fact that the top driven electrode, which is subjected to the higher energy bombardment, has the %C > %F whereas the grounded surface has %C < %F as seen in Table 15.

4.1.2.3)ERDA.

Sample	Layer depth Å C	H	ETCH GAS
Si	$1.3x10^{16}$	$1.6x10^{16}$	CF_4
SiO_2	--------	--------	
Si	$3.2x10^{17}$	$2.3x10^{16}$	C_3F_8
SiO_2	$5.5x10^{17}$	$3.2x10^{16}$	
Si	$5.5x10^{17}$	$3.2x10^{16}$	CHF_3
SiO_2	$5.5x10^{17}$	$2.5x10^{16}$	

The relevant spectra are shown in Figure 35. Additional spectra were obtained from CHF_3 with the peaks in different locations due to a change in geometry. This was in an attempt to obtain a fluorine peak separated from the background noise. Also included is C_3F_8/H_2 (70%-30%). Elemental

concentrations could not be quantitatively obtained due to the very much thicker polymer films, since these were of unknown stopping powers.

Figure 35.

ERDA Results.

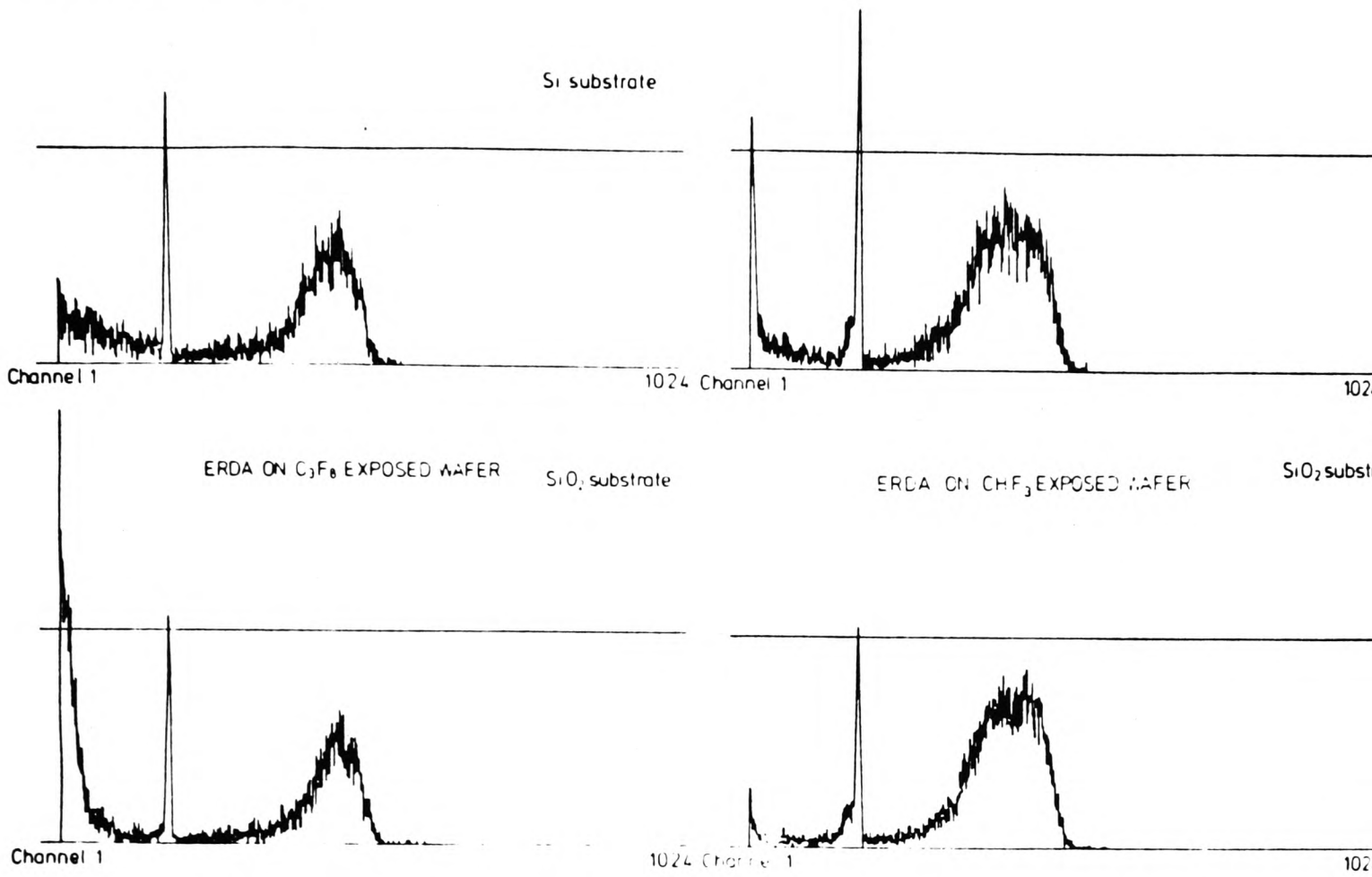

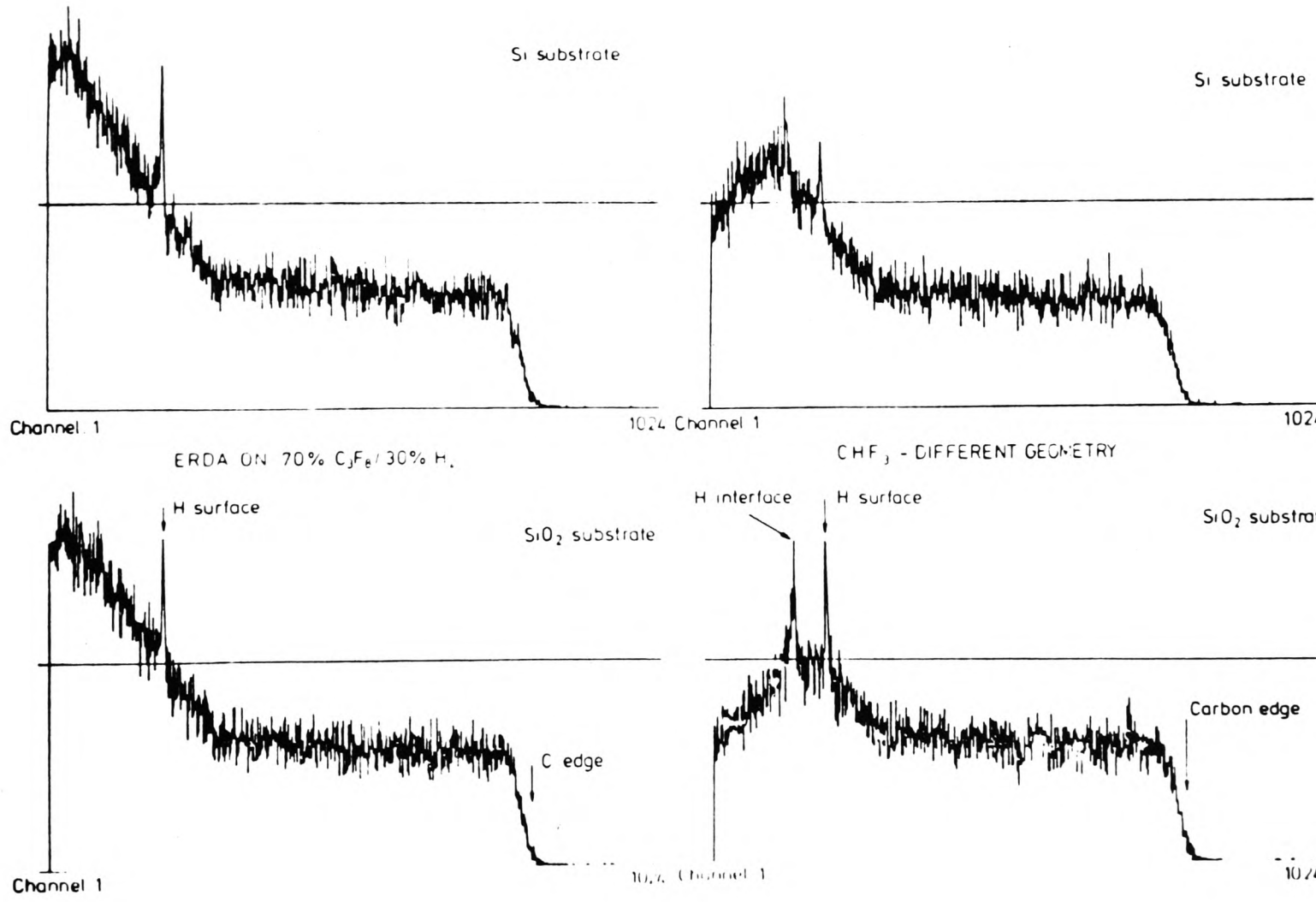

4.1.2.4)Rutherford Backscattering.

Overall the RBS spectra of all specimens exposed to CF_4 and C_2F_6 plasmas show that only thin films, heavily contaminated with the appropriate electrode material were formed. This was consistent with the quartz crystal microbalance data, as these gases do not form polymer to any significant extent, and the sputtering of electrode material is known to be the predominant characteristic. Thick polymer films were produced on the substrate surfaces exposed to C_3F_8 and CHF_3 plasmas, with much less metal contamination. The results are given for CF_4, C_2F_6, C_3F_8 and CHF_3 plasmas using Stainless Steel electrodes (Figure 36), and Titanium (Figure 37).

Sample.	"Fe" concn at surface atoms cm^{-2}. Si	SiO_2
CHF_3/Al	$< 10^{14}$	$< 10^{14}$
CHF_3/SS	$< 10^{14}$	7.0×10^{14}
CF_4/SS	4.2×10^{16}	3.3×10^{16}
C_2F_6/SS	1.5×10^{16}	1.4×10^{16}
C_2F_6/Al	1.2×10^{15}	1.8×10^{15}
C_3F_8/SS	#	#
C_3F_8/Al	$< 10^{14}$	$< 5 \times 10^{14}$
# - The polymer film is thick and contains "Fe" at about 0.2-0.3% of the fluorine concentration		

Gas comp	"Fe" concentration Si	SiO_2
CF_4	5.8×10^{16}	7.9×10^{16}
C_2F_6	2.1×10^{16}	2.2×10^{16}
C_3F_8	#	#
CHF_3	#	#
#- Little metal found in the film.		

Figure 36.

RBS results, St-St Electrodes.

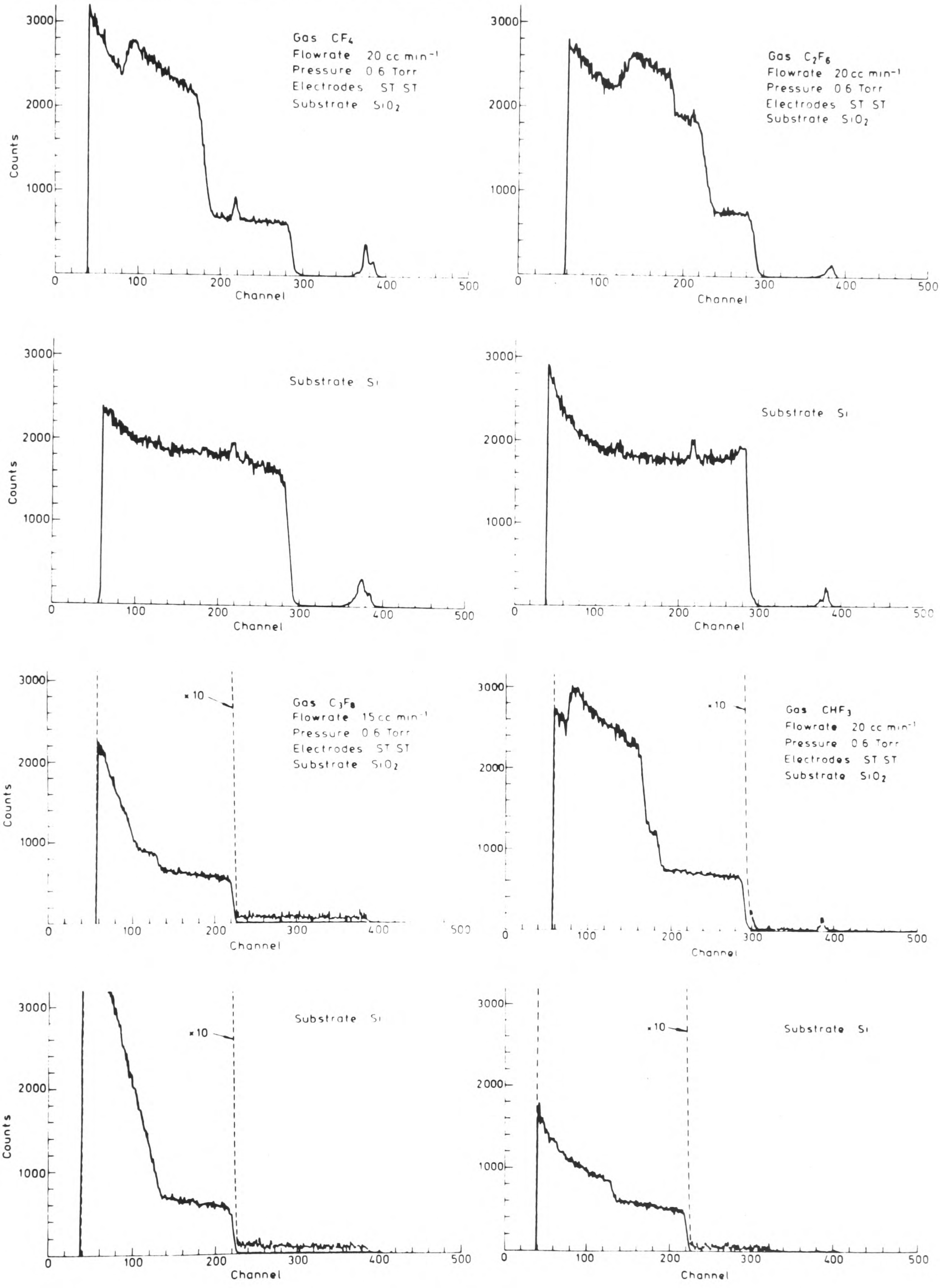

In the case of CHF_3 this is more than simple dilution effect for the Si surface. The SiO_2 surface on the other hand can be seen to be uncontaminated by polymer in most cases and is also thinner showing that SiO_2 etching has taken place. A graphical comparison of the amount of "Fe" (Fe,Ni,Cr) transferred from each of the four gases at 600mT with stainless-steel electrodes is shown in Figure 37. Comparison should be made with the CF_2 emission under the same conditions. The effect is underemphasised however by the fact that there is almost certainly a significant sputtered "Fe" contribution from the oxygen preclean plasma in each case. Thus the baseline is probably very near the top of the CHF_3 peak resulting in a greater ratio between the four results overall.

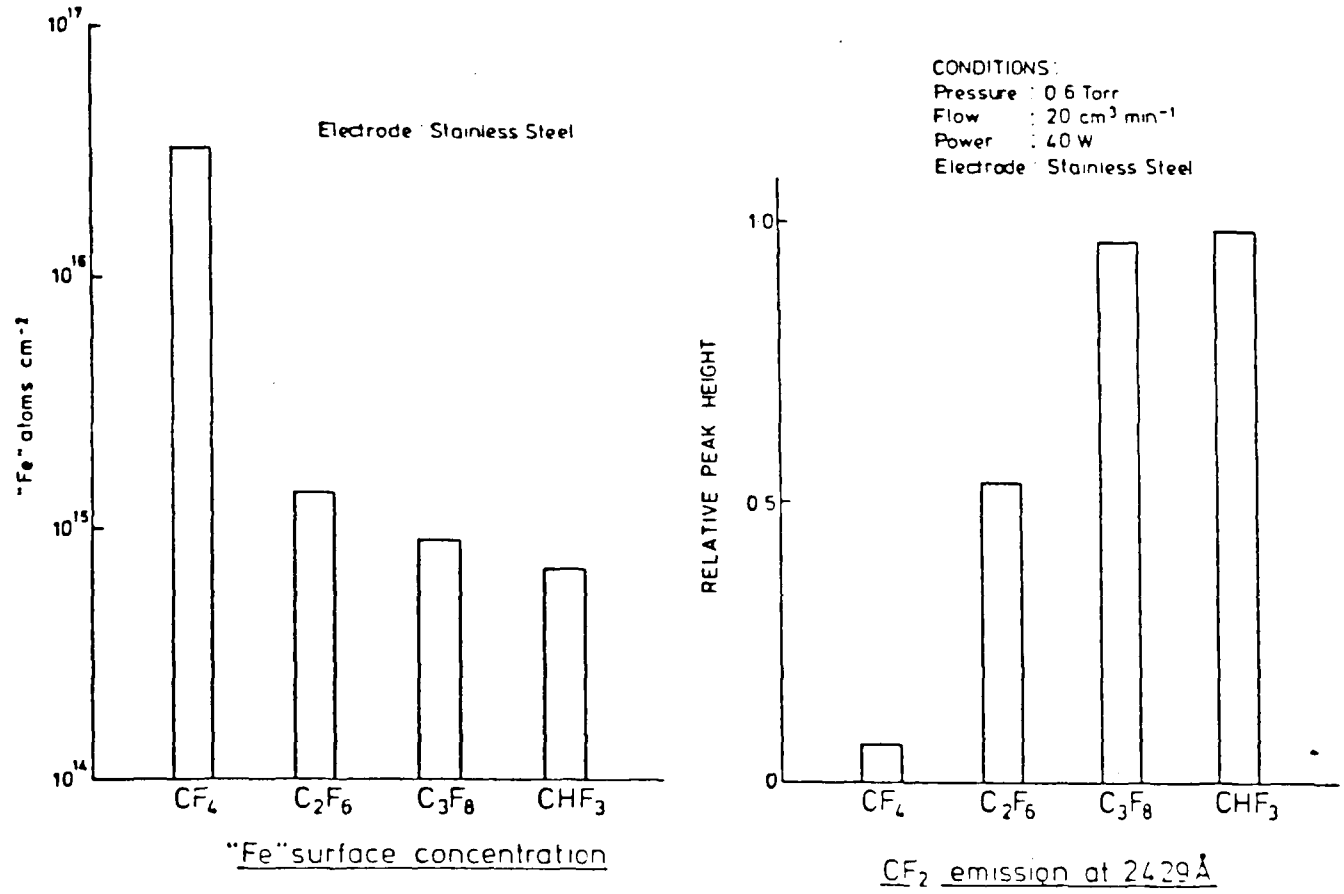

Figure 37.

RBS Results, Transferred "Fe".

Figure 38.

RBS Results, Ti Electrodes.

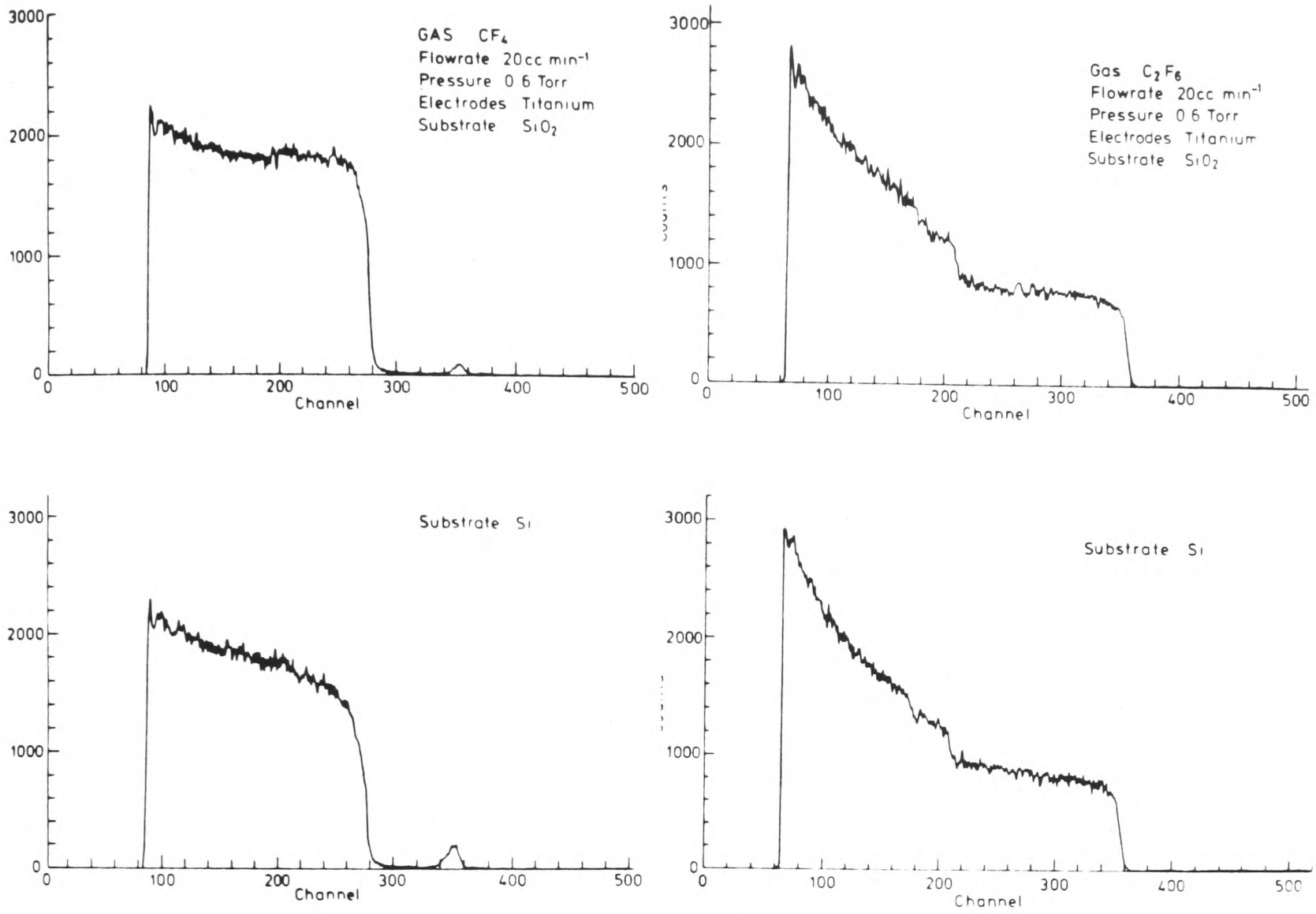

The anomalous behaviour of the Ti electrodes can again be seen.

4.1.2.5)Microscopy.

The Phillips SEM at Harwell was used to examine some commercial samples to see the effect of the polymer formation on some device wafers etched in a commercial machine. It was reassuring to see that both the etch profiles and the morphology of the polymers encountered occurred on the test samples etched in this apparatus. Figures 39 -41 show some of these features.

Using the Cambridge Stereoscan in I. & A. P., the surfaces of the four specimens from each of the pure gases was examined. These were all with Stainless-Steel electrodes at a pressure of 600mT. The specimens had to be gold coated due to the severe charging. The surface features shown are the regions: Masked Si/SiO_2, exposed Si/SiO_2 and the intersection of these two areas. Since small fragments of wafer were laid on top as a mask, in this case, the edge of the etch is somewhat diffuse. At very high magnifications a grassy surface was seen and it was possible to imagine a "Fe" signal from the tips, indicating sputtered electrode material was acting as a mask. These features were apparently much less in height than the expected etch depth since the etch would tend to undercut and break off the full height features.

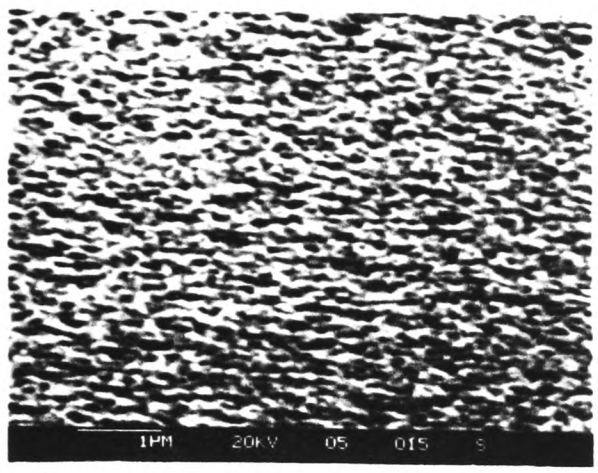

SiO_2

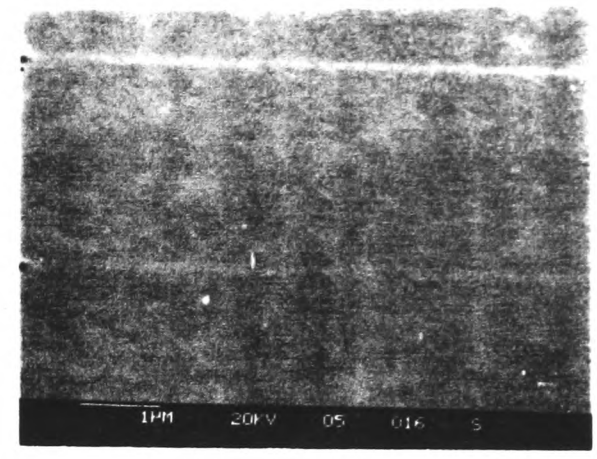

Plasma exposed

CF_4 **a**

'Clean'

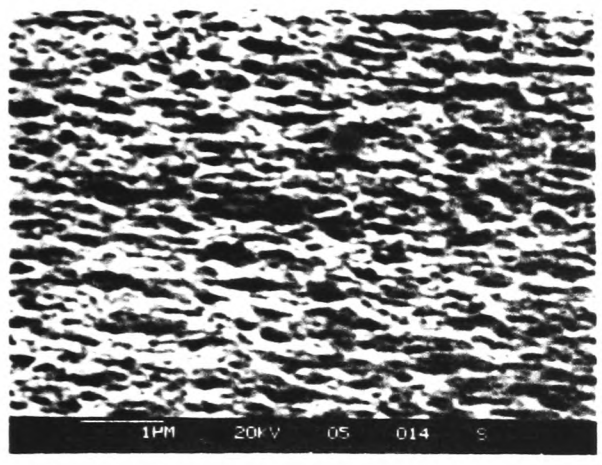

Si

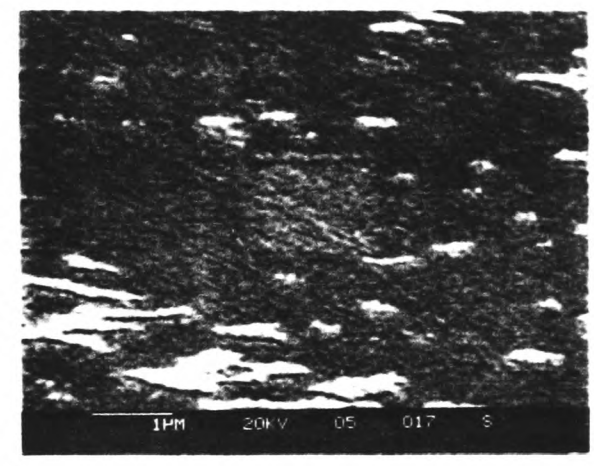

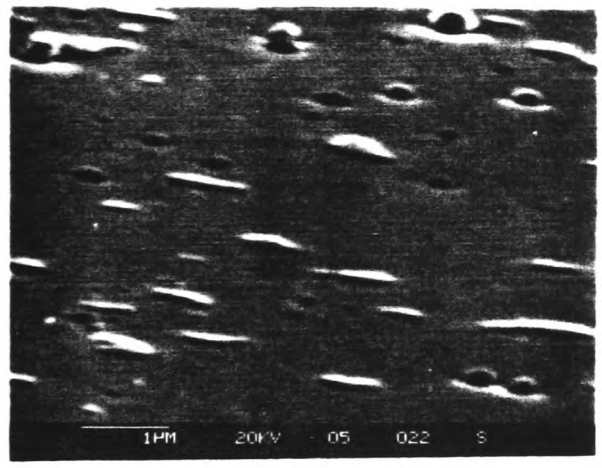

SiO_2

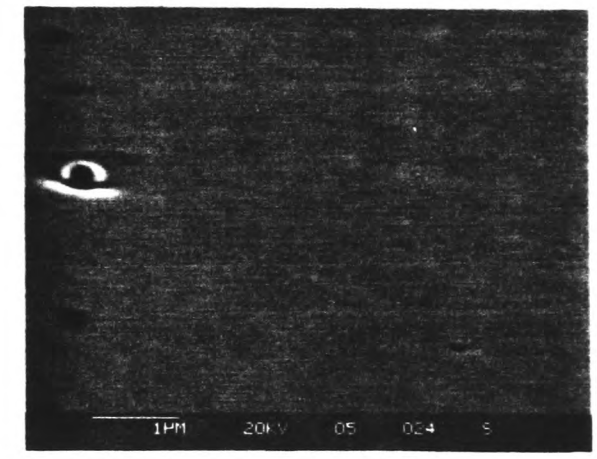

Plasma exposed

C_2F_6 **b**

'Clean'

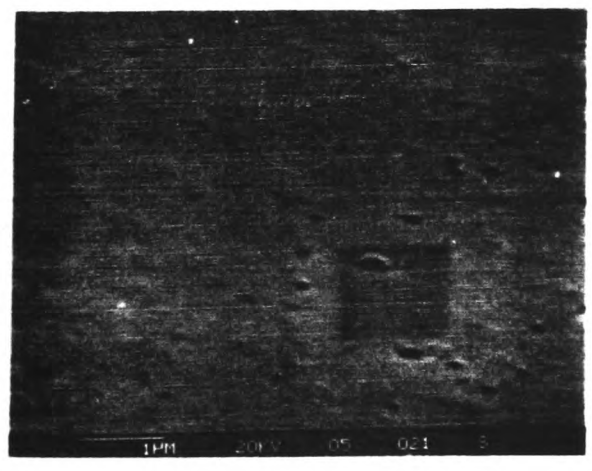

Si

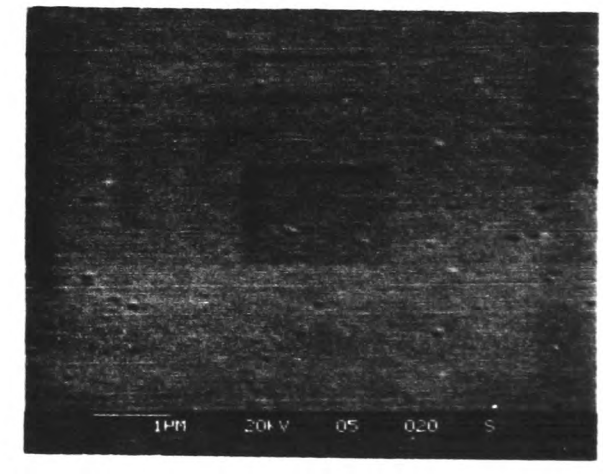

Fig 39

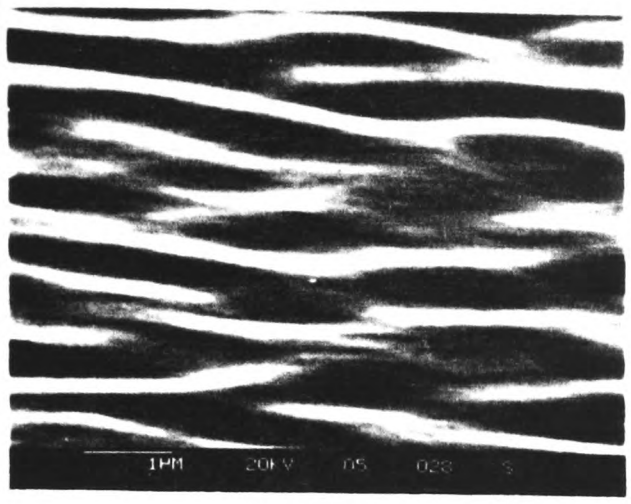

SiO_2

Plasma exposed

C_3F_8 **a**

'Clean'

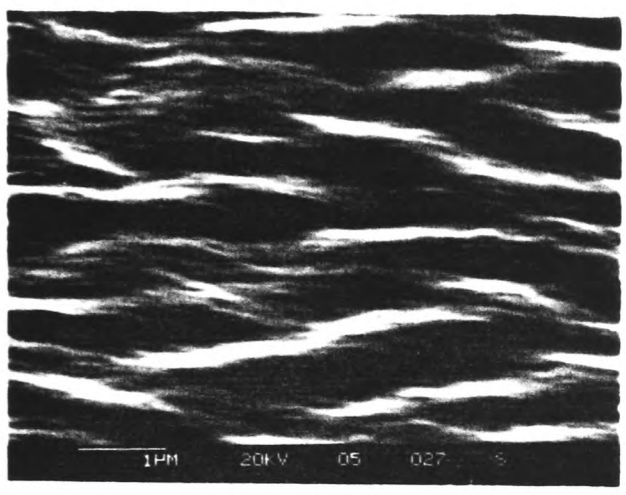

Si

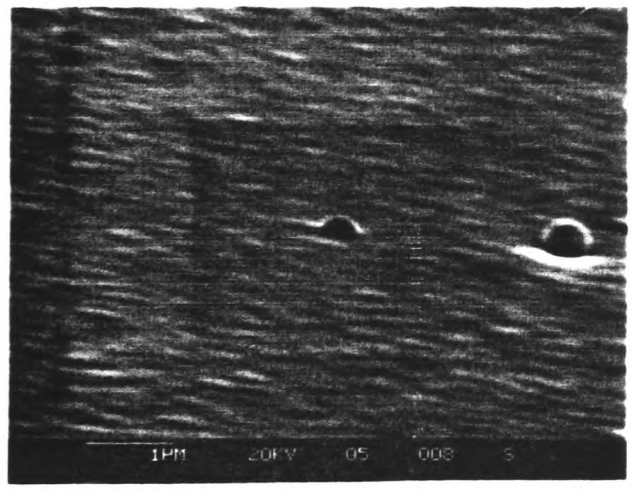

SiO_2

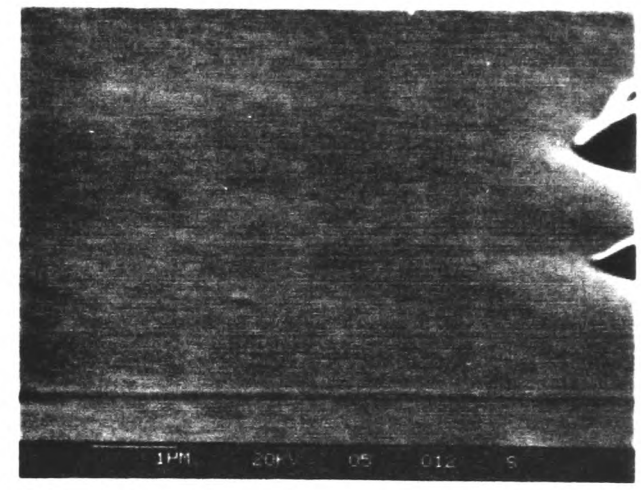

Plasma exposed

CHF_3 **b**

'Clean'

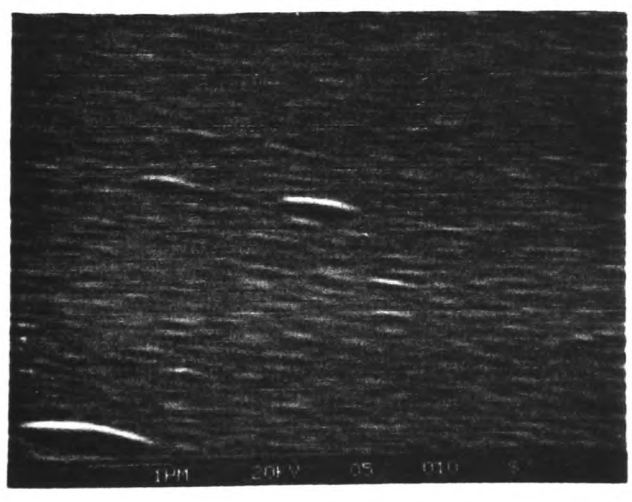

Si

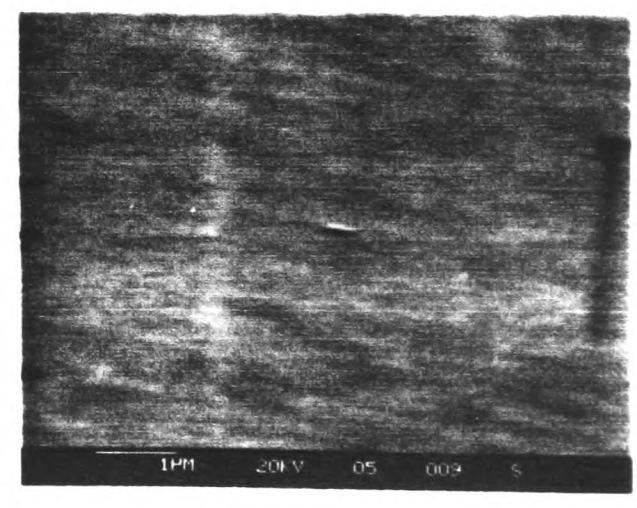

Fig 40

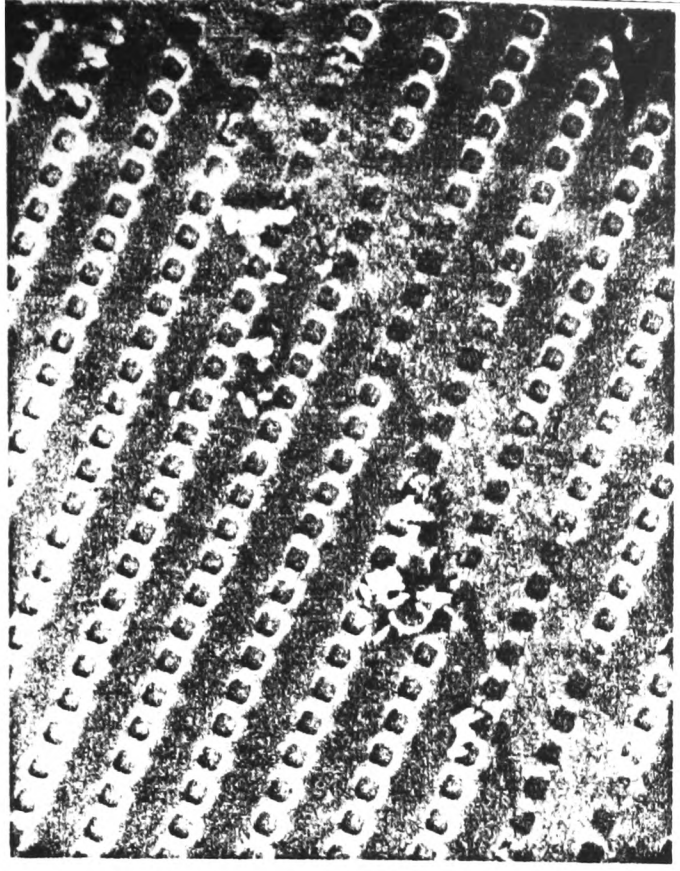

X640

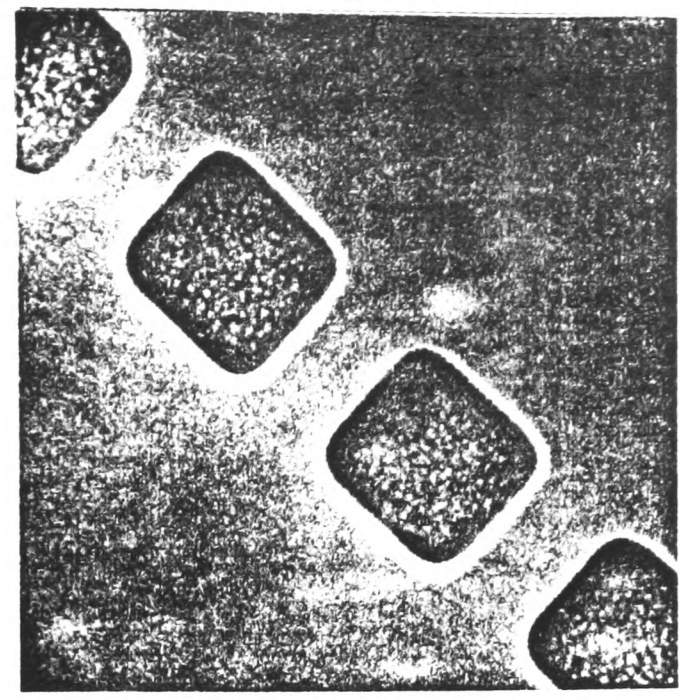

X5000

Commercial sample etched in

70% CF_4 , 30% H_2

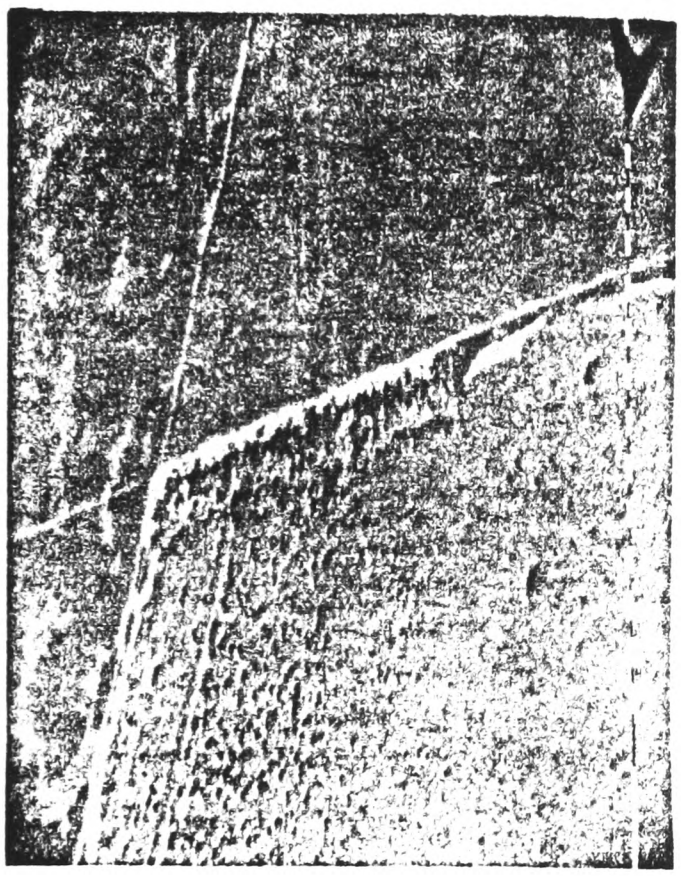

X320

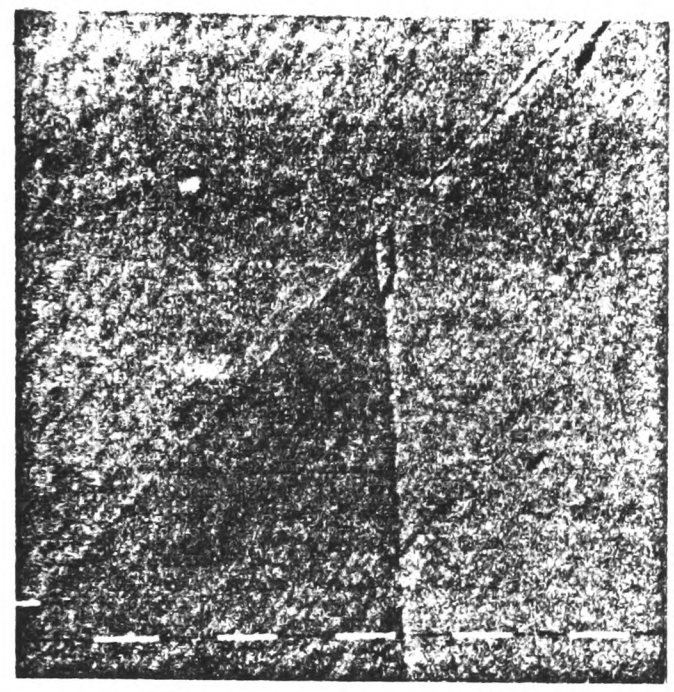

X80

Al | Si / SiO_2 interface

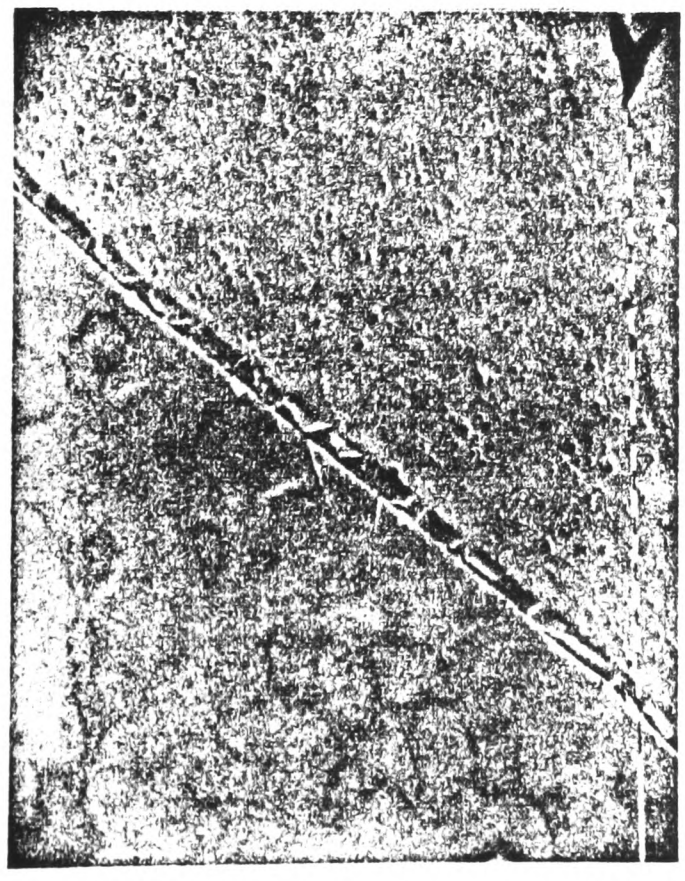

X640

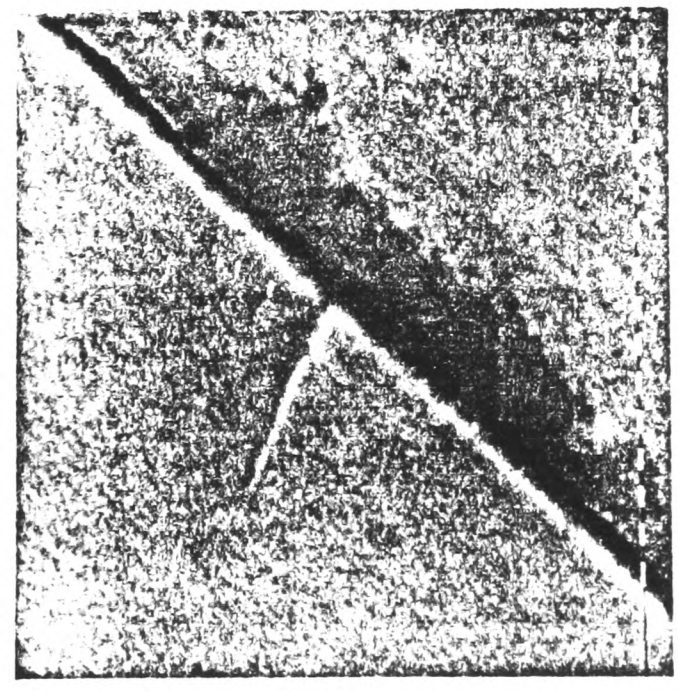

X640

Si/SiO_2 edge

FIG.**41** SEM PHOTOS OF POLYMER DEPOSITION

4.1.2.6)Infrared Studies of Polymers.

Transmission and some reflection spectra were recorded from 5mm diameter masked regions over the range 4000-200 cm^{-1} for CF_4 and CHF_3 exposed electrodes and samples to confirm the principle features of the polymer as suggested by XPS. Comparisons were made with reference spectra of a silicon wafer blank and again after coating with a fully fluorinated oil, Fluorolube. Also spectra were recorded of a 5 micron Teflon powder in a 16mm diameter KBr disc.

The results were encouraging so a more comprehensive set of transmission spectra were recorded directly from the films on the silicon wafers and also from the upper and lower electrodes after reflection from the metal substrates, (double transmission) for each of the four gases for different electrode materials. Further IR spectra were recorded from scrapings of the yellow deposit on the upper electrode when incorporated in KBr pellets. Vapours arising on vacuum pyrolysis of this deposit mixed with KBr were also examined in a 10cm pathlength, minimum volume cell.

Some IR results for pure gas fluorocarbon plasmas are shown in Figure 42 for Stainless-Steel electrodes, and Figure 43 for Titanium.

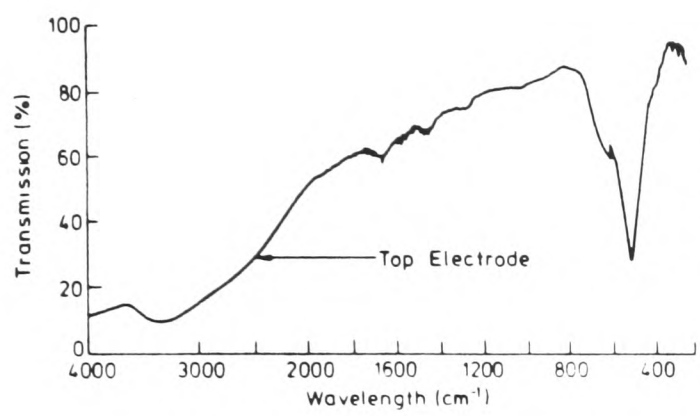

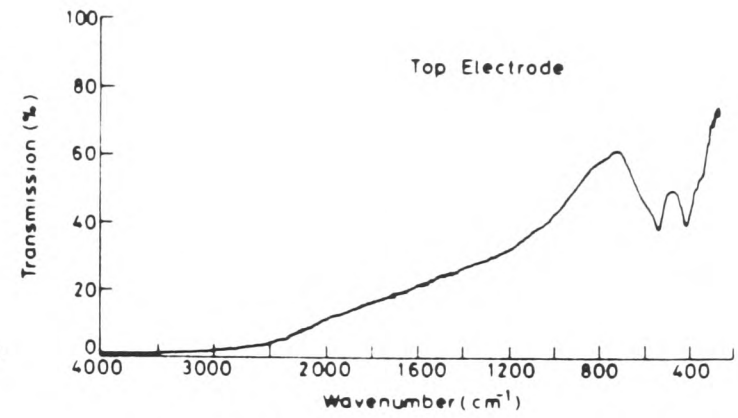

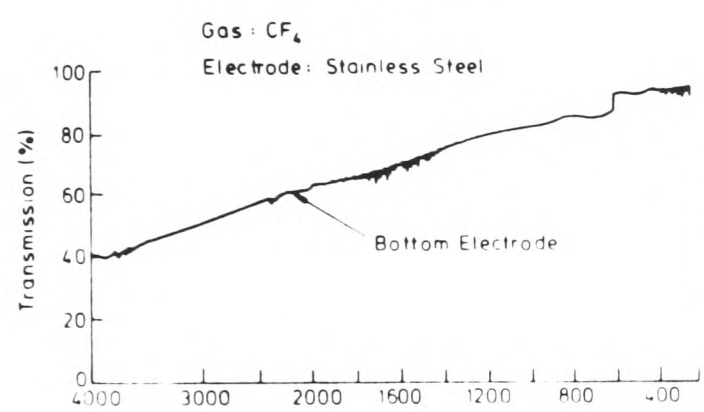

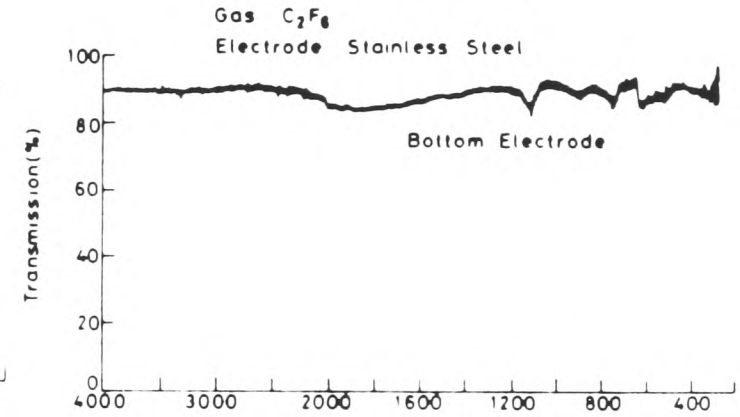

Figure 42.

IR Results Stainless-Steel.

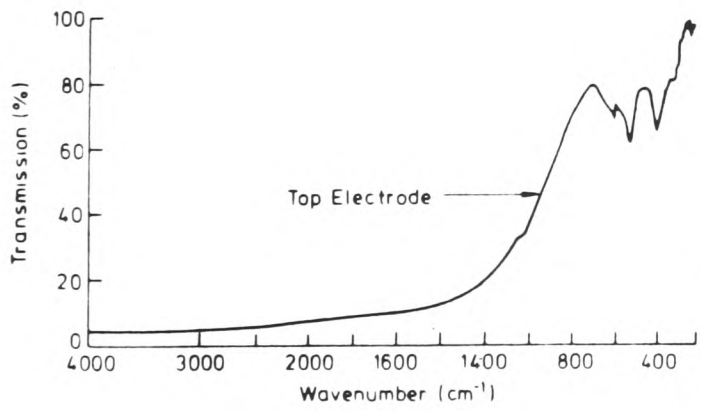

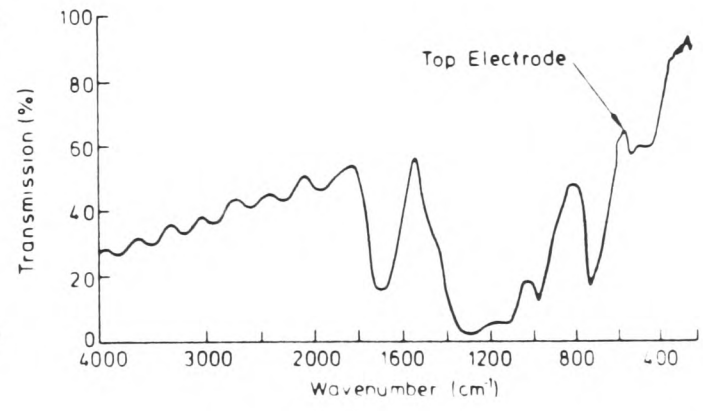

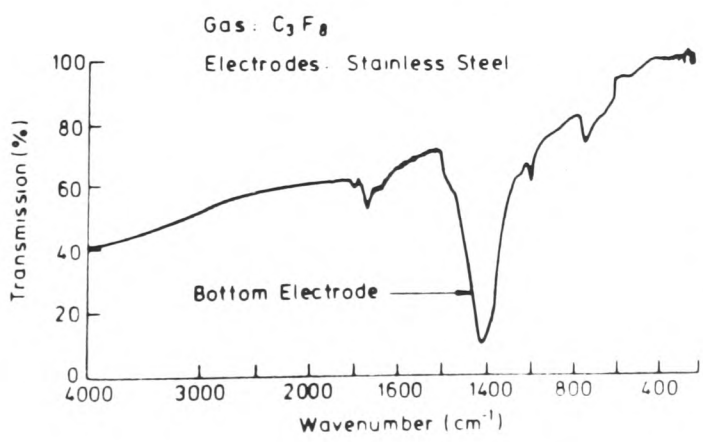

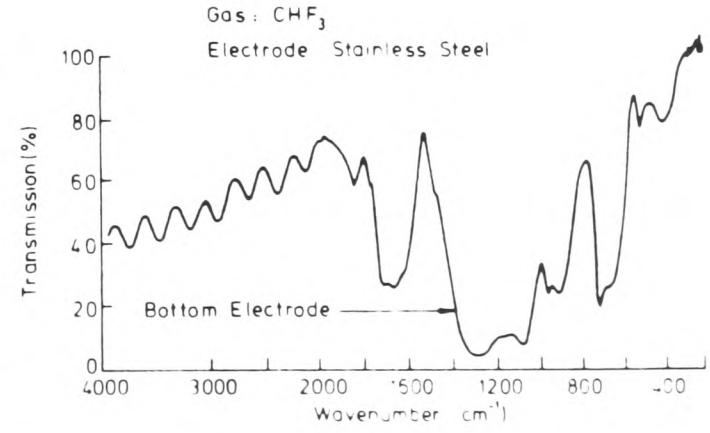

Figure 43.

IR Results Titanium.

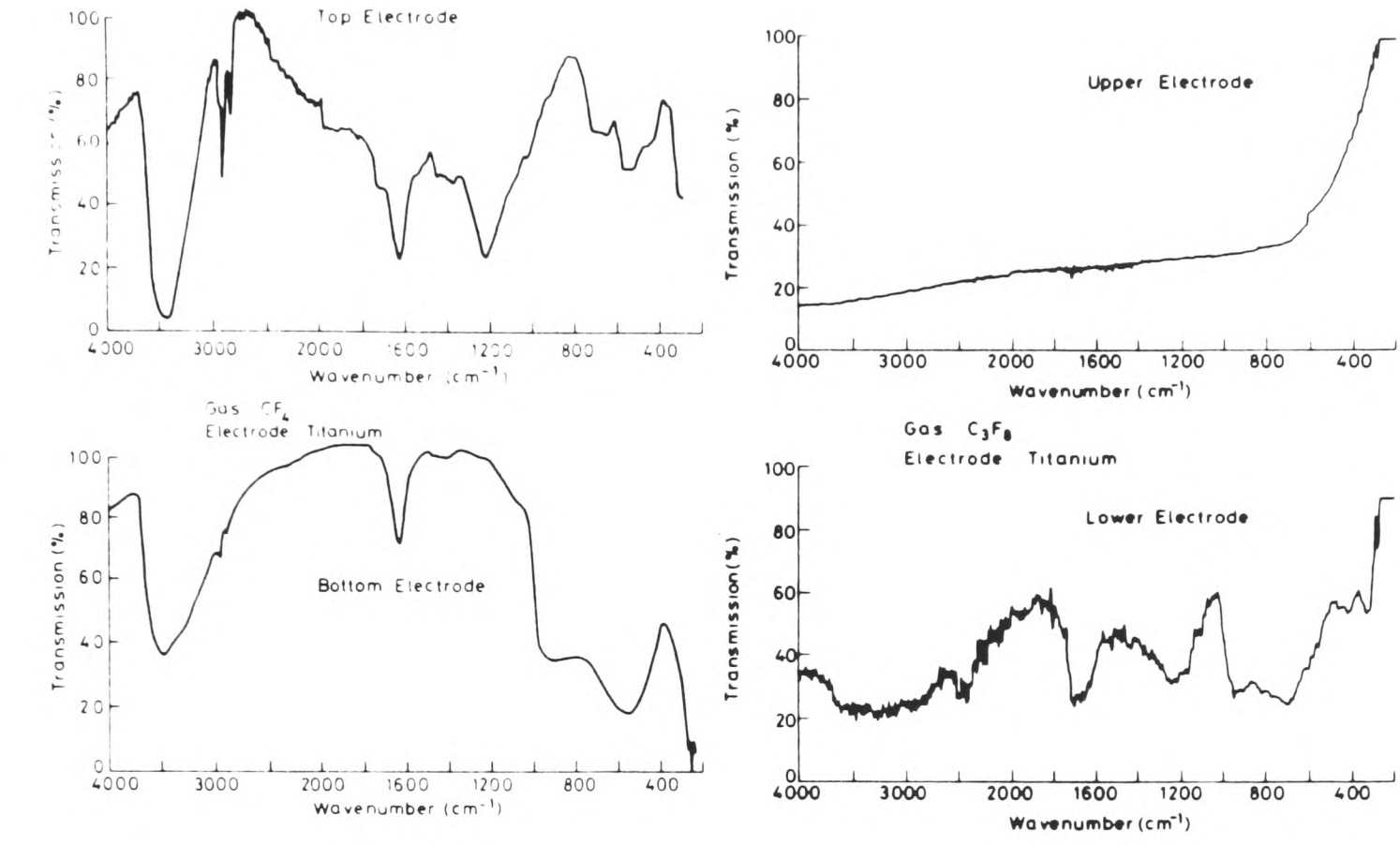

No evidence for polymeric material was found on either of the electrodes nickel, stainless-steel or aluminium in either CF_4 or C_2F_6 plasmas and the driven electrodes usually had traces of metal fluoride absorptions. This was most pronounced for stainless-steel with CF_4, and C_2F_6. These show a strong peak at ca.510cm^{-1} and 3300cm^{-1} due to water associated with the fluoride[477-478] after exposure to atmosphere. The spectra associated with the titanium electrodes show strong peaks due to the titanium oxyfluoride with traces of C-F absorptions. The unexpected appearance of the fluoropolymer is probably due to the scavenging effect of the titanium suppressing the back reaction between fluorine and "CF_2" on the electrode surface to reform the reactant gas mixture.

For C_3F_8 the top electrodes are characteristically 'clean' with traces of metal fluoride peaks in the regions seen for the CF_4, C_2F_6 spectra. However typical C-F stretching peaks could be seen in the film that has deposited on the bottom, grounded electrodes. These are at ca. 1230cm^{-1} for CF_3 and CF_2, 980cm^{-1} for isolated C-F, and 740cm^{-1} for CF-CF_3. The absorption near 1370cm^{-1} (shoulder on the 1230cm^{-1} peak) is tentatively assigned also to CF-CF_3. Possible unsaturation in the fluorocarbon film is consistent with the presence of the weak 1730cm^{-1} band (>C=F_2, -CF=CF_2 and -CF=CF- are possibilities). The increase in

polymer deposition as the pressure is lowered, as evidenced by the quartz crystal microbalance results for C_3F_8 (Figure 30), could also be seen by comparing C_3F_8/Ni (600mT) and C_3F_8/Ni (300mT). Again the Ti electrodes gave anomalous spectra. The driven electrode, though 'clean', showed no oxyfluoride bands but was etched, though to a far lesser extent than shown for the CF_4 and C_2F_6 discharges. This is consistent with the lesser amount of free fluorine present in C_3F_8 plasmas. The grounded Ti counter electrode showed both oxyfluoride and polymeric peaks. Material was scraped off this electrode and this spectrum is illustrated along with the similar transmission spectrum from the silicon wafer. This was done because the IR spectra are clearer than those of the electrodes, which were complicated by the uneven deposit formed.

The spectra of the films on the electrodes from CHF_3 plasmas were surprisingly similar to each other and also to the material formed on the grounded electrode from C_3F_8 discharges, with very little C-H present in the film. This was despite the differences revealed by XPS. The 1230cm^{-1} band is broadened by the enhanced 1370cm^{-1} CF-CF_3 due to greater cross-linking, and the 1720cm^{-1} 'unsaturation band' is also stronger. Virtually complete suppression of free fluorine is indicated by the Ti spectrum being closely related to those obtained from the other electrode materials Ni,

Stainless-Steel and Al. However the hydrolysis peaks are still in evidence. There is also proportionately greater unsaturation and cross-linking in the polymer film due to loss of fluorine from the growing film from bombardment induced HF formation and the generation of TiF_4.

A comprehensive search of the IR reference library failed to produce anything near the spectra obtained, but some common features were found with:

1. PTFE

2. Vinylidine fluoride - hexafluoropropylene copolymer:

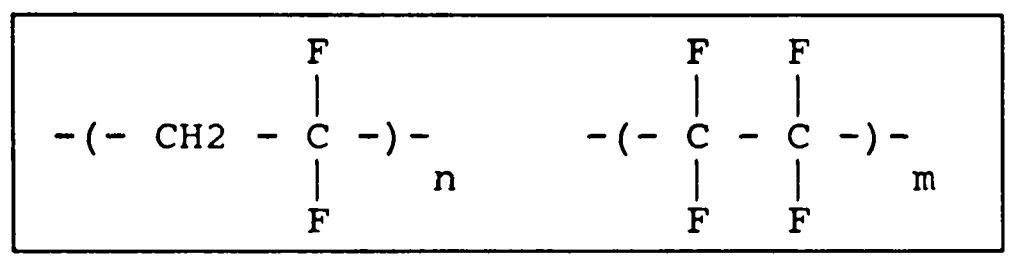

This polymer has been observed before as a result of pyrolysis of C_2F_4 and decomposition of various fluorocarbon gases in the presence of a catalytic platinum filament{477}.

A copy of the spectrum of the scrapings from the top stainless-steel electrode, run in CHF_3 at 600mT, was submitted to Mond Research Services (ICI) for comparison with their reference collection. They reported sodium hydrogen fluoride as the likely major component.

Checking with a reference spectrum of $NaHF_2$, and also KHF_2 did not support this interpretation. Also $NaHF_2$ and KHF_2 are both water-soluble with densities greater than 2, and the film scrapings were found to float on water and were obviously insoluble. Little solubility could be obtained on boiling with aqua regia and ICP analysis failed to detect significant amounts of metallic elements. LECO analysis for carbon on a small amount of sample indicated its presence as a major component[480].

4.1.2.7)Thermogravimetric Analysis.

When sufficient material could be obtained, scrapings of the polymer film from electrodes or the chamber walls were analysed to obtain some insight into the thermal stabilities of the materials that could be formed in an R.F. discharge.Samples were analysed under the following standard conditions: ca. 10mg sample, with a heating rate of $20^{o}C\ min^{-1}$ and an air flow of $10cc\ min^{-1}$. Standard samples run for comparison purposes included PTFE, PVDF (Polyvinyldifluoride $-(CH_2CF_2)_n-$), PFA (Perfluoroalkoxy-teflon), Polythene, and FEP 140 (Hexafluoropropylene).

Sample	Major peak temp		Minor peaks.	
PTFE	560°C	93.2%	520°C	23.2% (s)
PTFE **L**	575°C	78.8%	560°C	66.8%
PTFE **M**	550°C	96.0%	520°C	22.2% (s)
PFA	550°C	82.0%	525°C	a46.0% (s)
Polythene	350°C	71.6%	530°C	2.0%
PVDF	470°C	>100.0%	545°C	9.2%
FEP-140	505°C	73.8%	565°C	64.0%
CHF_3 Top	370°C	53.6%	435°C 30%, 635°C 10%	
" Bott	330°C	45.6%	225°C	a16.0% (s)

(s) -Shoulder on main peak, (a) -About
L -Low molecular weight material
M -Medium molecular weight material

These results are illustrated in Figure 44, and include the weight losses for CHF_3 derived polymer run with Al electrodes. Care had to be taken not to scape off metal from the electrodes as this will cause a loss in sensitivity as a certain fraction of the mass, corresponding to the metal, will not change weight except by oxidation. The overall shift of decomposition temperature that would be expected if the top electrode was at an elevated temperature can be clearly seen in the shape of the envelope. Extra thermal stability is also gained due to cross linking of the polymer on the driven electrode.

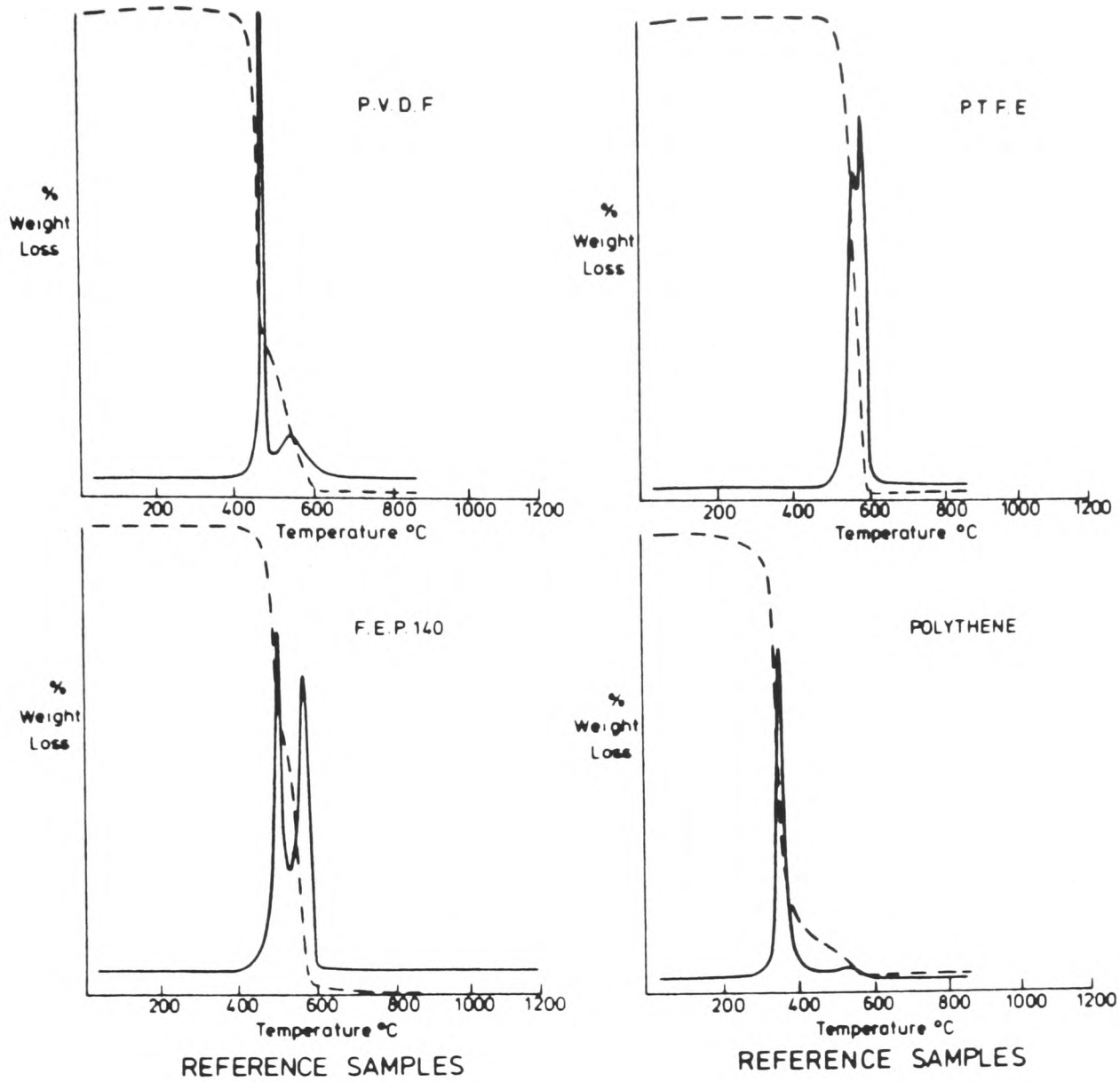

Figure 44.

TGA Results.

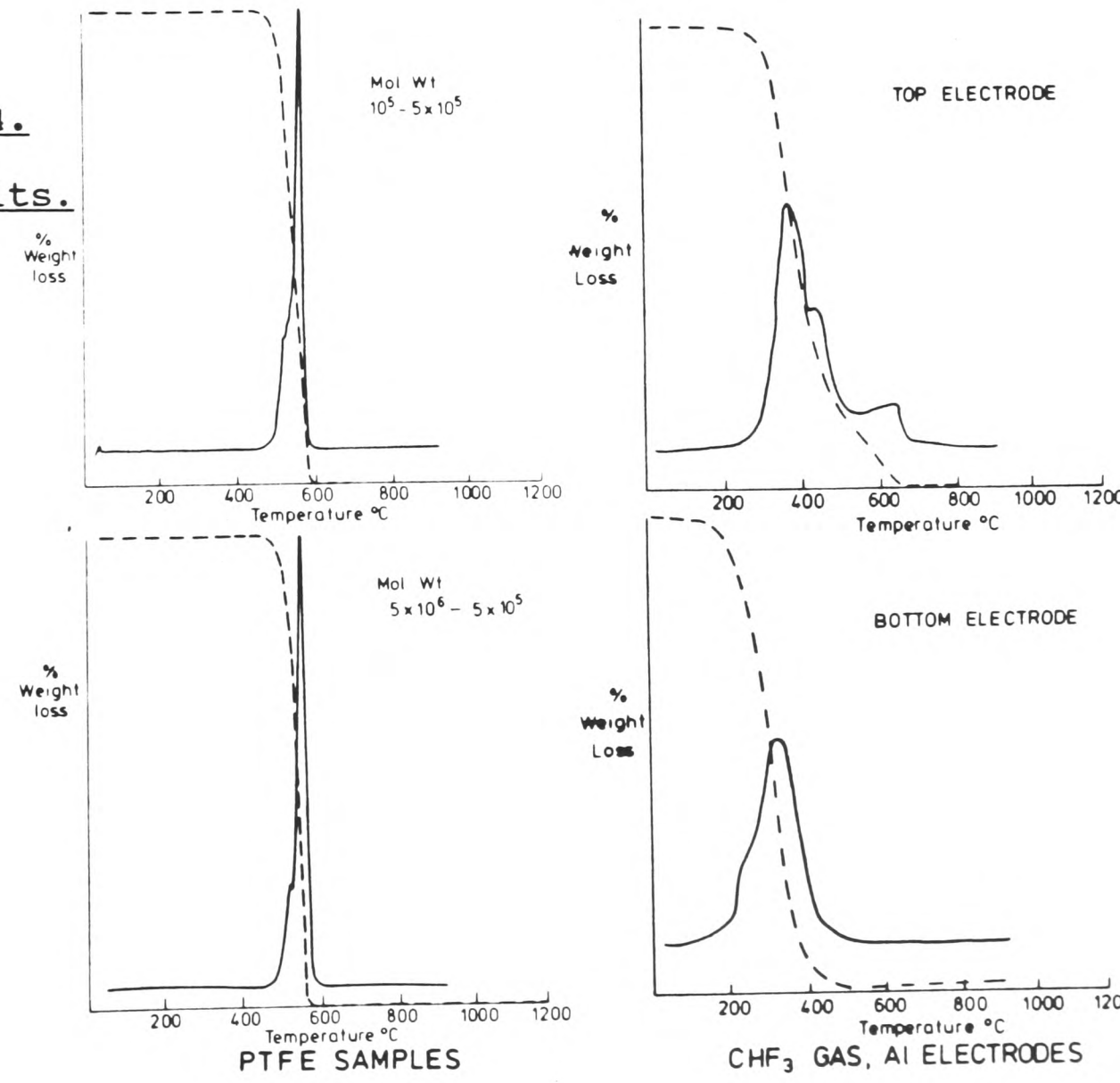

4.1.3)Interim Summary -Pure Gases.

Before discussing the fluorocarbon with hydrogen plasma measurements, it can be seen that the different techniques give a very consistent series of results. Variations in the rates of deposition from the pure gas plasmas can be correlated with the breakdown schemes proposed in "5.2 Thermodynamic calculations." and the separate studies done with a mass spectrometer. For CF_4 and C_2F_6, the dominant processes are the formation of the etching species $CF_3\cdot$ and F by ion bombardment. For C_3F_8 and particularly CHF_3 the generation of species for formation of the polymer precursors is the most favorable.All of this behaviour is predicted by the F : C model. Though optical emission monitors excited CF_2 and not the ground state, it can still be seen that there was a close correlation between the rate of polymer formation and the CF_2 intensity as illustrated for the three main electrode materials used. It should be borne in mind though, that CF_2 is still not necessarily the actual polymer precursor. Of most interest from these pure gas depositions was the fact that C_3F_8 polymer deposition was strongly dependent on the chemical nature of the electrode material used, as discussed further in the next section "Electrode effect $-C_3F_8$".

The second effect, particularly noticeable in the RBS spectra of Si and SiO_2 surfaces exposed to CHF_3 discharges, was the preferential polymer formation on the Si surfaces compared to the SiO_2 for most of these runs. This can be seen in the different positions of the Si 'edge' when comparing SiO_2 with Si substrates.

Overall the material from C_3F_8 plasmas appears to be thermally unstable, or easily degraded by ion bombardment. This can be seen in that the top driven electrode material remains exposed. The predominant mechanism for stabilisation of the CHF_3 derived material is cross-linking of the chains by radiation induced elimination of HF. This is feasible due to the intense UV radiation generated by the discharge. This would account for the only minor differences between the material from the driven and ground electrodes for CHF_3, which would not be found for a predominantly ion-induced polymerisation reaction.

4.1.3.1)Electrode Effect- C_3F_8.

This is due to formation of an unstable polymeric material which can deposit on the water-cooled ground surfaces, but is unable to remain on the driven electrode which is subjected to energetic ion bombardment among other processes. This ion bombardment causes ion-enhanced fluoridation and physical sputtering of both metal and the consequent metal fluorides. This material arriving at the grounded surface can act as a catalytic chain initiators for the $(CF_2)_n$ species found. However the overall 'electrode effect' is a combination of several factors of varying importance:

1. Ease of formation of a protective layer on the electrode, e.g. Fluoride or a stable polymer film.

2. Rate of sputtering of the metal.

3. Rate of sputtering/decomposition of the fluoride/polymer.

4. Catalytic activity of the metal.

5. Catalytic activity of the metal fluoride.

Hence even if a parent material is known to be catalytically active this could be masked if the fluoride, for example, was easily formed and had a low sputtering rate. The low rate of formation of polymer using Fecralloy electrodes is most likely due to case 1., the ready formation of an inert alumina/aluminium fluoride surface layer.

With the XPS data showing that the degree of cross-linking in the polymer derived from CHF_3 was very much greater than that from C_3F_8, when comparing material deposited on the grounded Si in both cases, it is proposed that this was due to ion-enhanced elimination of HF to give a highly cross-linked material. This is supported also by the low component of CH in the same XPS C-1s spectrum. This effect is even more pronounced on the driven electrode as the energies of the ions striking the surface are greater, but the effect of the elevated temperature must also be considered.

4.1.3.2)Substrate Effect- CHF_3.

This effect has been observed before, and explained as being due to the reaction of the forming polymer film with oxygen from the SiO_2 lattice, giving rise to products such as COF_2 and CO. As already stated, this reaction could be followed by monitoring 483.5nm CO^*. This leaves a fresh damaged Si surface with plenty of reaction sites since oxygen is missing from the lattice. Fluorine atom attack is then more favorable, till the oxygen atoms of the underlying SiO_2 lattice are once more exposed for the cycle to repeat itself. Thus this effect is enhanced in low C:F ratio etching gases where polymer forms easily, but is not

found for mixtures where the polymer forming species are suppressed i.e. CF_4/O_2. With excess polymer formation this effect will be suppressed by the inability of the ion bombardment to remove the film sufficiently quickly.

In the case of the Si surface there is no corresponding mechanism for removal of the growing polymer film, thus the surface tends to become protected against chemical attack.

4.2)Runs With Fluorocarbon/Hydrogen Mixes.

Following the study on the deposition rates from the series CF_4, C_2F_6, C_3F_8 and CHF_3, the effects of the addition of hydrogen to these fluorocarbon plasmas was investigated. This concentrated primarily on C_3F_8/H_2 and to a lesser extent on CF_4/H_2. It was hoped that the C_3F_8/H_2 gas mixtures would lead to the same type of behaviour and generate polymeric material with the same characteristics as that from CHF_3. The CF_4/H_2 plasmas were examined to observe the effect of suppressing the F atom concentration, and to study the reactions of a commercial etching mixture with a known high selectivity.

These experiments were performed by establishing a gas composition using the three channel mass flow controller and allowing it to equilibrate for quarter of an hour before striking the plasma. Microbalance frequency readings were then taken every quarter of an hour until a linear increase in weight, as measured by the change in frequency, was obtained. The cycle was then repeated for the next ratio of halocarbon to hydrogen. By using this method neither the chamber or optical system was disturbed for the duration of the run.

A few measurements were also made with mixtures of CF_4/H_2 with inert gases to investigate changing the electrical characteristics of the discharge and are noted at the end.

4.2.1)Results From Rig.

4.2.1.1)Quartz Crystal Microbalance.

The result of an increasing percentage of hydrogen in a CF_4 plasma was found to lead to an abrupt change from an etching plasma to one that deposits polymer easily. This has a maximum effect up to 10% added H_2 after which the increase in rate lessens. The optical emission from CF_2^* also passes through a maximum at the same percentage of hydrogen as given by the microbalance results.

With the C_3F_8/H_2 gas mixtures no limit could be found for the increase in rate of polymer deposition up to 50% H_2. There were problems in that the rates of deposition from C_3F_8 plasmas were already high and the increase soon swamped the available range of frequency of the Quartz crystal microbalance. similarly there was no clear maximum to the CF_2^* emission.

The results for CF_4/H_2, C_2F_6/H_2, and C_3F_8/H_2 mixtures are illustrated in Figure 45. Some sample CF_4/H_2 with inert gas results are also given.

Figure 45. H_2 Addition Deposition Rates.

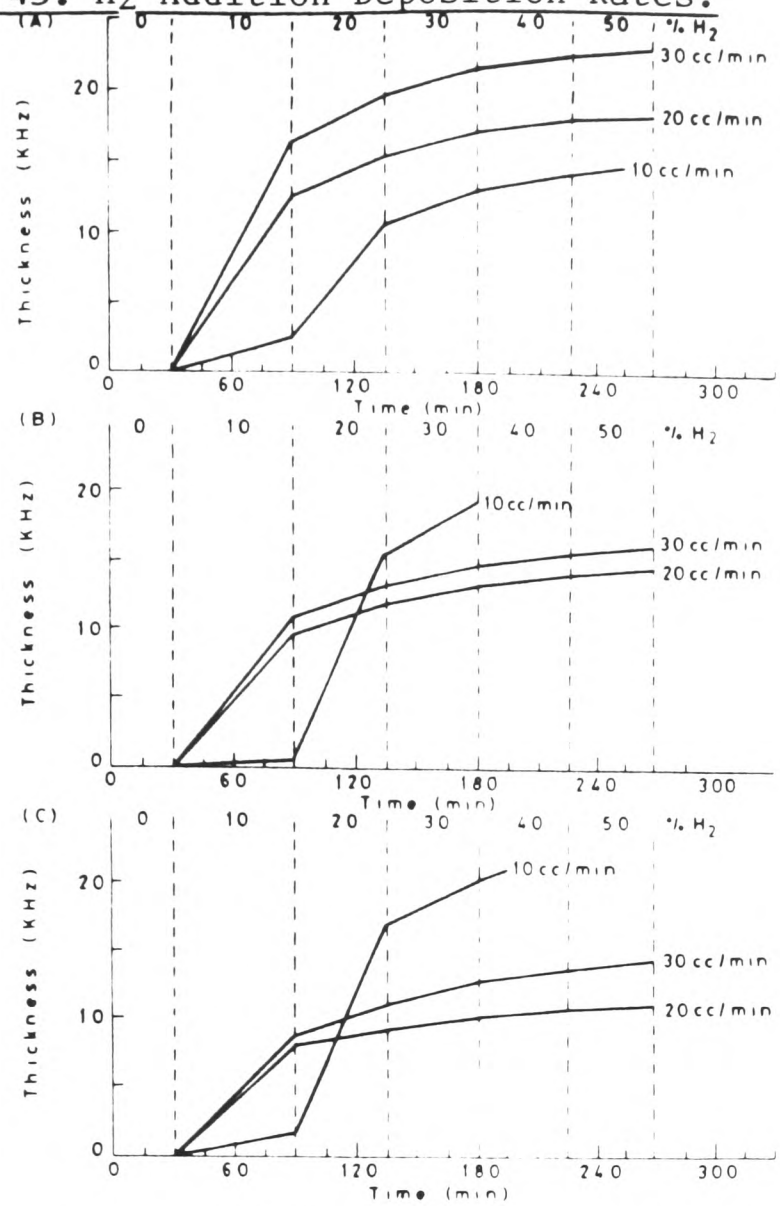

CF_4/H_2 polymer deposition with flow rates of 30, 20 and 10 cc/min at 0.6T and 40 W power (A) Nickel (B) Stainless Steel (C) Aluminium

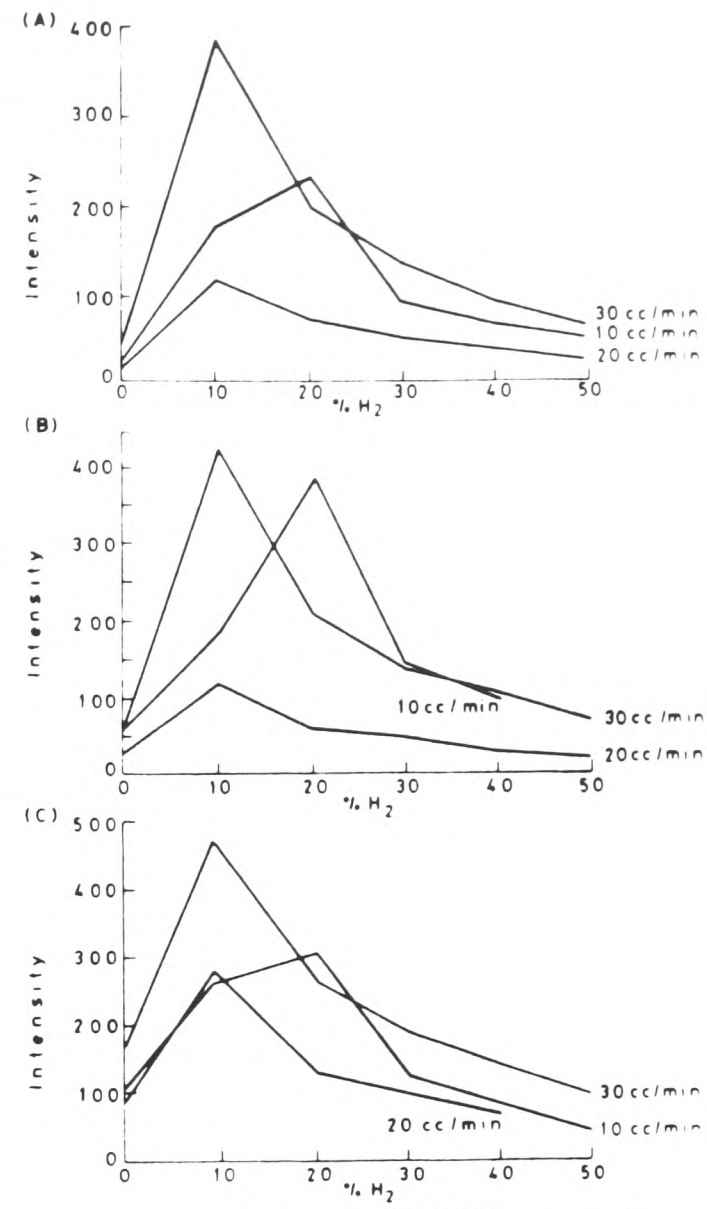

CF_4/H_2- CF_2 (2490 Å) emission intensities with flow rates of 30, 20 and 10 cc/min at 0.6T and 40W power (A) Nickel (B) Stainless Steel (C) Aluminium

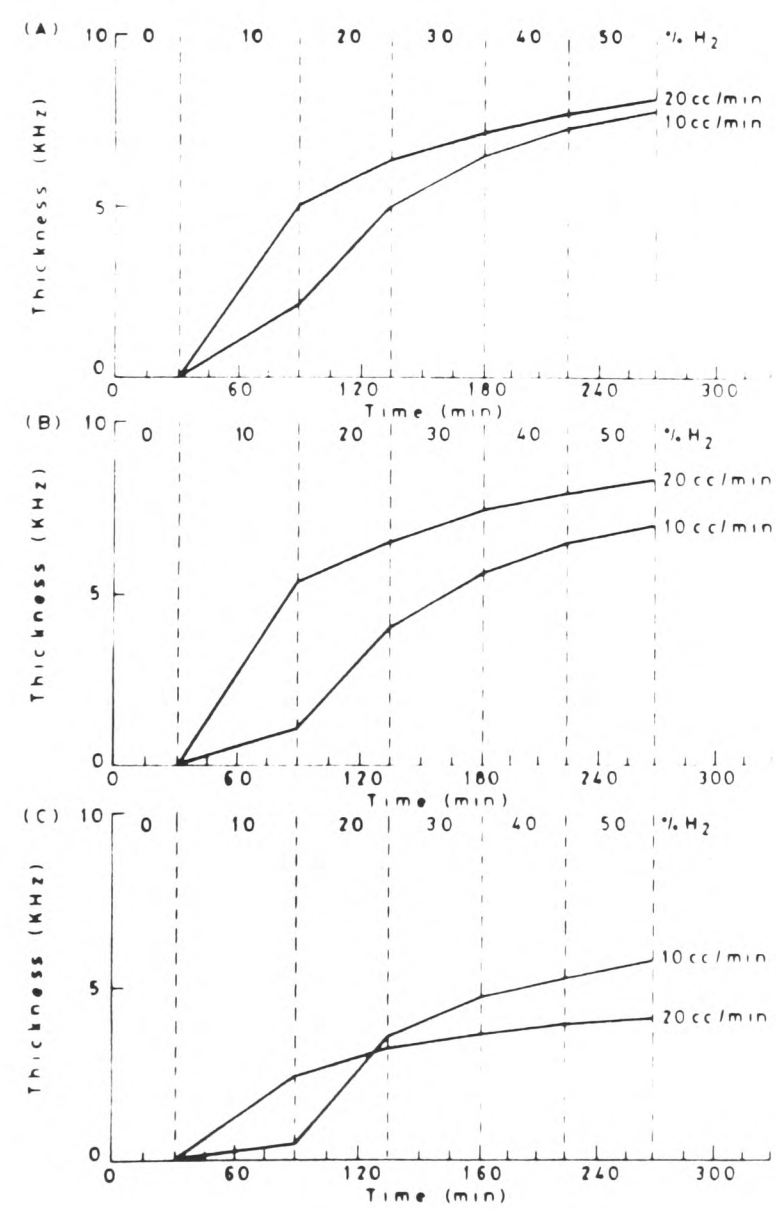

CF_4/H_2 polymer deposition with flow rates of 20 and 10 cc/min at 0.3T and 40W power. (A) Nickel (B) Stainless Steel (C) Aluminium

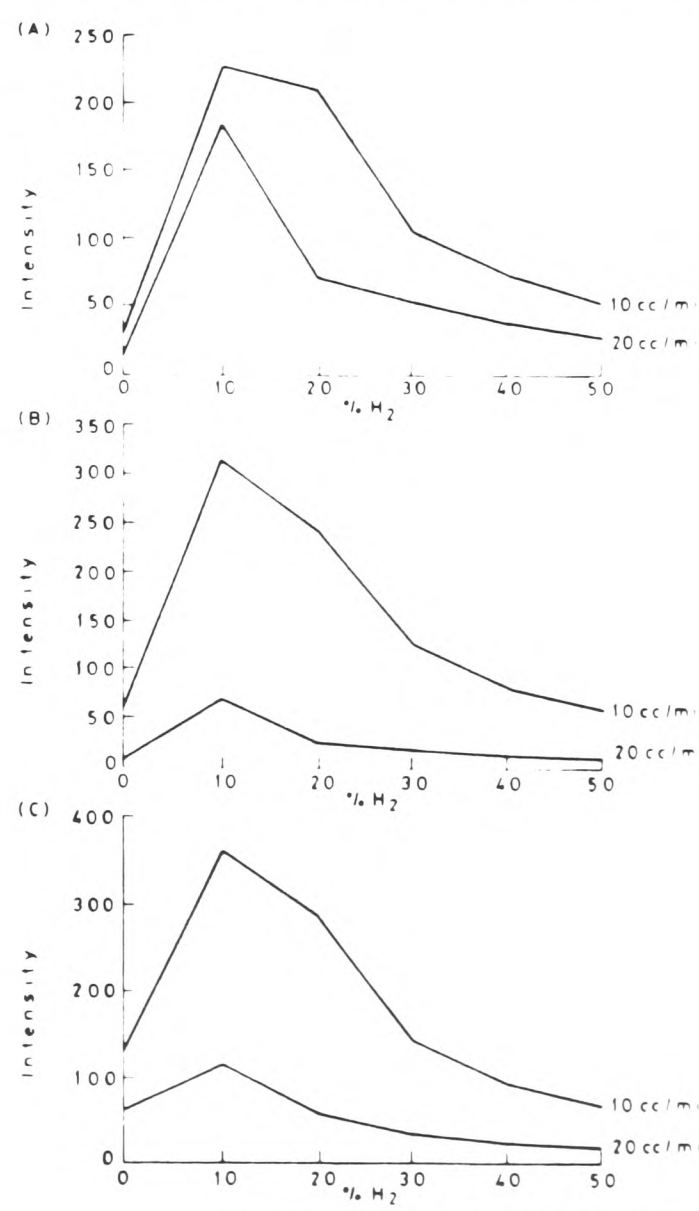

CF_4/H_2-CF_2 (2490 Å) emission intensities with flow rates of 20 and 10 cc/min at 0.3T and 40W power (A) Nickel (B) Stainless Steel (C) Aluminium

Figure 46. H_2 Addition Deposition Rates.

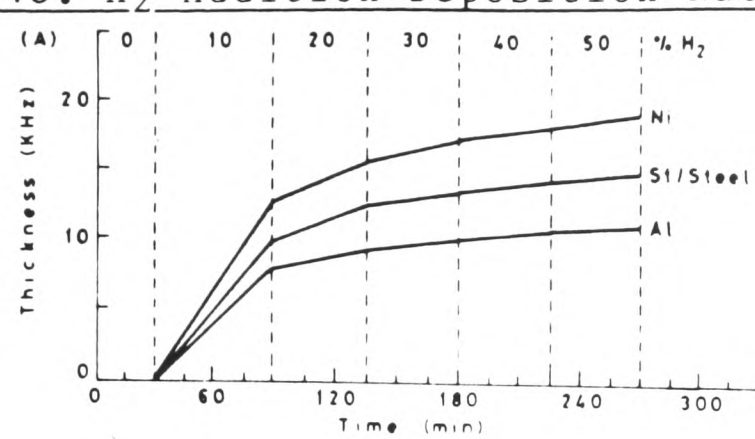

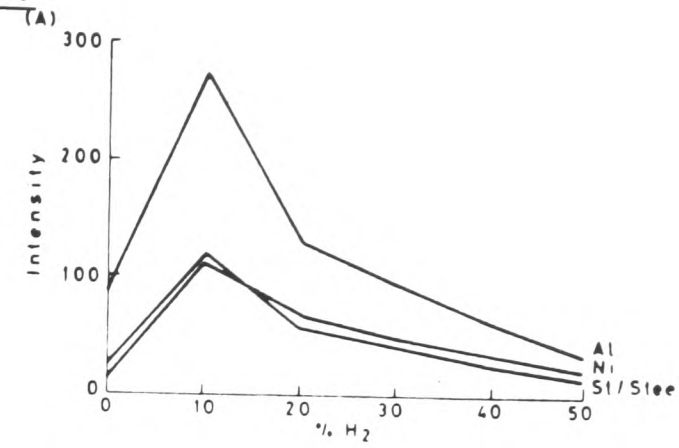

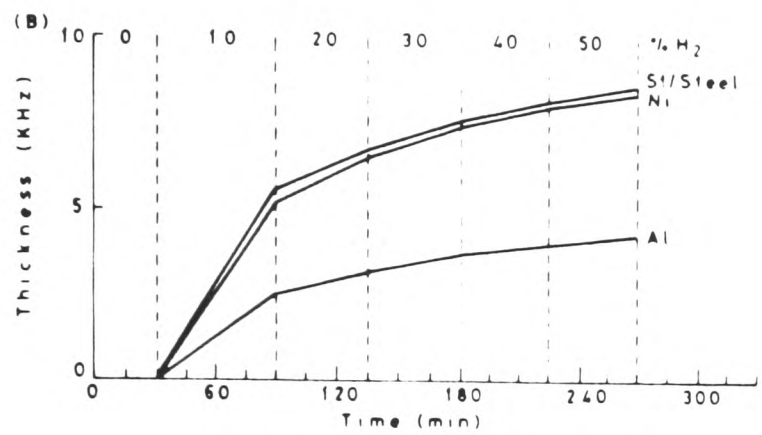

CF_4/H_2 polymer deposition on nickel, stainless steel and aluminium electrodes with a flow rate of 20 cc/min and 40W power (A) 0·6T (B) 0·3T

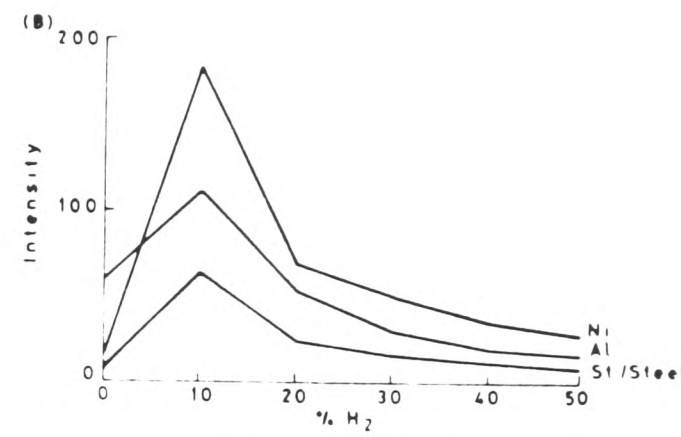

CF_4/H_2-CF_2 (2490Å) emission intensities for nickel, stainless steel and aluminium electrodes with a flow rate of 20 cc/min and 40W power (A) 0·6T (B) 0·3T

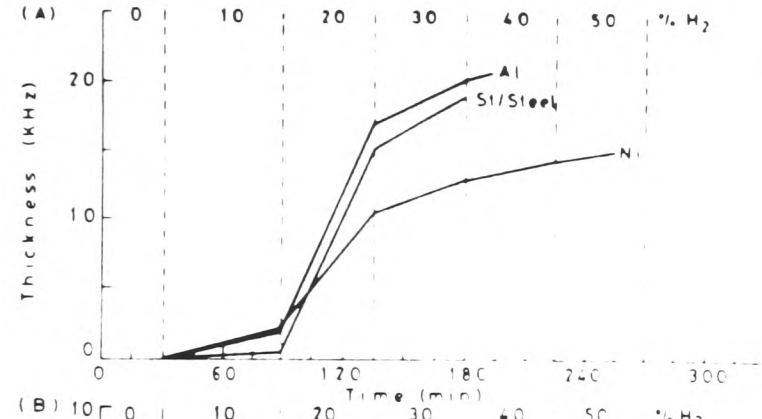

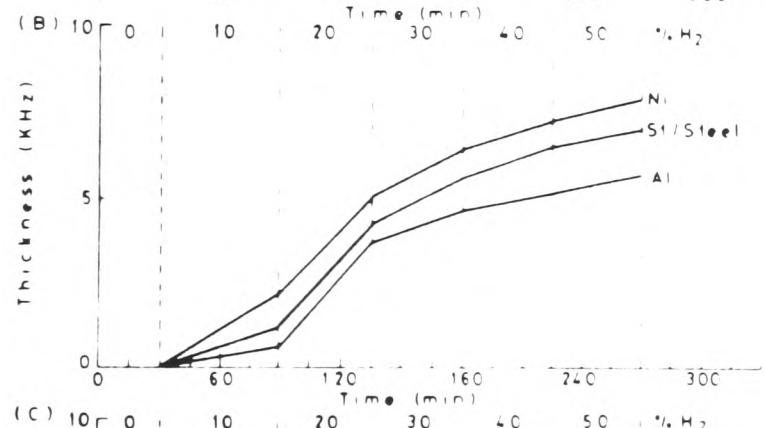

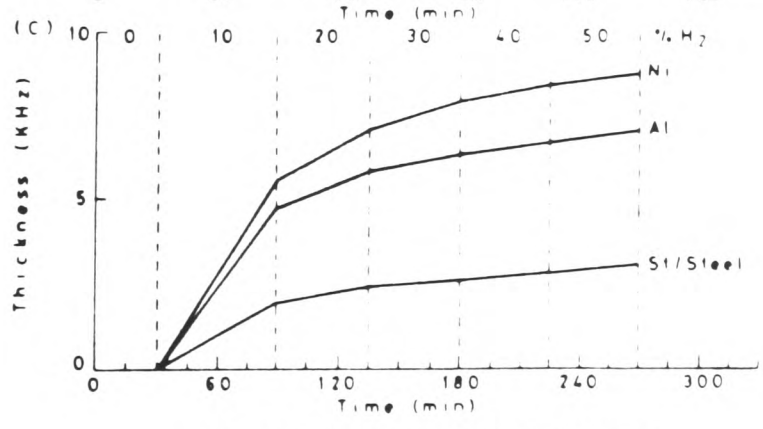

CF_4/H_2 polymer deposition on nickel, stainless steel and aluminium electrodes with a flow rate of 10 cc/min and 40 W power (A) 0·6T (B) 0·3T (C) 0·2T

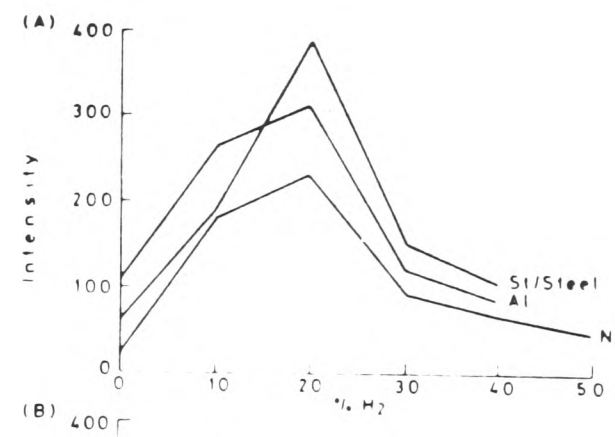

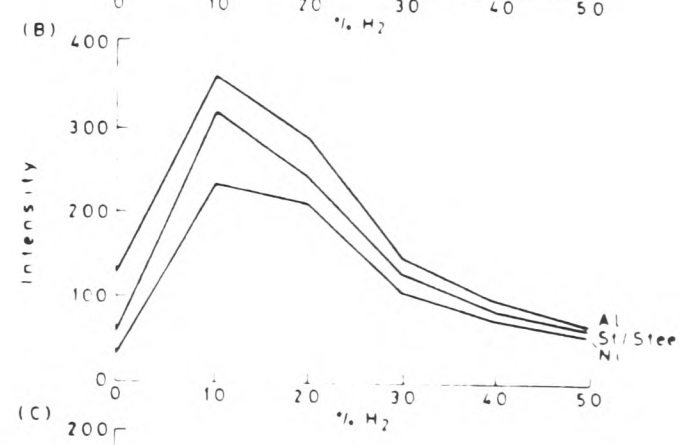

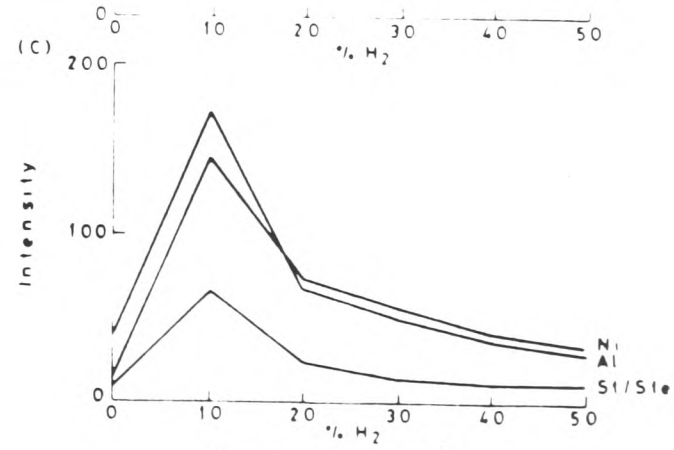

CF_4/H_2-CF_2 (2490Å) emission intensities for nickel, stainless steel and aluminium electrodes with a flow rate of 10 cc/min and 40W power (A) 0·6T (B) 0·3T (C) 0·2T

Figure 47. H_2 Addition Deposition Rates.

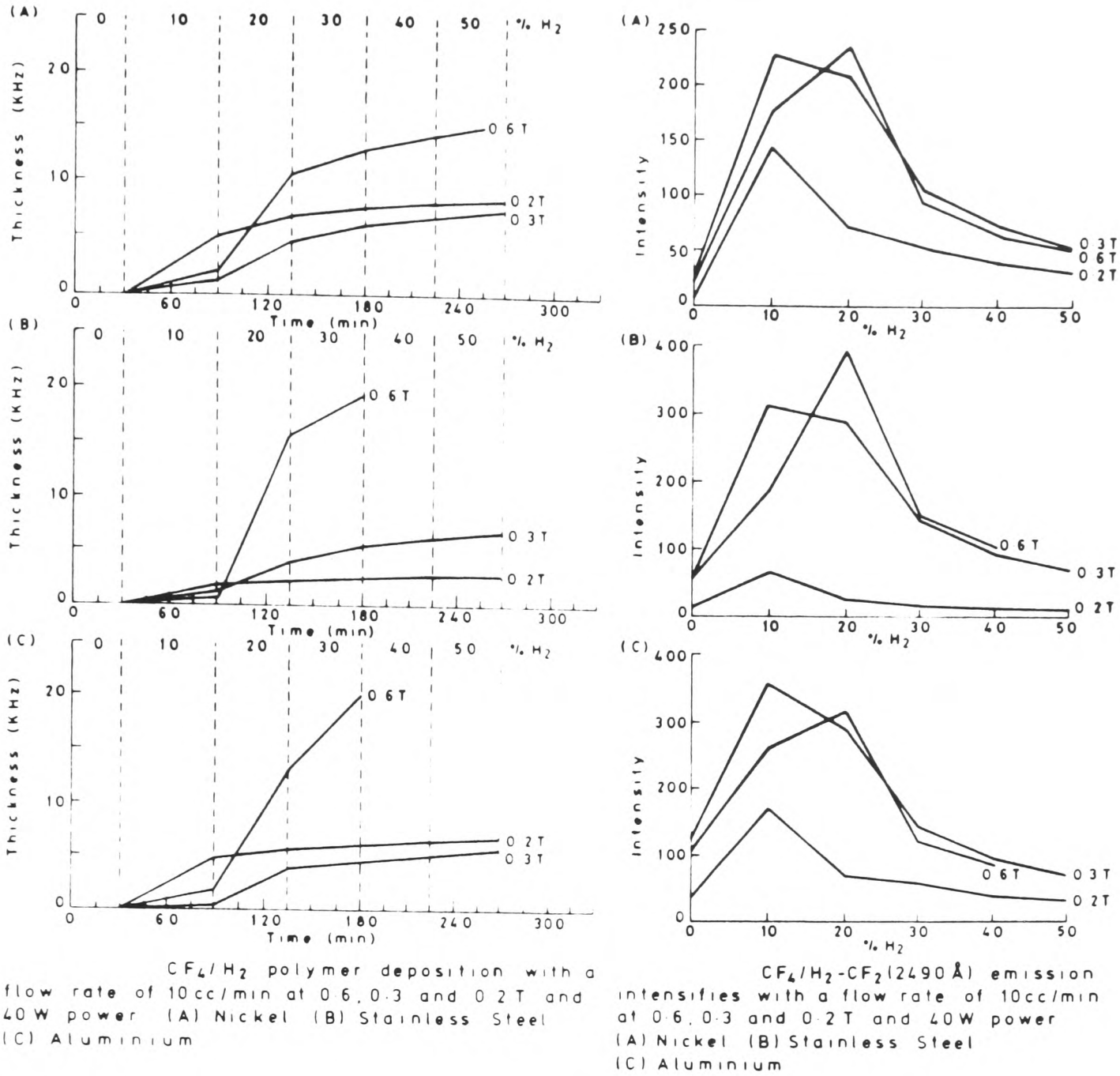

CF_4/H_2 polymer deposition with a flow rate of 10 cc/min at 0·6, 0·3 and 0·2 T and 40 W power (A) Nickel (B) Stainless Steel (C) Aluminium

CF_4/H_2-CF_2 (2490 Å) emission intensifies with a flow rate of 10 cc/min at 0·6, 0·3 and 0·2 T and 40 W power (A) Nickel (B) Stainless Steel (C) Aluminium

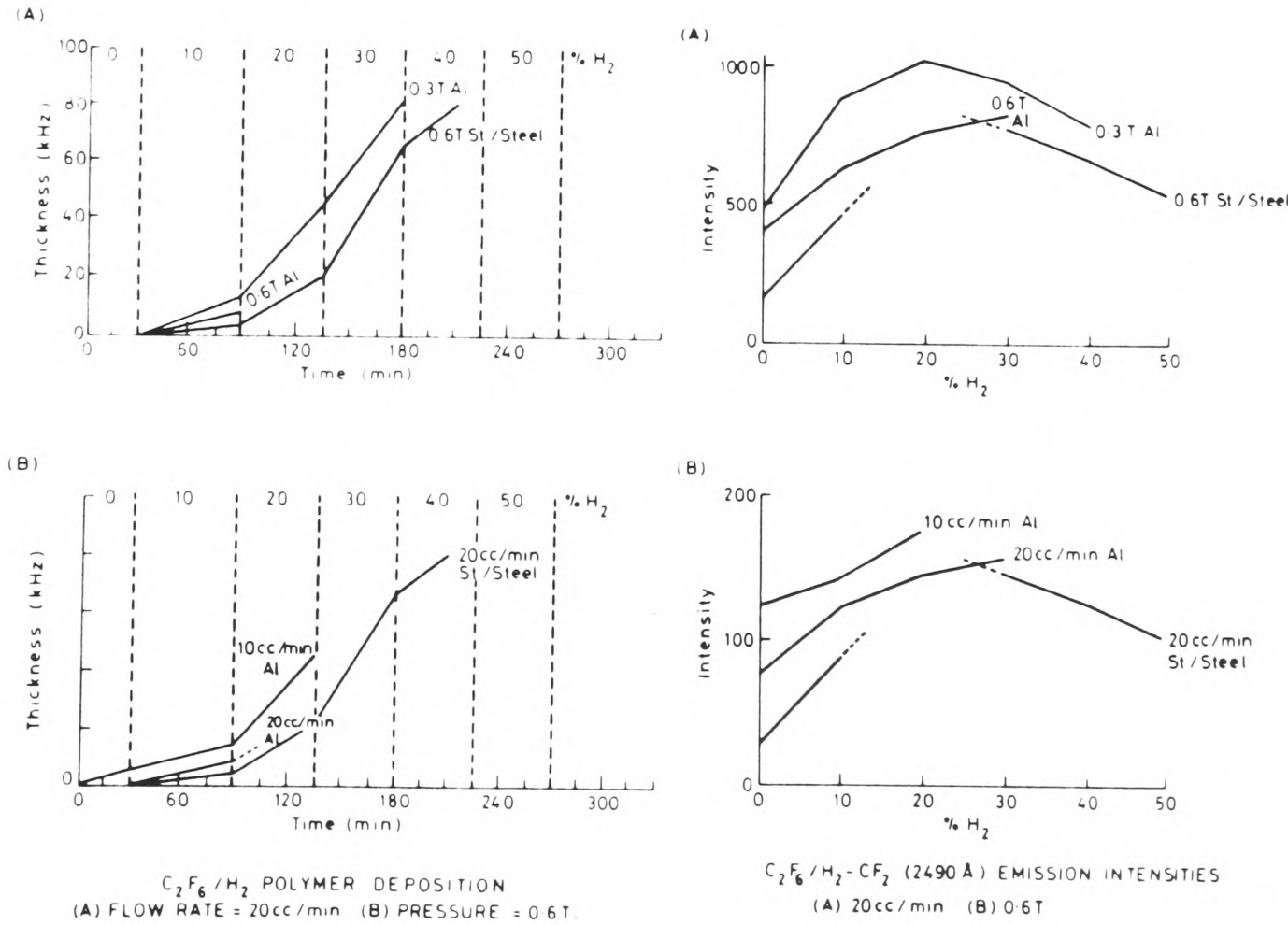

C_2F_6/H_2 POLYMER DEPOSITION
(A) FLOW RATE = 20 cc/min (B) PRESSURE = 0·6 T.

C_2F_6/H_2-CF_2 (2490 Å) EMISSION INTENSITIES
(A) 20 cc/min (B) 0·6 T

Figure 48. H_2 Addition Deposition Results.

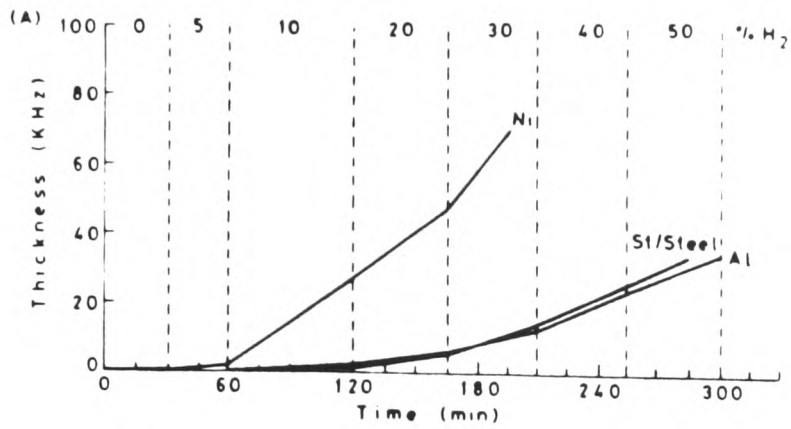

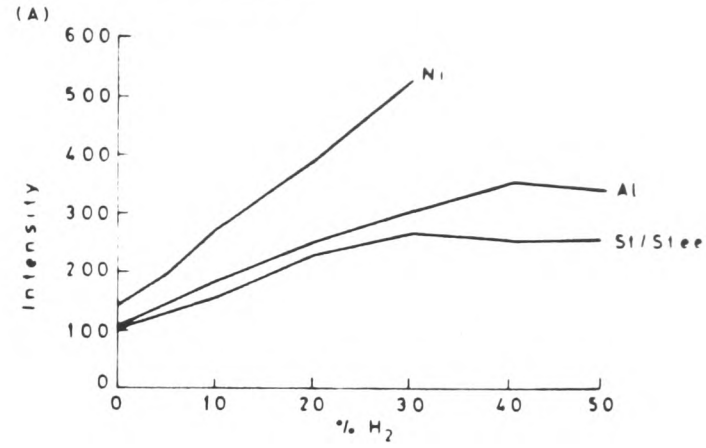

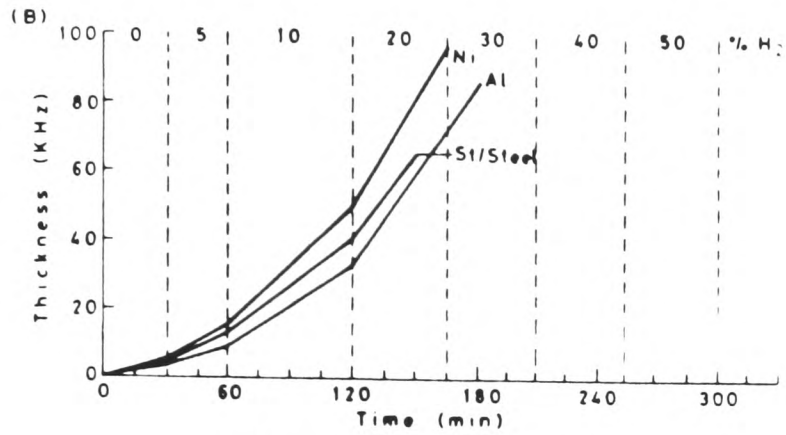

C_3F_8/H_2 polymer deposition on nickel, stainless steel and aluminium electrodes with a flow rate of 15cc/min and 40W power (A) 0·6T (B) 0·3T

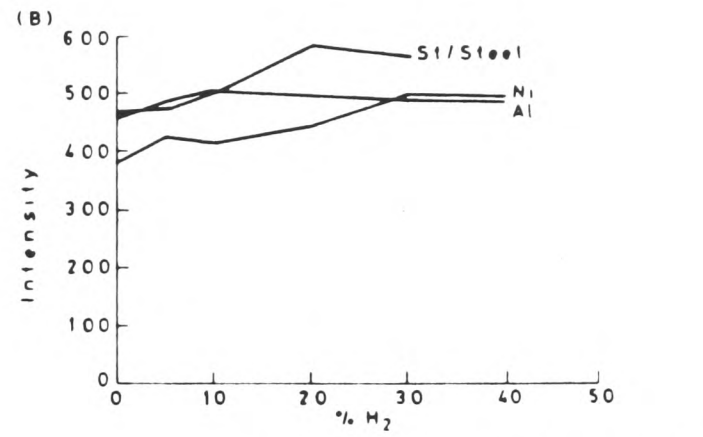

C_3F_8/H_2 - CF_2 (2490 Å) emission intensities for nickel, stainless steel and aluminium electrodes with a flow rate of 15cc/min and 40W power (A) 0·6T (B) 0·3T

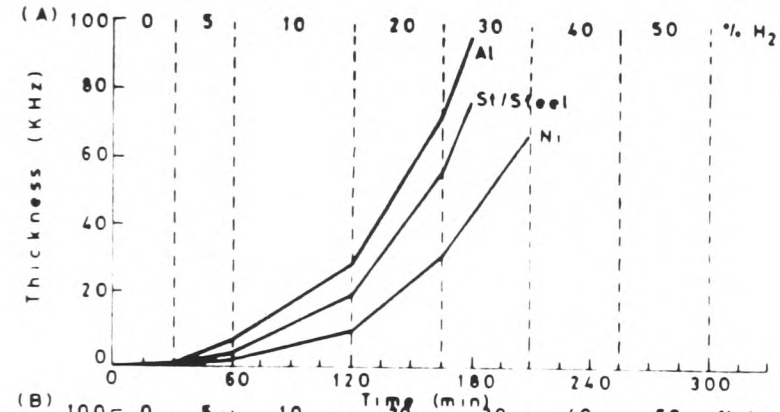

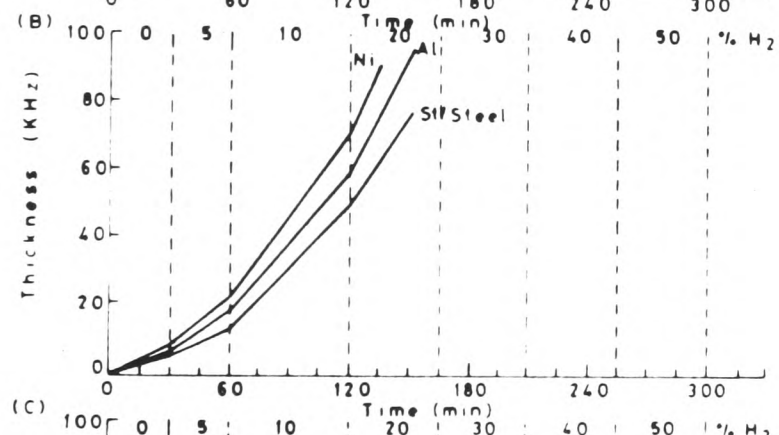

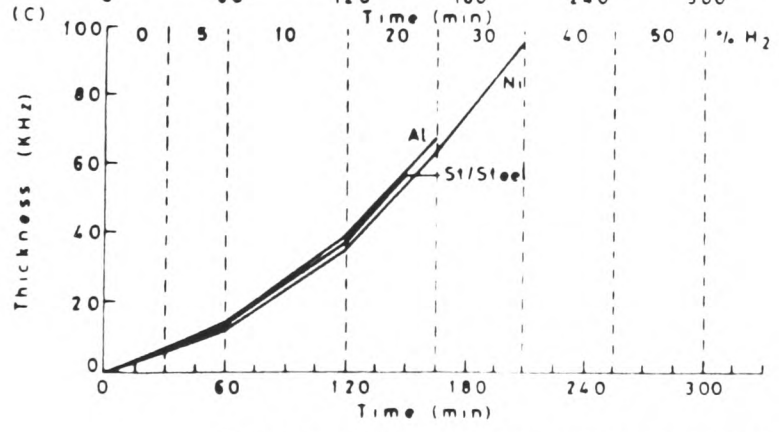

C_3F_8/H_2 polymer deposition on nickel, stainless steel and aluminium electrodes with a flow rate of 7·5cc/min and 40W power (A) 0·6T (B) 0·3T (C) 0·2T

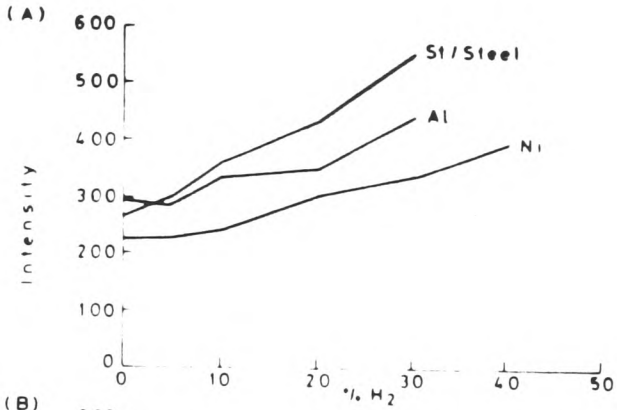

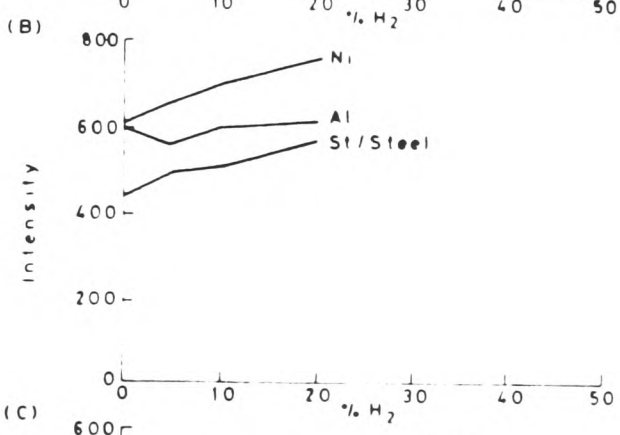

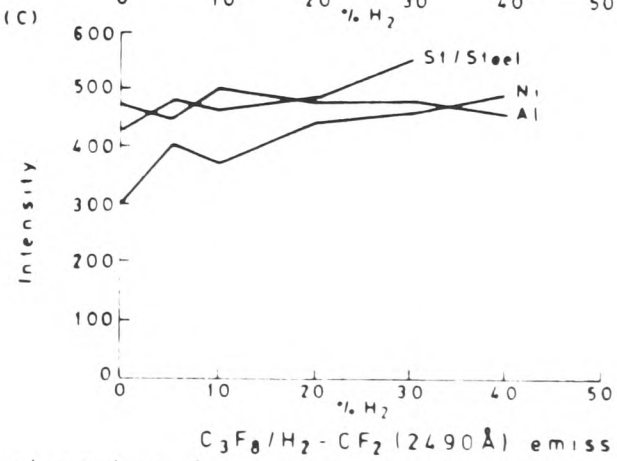

C_3F_8/H_2 - CF_2 (2490 Å) emission intensities for nickel, stainless steel and aluminium electrodes with a flow rate of 7·5cc/min and 40W power (A) 0·6T (B) 0·3T (C) 0·2T

Figure 49. H_2 Addition Deposition Rates.

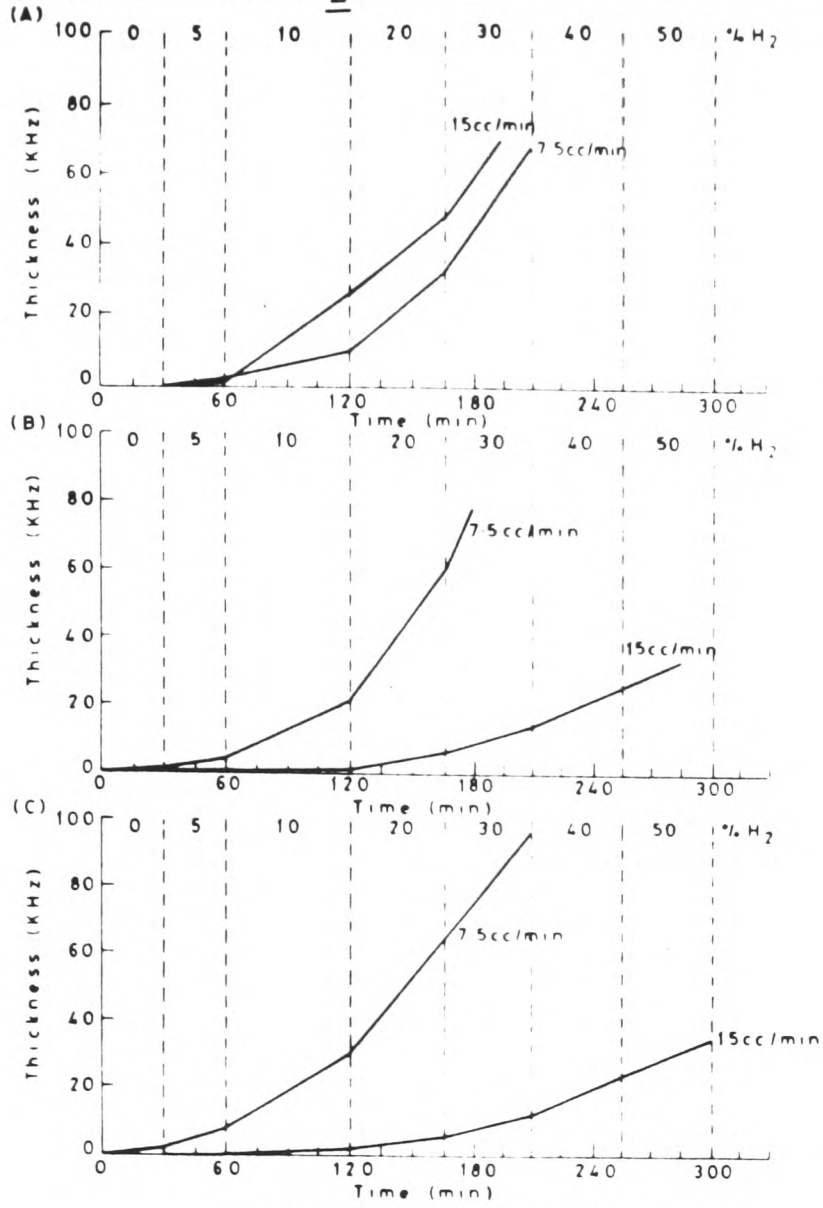

C_3F_8/H_2 polymer deposition with flow rates of 15 and 7.5 cc/min at 0.6T and 40W power (A) Nickel (B) Stainless Steel (C) Aluminium

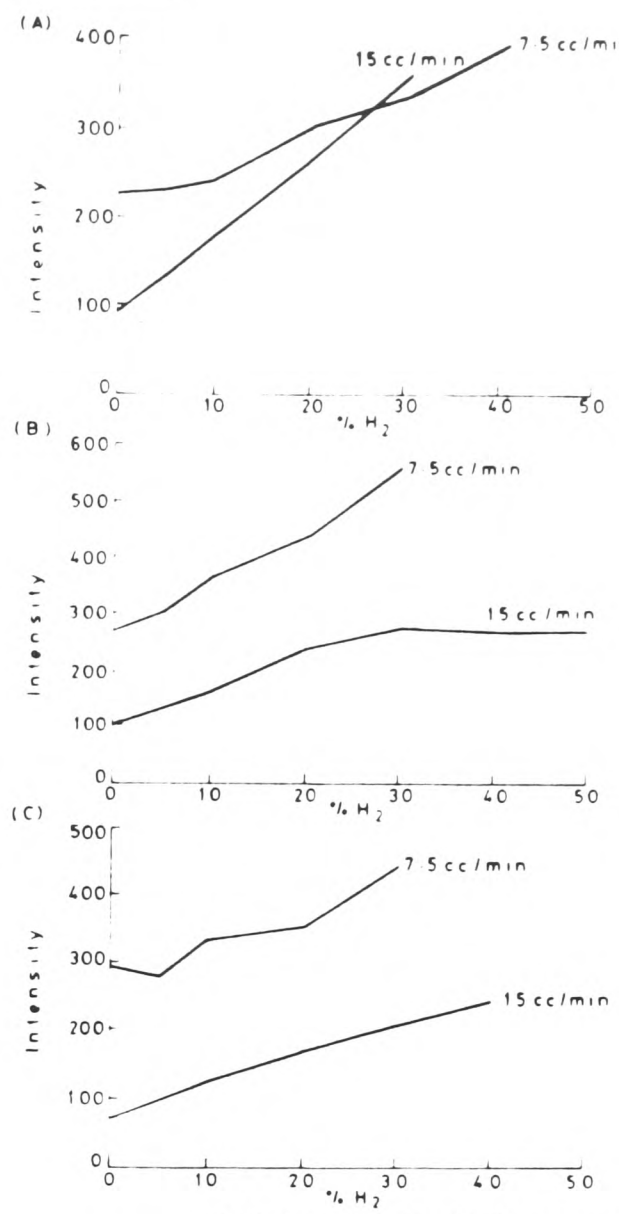

C_3F_8/H_2-CF_2(2490 Å) emission intensities with flow rates of 15 and 7.5 cc/min at 0.6T and 40W power (A) Nickel (B) Stainless Steel (C) Aluminium

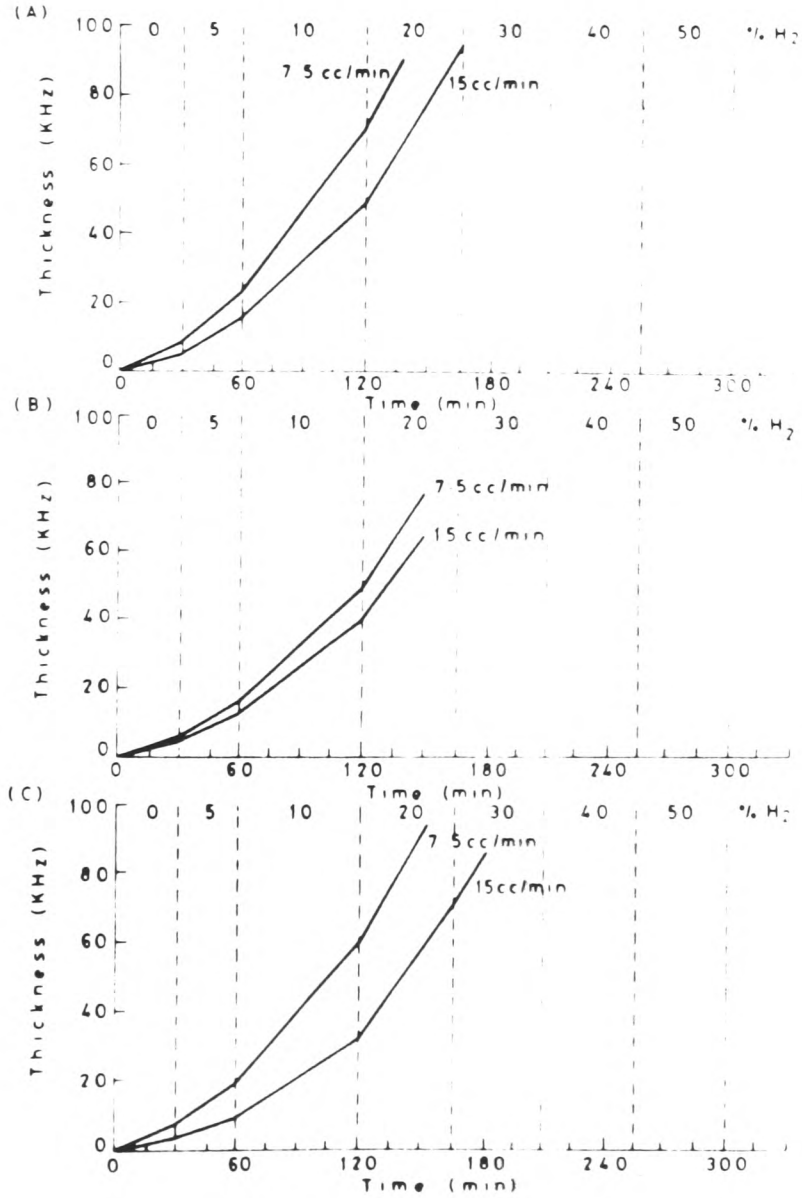

C_3F_8/H_2 polymer deposition with flow rates of 15 and 7.5 cc/min at 0.3T and 40W power (A) Nickel (B) Stainless Steel (C) Aluminium

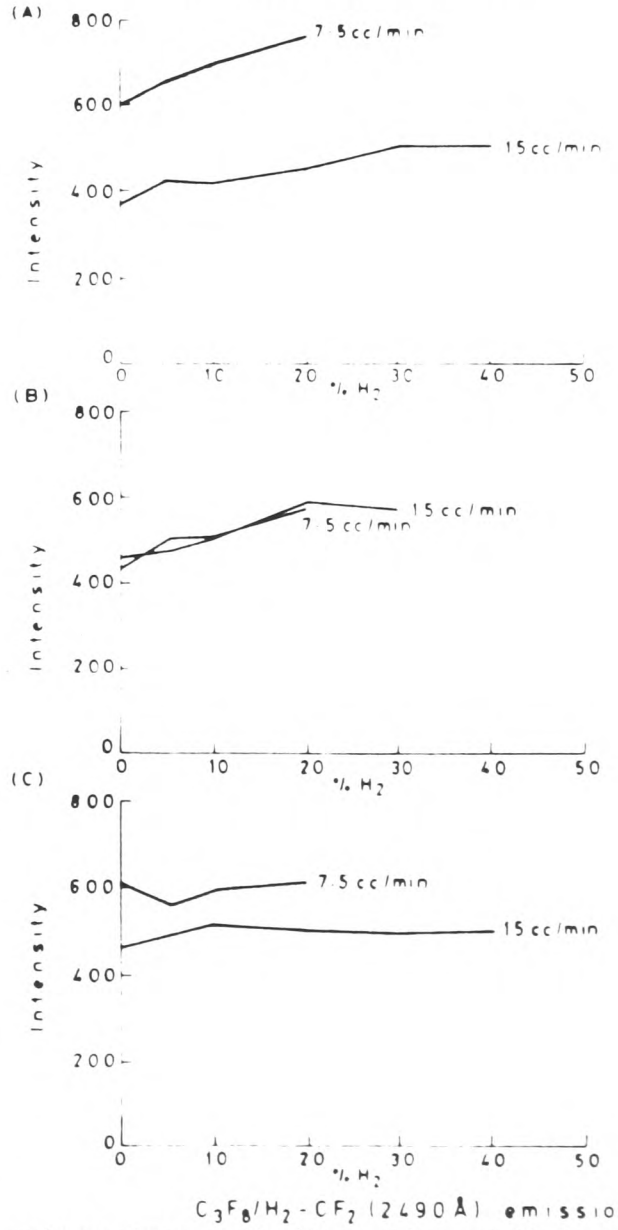

C_3F_8/H_2-CF_2(2490 Å) emission intensities with flow rates of 15 and 7.5 cc/min at 0.3T and 40W power (A) Nickel (B) Stainless Steel (C) Aluminium

Figure 50.

H_2 Addition Deposition Rates.

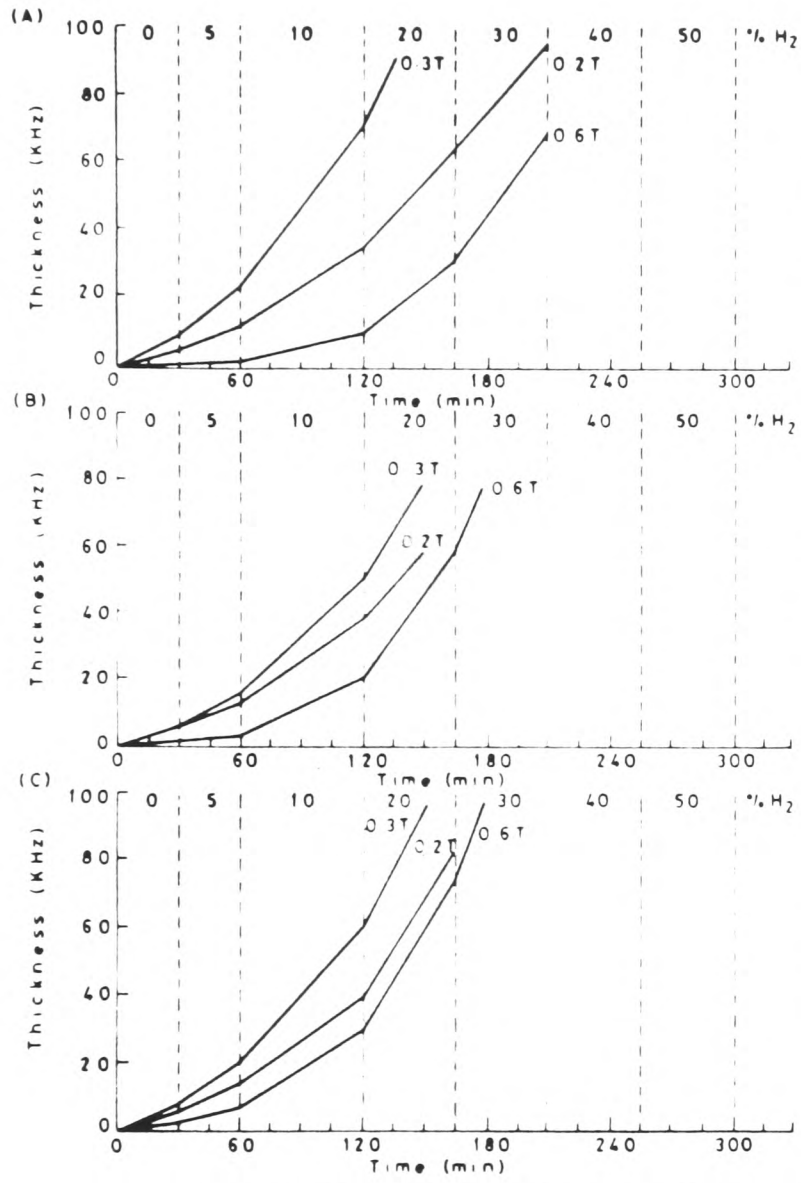

C_3F_8/H_2 polymer deposition with a flow rate of 7·5 cc/min at 0·6, 0·3 and 0·2T and 40 W power. (A) Nickel (B) Stainless Steel (C) Aluminium

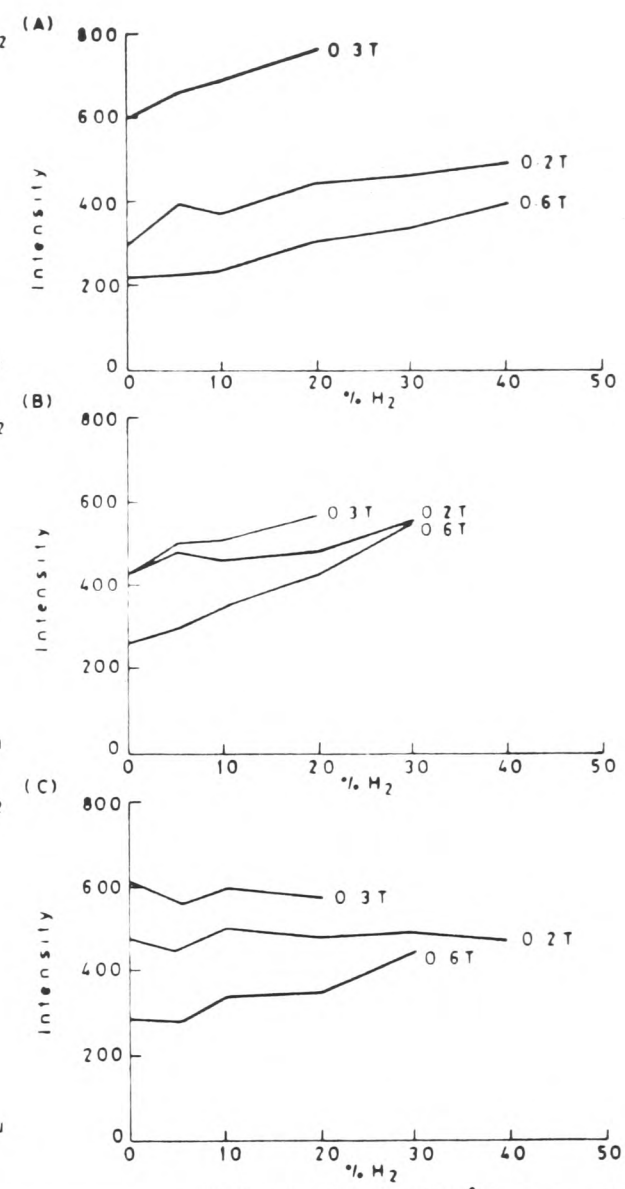

C_3F_8/H_2-CF_2(2490 Å) emission intensities with a flow rate of 7·5 cc/min at 0·6, 0·3 and 0·2T and 40 W power (A) Nickel (B) Stainless Steel (C) Aluminium

Figure 51.

H_2/Inert Addition Deposition Rates.

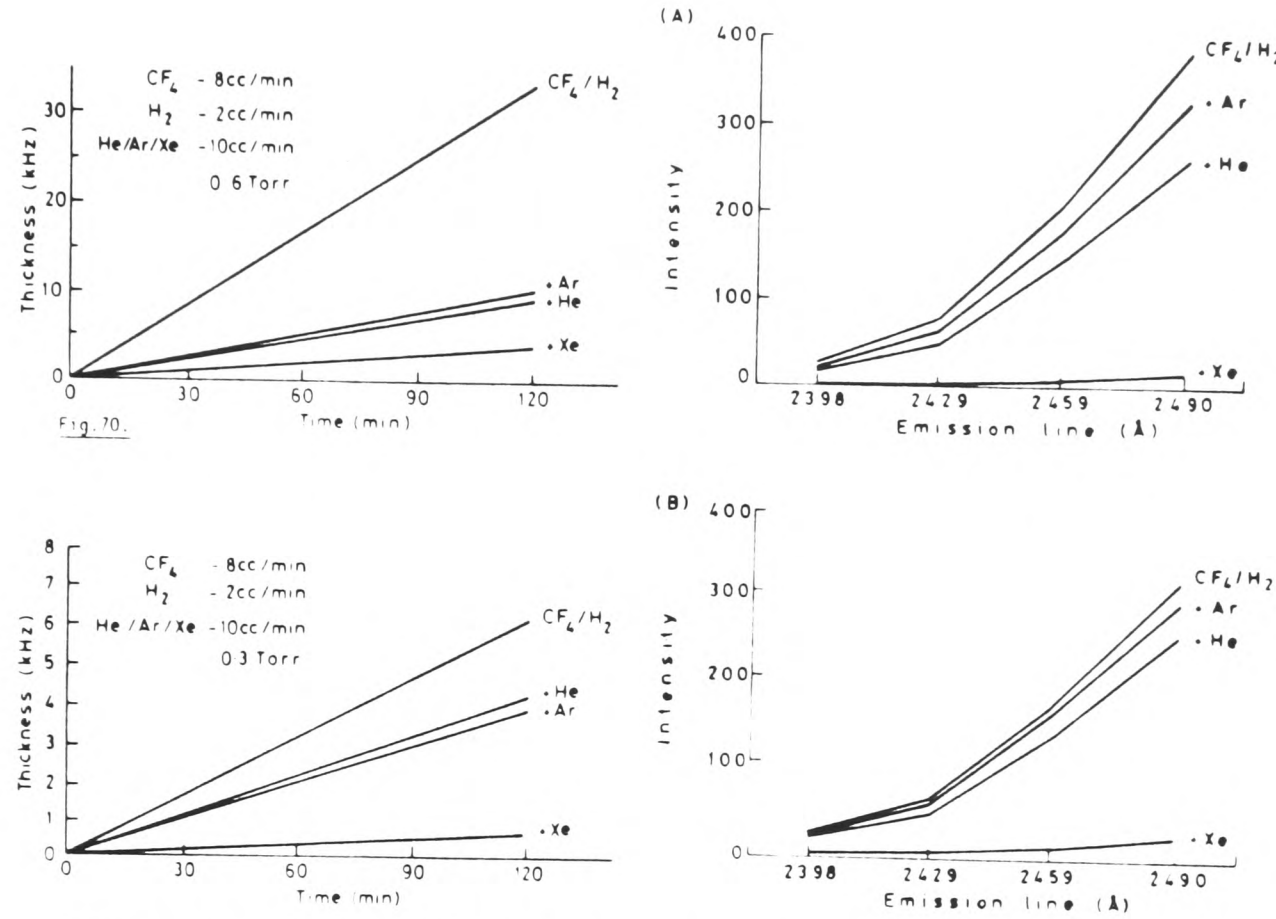

Fig. 70.

EFFECT OF INERT GAS ADDITIONS ON THE RATE OF POLYMER DEPOSITION IN A CF_4/H_2 (80%-20%) PLASMA.

CF_2 emission intensities for a CF_4/H_2 (80% / 20%) plasma with additions of helium, argon and xenon. (A) 0 6T (B) 0 3T

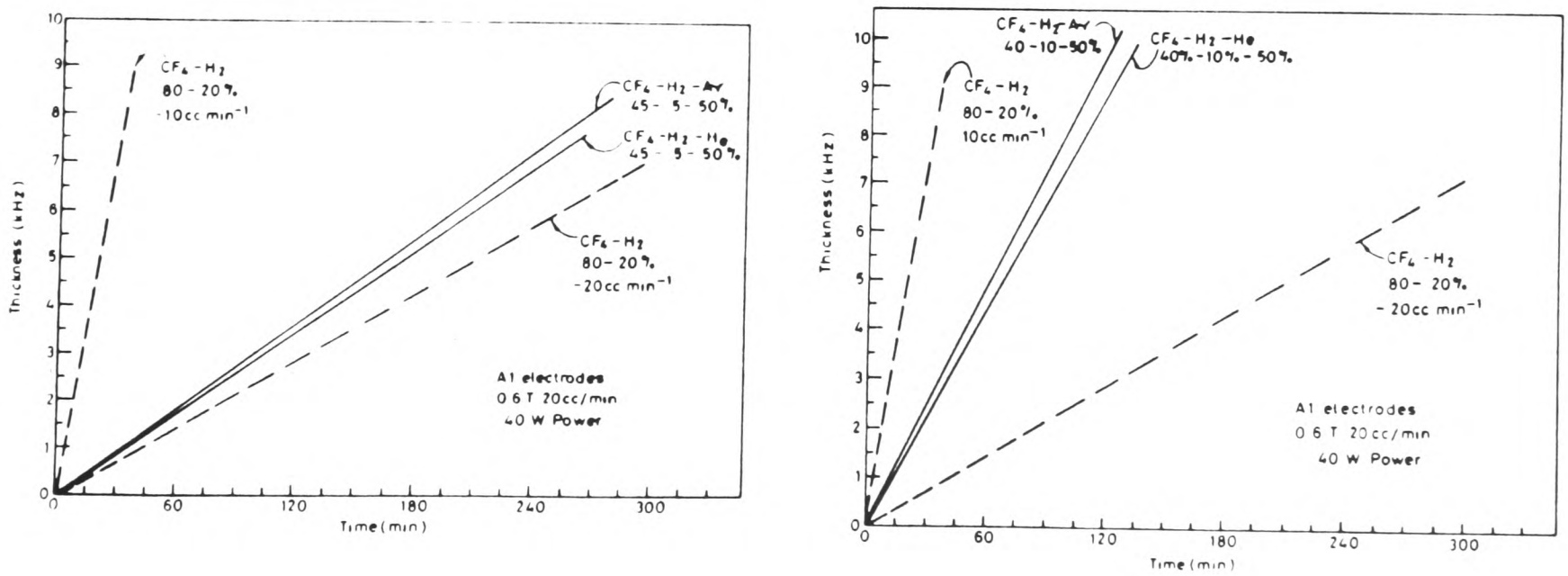

4.2.1.2)Dynamic Optical Spectroscopy.

Again this was used for a comparison of intensities of CF_2^* (249nm) vs. polymer build-up rate. As stated in the quartz crystal microbalance section the optical emission from CF_2^* also passes through a maximum at the same percentage of hydrogen. At the same time, though the atomic hydrogen emissions were always observed, no H_2 molecular emissions were clearly visible until 10% H_2 by volume had been exceeded. The F atom emission was markedly quenched by addition of H_2. The HF emission lines were looked for but not observed, they are known though to be weak.

With the C_3F_8/H_2 gas mixtures no limit could be found for the increase in rate of polymer deposition up to 50% H_2. Similarly there was no clear maximum in the CF_2^* emission.

4.2.2)Examination of Surfaces.

4.2.2.1)XPS Results CF_4/H_2, C_3F_8/H_2.

CHF_3	Top electrode	Si sample.
F	47.1%	51.3%
C	51.4%	47.8%
O	1.5%	0.8%
CF_3	1188	1187
CF_2	1190.3	1188.9
CF	1192.7	---
$C-CF_n$	1194.7	1193.3
CF_4/H_2		
F	15.2%	63.3%
C	8.3%	1.7%
O	76.3%	35.0%
Al	0.2%	0.0%
C_3F_8/H_2		
F	44.8%	45.0%
C	2.4%	2.1%
O	52.8%	53.0%
Al	0.0%	0.0%
CF_3	1189.3	1190.0
CF_2	1191.7	1192.6
$C-CF_n$	1193.8	1194.7
C	1196.1	1197.0
C-H	1198.3	---

The spectra are given in Figure 52 for C_3F_8, CF_4/H_2, CHF_3 and C_3F_8/H_2 respectively.

Figure 52.

XPS -H_2 Addition Results.

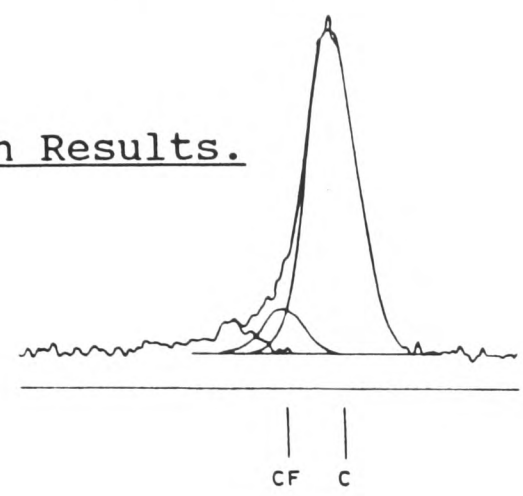

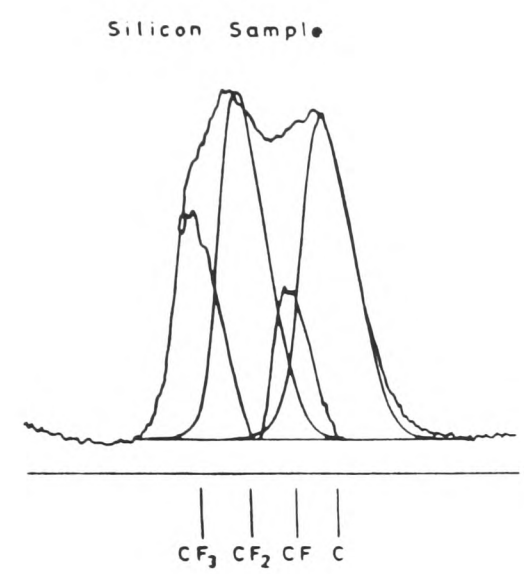

Figure 78. Carbon 1s spectra C_3F_8 plasma

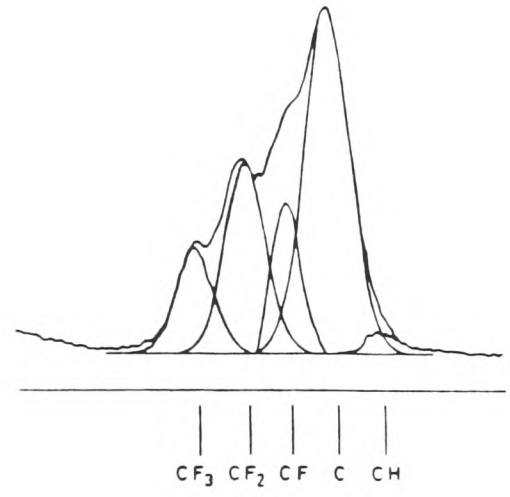

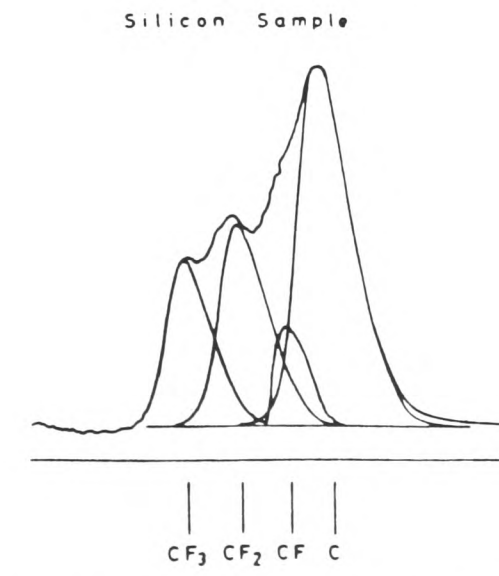

Figure 79. Carbon 1s spectra CHF_3 plasma

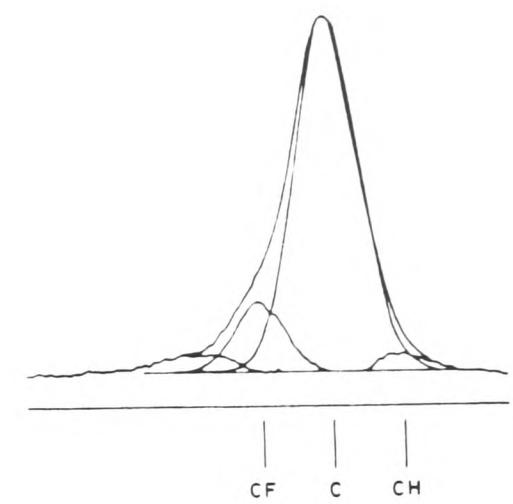

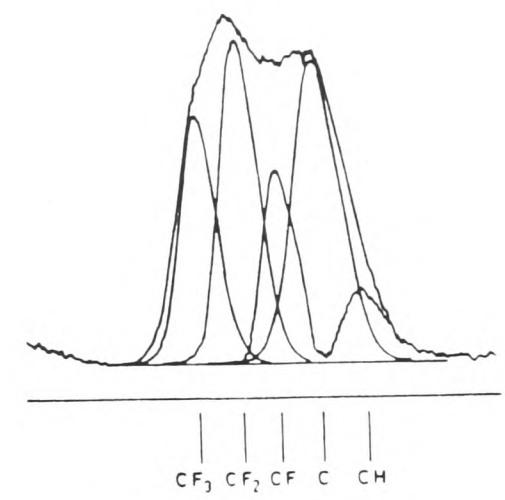

Figure 80 Carbon 1s spectra CF_4/H_2 plasma

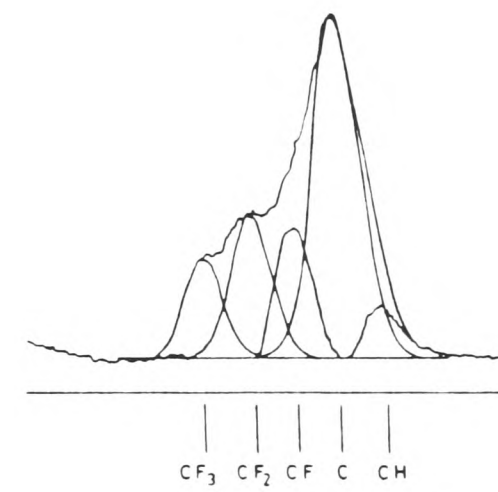

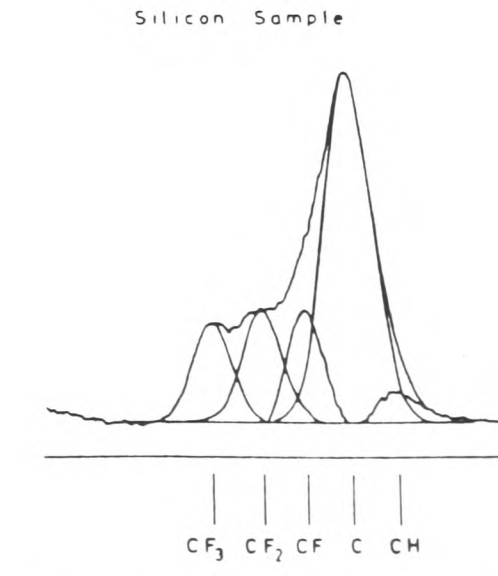

Figure 81. Carbon 1s spectr C_3F_8/H_2 plasma

4.2.2.2)Rutherford Backscattering.

The level of metal contamination found with fluorocarbon/hydrogen plasmas is found to be very low, < 0.05 atomic% except for ($Ti/Si/C_3F_8$) ca. 0.5 atomic%. Despite the XPS data seeming to indicate that the structure of the C_3F_8/H_2 polymer was similar to that from CHF_3, no substrate effect was observed. This could have been swamped as the polymer deposition rates were extremely high from this mixture.

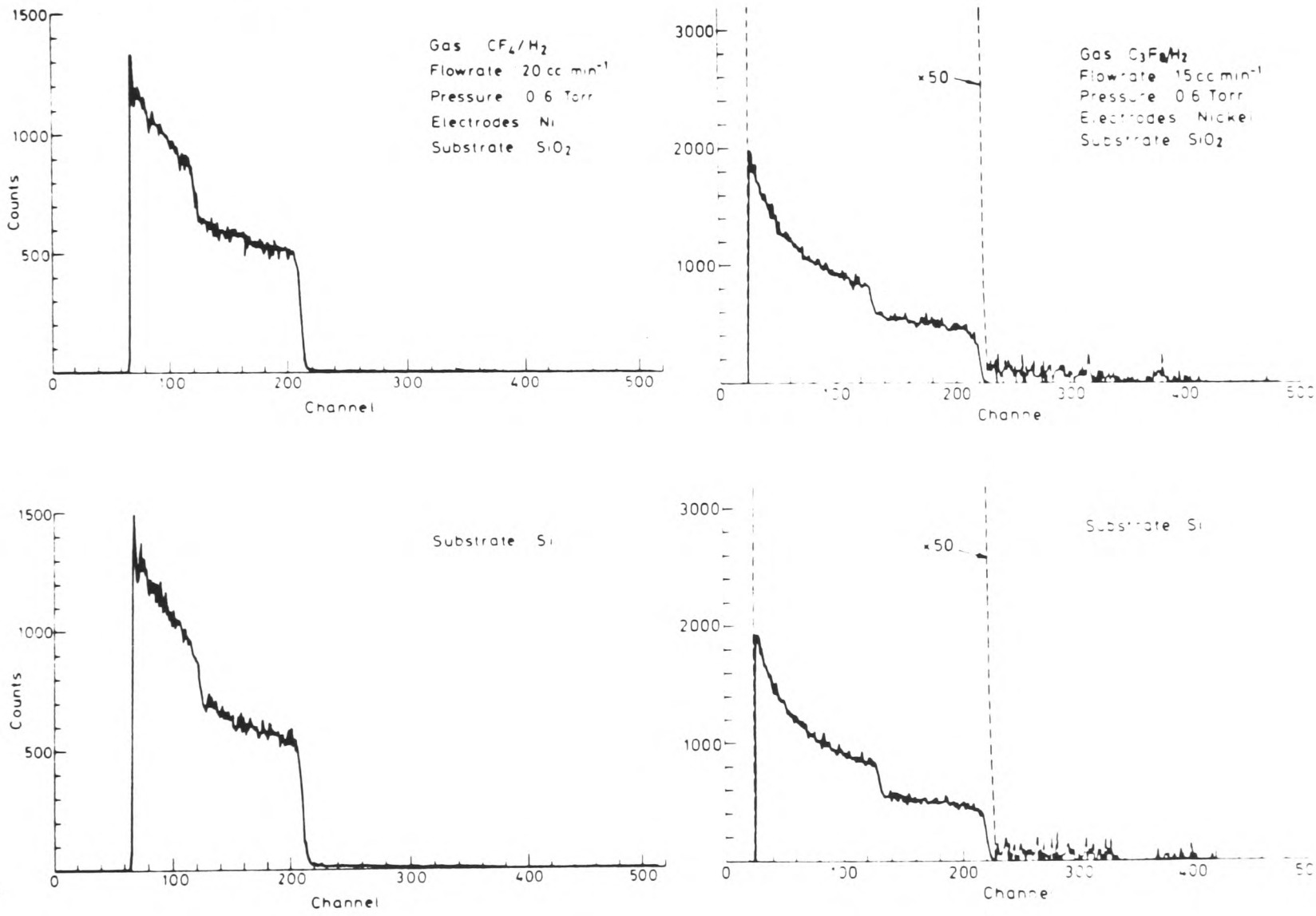

Figure 53.

RBS H_2 Addition.

4.2.2.3)Infrared Studies.

A range of electrodes and SiO_2 wafers from C_xF_y/H_2 mixtures were also examined by IR. These are shown in Figure 53. All of these mixtures were characterised by thick polymer films deposited on both electrodes.

CF_4/H_2 top electrodes indicated traces of metal fluorides - presumably due to the initial pure CF_4 plasma. These also show a lesser C-H content than the corresponding ground electrodes. The similarity shown by XPS between the CF_4/H_2 generated material and that from C_3F_8 is not shown by the IR to any significant degree. However the spectra do indicate that there are similarities between the material from C_3F_8/H_2 and CHF_3 on the top electrodes that was also shown by XPS.

The experiments that were done with Al electrodes and CF4/H2 and C2F6/H2 discharges showed some evidence for the substrate effect in that, whereas the bottom electrodes were coated in polymer, the SiO_2 surfaces examined show very little $(CF_x)_n$ material.

Figure 54.

IR H_2 Addition.

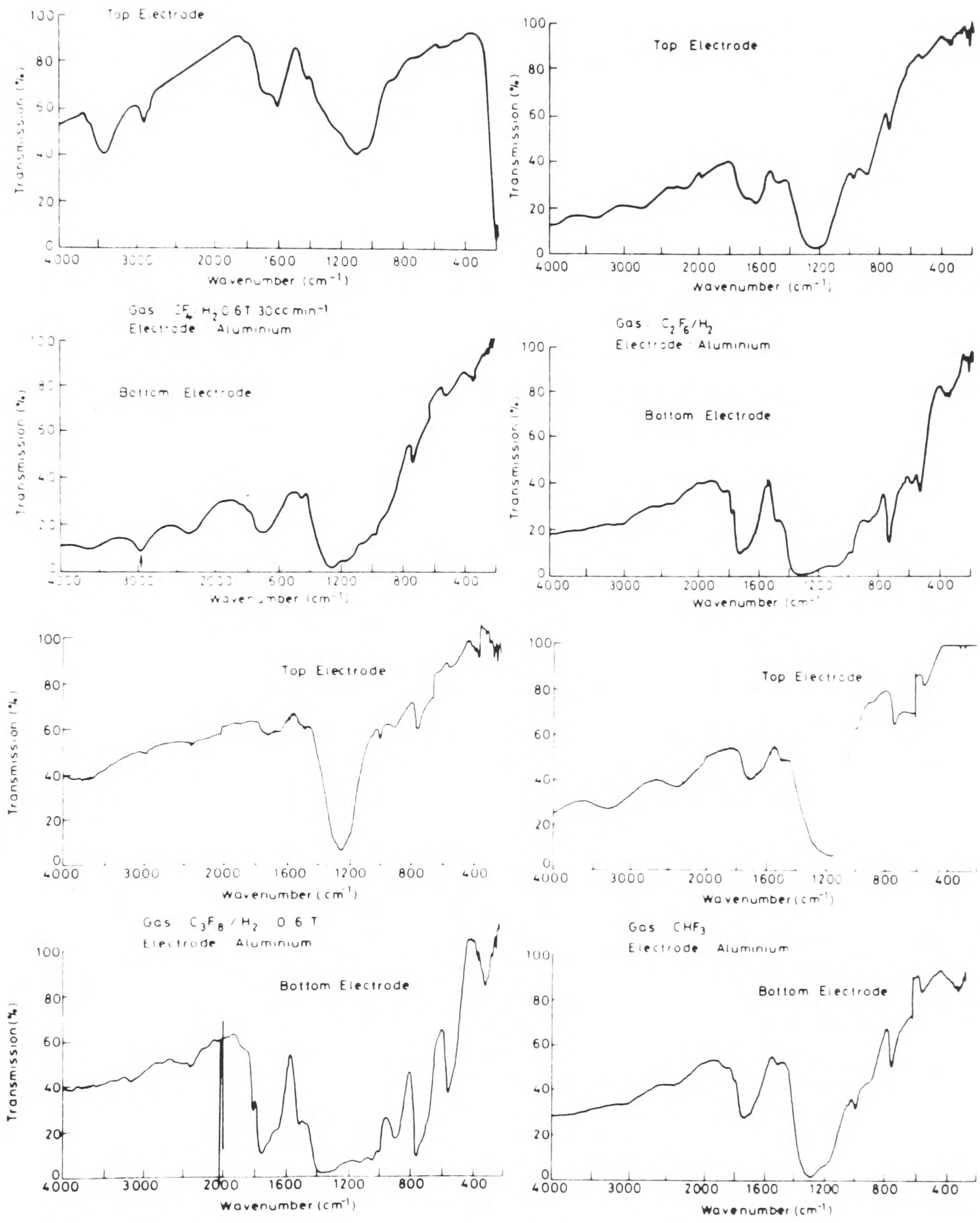

4.2.2.4)Thermogravimetric Analysis.

Sample	Major peak temp °C	Minor peaks.
Polythene	350°C 71.6%	530°C 2.0%
PVDF	470°C >100.0%	545°C 9.2%
CHF_3 Top	370°C 53.6%	435°C 30%, 635°C 10%
B	330°C 45.6%	225°C a 16.0%(s)
CF_4/H_2 T	495°C 11.4%	330°C 7.2%
" B	375°C 40.8%	490°C 20.8%
C_2F_6/H_2 T	412°C 52.0%	510°C 36.0%
" B	591°C 52.8%	310°C 51%, 96°C 6.4%
C_3F_8/H_2 T	415°C 12.1%	520°C 12.5%
" B	315°C 26.1%	a550°C 4.0%

(s) -Shoulder on main peak, (a) -About
Conditions: ca. 10mg sample.
Heating rate 20°C min^{-1}
Air flow of 10cc min^{-1}

Figure 55. TGA, H_2 Addition.

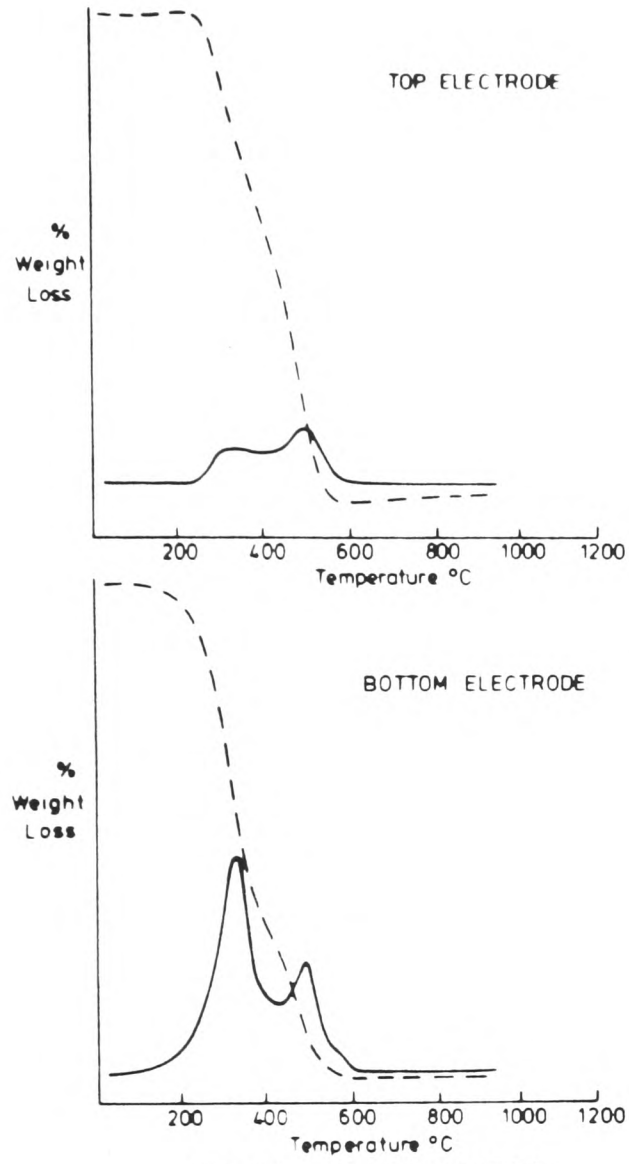

4.2.3)Overall Summary and Conclusions.

A number of fluorocarbon gases, viz CF_4, C_2F_6, C_3F_8, and CHF_3 were compared for their relative tendencies to deposit polymeric material during the plasma etching of Si/SiO_2. Emission spectroscopy confirmed the correlation between the production of CF_2^* in the plasma and the corresponding rate of polymer deposition. The role of the composition of the electrodes in the polymer production process has also been examined, particularly for the two gases C_3F_8 and CHF_3, which produce the greatest abundance of polymers. It was found that polymer production from C_3F_8 is much more sensitive to electrode composition than that from CHF_3. On the other hand, polymers produced from C_3F_8 can accumulate at similar rates on Si and SiO_2, whereas those from CHF_3 show a much greater likelihood of building up on Si than on SiO_2. XPS and Infrared spectroscopy were used to demonstrate that polymers arising from these two gases exhibit marked structural differences, which can be minimised by mixing hydrogen with C_3F_8.

It is proposed that the 'electrode effect' associated with C_3F_8 is as a result of metal or metal fluorides being transferred from the driven electrode (where the dominant process is ion enhanced fluoridation), to the substrate surface where they may act as catalytic chain initiators for

the polymerisation process. The effect is not observed for CHF_3, since the formation of the more thermally stable polymer film on the surface of the top electrode acts as a mask and inhibits sputtering of electrode material.

Rutherford Backscattering Spectrometry was used to examine the polymer films, especially for the presence of metal contamination from the electrodes. This technique is especially suitable for the quantitative detection of the distribution of relatively heavy elements in light matrices. These spectra confirmed the presence of metal contamination in the polymer films laid down from C_3F_8 plasmas, which also showed a layer of polymer on both Si and SiO_2. This was in contrast to the spectra from CHF_3 where it was found that preferential polymer deposition occurred on the Si surface. This phenomenon, the 'substrate effect is generally ascribed to oxygen in the SiO_2 lattice being able to oxidise the fluorocarbon polymer, as it forms, to CO, CO_2, and COF_2, which can then desorb from the surface. No such effect was observed for C_3F_8, perhaps because the presence of catalytic material on the substrate surface readily promotes new polymer formation.

The RBS spectra of all specimens from CF_4 and C_2F_6 plasmas showed that only thin films, heavily contaminated with metal, were deposited. This was

consistent with the fact that these gases are essentially etching in nature, forming little or no polymer, and so sputtering of electrode material can occur readily. For this reason, their RBS spectra are very similar to those to be expected from 'clean' Si and SiO_2 substrates, but with traces of sputtered metal on the surface.

XPS studies of the polymers deposited in C_3F_8 and CHF_3 plasmas were performed to give an insight into the types of fragments present in their molecular structure. When C_3F_8 was used, the top electrode showed a carbonaceous deposit visible as a black film mainly around the edge of the electrode surface. The Si sample, which was covered by a layer of light yellow polymer, showed contributions from four main structural types. These differences may be attributed to the fact that while polymerisation is the dominant process occurring at all grounded surfaces, ion-enhanced fluoridation and physical sputtering dominate at the driven electrode which, in this system, can be about 250^{o}C hotter.

On the other hand, the polymers deposited from a CHF_3 plasma on to the top electrode and the silicon substrate were found to be very similar. Also the degree of cross-linking in this material was apparently far more extensive than those from C_3F_8. It is proposed that this is due to the presence of H atoms in CHF_3 derived polymers which is likely to

give rise to adjacent C-H and C-F in the material. The elimination of HF is then a favorable process (ΔH ca. -302kJ/mol), leading to stabilisation by cross-linking and formation of double bonds. This elimination mechanism in polymers from CHF_3 would also account for the low intensities of the C-H component of the XPS C_{1s} spectrum.

In order to detect the presence of fluorocarbon deposits on the electrode surfaces, infrared double transmission spectra were recorded. No evidence for polymeric material was found on the electrodes from CF_4 and C_2F_6 plasmas, though some metal fluoride absorptions were observed. Under the present operating conditions, these gases are therefore etching in nature and do not form any polymeric fluorocarbon films to any significant extent.

The top electrode surface from a C_3F_8 plasma gave two peaks in the region 600-400cm^{-1} that may be assigned to metal fluorides, while the bottom electrode showed extensive absorptions in the fluorocarbon region, which correlated well with the results obtained by XPS. Good agreement between XPS and IR was also found with the CHF_3 samples, where extensive C-F absorptions were found for both top and bottom electrode surfaces.

Following this initial study of the deposition rates, and the characterisation of polymers laid down by pure fluorocarbon gases, the C_3F_8/H_2 system

was examined. Hydrogen addition to the C_3F_8 plasma suppressed the F atom concentration by formation of HF, and reduced the rate at which species such as CF_2 were consumed by recombination reactions to give, for example, CF_3. This resulted in a considerable increase in the polymer deposition rate. The electrode effect, a characteristic of the pure C_3F_8 plasma, was drastically reduced as well. This was presumably due to a masking layer of polymer being laid down on the top electrode which prevented sputtering of catalytically active material. This was reflected in the RBS results which showed only a very low level of metal contamination in the polymer films. There was no evidence of any substrate effect, but this was not totally unexpected, since the high rates deposition would tend to swamp any such effect. XPS C_{1s} spectra of the polymers deposited on the top electrode and the silicon substrate were very similar and closely resembled those from CHF_3. The C-H component did appear to be more intense though. Unlike the pure C_3F_8 plasmas, there was again an apparent high degree of cross-linking within the polymer, made possible by the presence of hydrogen which, after incorporation, could presumably be eliminated as HF from the polymeric structure. IR double transmission spectra were again recorded, and both electrode surfaces showed strong absorptions in the fluorocarbon region, although they were less

extensive on the top electrodes where a metal fluoride absorption could also be observed. This is consistent with the fact that pure C_3F_8 was used at the start of the run, before H_2 was added. There was a strong similarity between the spectrum obtained from the bottom electrode and that from a CHF_3 plasma. This agrees well with the similarities also observed by XPS between the polymers on the silicon samples comparing C_3F_8/H_2 and CHF_3 plasmas.

Hence overall this study has confirmed the relationship between polymer deposition and the presence of certain species, such as CF_2 in the plasma. It has used Rutherford Backscattering Spectometry to interrogate the polymers, especially for the detection of metal transferred from the electrodes, and thereby highlighting the role of the electrodes in influencing the likelihood of polymer formation. Furthermore it has demonstrated significant differences between the two gases viz. C_3F_8 and CHF_3, which in this work have given rise to the highest rates of polymer deposition. The former gas shows a sensitivity to the nature of the electrode material. This is ascribed here to the fact that the polymer from the C_3F_8 discharge is unstable to a combination of ion bombardment and high temperatures. Hence the electrode material is always available for the production of catalytic species and is also likely to remove atomic fluorine from the system as metal fluorides, thereby further

enhancing the probability of polymer formation. On the other hand, the polymers arising from CHF_3 are thermally more stable and do not allow the electrode to participate in the various reactions. The structure of the latter polymers, confirmed by XPS, is consistent with their being formed via an HF elimination mechanism. This concept is supported by the similar structures formed from C_3F_8/H_2 mixtures.

Parts of this work have already been published as "A Study of the Deposition of Polymeric Material onto Surfaces from Fluorocarbon RF Plasmas", in Plasma Chemistry and Plasma Processing Vol.6 No.4, 417-427, (1986).

5)APPENDICES.

5.1 CONTROLLED ATMOSPHERE SEM.

As the project was involved in etching as well as deposition studies on Si/SiO2 substrates, some mention will be made of the work that was done in a controlled atmosphere scanning electron microscope.

5.1.1)Introduction.

Most of the work so far, in the field of controlled atmosphere scanning electron microscopy, has concentrated on two main areas[481-484]:

1. Atmospheric SEM -detection takes place above a pressure limiting aperture with the sample pressure usually below atmospheric.

2. Environmental SEM -detection takes place below a pressure limiting aperture -sample generally at atmospheric pressure.

The main limitation is the electron-beam scattering due to gas molecules present which takes place in three distinct regions; firstly between the electron gun and objective aperture, between the objective and pressure limiting aperture, and also between the pressure limiting aperture and the sample.

The microscope operates by generating a fine beam of electrons from a heated tungsten filament. These are accelerated by a potential of typically 20kV and focussed as a fine spot on the surface of the specimen by electromagnetic lenses. Electrons leaving the surface and up to a micron below, due to the action of the primary beam, are attracted to the secondary electron collection system.

Apart from producing an image of the specimen, the second important effect of the incident electron beam is the possibility of breakdown of any species chemisorbed on the sample surface. This process is achieved in the plasma rig by the high electron energies produced by the R.F. field.

With the very much lower pressures used the specimen detail resolution should be better than 500Å and could be as good as 150Å. This is in a system with magnifications from 20X to 50,000X. Hence, if successful etching can be achieved, sub-micron masks and device features could be fabricated, in scanned areas of 5mm to 2 microns. The three major observable effects should be loss of surface material as volatile products, formation of growths on the sample or the laying down of coatings- the major effect so far observed.

In this study the microscope was intended to be used as a very fine Reactive Ion Beam etch type system, but using electrons as the charged particles

instead. In this way it was hoped to be able to demonstrate 'maskless' etching of Si and SiO_2 surfaces with very fine dimensions. The possibility of pattern delineation by the deposition of material, and/or oxygen atmosphere etching was also examined.

5.1.2)Instrument.

A Cambridge S2A scanning electron microscope, illustrated in Figure 62, was adapted for use as a controlled atmosphere instrument. The main advantage with this particular model is that the column is sealed from the chamber except at the aperture. This is due to the quick specimen change feature offered by Cambridge Instruments, in that the chamber can be brought up to atmosphere without breaking the vacuum in the electron-optics. This particular instrument has a major disadvantage in that the electron-gun to objective aperture is pumped centrally. This is unsatisfactory for CASEM work, because the gun and objective should be pumped separately. This is to ensure that the pressure in the gun chamber is as low as possible. This was particularily important when it was intended to have fluorine containing species present, whilest using a tungsten filament. Unfortunately modifications here are difficult on this instrument, but using the smallest of the three supplied apertures, the chamber pressure can be at

2mT (at the vacuum trip level), without bringing the gun pressure above 2 X 10^{-5} torr at a backing pressure of 0.2 torr.

5.1.2.1)Vacuum System.

Only slight modifications were carried out on the vacuum system of the Cambridge S2A scanning electron microscope, for the controlled atmosphere work. The diffusion pumps for the electron gun and specimen chamber had the standard oil supplied changed to Convalex-10, a special high efficiency low contamination poly-phenyl ether. The main backing/roughing pump used a standard hydrocarbon oil, which did lead to problems with degassing when the system was in use. It was found that the safe limit for controlled atmosphere work at the highest pressure the microscope would allow was about two hours. Longer than this, and the filament lifetime was seriously degraded due to the increased pressure as well as oxidation, carbon buildup and formation of volatile WF_6 -from breakdown of the etching gases. When the pumps have had time to degas, preferably overnight, work can safely be recommenced. Whilest no serious problems with oil breakdown were found due to effluent contamination, a single stage Fomblin oil containing pump as fitted to the plasma rig was on order. Though oil contamination and carbonaceous buildup are claimed

to be reduced in Scanning Electron Microscopes[485-488], this will have the disadvantage that the backing pressure to the diffusion pumps will be higher, with consequent problems.

5.1.2.2)Hardware and Stages.

The microscope has two stages that have been modified for controlled atmosphere work:

* A standard X-Y stage with rotate.
* A 25-1100^{o}C controlled temperature stage.

5.1.2.2.1)X-Y Stage with Rotate.

This used standard 5cm thin aluminium discs on to which the samples were attached with aquadag, silverdag or some other suitable conducting medium. The stage was used for larger specimens since a reasonable range of movement was allowed. The gas inlet nozzle was positioned initially directly above the holder. The stage was also tilted at 45^{o} towards the scintillator to collect the maximum number of electrons.

Construction of the Gas Cell.

One of the problems was the amount of gas actually at the surface of the surface being low due to the distance between the jet and the specimen. Initial work with CF_4 and C_2F_6 indicated that a layer would build up and be retained by the surface but etching would only proceed at very low rates. The main influence of the electron-beam was to cause deposition of carbon on the surface. With a higher pressure of gas at the surface there is more chance of electron induced ionisation to generate active F atoms.

With a small piece of clean Silicon loaded onto the stage the electron beam was scanned across the surface in line mode. This was to ensure that the effect of electron beam degradation of the residual hydrocarbon oil in the system was not confused for an etchant gas effect. With a small flow of CF_4 introduced an effect was observed; showing that there was a small but significant pressure of gas above the surface. However the change in morphology of the surface of the sample was extremely slow with the most likely explanation being the low concentration of gas present. A confining cell was therefore designed and built to increase the gas concentration above the specimen as much as possible, on this stage. This consisted of a brass cap machined to very close tolerances to fit over

the rotating stage on which the sample was mounted. It was necessary also to coat the edge of the observation port with carbon to minimise secondary electron emission from the cell. Then with vacuum grease applied to the edge of the stage as an additional seal, the pressure in the cell could be increased so as to destroy the image completely by electron scattering, without approaching near the vacuum trip. This stage is illustrated in Figure 63 in the photographs.

5.1.2.2.2)Temp. Controlled Stage.

This was a heated stage for small samples, thus allowing deposition and etch rates as a function of temperature to be studied. However temperatures above 100^{o}C when power is applied to the heater, lead to noisy images due to the thermal electrons emitted. This was partially countered by a fine grid which is held at -5 volts with respect to the sample, to supress all the very low energy electrons. This was in practice difficult to use as it has to be carefully installed electrically isolated from the sample boat and thermocouple probes. The detection system scintillator voltage was also reduced to discourage the low energy thermal electrons from entering the electron

collection system. A range of conditions had to be determined to obtain the best signal to noise ratio in each experiment.

A photo of the heating stage is shown in Figure 64, and the details of the hot module in Figure 56.

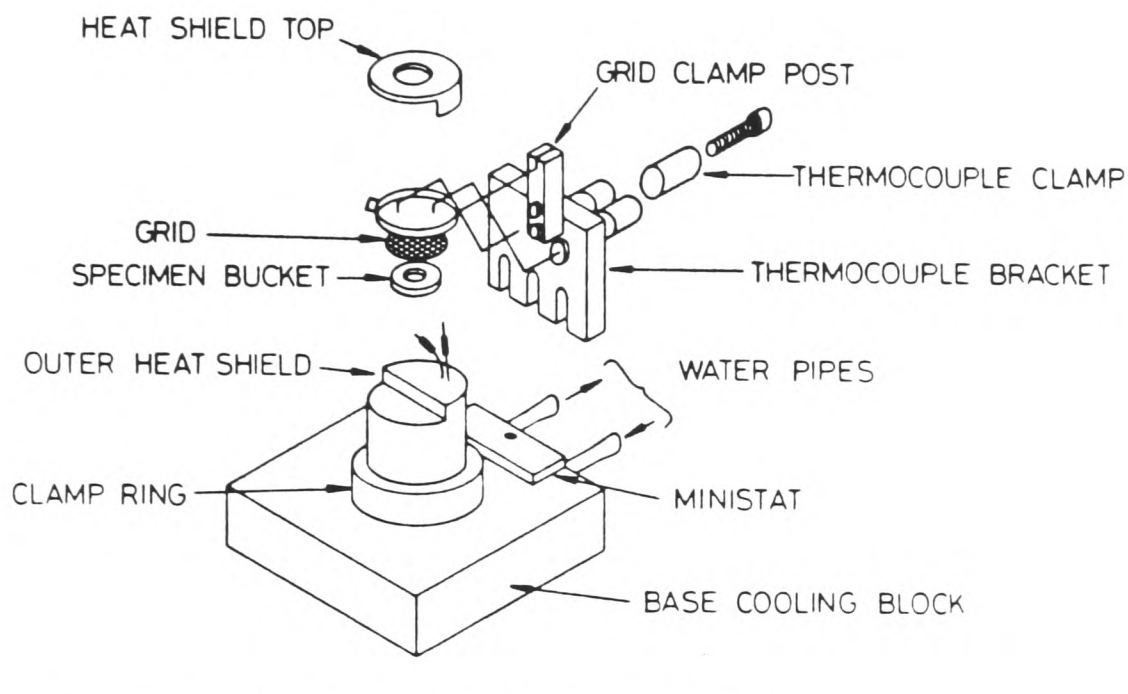

Figure 56. Diagram of Hot Stage.

5.1.2.3)Mass Spectrometers.

There were two mass spectrometers fitted to the microscope:
There was a 1-100 m/e Q-50 quadrupole, and also a 1-240 m/e Micromass-1 magnetic mass spectrometer. As with the plasma rig considerable effort was expended to get the systems operational without much sucess.

5.1.3)Progress and Results.

In the controlled atmosphere role some etching, but mainly deposition was oberved, using CF_4 with SiO_2 specimens. Some films were shown to be due to the influence of the primary beam on the pump oil present above the sample, but filament growth and polymer film growth has been demonstrated. Unfortunately the age of the microscope means that it is tempramental with trouble both in the sequencing of the vacuum system operation and the high voltage supply to the gun. Thus only a few preliminary results are presented here.

5.1.3.1)AGR Fuel Pin Studies.

As well as examining semiconductor specimens, samples consisting of H_2 annealed Advanced Gas Cooled Reactor fuel elements were studied. Work on AGR fuel pins showed that it was possible to grow filaments on the ferrous metal surface about 100Å long at temperatures between 500-800^{o}C in a pure CO atmosphere. The electron-beam however had only a slight additional effect. The filaments could not be observed in situ as their size was below the resolution of the instrument in the scanning mode. They could however easily be observed in the other SEMS, but this meant that the particular area exposed to the electron beam in the first microscope

was difficult to find. Typical deposits that could be obtained are illustrated in a photo at the end, Figure 66.

5.1.3.2)SiO_2, W, Mo on Si Studies.

The microscope was used for the initial examination of etched and coated specimens from the plasma rig. Initial examination of some etched samples, where the SiO_2 on Si has clearly been removed, failed to detect the edge profile, due to the isotropic nature of the etch and the poorly defined edge of the mask, even with lowered accelerating voltages. The method of measuring edge discontinuities by observing fringes in a drop on the surface and by using the Talystep was however adequate.

Work was done with both CF_4 and C_2F_6 as the etchant gases. The theoretically more reactive CF_4/O_2, C_2F_6/O_2 mixes were also tried, as being the various gases used in commercial plasma etching systems on SiO2, Mo and W films on Si. These mixtures were made up on the plasma rig gas mixing system, hence allowing the possibility of direct comparisons between the two systems. The mixtures were introduced through a micrometer needle valve, the maximum pressure allowable in the chamber again being determined by the vacuum trip. One interesting

area would be the effect of using XeF_2, if fluorination problems of the microscope can be overcome, as a comparison to XeF_2 with Ar^+ bombardment.

There was some evidence for a change in the X-ray emission from the surface as W or Mo films on Si were etched. Thus the Kevex detector was indicating the end of etch. However the absorption of Si characteristic radiation is high and hence care would have to be taken with this method for thicker films. Loss of the products WF_6, MoF_6, SiF_4 was easily obtained due to the high vacuum conditions and low boiling points, but breakdown products were not detected by the mass spectrometers. The fact that the electron beam is reducing, thus possibly producing lower valent higher melting point ionic compounds should be noted.

Work was stopped on this instrument due to the time it consumed because of the difficulties associated with controlled atmosphere microscopy, and the effort concentrated on the main plasma rig. Other work that was hoped to be achieved in the laying down of polymers and other coatings on substrates had to be abandoned.

5.2)GAS BREAKDOWN IN MASS SPECTROMETER.

A V.G. Magnetic Mass Spectrometer was used to study the breakdown of the homologous series of fluorocarbon gases as a function of varying ion energy. The measurements were made at energies of 15, 20, 40, and 100eV with the four pure gases. This was to study the ion induced reactions of these gases and also because there have been previous studies on measuring the appearance potentials of various CF_x species. Results obtained are shown below in Figure 57 for CF_4, C_2F_6, C_3F_8 and CHF_3 respectively. Attempts were then made to correlate this data with the thermodynamically favorable reaction routes calculated from the thermodynamic information available. Again due to hardware problems, now with its control computer, this mass spectrometer was unavailable for the more interesting C_xF_y/H_2 measurements.

In all cases, except CHF_3, the highest intensity signal was from CF_3^+, and the concentrations follow a pattern that is to be expected from the bond energies. For CHF_3 though, the CF_3^+ signal appears to be lower than expected, possibly due to CF_3 + H ---> CF_2 + HF.

Figure 57.

Gas Breakdown Studies in the Mass Spec Results

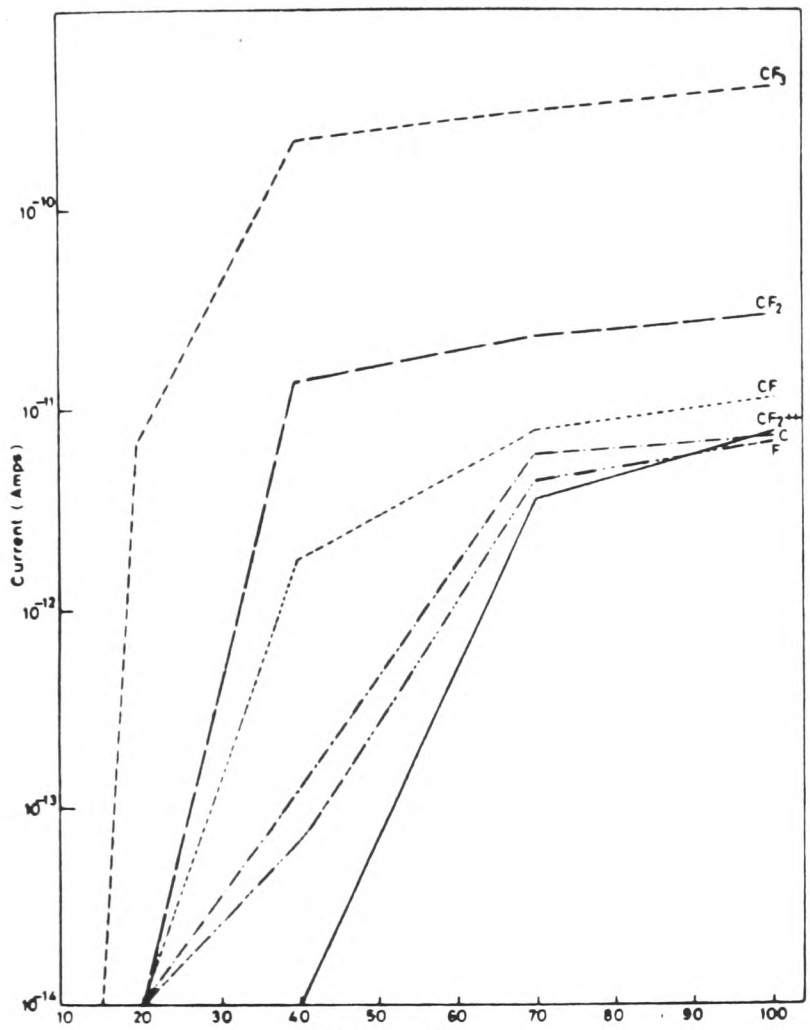

CF_4 GAS

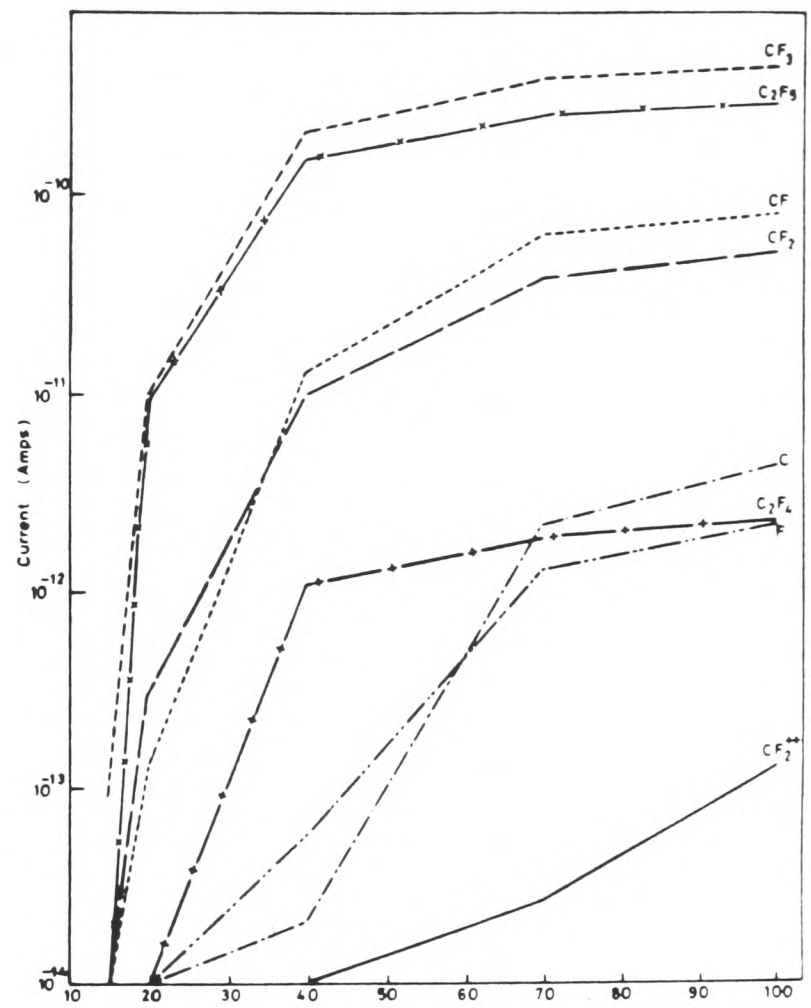

C_2F_6 GAS

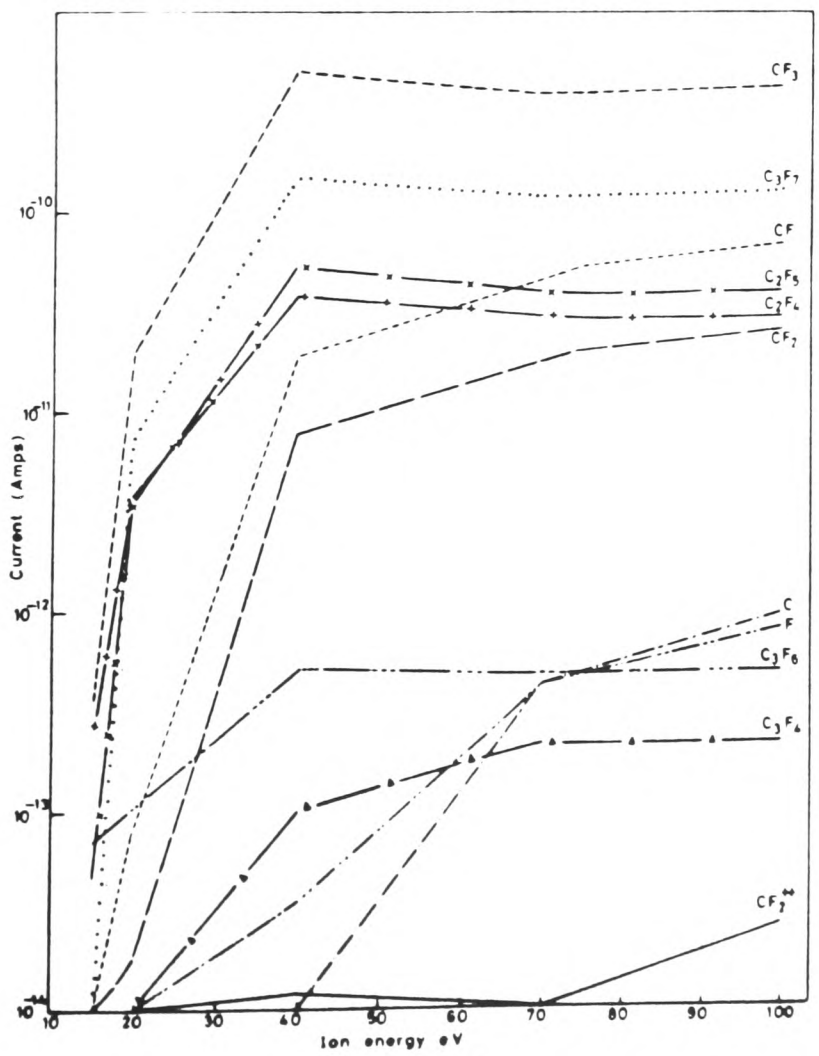

C_3F_8 GAS

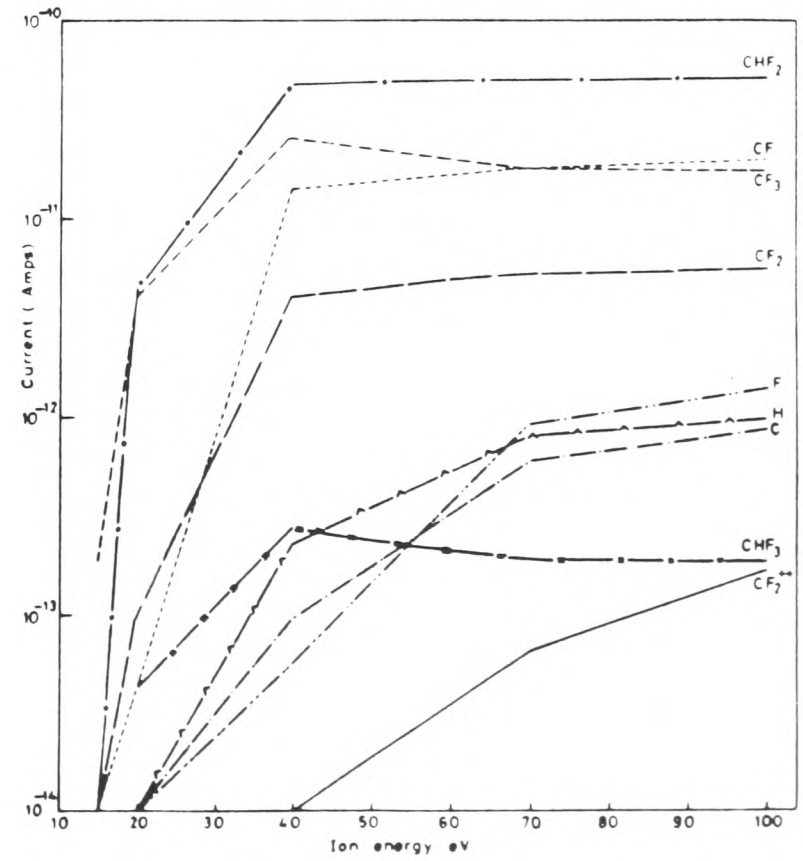

CHF_3 GAS

5.3)THERMODYNAMIC CALCULATIONS.

5.3.1)CF_n Species.

5.3.1.1)Heats of Formation.

Species.	kJ mol^{-1}
CF	+255
CHF	+126
CF_2	-182 (-171/-194)
CH_2F	-33
CHF_2	-248
CF_3	-472 (-469)
C_2F_5	-887 (-909)
CH_3CF_2	-303
C_3F_7	-1282
$CF=CF_2$	-192
H	+218
F	+79.1
CF_4	-911
CH_2F_2	-451
C_2F_4	-636
C_2F_6	-1324
C_3F_6	-1083
C_3F_7H	-285
C_3F_8	-1720
CHF_3	-680 (-698)
HF	-64.8
COF	-172
COF_2	-639
CF_3OF	-765

5.3.1.2)Bond Energies.

Species.					kJ mol^{-1}
H_2	--->	2H			436
F_2	--->	2F			157
HF	--->	H	+	F	569
# C_2F_4	--->	$2CF_2$			309 (293)
CF_3-F	--->	CF_3	+	F	519
CH_3-F	--->	CH_3	+	F	452
CHF_3	--->	CHF_2	+	F	505
CHF_3	--->	CF_3	+	H	427 (444)
C_2F_6	--->	C_2F_5	+	F	515 (477)

Notes:

C2F4 sigma-bond (142.1), pi-bond (163.3)

Average bond energies: C-C (607), C-F (536), C-H (337)

5.3.2)$C_xF_yH_z$ Reactions- Pure Gases.

Parent		Products			kJ mol^{-1}
CF_4	---->	CF_3	+	F	520
C_2F_6	---->	CF_3	+	CF_3	402
		C_2F_5	+	F	477
C_3F_8	---->	C_2F_5	+	CF_3	361
		C_3F_7	+	F	437
CHF_3	---->	CF_3	+	H	427
		CHF_2	+	F	505
Then:		CF_3 ----> CF_2 + F			
except for		CHF_3 ----> CF_2 + HF			

Note{489}: $2CF_2 + M \longrightarrow C_2F_4 + M$

k(3) ca. 2.1×10^7 $dm^3 mol^{-1} s^{-1}$ @ 298K

5.3.3)$C_xF_yH_z$ Reactions- H_2 Additions.

Parent	Products	kJ mol^{-1}
$CF_4 + H_2$ ---->	$CF_3 + HF$	502
$C_2F_6 + H_2$ ---->	$CF_3 + CF_3$	402
	$C_2F_5 + HF$	477
C3F8/H2 ---->	$C_2F_5 + CF_3$	361
	$C_3F_7 + HF$	437
CHF3/H2 ---->	$CF_3 + H$	427
	$CHF_2 + HF$	505
Then: CF3 + H ----> CF2 + HF except for CHF2 ----> CF + HF		

5.3.4)Si/SiO_2 processes.

5.3.4.1)Heats of Formation.

Species.	kJ mol^{-1}
SiF	ca. 4.2
SiF_2	-618.2
SiF_4	-1613

Ref{490}.

5.3.4.2)Bond Energies.

Species.	kJ mol^{-1}
Si-O	79
Si-F	540
Si-H	298.4

REFERENCES.

1) Sze.S.M.
Physics of Semiconductor Devices. Wiley; (1981)

2) Starbuck.C.
Priv Comm. Southampton Univ; (1984)

3) Wolf.S., Tauber.R.N.
Silicon Processing for the VLSI era. Lattice; (1986)

4) Sze.S.M.
VLSI Technology McGraw-Hill; (1983)

5) Ghandi.S.K.
VLSI Fabrication Principles. Wiley; (1983)

6) Integrated Circuit Engineering Corp.
Practical Integrated Circuit Fabrication. (1982)

7) Elliott.D.J.
I.C. Fabrication Technology. McGraw-Hill; (1982)

8) Howard.R.E., Hu.E.L., Namba.S., Pang.S.W. Eds.
Sci. & Technol. of Microfabrication. MRS Vol-76; (1987)

9) Matlock.J.H.
Proc. Electrochem. Soc. 77-5; 32, (1977)

10) Wittmer.M., Stimmell.J., Strathman.M. Eds.
Matrl. Issues in Si. IC. Processing. MRS Vol-71; (1986)

11) Bardsley.W.
Vacuum. 34(3-4); 391, (1984)

12) Bloem.J.
J. Electrochem. Soc. 117; 1397, (1970)

13) Pollack.M.A., Nahory.R.E., DeWinter.J.C., Ballman.A.A.
Applied Physics Letters. 33; 314, (1980)

14) Wang.F.F.Y., Ed.
Impurity Doping Processes in Si. North-Holland; (1981)

15) Lindhard.J., Scharff.M., Schiott.H.
Mat-Fys. Med. Dan. Vid. Selsk. 33(14); 1, (1984)

16) Introduction to Microlithography.
American Chemical Society. Series-219; (1983)

17) Moss.S.J., Ledwith.A.
The Chem. of the Semiconductor Ind. Blackie;Ch.9-10,(1986)

18) Flamm.D.L., Mucha.J.A.
Chapter in (17) (1986)

19) Vossen J.L., Kern W. Eds.
Thin Film Processes Academic; (1978)

20) Mort.J., Jansen.F. Eds.
Plasma Deposited Thin Films. CRC; (1986)

21) Heincke.R.A.H.
Solid State Electronics. 18(12); 1146, (1975)

22) Heincke.R.A.H.
Solid State Electronics. 19(12); 1039, (1976)

23) Mathad.G.S., Schwartz.G.C., Gottscho.R.A. Eds.
Plasma Processing. Proc. Electrochem. Soc. 87-6; (1987)

24) Chang.R.P.H., Abeles.B. Eds.
Plasma Synthesis & Etching MRS Vol-38; (1985)

25) Coburn.J.W., Gottscho.R.A., Hess.D.W. Eds.
Plasma Processing. MRS Vol-68; (1986)

26) Donnelly.V.M., Herman.I.P., Hirose.M. Eds.
Photon, Beam & Plasma Processes MRS Vol-75; (1987)

27) ALVEY VLSI, Users Guide to New Si Technology.
DTI/PUB003/5k/06/87; (1987)

28) Coburn.J.W., Winters.H.F.
Annual Rev. Materials Science. 13; 91, (1983)

29) Maleham.J.
IEE Vacation School. Lecture-1; (1986)

30) Koenig.H.R., Maissel.L.I.
IBM J. Res. Development. 168, (1970)

31) Lee.R.E.
J. Vac. Sci. Technology. 16; 164, (1979)

32) Carter.G., Lewis.G.N., Nobes.M.J., Cox.J., Begemann.W.
Vacuum. 34(3-4); 445, (1984)

33) Bondur.J.A.
J. Vac. Sci. Technol. 13(5); 1023, (1976)

34) Schwartz.G.C., Schaible.P.M.,
J. Electrochem. Soc. 130(9); 1898, (1983)

35) Chang.J.S.
Solid State Technology. 27(4); 214, (1984)

36) Downey.D.F., Bottoms.W.R., Hanley.P.R.
Solid State Technology. 24; 181, (1981)

37) Mayer.T.M., Barker.R.A.
J. Electrochem. Soc. 129(3); 585, (1982)
or Proc. Electrochem. Soc. 82-6; 436, (1982)

38) Chinn.J.D., Phillips.W., Adesida.I., Wolf.E.D.
J. Electrochem. Soc. 131(2); 375, (1984)

39) Bersin.R.A.
Solid State Technology. 19(5); 31, (1975)

40) Donnelly.V.M., Flamm.D.L., Tu.C.W., Ibbotson.D.E.
J. Appl. Phys. 55(1); 242, (1984)

41) Class.W.H., Hurwitt.S.D., Hill.M.l., Hutt.M.K.
European Patent 0,084,970 A2 (1983)

42) Broydo.S.
Solid State Technology. 26(4); 159, (1983)

43) Bondur.J.A., Clarke.H.A.
Solid State Technology. 23(4); 122, (1980)

44) Bruce.R.H.
Solid State Technology. 24(10); 64, (1981)

45) Parry.P.D., Rodde.A.F.
Solid State Technology. 24(4); 125, (1981)

46) Bruce.R.H.,Reinberg.A.R.
J. Electrochem. Soc. 129(2); 393, (1982)

47) Armstrong.N.P., Maleham.J.
Vacuum. 33(5); 291, (1983)

48) Zarowin.C.B.
Proceedings Electrochem. Soc 83-10; 11, (1983)

49) Poulsen.R.G., Brochu.M.
Proc. Symp. Etch. Pattern Definition. 111, (1977)

50) Enomoto.T., Denda.M., Yasuoka.A., Nakata.H.
Jpn. J. Appl. Phys. 18(1); 155, (1979)
or Solid State Technology. 23(4); 117, (1980)

51) Reinberg.A.R., et al.
Electrochem. Soc. Abstr. 81-1; 669, (1981)

52) Chang.J.S.
Solid State Technology. 27(4); 214, (1984)

53) Reinberg.A.R., Dalle-Ave.J., Steinberg.G., Bruce.R.
Proceeding of Electrochem. Soc. 82-6; 198, (1984)

54) Mogab.C.J.
J. Electrochem. Soc. 124(8); 1262, (1977)

55) Chapman.B.N., Hansen.T.A., Minkiewicz.V.J.
J. Applied Physics. 51(7); 3608, (1980)

56) Doken.M., Miyata.I.
J. Electrochem. Soc. 126(12); 2235, (1979)

57) Aktik.M., Segui.Y., Bui Ai.
J. Appl. Physics. 50(10); 6567, (1979)

58) Mathad.G.S.
Electrochem. Soc. Abstr. 81-1; 720, (1981)

59) Brosset.D., Bui Ai., Segui.Y.
Applied Physics Letters. 33(1); 87, (1978)

60) Pang.S.W.
Solid State Technology. 27(4); 249, (1984)

61) Watanabe.T., Yoshida.Y.
Solid State Technology. 27(4); 213, (1984)

62) Ephrath.L.M., DiMara.D.J.
Solid State Technology. 24(4); 182, (1981)

63) Watanabe.T., Yoshida.Y.
Solid State Technology. 27(4); 213, (1984)

64) Deshmukh.V.G.I.
IEE Vacation School. Lecture-16; (1986)

65) Jackson.G.N.
Vacuum. 21(11); 533, (1971)

66) Chapman.B.N.
Glow Discharge Processes Wiley; (1980)

67) Smith.D., Adams.N.G.
Pure & Applied Chem. 56(2); 175, (1984)

68) Gill.M.D.
Vacuum. 34(3-4); 357, (1984)

69) Chatterton.P.A.
IEE Vacation School. Lecture-2; (1986)

70) Bell.A.T.
J. Vac. Sci. Technol. 16(2); 418, (1979)

71) Bell.A.T.
Proc. Electrochem. Soc. 77-5; 205, (1980)

72) Winters.H.F. in
Topics in Current Chemistry. 94; 69, (1980)

73) Venugopalen.M., Verprek.S.
Topics in Current Chemistry. 107; 47, (1983)

74) Bondur.J.A.
J. Vac. Sci. Technol. 13(5); 1023, (1976)

75) Holland.L.
J. Vac. Sci. Technol. 14(1); 5, (1977)

76) Poulsen.R.G.
J. Vac. Sci. Technol. 14(1); 266, (1977)

77) Lehmann.H.W., Widmer.R.
J. Vac. Sci. Technol. 15; 319, (1978)

78) Bell.A.T.
Solid State Technology. 21(4); 89, (1978)

79) Kalter.H., van de Ven.E.P.G.T..
Phillips Technical Review. 38(7-8); 200, (1978)

80) Melliar-Smith.C.M., Mogab.C.J.in:
(19) Thin Film Processes. Academic; 497, (1978)

81) Coburn.J.W., Winters.H.F.
J. Vac. Sci. Technol. 16(2); 391, (1979)

82) Lehmann.H.W., Widmer.R.
J. Vac. Sci. Technol. 17)5; 1177, (1980)

83) Booth.R.C., Heslop.C.J.
Thin Solid Films. 65; 111, (1980)

84) Mogab.C.J.
Inst. Physics Conference. Serial-53; 37, (1980)

85) Curran.J.E.
Thin Solid Films. 86; 101, (1981)

86) Dieleman.J.
Thin Solid Films. 86; 147, (1981)

87) Ephrath.L.M.
Proceedings Electrochem. Soc. 81-5; 627, (1981)

88) Flamm.D.L., Donnelly.V.M.
Plasma Chem. Plasma Process. 1; 317, (1981)

89) Kurogi.Y.J.
Thin Solid Films. 92; 33, (1982)

90) Ephrath.L.M.
J. Electrochem. Soc. 129(3); 62C, (1982)

91) Coburn.J.W.
Plasma Chem. Plasma Process. 2; 1, (1982)

92) Flamm.D.L., Donnelly.V.M., Ibbotson.D.E.
J. Vac. Sci. Technol.-B. 1(1); 23, (1983)

93) Curran.J.E.
Vacuum. 34(3-4); 343, (1984)

94) Turban.G.
Pure & Applied Chem. 56(2); 215, (1984)

95) Turban.G.
Electrochem. Soc. Abstr. 81-1; 636, (1981)

96) Valente.M., Queirolo.G.
J. Electrochem. Soc. 131(5); 1132, (1984)

97) Brewer.J.A., Miller G.N.
J. Vac. Sci. Technol.-B. 1(4); 932, (1983)

98) Horiike.Y., Sugawara.T., Okano.H., et al.
Jpn. J. Appl. Physics. 20(4); 803, (1981)

99) Nagy.A.G., Hess.D.W.
J. Electrochem. Soc. 129(11); 2530, (1982)

100) Coburn.J.W., Winters.H.F.
J. Appl. Physics. 48(8); 3532, (1977)

101) Coburn.J.W., Winters.H.F., Chuang.T.J.
J. Appl. Physics. 50(5); 3189, (1979)

102) Coburn.J.W., Winters.H.F.
J. Vac. Sci. Technol. 18(3); 825, (1981)

103) Tachi.S., Miyake.K., Tokuyama.T.
Jpn. J. Appl. Physics (Suppl). 21(1); 141, (1982)

104) Gerlach-Meyer.U., Coburn.J.W., Kay.E.
Surface Science. 103; 177, (1981)

105) Mayer.T.M., Barker.R.A.
J. Vac. Sci. Technol. 21(3); 757, (1982)

106) McNevin.S.C., Becker.G.E.
J. Vac. Sci. Technol-A. 2(2); 505, (1984)

107) McNevin.S.C., Becker.G.E.
J. Vac. Sci. Technol-B. 2(1); 27, (1984)

108) Coburn.J.W., Winters.H.F.
J. Appl. Physics. 50(5); 3189, (1979)

109) Winters.H.F.
J. Vac. Sci. Technol-B. 1(4); 927, (1983)

110) Astell-Burt.P.J., Ditmer.G.A., Webb.D.R., et al.
MRS Symposium Proceedings. Fall meeting; (1987)

111) Winters.H.F., Coburn.J.W., Kay.E.
J. Appl. Physics. 48(12); 4973, (1977)

112) Winters.H.F.
J. Appl. Physics. 49(10); 5165, (1978)

113) Coburn.J.W.
IBM. J. Research & Development. 23; 1, (1979)

114) Flamm.D.L., Mogab.C.J., Sklaver.E.R.
J. Appl. Physics. 50(10); 6211, (1979)

115) Flamm.D.L., Donnelly.V.M., Mucha.J.A.
J. Appl. Physics. 52(5); 3633, (1981)

116) Ibbotson.D.E., Flamm.D.L.
IEEE Transactions. EI-17(2); 163, (1982)

117) Vinogradov.G.K., Nevzorov.P.I., Polak.L.S., Slovetsky.D.I.
Vacuum. 32(9); 529, (1982)

118) Vasile.M.J., Stevie.F.A.
J. Appl. Physics. 53(5); 3799, (1982)

119) Flamm.D.L., Donnelly.V.M., Ibbotson.D.E.
J. Vac. Sci. Technol-B. 1(1); 23, (1983)

120) Winters.H.F., Coburn.J.W., Chuang.T.J.
J. Vac. Sci. Technol-B. 1(2); 469, (1983)

121) Kay.E., Coburn.J.W., Dilks.A.
Topics in Current Chem. 94; 1, (1982)

122) Mogab.C.J., Adams.A.C., Flamm.D.L.
J. Appl. Phys. 49(7); 3796, (1978)

123) Truesdale.E.A., Smolinsky.G.
J. Appl. Physics. 50(11); 6594, (1979)

124) Degenkolb.E.O., Mogab.C.J., Goldrick.M.R.
Applied Spectroscopy. 30; 520, (1976)

125) Griffiths.J.E., Degenkolb.E.O.
Applied Spectroscopy. 31(2); 134, (1977)

126) Harshbarger.W.R., Porter.R.A., Miller.T.A., Norton.P.
Applied Spectroscopy. 31(3); 201, (1977)

127) Harshbarger.W.R., Porter.R.A.
Solid State Technology. 21(4); 99, (1978)

128) Harshbarger.W.R.
Solid State Technology. 25(4); 126, (1982)

129) Flamm.D.L.
Solid State Technology. 22(4); 109, (1979)

130) Flamm.D.L.
Plasma Chem. Plasma Processing. 1(1); 37, (1981)

131) Saunders.F.H.M., Dielman.J.
Proceedings Electrochem. Soc. 81-5; 638, (1981)

132) Kushner.M.J.
J. Appl. Physics. 53(4); 2923, (1982)

133) Lee.Y.H., Chen.M-M.
J. Appl. Physics. 54(10); 5966, (1983)

134) Korman.C.S.
J. Vac. Sci. Technol. 20; 476, (1982)

135) Burton.R.H., Smolinsky.G.
J. Electrochem. Soc. 129(7); 1599, (1982)

136) Smolinsky.G., Gottscho.R.A., Abys.S.M.
J. Appl. Phys. 54(6); 3518, (1983)

137) Heicklen.J., Knight.V., Greene.S.A.
J. Chem. Physics. 42(1); 221, (1965)

138) D'Agostino.R., Cramarossa.F., DeBenedictus.S.
Plasma Chem. Plasma Processing. 2; 213, (1982)

139) D'Agostino.R., Cramarossa.F., et al.
J. Appl. Physics. 54(3); 1284, (1983)

140) Millard.M.M., Kay.E.
J. Electrochem. Soc. 129(1); 160, (1982)

150) Brown.W.A., Kamins.T.I.
Solid State Technology. 22(4); 51, (1979)

151) Adams.A.C.
Solid State Technology. 26(4); 135, (1983)

152) Rand.M.J.
J. Vac. Sci. Technol. 16(2); 420, (1979)

153) Endo.A., Yada.T.
J. Appl. Physics. 23(3); 384, (1983)

154) Bell.A.T.
Topics in Current Chemistry. 94; 43, (1980)

155) Bell.A.T.
Polymer Preprints. 16(1); 27, (1975)

156) Hollahan.J.R., Bell.A.T.
Techn. & Applications of Plasma Chem. Wiley; (1974)

157) Lam.D.K.
Polymer Preprints. 16(1); 50, (1975)

158) Morita.S., Sawa.G., Ieda.M.
Polymer Preprints. 16(1); 73, (1975)

159) Tibbitt.J.M., Shen.M., Bell.A.T.
J. Macromol. Sci. Chem. A10(8); 1623, (1976)

160) Morosoff.N., Newton.W., Yasuda.H.
J. Vac. Sci. Technol. 15(6); 1815, (1978)

161) Henis.N.B.H., So.Y-H., Miller.L.L.
J. Am. Chem. Soc. 103; 4634, (1981)

162) Miller.L.L., So.Y-H.
J. Am. Chem. Soc. 103; 4204, (1981)

163) Inspektor.A., Carmi.U., Avni.R., Nickel.H.
Plasma Chem. Plasma Process. 1(4); 377, (1981)

164) Drauglis.E., Wielsonski.R.F., Sliemens.F.A.
Organic Coat. & Plastics Chem. ACS-184; 554, (1982)

165) Martinu.L., Biederman.H.
Vacuum. 33(5); 253, (1983)

166) Kinzig.B.J.
Polymer Preprints. (21)2; 66, (1982)

167) Millard.M.M., Windle.J.J., Pavlath.A.E.
J. Appl. Polymer Sci. 17; 2501, (1973)

168) Kay.E.
Int. Symp. Plasma Chem-4th. 30, (1979)

169) Kaganowicz.G.,Datta.P.,Robinson.J.W.
Int. Symp. Plasma Chem-4th. 152, (1979)

170) Retajczyk.T.F.,Gallagher.P.K.
Materials Letters. 2(1); 23, (1983)

171) Boothanom.N., White.M.
Thin Solid Films. 24; 395, (1974)

172) Roy.R.A., Messier.R., Krishnaswamy.S.V.
Thin Solid Films. 109; 27, (1983)

173) Sadhir.R.K., James.W.J., Auerbach.R.A.
Thin Solid Films. 97; 17, (1982)

174) Mathad.G.S.
Electrochem. Soc. Abstr. 81-1; 720, (1981)

175) Peccoud.L., LaPorte.Ph., Chevallier.M.
Vide Couches Minces. 212; 71, (1982)

176) Poll.H.U., Meichsner.J., Steinrucken.A.
Thin Solid Films. 112(4); 369, (1984)

177) Wielonski.R.F., Beale.H.A.
Thin Solid Films. 84; 425, (1981)

178) Asano.Y.
Thin Solid Films. 105; 1, (1983)

179) Asano.Y., Yamazaki.H., Morinaka.A.
Jpn. J.Appl.Phys. 22(3); 480, (1983)

180) Kay.E., Dilks.A., Hetzler.U.
J. Macromol. Sci. Chem.-A. 12(9); 1393, (1978).

181) Kay.E., Dilks.A.
J. Vac. Sci. Technol. 16(2); 428, (1979)

182) Kay.E., Dilks.A.
ACS Symposium. 108; 195, (1979)

183) Kay.E., Dilks.A.
Topics in Current Chem. 94; 1, (1980)

184) Kay.E., Dilks.A., Seybold.D.
J. Appl. Physics. 51(11); 5678, (1981)

185) Kay.E., Dilks.A.
Thin Solid Films. 78; 309, (1981)

186) Kay.E., Dilks.A.
J. Vac. Sci. Technol. 18(1); 1, (1981)

187) Bubeck.C., Kay.E.
J. Vac. Sci. Technol. 18(2); 320, (1981)

188) Kay.E., Hecq.M.
J. Appl. Physics. 55(2); 370, (1983)

189) Biederman.H.
Vacuum. 34(3-4); 405, (1984)

190) Biederman.H., Holland.L.
Nuclear Instruments & Methods. 212; 497, (1983)

191) Hecq.M., Zieman.P., Kay.E.
J. Vac. Sci. Technol-A. 1(2); 364, (1983)

192) Kay.E., Hecq.M.
Surface Science -preprint. (1983)

193) Greene.J.E.
J. Vac. Sci. Technol. 15(2); 203, (1978)

194) Marcoux.P.J., Dow Foo.P.
Solid State Technology. 24(4); 115, (1981)

195) Korman.C.S.
Solid State Technology. 25(4); 115, (1982)

196) Kolodner.P., Katzir.A., Hartsough.N.
Proc. Electrochem. Soc. 83-10; 452, (1983)

197) Kolodner.P., Katzir.A., Hartsough.N.
J. Vac. Sci. Technol.-B. 1(2); 501, (1983)

198) Curtis.B.J., Brunner.H.J.
J. Electrochem. Soc. 125(5); 829, (1978)

199) Harshbarger.W.R., Porter.R.A., Norton.P.
J. Electron. Mater. 7(3); 429, (1978)

200) Hirobe.K., Tsuchimoto.T.
J. Electrochem. Soc. 127(1); 234, (1980)

201) Zijlastra.P.A., Beenakker.C.I.M.
Applied Spectroscopy. 35(4); 413, (1981)

202) Gelerent.B.
European Patent 0,062,302. (1982)

203) Donnelly.V.M., Flamm.D.L.
US Patent 4,377,436. (1983)

204) Bunyard.G.B., Raby.B.A.
Solid State Technology. 20(12); 53, (1977)

205) Oshima.M.
Jpn. J. Appl. Phys. 17(3); 579, (1978)

206) Brown.H.L., Bunyard.G.B., Lin.K.C.
Solid State Technology. 21(7); 35, (1978)

207) Busta.H.H., Lagos.R.E., Kiewit.D.A.
Solid State Technology. 22(2); 61, (1979)

208) Curtis.B.J., Brunner.H.R.
Int. Symp. Plasma Chem-4th. 139, (1979)

209) Sternheim.M., VanGelder.W.
Electrochem. Soc. Abstr. 81-1; 717, (1981)

210) Trumpp.H.J., Greschner.J.
Proc. Electrochem. Soc 82-6; 348, (1982)

211) Sternheim.M., Van Gelder.W., Hartman.A.W.
Proc. Electrochem. Soc 82-6; 356, (1982)

212) Sternheim.M., VanGelder.W., Hartman.A.W.
J. Electrochem. Soc. 130(3); 655, (1983)

213) Coe.M.E.B.
US Patent 4,345,968. (1982)

214) Coe.M.E.B.
PCT 00660. (1982)

215) Ukai.K., Hanazawa.K.
J. Vac. Sci. Technol. 16(2); 385, (1979)

216) Tretola.A.R.
US Patent 4,207,137. (1980)

219) Duval.P.
Revue Phys. Appl. 15; 1479, (1980)

220) O'Hanlon.J.F.
Solid State Technology. 24(10); 89, (1981)

221) Duval.P.
Solid State Technology. 25(9); 124, (1982)

222) O'Hanlon.J.F.
J. Vac. Sci. Technol-A. 2(2); 174, (1984)

223) Lam.D.K., Koch.G.R.
Solid State Technology. 23(8); 199, (1980)

224) Peterson.J.F., Steinherz.H.A.
Solid State Technology. 24(11); 82, (1981)

225) Peterson.J.F., Steinherz.H.A.
Solid State Technology. 25(1); 104, (1982)

226) Laurenson.L., Dennis.N.T.M., Newton.J.
Vacuum. 29(11-12); 433, (1979)

227) Sirkin.E.R., Powell.R.D.
J. Vac. Sci. Technol-B. 1(1); 74, (1983)

228) Herb.G.K., et al.
Solid State Technology. 26(8); 185, (1983)

229) Bance.U.R., Drummond.I.W., et al
Vacuum. 28(10-11); 489, (1978)

230) Ferran.R.J., Sullivan.J.J.
J. Vac. Sci. Technol. 12(1); 560, (1975)

231) Reed.T.B.
J. Appl. Phys. 32(5); 821, (1961)

232) Fassel.V.A.
Science. 202; 183, (1978)

233) Coburn.J.W., Kay.E.
J. Appl. Phys. (43)12; 4965, (1972)

234) Class.W.H.
M.R.C. Book of Basics 2nd.Ed; (1983)

235) Kern.W., Vossen.J.L. (Ed).
Thin Film Processes. Academic; (1978)

236) Kingsnorth.R.
IEEE. ED-27(12); 105, (1983)

237) Clark.W.R., Sullivan.J.J.
Solid State Technology. (25)3; 82, (1981)

238) Mauer.J.L., Logan.J.S.
J. Vac. Sci. Technol. 16(2); 404, (1981)

239) Kiesling.R.A., Sullivan.J.J.
J. Vac. Sci. Technol. 15(2); 771, (1978)

240) Chapman.B.N., Minkiewicz.V.J.
J. Vac. Sci. Technol. 15(2); 329, (1978)

241) Shibagaki.M., Horiike.Y., Yamazaki.T.
USP 4,160,690. (1979)

242) Chapman.B.N., Hansen.T.A., Minkiewicz.V.J.
J. Appl. Phys. 51(7); 3608, (1980)

243) Turban.G., Pasquereau.J., Rapeaux.M., et al.
Electrochem. Soc. Extended Abstr. 81-1; 636, (1981)

244) Curran.J.E.
Vacuum. 34(3-4); 343, (1984)

245) Logan.J.S., Mazza.N.M., Davidse.P.D.
J. Vac. Sci. Technol. 6; 120, (1968)

246) Kobayashi.H., Bell.A.T., Shen.M.
Polymer Preprints. 16(1); 44, (1975)

247) Koda.S.
J. Phys. Chem. 83(16); 2065, (1979)

248) Martinet.F.
Electrochem. Soc. Abstr. 81-1; 723, (1981)

249) Martinet.F.
Proc. Electrochem. Soc 82-6; 379, (1982)

250) Mosburg.E., Kerns.R., Abelson.J.
Electrochem. Soc. Abstr. 81-1; 727, (1981)
Proc. Electrochem. Soc 82-6; 410, (1982)

251) Bruce.R.H., Reinberg.A.R.
J. Electrochem. Soc. 129(2); 393, (1982)

252) Mantei.T.D.
J. Electrochem. Soc. 130(9); 1958, (1983)

253) Nagy.A.G.
Solid State Technology. 26(12); 173, (1983)

254) Thornton.J.A.
J. Vac. Sci. Technol. 15(2); 188, (1978)

255) Clements.R.M.
J. Vac. Sci. Technol. 15(2); 193, (1978)

256) Eser.E., Ogilive.R.E., Taylor.K.A.
J. Vac. Sci. Technol. 15(2); 199, (1978)

257) Steinbruchel.Ch.
J. Electrochem. Soc. 130(3); 648, (1983)

258) Hurley.R.E.
Vacuum. 34(3-4); 351, (1984)

259) Toyoda.H., Tobinga.M., Komiya.H.
Jpn. J.Appl.Phys. 20(3); 681, (1981)

260) Bruce.R.H., Flamm.D.L., Donnelly.V.M., Duncan.B.S.
Electrochem. Soc. Abstr. 81-1; 631, (1981)

261) Koyama.K., Takasaki.K., Maeda.M., Takagi.M.
Proc. Electrochem. Soc 82-6; 478, (1982)

262) Suzuki.K., Okudaira.S., Kanomata.I.
Jpn. J. Appl.Phys. 20(3); 681, (1981)

263) Jinno.K.
Jpn. J. Appl.Phys. 17(7); 1283, (1978)

264) Suzuki.K., Okudaira.S., Kanomata.I.
J. Electrochem. Soc. 126(6); 1024, (1979)

265) Hartman.D.C.
Electrochem. Soc. Extended Abstr. 81-1; 662, (1981)

266) Suzuki.K., Okudaira.S., Nishimatsu.S., et al.
J. Electrochem. Soc. 129(12); 2764, (1982)

267) Kay.E.
Priv. Comm. (1982)

268) EerNisee.E.P.
J. Vac. Sci. Technol. 12(1); 564, (1975)

269) Lu.C.S.
J. Vac. Sci. Technol. 12(1); 578, (1975)

270) Benes.E.
J. Appl. Phys. 56(3); 608, (1984)

271) Lue.J.T.
Vacuum. 32(12); 711, (1982)

272) Stevens.D.S., Tiersen.H.F., Sinha.K.A.
J. Appl. Phys. 54(4); 1704, (1983)

273) Sauerbrey.G.Z.
Phys. Verhandl. 8; 113, (1957)

274) Sauerbrey.G.Z.
Z.Physik. 155; 206, (1959)

275) Heyman.J.S., Miller.W.E.
J. Vac. Sci. Technol. 15(2); 219, (1979)

276) Chandler.P.J., Meek.P.R., Holland.L.
Thin Solid Films. 86(4); 183, (1981)

277) Curtis.B.J., Brunner.H.R.
Int. Symp. Plasma Chem. -5th. 318, (1981)

278) Beenakker.C.I.M., vanDommelen.J.H.J., van de Poll.R.P.
J. Appl. Phys. 52(1); 480, (1981)

279) Gottscho.R.A., Miller.T.A.
Pure & Appl. Chemistry. 56(2); 189, (1984)

280) Harshbarger.W.R., Porter.R.A., Miller.T.A., Norton.P.
Applied Spectroscopy. 31(3); 201, (1977)

281) Harshbarger.W.R., Porter.R.A.
Solid State Technology. 24(4); 99, (1978)

282) Frieser.R.G., Nogay.J.
Applied Spectroscopy. 34(1); 31, (1980)

283) Klinger.R.E., Greene.J.E.
Proc. Electrochem. Soc. 81-1; 257, (1981)

284) Frieser.R.G., Nogay.J.
Proc. Electrochem. Soc. 81-1; 275, (1981)

285) Zaidel.A.N., Prokofiev.V.K., Raiskii.S.M.
Tables of Spectral Lines. Pergamon; (1961)

286) Pearce.R.W.B., Gaydon.A.G.
Identification of Molecular Spectra. 4th Ed; (1978)

287) Hertzberg.G.
Electronic Spectra. Vol.III. Van Nostrand; (1955)

288) Ramsay.D.A.
Annual Rev. New York Acad. Sci. 67; 485, (1957)

289) Hesser.J.E.
J. Chem. Phys. 48(6); 2518, (1968)

290) Andrews.E.B., Barrow.R.F.
Nature. 165; 890, (1950)

291) Andrews.E.B., Barrow.R.F.
Proc. Phys. Soc. 64; 481, (1951)

292) Kuzyakov.Y.Y., Tatevskii.V.M.
Optika. Spektrosk. 5; 699, (1959)

293) Mann.D.E., Broida., Squires.B.E.
J. Chem. Phys. 22; 348, (1954)

294) Porter.T.L., Mann.D.E., Acquista.N.
J. Mol. Spec. 16; 228, (1965)

295) Carroll.P.K., Grennan.T.P.
J. Phys. B. 3; 865, (1970)

296) Tiee.J.J., Wampler.F.B., Rice.W.W.
Chem. Phys. Letters. 68(2-3); 403, (1979)

297) Bass.A.M., Mann.D.E.
J. Chem. Phys. 36; 3501, (1962)

298) Laird.R.K., Andrews.E.B., Barrow.R.F.
Transactions of Faraday Soc.-334. 46(10); 803, (1950)

299) Venkateswarlu.P.
Physics Review. 77(5); 676, (1950)

300) Margrave.J.L., Wieland.K.
J. Chem. Phys. 21; 1552, (1953)

301) Mann.D.E., Thrush.B.A.
J. Chem. Phys. 33(6); 1732, (1960)

302) Simons.J.P., Yarwood.A.J.
Nature. 187; 316, (1960)

303) Simons.J.P., Yarwood.A.J.
Nature. 192; 943, (1961)

304)

305) Nelson.L.S., Kuebler.N.A.
J. Chem. Phys. 37(1); 47, (1962)

306) Thrush.B.A., Zwolenik.J.J.
Transactions of Faraday Soc. 59; 582, (1963)

309) Mathews.C.W.
J. Chem. Phys. 45; 1068, (1966)

310) Mathews.C.W.
Canadian J. Phys. 45; 2355, (1967)

311) Marsigny.L., LeBreton.J., Ferran.J., LaGrange.R.
Comptes. Rendu. Acad. Sci.-C. 266; 9, (1968)

312) Marsigny.L., Ferran.J., LeBreton.J., LaGrange.R.
Comptes. Rendu. Acad. Sci.-C. 266; 507, (1968)

313) Gilbert.R., Theoret.A.
J. Phys. Chem. 80(9); 1017, (1976)

314) Quach-Tat-Trung., Durocher.G., et al.
Chem. Phys. Letters. 47(3); 404, (1977)

315) Johnson.C.A.F., Ross.H.J.
J. Chem. Soc. Farad. Trans.-I. 2930, (1978)

316) Wampler.F.B., Tiee.J.J., Rice.W.W., Oldenberg.R.C.
J. Chem. Phys. 71(10); 3926, (1979)

317) Dalby.F.W.
J. Chem. Phys. 41(8); 2297, (1964)

318) Akins.D.L., King.D.S., Stephenson.J.C.
Chem. Phys. Letters. 65(2); 257, (1979)

319) Koda.S.
J. Phys. Chem. 83(16); 2065, (1979)

320) DePristo.A.E.
J. Chem. Phys. 73(9); 4329, (1980)

321) Hack.W., Langel.W.
J. Photochemistry. 21; 105, (1983)

322) Hack.W., Langel.W.
J. Phys. Chem. 87(18); 3462, (1983)

323) Dornhofer.G., Hack.W., Langel.W.
J. Phys. Chem. 87(18); 3456, (1983)

324) Kerr.K.C., Pimental.G.C.
Applied Optics. 4(1); 25, (1965)

325) Powell.F.X.
J. Chem. Phys. 45; 1067, (1966)

326) Suto.M., Washida.N.
J. Chem. Phys. 78(3); 1007, (1983)
& cont: Pt.II, III, IV pp. 1012, 1019, 1025.

327) Carson.G.A., Pimental.G.C.
J. Chem. Phys. 44; 4053, (1966)

328) Johnson.R.C., Jenkins.H.G.,
Proceedings Royal Soc.-A. 116; 327, (1927)

329) Asundi.R.K., Samuel.R.
Proceedings Ind. Acad. Sci. 3; 346, (1936)

330) Eyster.E.H.
Physics Rev. 51; 1078, (1937)

331) Barrow.R.F., Butler.D., Johns.J.W.C., Powell.J.L.
Proceedings Phys. Soc. 73; 317, (1959)

332) Verma.R.D.
Canadian J. Physics. 40; 586, (1962)

333) Sankaranayanan.S., Narayanan.P.S.
Proc. Nat. Inst. Sci. India-A. 32; 56, (1966)

334) Appleblad.O., Barrow.R.F., Verma.R.D.
J. Phys. B. 1; 274, (1968)

335) Johns.J.W.C., Barrow.R.F.
Proceedings Physics Soc. 71; 476, (1958)

336) Dovell.W.H., Barrow.R.F.
Proceedings Physics Soc.-A. 64; 98, (1951)

337) Johns.J.W.C., Chantry.G.W., Barrow.R.F.
Transactions Farad. Soc.-431. 54(11); 1589, (1958)

338) Rao.D.R.
J. Molecular Spectroscopy. 34; 284, (1970)

339) Rao.V.M., Curl.R.F., Timms.P.L., Margrave.J.L.
J. Chem. Phys. 43; 2557, (1965)

340) Rao.V.M., Curl.R.F.
J. Chem. Phys. 45(6); 2032, (1966)

341) Bassler.J.M., Timms.P.L., Margrave.J.L.
J. Am. Chem. Soc. 5(5); 729, (1966)

342) Rao.D.R., Venkateswarlu.P.
J. Mol. Spec. 7; 287, (1961)

343) Khanna.V.M., Besenbruch.G., Margrave.J.L.
J. Chem. Phys. 46(6); 2310, (1967)

344) Dixon.R.N., Halle.M.
J. Mol. Spec. 48; 192, (1970)

345) Wang.J.L-F., Krishman.C.N., Margrave.J.L.
J. Mol. Spec. 48; 346, (1973)

346) Donnelly.V.M., Flamm.D.L., Mucha.J.A.
Proceedings Electrochem. Soc. 81-1; 270, (1981)

347) Flamm.D.L., Donnelly.V.M., Mucha.J.A.
J. Appl. Phys. 52(5); 3633, (1981)

348) Porlezza.C.
Rend. Acad. Linc. 33; 283, (1924)

349) Karlicek.R.F., Donnelly.V.M., Johnson.W.D.
Material Research Soc. Symp. Proc. 17; 151, (1983)

350) Karlicek.R.F., Donnelly.V.M., Johnson.W.D.
Material Research Soc. Symp. Proc. 17; 151, (1983)

351) Ashfold.M.N.R., Castano.F., Hancock.G., Ketley.G.W.
Chem. Phys. Letters. 73(3); 421, (1980)

352) Hancock.G., Ketley.G.W.
J. Chem. Soc. Faraday Trans.-2. 78; 1283, (1982)

353) Hancock.G., Ketley.G.W., MacRobert.A.J., McKendrick.K.
Bulletin Soc. Chim. Belg. 92; 638, (1983)

354) Hancock.G., Ketley.G.W., MacRobert.A.J.
J. Phys. Chem. 88; 2104, (1984)

355) King.D.S., Stephenson.J.C.
Chem. Phys. Letters. 51(1); 48, (1977)

356) King.D.S., Stephenson.J.C.
J. Am. Chem. Soc. 100; 7151, (1978)

357) Hancock.G.
Priv. Comm. (1982)

358) Sam.C.L., Yardley.J.T.
Chem. Phys. Letters. 61(3); 509, (1979)

359) Huie.R.E., Long.N.J.T., Thrush.B.A.
Chem. Phys. Letters. 51(2); 197, (1977)

360) Bialkowski.S.E., King.D.S., Stephenson.J.C.
J. Chem. Phys. 71(10); 4010, (1979)

361) Tiee.J.J., Wampler.F.B., Rice.W.W.
Chem. Phys. Letters. 65(3); 425, (1979)

362) Hancock.G.
Priv. Comm. (1987)

367) Gottscho.R.A., Burton.R.H., Flamm.D.L., et al.
J. Appl. Phys. 55(7); 2707, (1984)

368) Nishizawa.J., Hayasaka.N.
Thin Solid Films. 92(1-2); 189, (1982)

369) Pang.S., Brueck.S.R.J.
Masterials Research Society Symp. Proc. 17; 161, (1983)

370) Hargis.P.J., Kushner.M.J.
Appl. Phys. Letts. 40(9); 779, (1982)

371) Raby.B.A.
J. Vac. Sci. Technol. 15(2); 205, (1978)

372) Granger.P.F., Duchemin.J.P.
Thin Solid Films. 67; 279, (1980)

373) Lehmann.H.W., Heeb.E., Frick.K.
Solid State Technology. 24(10); 69, (1981)
Electrochem. Soc. Abstr. 81-1; 615, (1981)

374) McOmber.J.I., Pender.M.
Electrochem. Soc. Abstr. 81-1; 634, (1981)

375) Dylla.H.F., Blanchard.W.R.
J. Vac. Sci. Technol.-A. 1(2); 1297, (1983)

376) Coburn.J.W., Eckstein.E.W., Kay.E.
J. Vac. Sci. Technol. 12(1); 151, (1975)

377) Coburn.J.W.
Rev. Scientific Instruments. 41(8); 1219, (1970)

378) Coburn.J.W., Kay.E.
Solid State Technology. 12(12); 49, (1971)

379) Coburn.J.W., Kay.E.
Applied Physics Letters. 18(10); 435, (1971)

380) Coburn.J.W., Kay.E.
Applied Physics Letters. 19(9); 350, (1971)

381) Oechsner.H., Gerhard.W.
Surface Science. 44; 480, (1974)

382) Coburn.J.W., Taglauer.E., Kay.E.
J. Appl. Phys. 45(4); 1779, (1974)

383) Coburn.J.W., Eckstein.E.W., Kay.E.
J. Appl. Phys. 46(7); 2828, (1975)

384) Shinoki.F., Itoh.A.
J. Appl. Phys. 46(8); 3381, (1975)

385) Oechsner.H., Stumpe.E.
Applied Physics. 14; 43, (1977)

386) Beenakker.C.I.M., Van de Poll.R.P.J., Dieleman.J.
Electrochem. Soc. Abstr. 81-1; 618, (1981)

387) Wagner.J.J., Brandt.W.W.
Plasma Chem. Plasma Processing. 1(4); 201, (1981)

388) Hays.A.K.
Electrochem. Soc. Abstr. 81-1); 741, (1981)

389) Weakliem.H.A.
Electrochem. Soc. Abstr. 81-1; 729, (1981)

390) Kay.E., Coburn.J.W., Kruppa.G.
Le Vide. 183; 89, (1976)

391) Canning Handbook
Electroplating. 22nd Ed; 794, (1978)

392) Ephrath.L.M.
J. Electron. Mater. 7(3); 415, (1981)

393) Levenstein.H.J., Vratny.F.
US Patent 4,419,201. (1983)

394) AERE Codes of Practice.
Vacuum systems and components. 1st. Ed;Reprint (1982)

395) Alcaide.H.D.
Solid State Technology. 25(4); 171, (1982)

396) Hozumi.N., Morosoff.N.
Polymer Preprints. 16(1); 38, (1975)

397) Coburn.J.
Jpn. J. Appl. Phys. 22(4); 631, (1983)

398) Hetzler.U., Kay.E.
J. Appl. Phys. 49; 4619, (1979)

399) Nicholas.M.G.
Priv. Comm. AERE; (1981)

400) Nomarskii.G., Weill.A.R.
Rev. Metall. 52; 121, (1955)

401) Griffiths.D.P., Bradley.S.H.
J. Mater. Sci. 12; 1019, (1977)

402) Robinson.H., Rawlinson.W.F.
Philosophical Magazine 28; 277, (1914)

403) Robinson.H., Rawlinson.W.F.
Proc. Royal Soc. Ser.A. 104; 274, (1923)

404) Robinson.H., Rawlinson.W.F.
Philosophical Magazine. 50; 241, (1925)

405) deBroglie.M.
Comptes Rendu. 172; 274, (1921)

406) Auger.P.
Comptes Rendu. 180; 65, (1925)

407) Auger.P.
J. Phys. Rad. 6; 205, (1925)

408) Scheibner.E.J., Tharp.L.N.
Surface Science. 8; 247, (1967)

409) Palmberg.P.W.
J. Appl. Phys. 38; 3137, (1967)

410) Weber.R.E., Peria.W.T.
J. Appl. Phys. 38; 4355, (1967)

411) Harris.L.A., Res.G.E.
J. Appl. Phys. 39; 1419, (1968)

412) Palmberg.P.W., Bohn.G.K., Tracy.J.C.
Appl. Phys. Lett. 15; 254, (1969)

413) Seah.M.P.
Vacuum. 34(3-4); 463, (1984)

414) Riviere.J.C.
AERE Report. R-9433; (1979)

415) Clark.D.T., Shuttleworth.D.
J. Polym. Sci. -Polymer Chem. Ed. 18(1); 32, (1980)

416) Clark.D.T.
Adv. in Polymer Friction & Wear. Plenum 5A; (1975)

417) Clark.D.T.
Adv. in Polym. Science. Springer-Verlag; (1977)

418) Korman.C.S., Dilks.A. Ed.
Electron Spectr. Theory, Techn. Academic. 4; (1982)

419) Clark.D.T., Dilks.A.
J. Polymer Science. 15; 2321, (1977)

420) Clark.D.T., Dilks.A.
J. Polymer Science. 16; 911, (1978)

421) Clark.D.T., Feast.W.J.
J. Macromol. Science. 12; 191, (1975)

422) Clark.D.T., Dilks.A., Shuttleworth.D.
Polymer Surfaces. Wiley. (1978)

423) Rice.D.W., O'Kane.D.F.
J. Electrochem. Soc. 123; 1308, (1976)

424) Clark.D.T., Shuttleworth.D.
J. Polym. Sci. -Polym. Chem. Ed. 18(1); 32, (1980)

425) Yasuda.H.
J. Macromol. Sci. Chem. A-10; 383, (1976)

426) Millard.M.M, Pavlath.A.E.
J. Macromol. Sci. Chem. A-10; 579, (1975)

427) Millard.M.M, Pavlath.A.E.
Polymer preprints. 16(1); 84, (1975)

428) Dilks.A., Kay.E.
Macromolecules. 14(3); 855, (1981)

429) Clark.D.T.
Pure & Applied Chemistry. 54(2); 415, (1982)

430) Mende.G.
Surface Science. 128; 169, (1983)

431) Yang.M.G., Koliwad.K.M.
J. Electrochem. Soc. 122(5); 675, (1975)

432) Davies.G.J., Tuppin.C.G., et al.
Analytical Proceedings. 20(9); 478, (1983)

433) Evans.C.A.
J. Anal. Chem. 44(13); 67A, (1972)

434) Oechsner.H., Gerhard.W.
Surface science. 44; 480, (1974)

435) Czanderna.A.W.
Methods of surface analysis. Elsevier; (1975)

436) Surman.D.J., van den Berg.J.A., Vickerman.J.C.
Surf. & Interface Analysis. 4(4); 160, (1982)

437) Kenway-Jackson.C.
Vacuum. 34(3/4); 479, (1984)

438) Vickerman.J.C.
Analytical Proceedings. 20; 482, (1984)

439) Sigmon.T.W.
SIMS-II. Springer Chem. 9; 80, (1979)

440) Christie.W.H., Warmack.R.J. , White.C.W., Narayan.J.
SIMS-II. Springer Chem. 9; 100, (1979)

441) Magee.C.W.
SIMS-II. Springer Chem. 9; 88, (1979)

442) Huber.A.M., Morillot.G., Merenda.P., Linh.N.T.
SIMS-II. Springer Chem. 9; 91, (1979)

443) Wang.K.L., Storms.H.A.
SIMS-II. Springer Chem. 9; 110, (1979)

444) Raman.C.V.
Nature. 121; 501, (1924)

445) Jenny.S.N.
Priv. Comm. AERE; (1982)

446) Mikklesen.J.C., Galeener.F.L.
Appl. Phys. Lett. 37(8); 712, (1980)

447) Adar.F., LeClerq.M., Grayzel.R.E.
American Laboratory. 59, (1982)

448) Needham.C.D.
L'Actualite chimique. 43, (1980)

449) Needham.C.D., Ramsey.J.N.
Semiconductor International. (1981)

450) L'Ecuyer.J., Brassard.C., Cardinal.C., Chabbal.J., et al.
J. Appl. Phys. 47(1); 381, (1976)

451) Terreault.B., Leroux.M., Martel.J.G., et al.
J. Vac. Sci. Technol. 14(1); 492, (1977)

452) Sofield.C., Woods.C.J., Butcher.J.M., et al.
Nuclear Instruments & Methods. 203(1/3); 509, (1982)

453) Read.P.M., Sofield.C., Franks.M.C., Scott.G.B., et al.
Thin Solid Films. 110; 251, (1983)

454) Read.P.M.
Priv. Comm (1984)

455) Michaelowicz.A.
Kinematics of Nuclear Reactions. Iliffe; (1967)

456) de Jager.C.W., de Vries.H., de Vries.C.
Nuclear Data Tables. 14; 479, (1974)

457) Geiger.H., Marsden.E.
Proc.Roy.Soc. 82; 495, (1909)

458) Rutherford.E.
Philosophical Magazine. 21; 669, (1911)

459) Ziegler.J. F.
New uses of Ion Accelerators. Plenum N.Y.; (1975)

460) Chu.W.K., Mayer.J.W., Nicholet.M.A.
Backscattering Spectrometry. Academic N.Y.; (1978)

461) Gildenblat.G., Heath.B.A., Katz.W.
J. Appl. Phys. 54(4); 1855, (1983)

462) Rabinzolm.P., et al.
J. Electrochem. Soc. 131(4); 905, (1984)

463) Eyre.N.J.
AERE Report. R-11178; (1984)

464) Stallhofer.P., Huber.D.
Solid State Technology. 26(8); 233, (1983)

465) Haslam.J., Willis.H.A., Squirrel.D.C.M.
Identification and analysis of plastics 419, (1965)

466) Bellamy.L.J.
IR Spectra of Complex Molecules. Wiley; 324, (1954)

467) Colthrup.N.B, Daly.L.H, Wiberley.S.E.
Introduction to IR & Raman Spectr. Academic; 313, (1964)

468) Adams.A.C.
Solid State Technology. 26(4); 135, (1983)

469) Grossel.M.C.
Priv. Comm. (1983)

470) Kaplan.S., Dilks.A.
Thin Solid Films. 84; 419, (1981)

471) Dilks.A., Kaplan.S.
Electrochem. Soc. Abstracts. 81-1; 743, (1981)

472) Dilks.A., Kaplan.S.
Proc. Electrochem. Soc 82(6); 31, (1982)

473) Coates.A., Redfern.J.
Analyst 88; 906, (1965)

474) Cox.J.M., Wright.B.A., Wright.W.W.
J. Appl. Polym. Sci. 8; 2935, (1964)

475) Cox.J.M., Wright.B.A., Wright.W.W.
J. Appl. Polym. Sci. 8; 2951, (1964)

476) ET Associates.
Nailsea, Bristol.

477) Lawson.K.E.
IR. Absn. Inorg. Substances. Reinhold. (1961)

478) Robinson.J.W.
Handbook of Specroscopy. CRC. 2; (1974)

479) Steunenberg.R.K., Cady.G.H.
J. Am. Chem. Soc. 74; 4165, (1952)

480) Pickford.C.
Priv. Comm. AERE; (1984)

481) Danilatos.G.D.
Scanning. 4; 9, (1981)

482) Danilatos.G.D.
J. Microscopy. 121; 235, (1981)

483) Cairns.J.A.,et al.
Appl.Phys.Lett. 30(8); 392, (1977)

484) Baker.R.T.K., Sherwood.R.D., Dumesic.J.A.
J. Vac. Sci. Technol. 16(2); 493, (1979)

485) Miller.D.E.
Scanning Electron Micros. 1; 513, (1978)

486) Holland.L., Laurenson.L., Hurley.R.E., Williams.K.
Nuclear Instr. Methods. 3; 555, (1973)

487) Holland.L., Laurenson.L., Fulker.M.J.
Jpn. J. Appl. Phys. 12(9); 1468, (1973)

488) Conru.H.W., Laberge.P.C.
J. Phys. E. 8; 136, (1975)

489) Tyerman.W.J.R.
Trans. Faraday Soc. 65; 1188, (1969)

490) Timms.P.L., et al.
J. Am. Chem. Soc. 87(13); 2824, (1965)

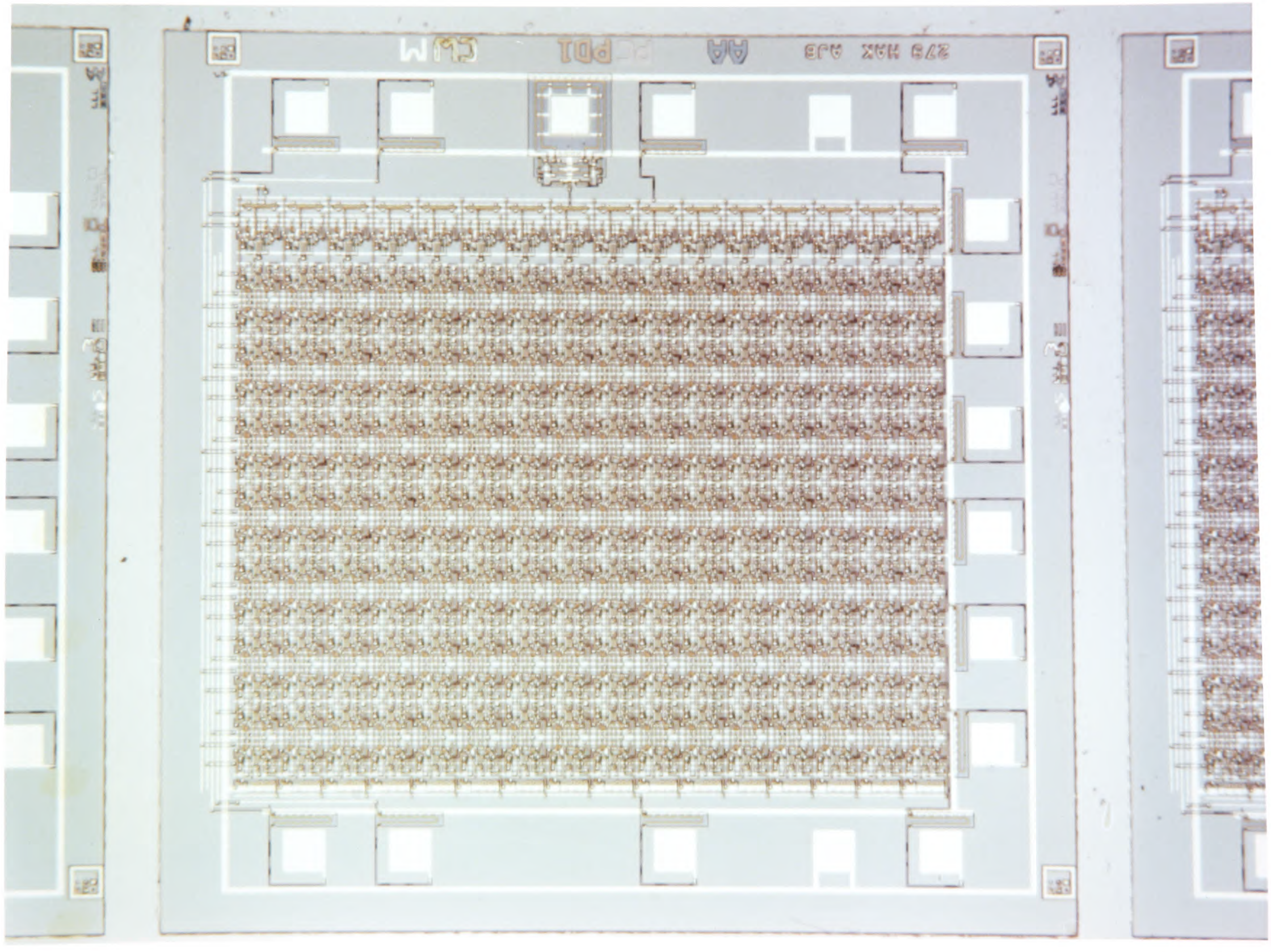
CLM
PDL
AA
2.3 MAX 2.3

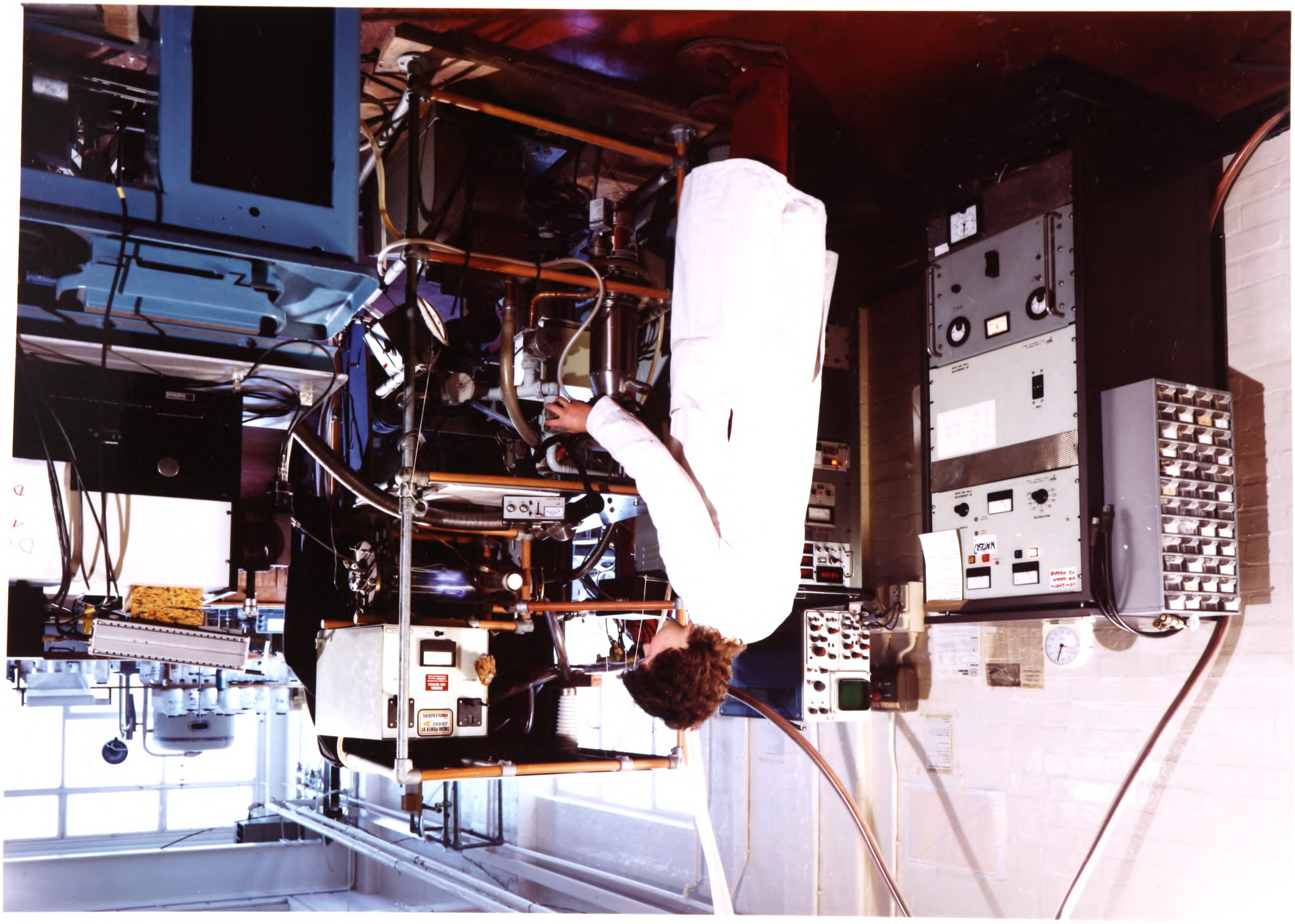

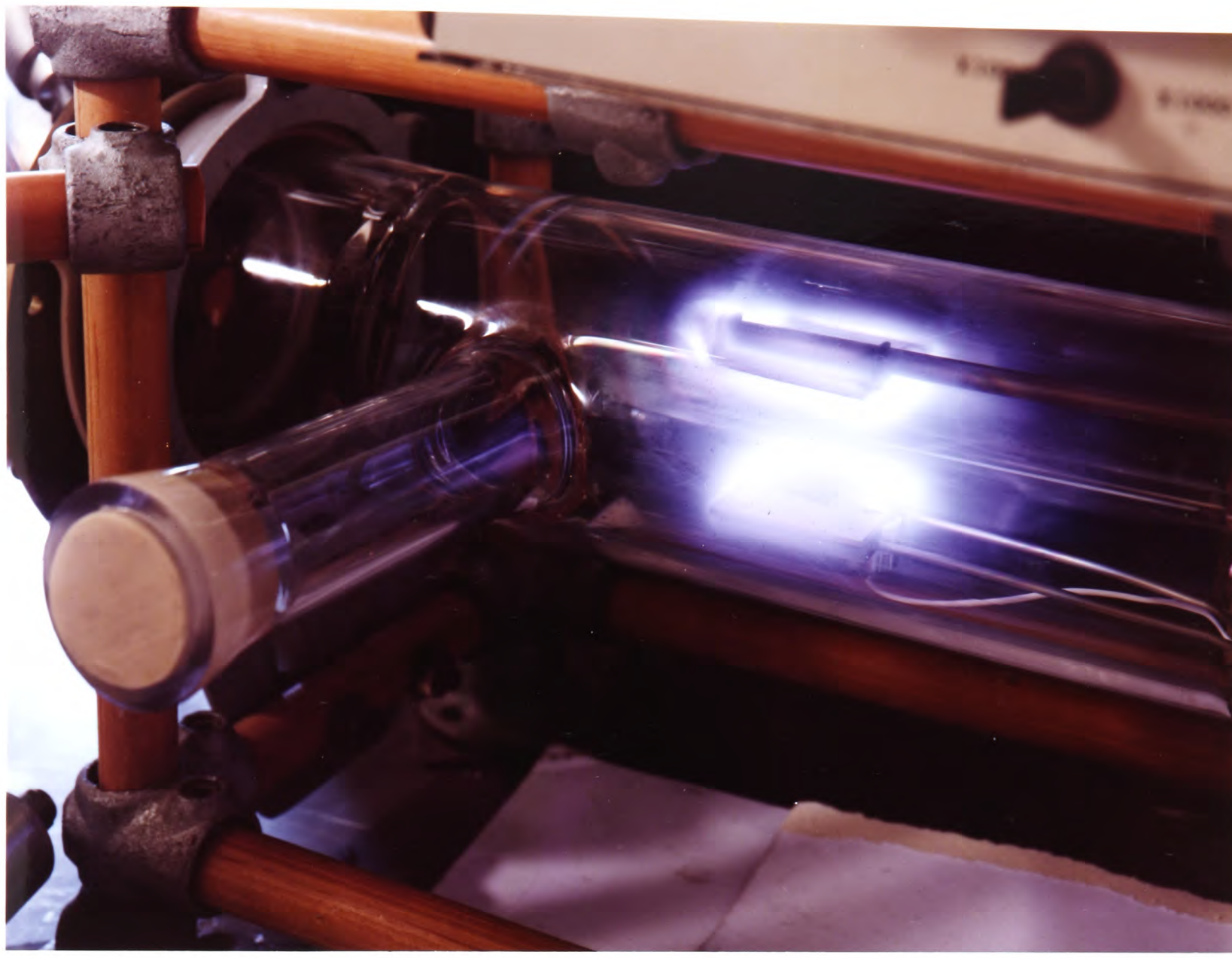

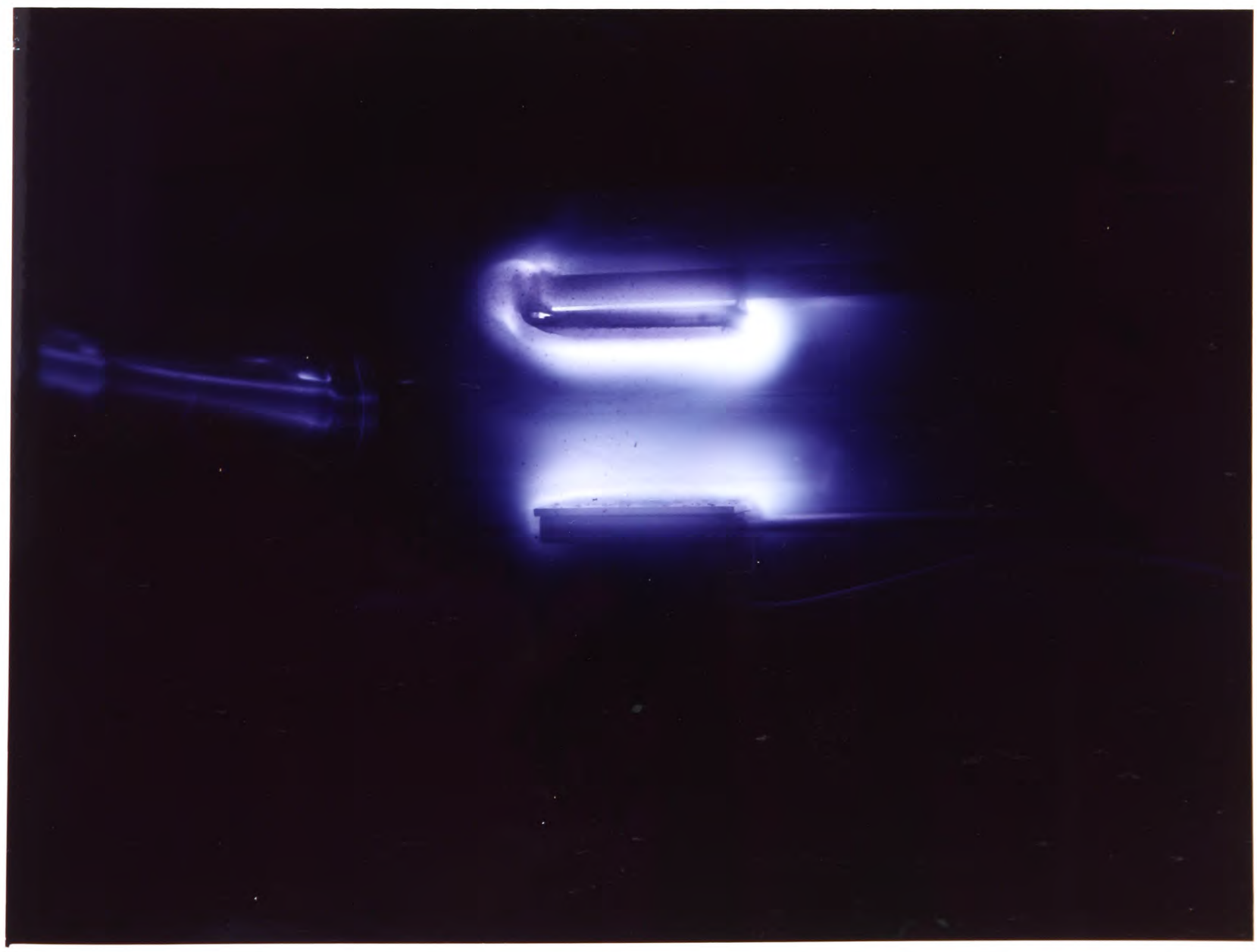

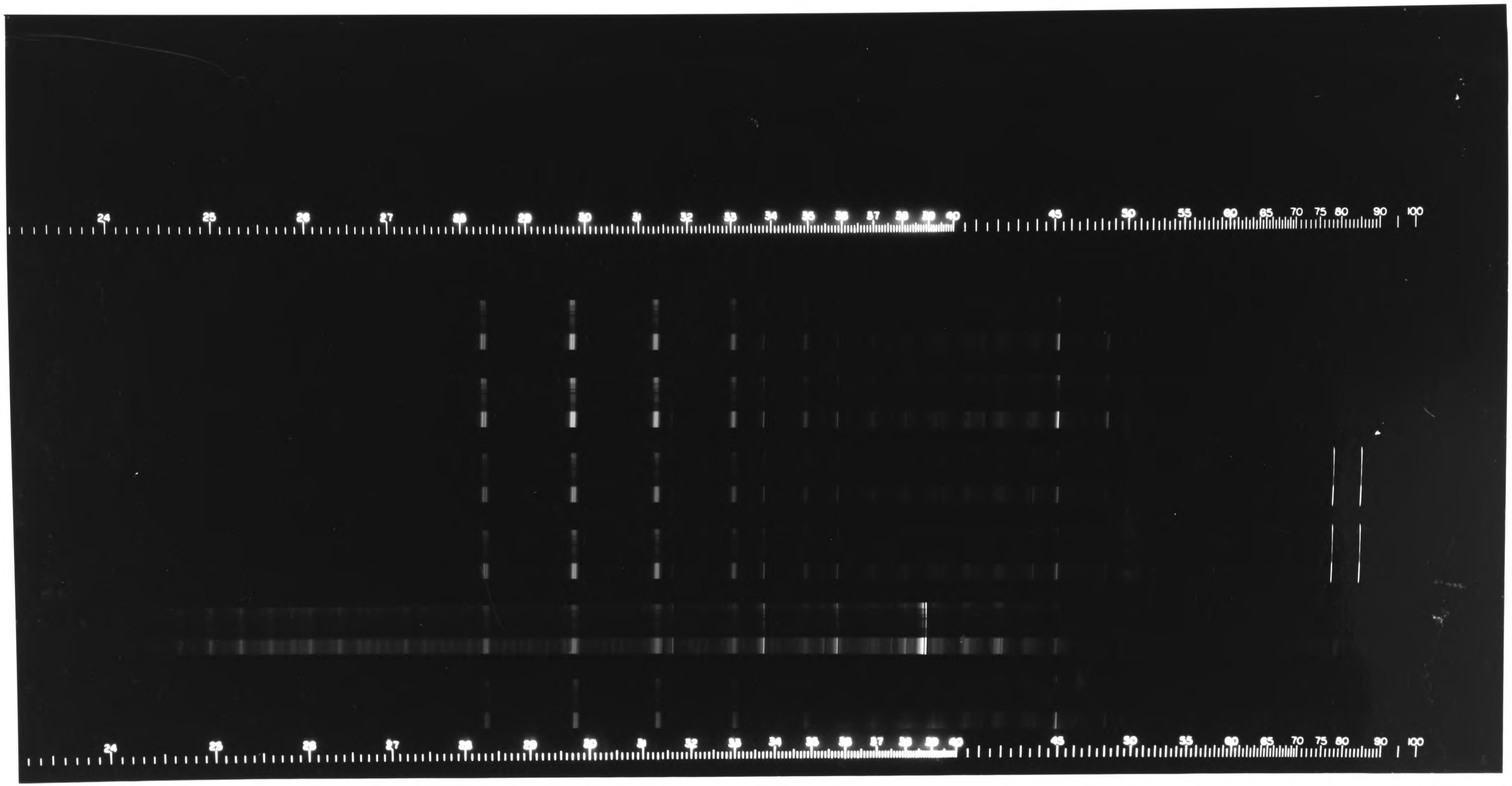

FIG. 61. SAMPLE 10" X 4" PLATE

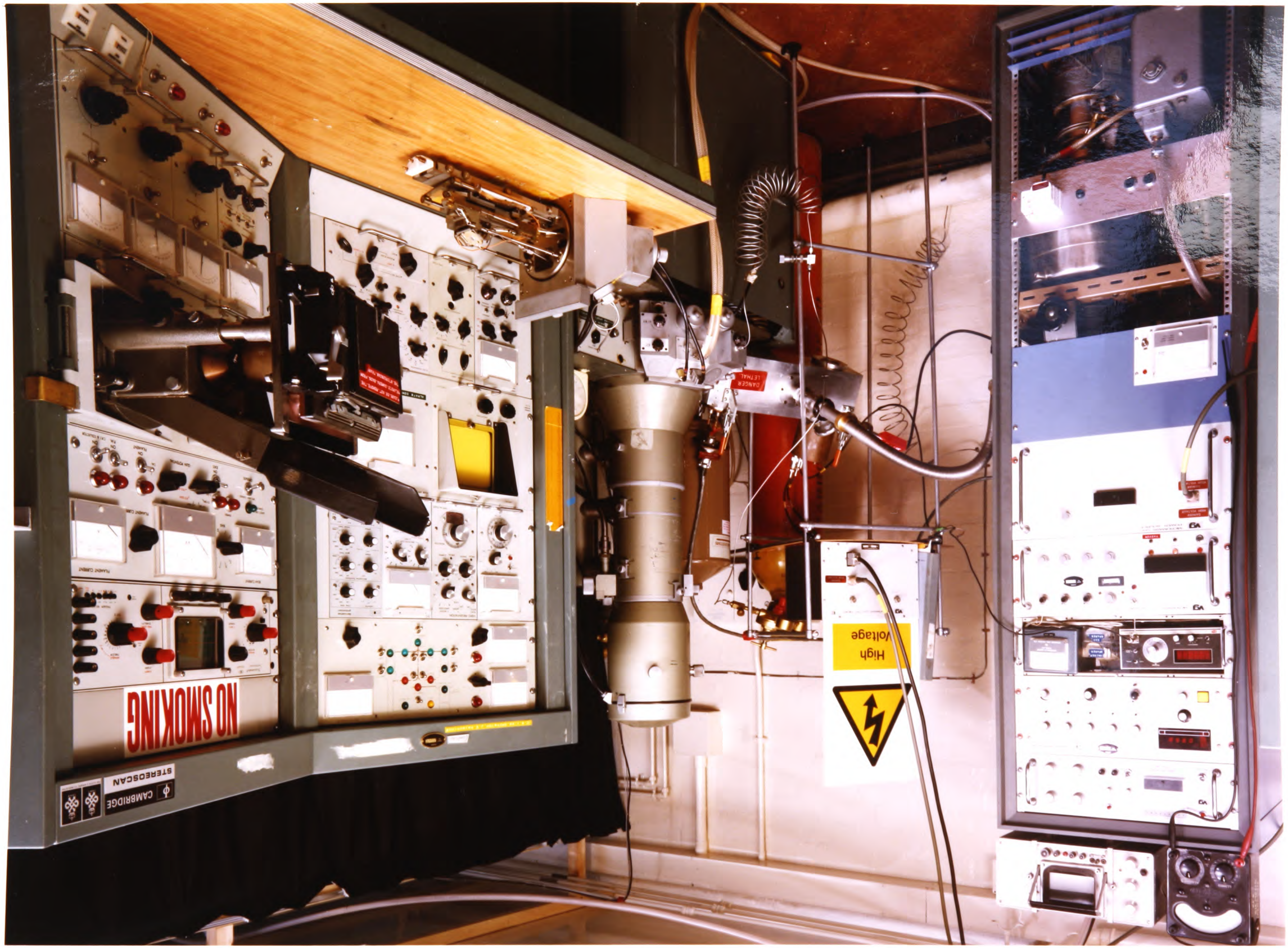
NO SMOKING
CAMBRIDGE
STEREOSCAN
High
Voltage

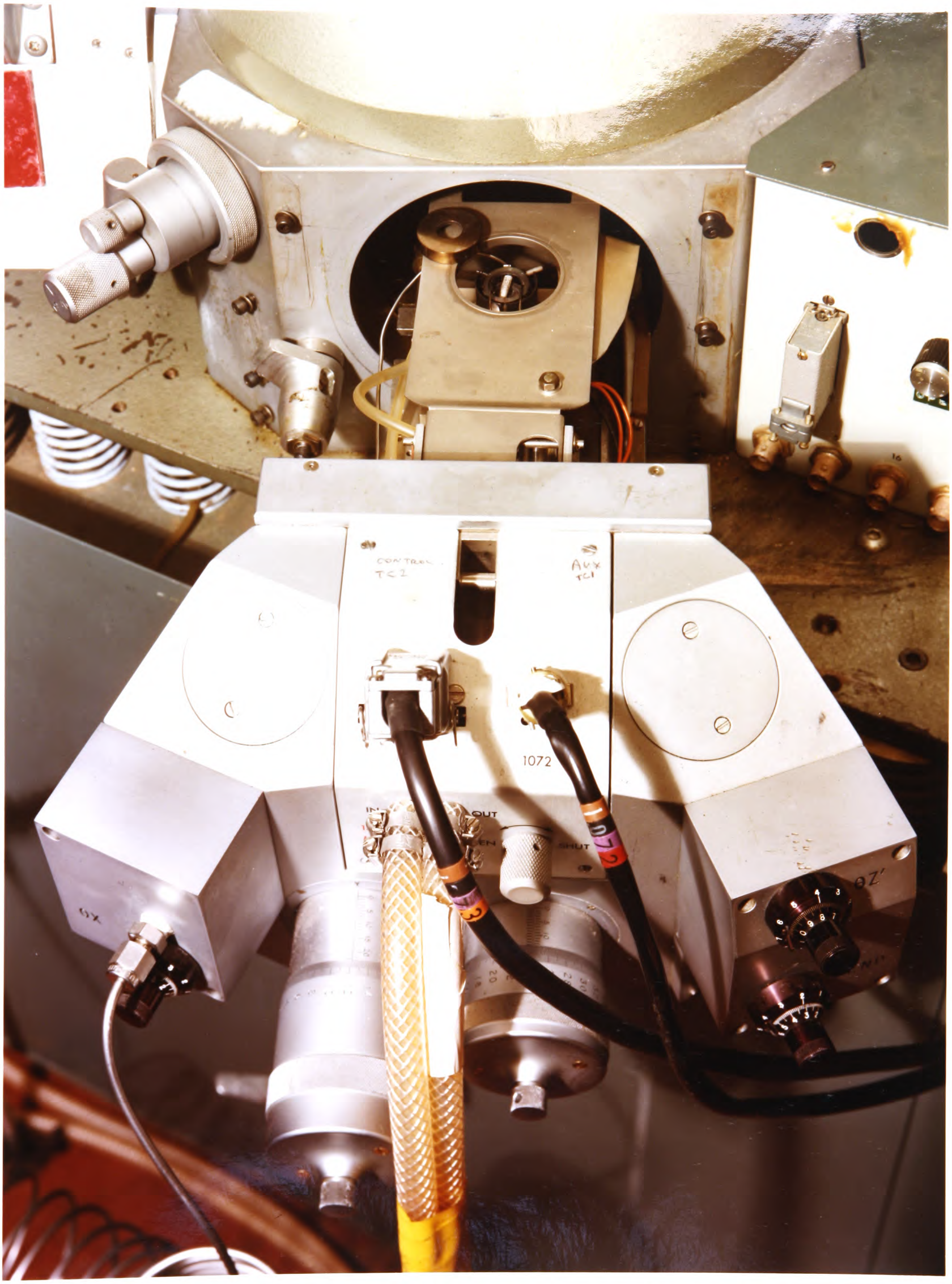
CONTROL
TC2
AUX
TC1
1072
OUT
SHUT
OZ'

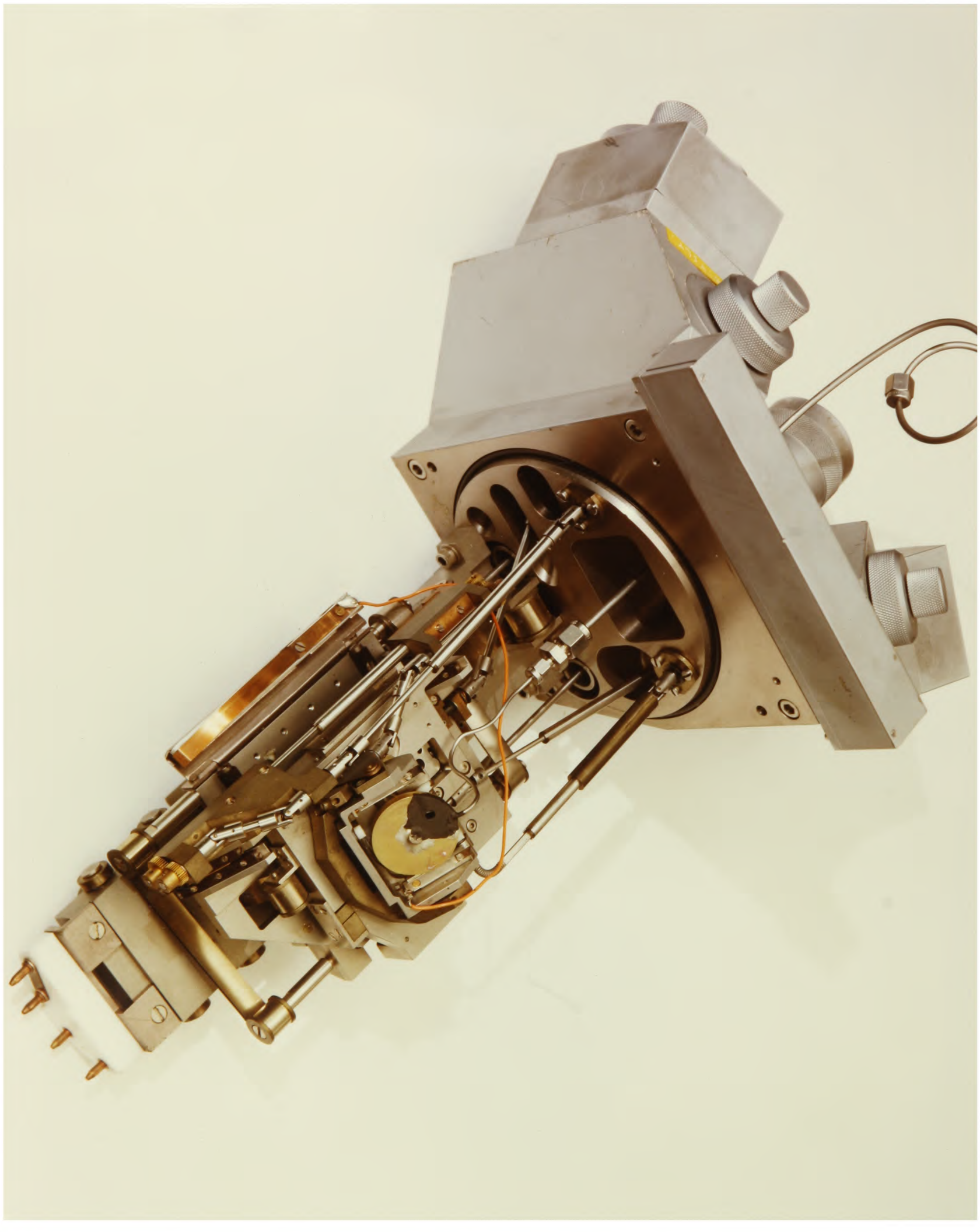

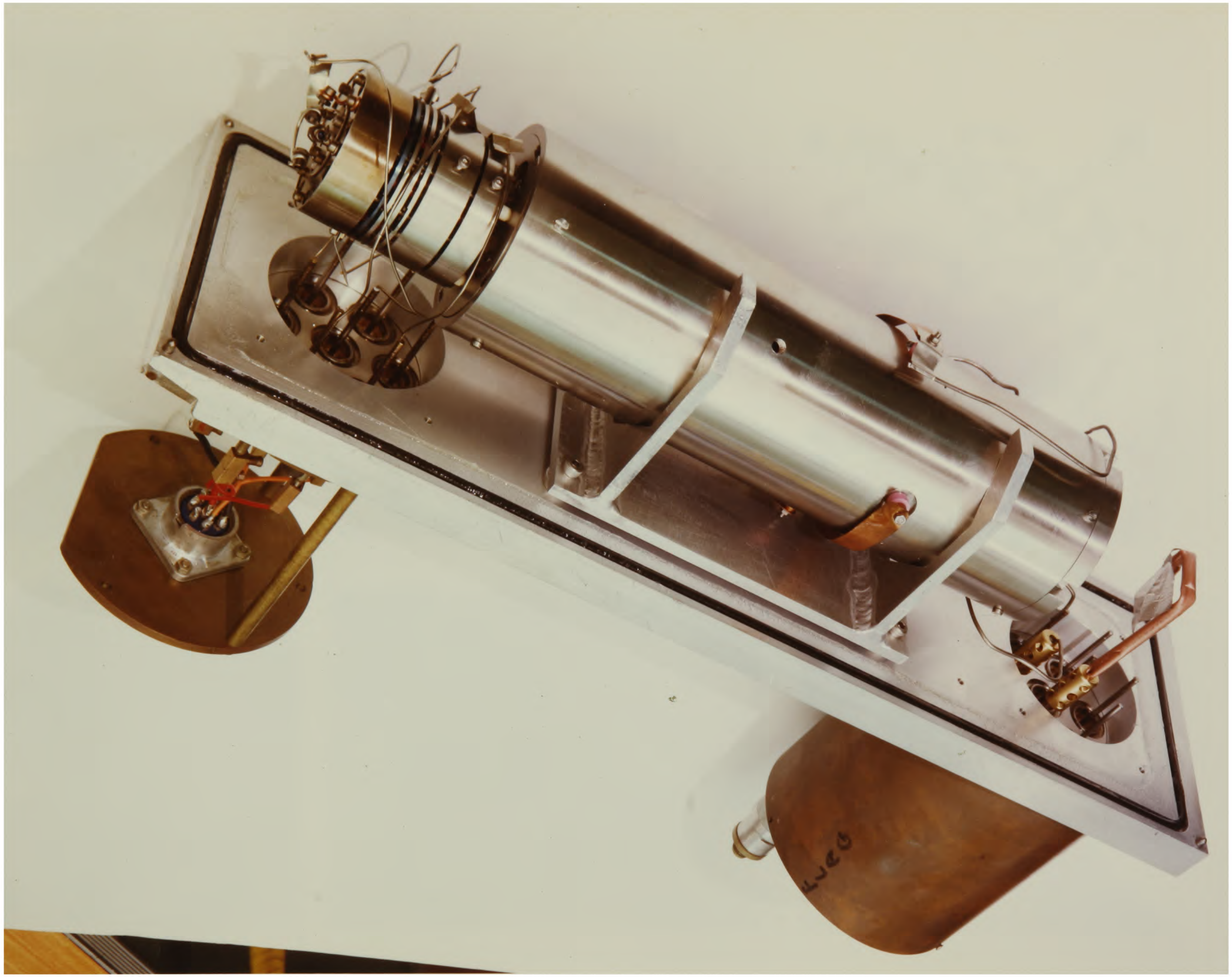

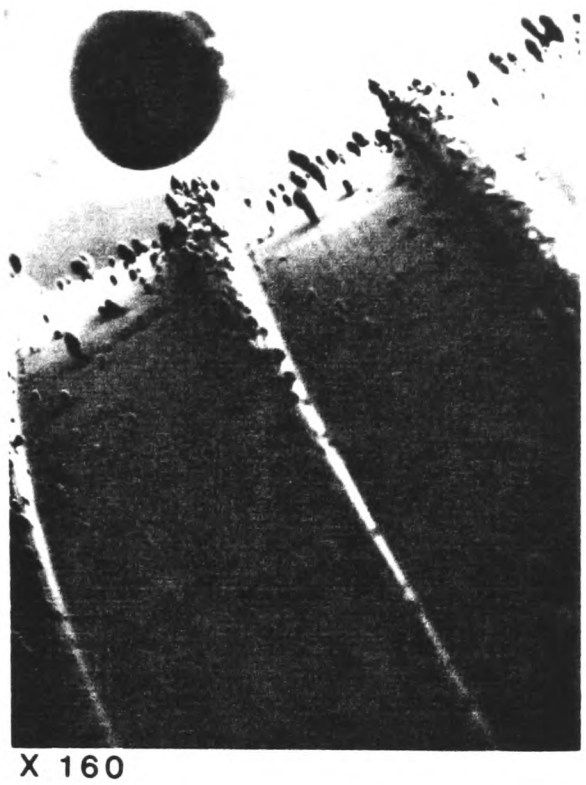

X 160

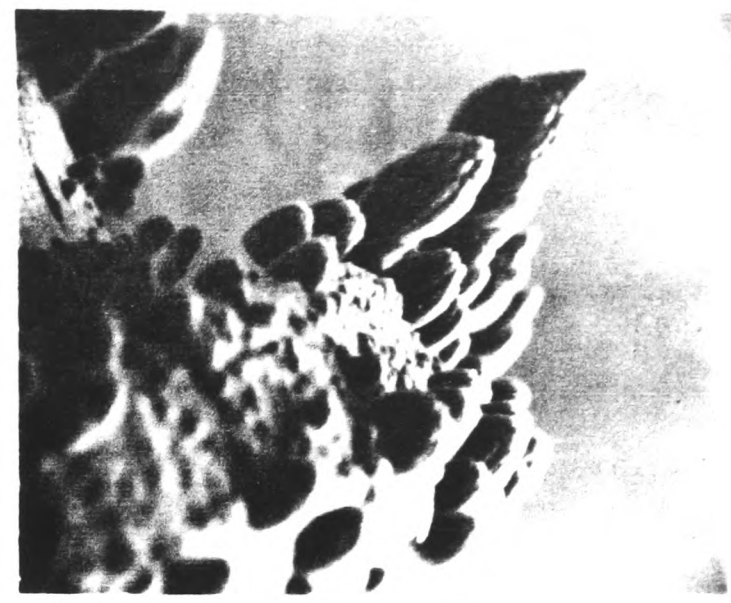

X 640

100 % CO

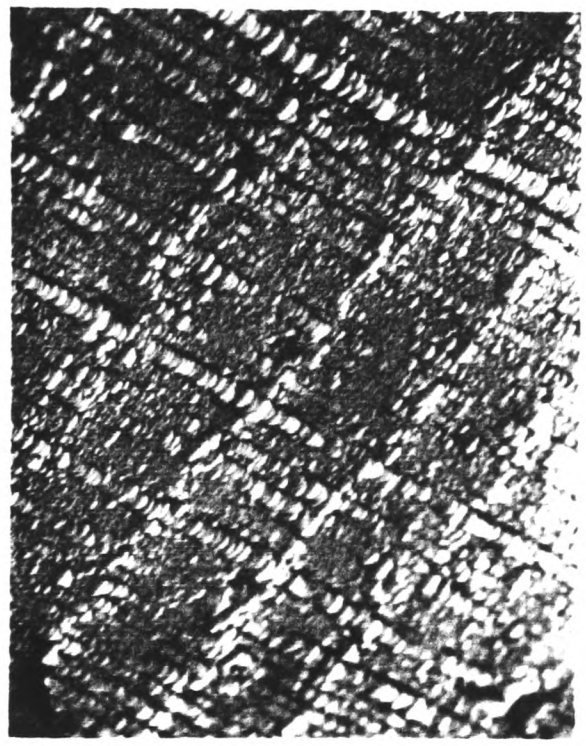

X 640

X 5,000

95 35 CO, 65 CO_2

X 640

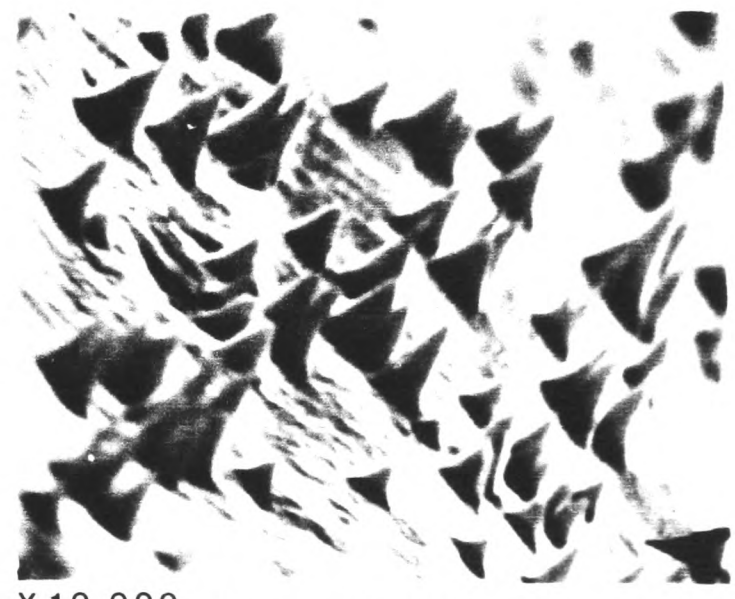

X 10,000

93 5 CO, 6 5 CO_2

FIG. CARBON DEPOSITION ON STEEL SAMPLES.

Index